

Université de Versailles Saint-Quentin-en-Yvelines
Thèse d'habilitation à diriger des recherches

École doctorale :
sciences de l'environnement

présentée par

M. Frédéric CHEVALLIER

Titre du mémoire :

**De l'application de la
théorie analytique des probabilités
pour l'étude de l'atmosphère**

soutenue publiquement le 26 mars 2009 devant le jury composé de

Présidente :	Mme	Sylvie	Thiria
Rapporteurs :	M.	Gérald	Desroziers
	M.	Hervé	Le Treut
	M.	Olivier	Talagrand
Examinateurs :	M.	Philippe	Ciais
	M.	Jean-Noël	Thépaut
	M.	Jacques	Verron

Table des matières

Résumé du mémoire et des travaux	5
Prospective personnelle	11
I Introduction	21
I.1 Petite histoire de la théorie des probabilités	21
I.2 Définition de la probabilité	23
I.3 Compendium du théorème de Bayes	24
I.4 Théorème de Bayes et étude de l'atmosphère	26
I.5 Présentation du mémoire	27
II Information a priori	29
II.1 Introduction	29
II.2 Caractérisation des erreurs	30
II.2.1 Introduction	31
II.2.2 Model and Data	31
II.2.3 Results	32
II.2.4 Discussion and Conclusions	34
III Observations	39
III.1 Introduction	39
III.2 Choix d'observations interprétables	40
III.2.1 Introduction	40
III.2.2 Theoretical framework of 4D-Var	41
III.2.3 Data and model	43
III.2.4 Accuracy of the observation operator	45
III.2.5 Linearity of the observation operator	50
III.2.6 Application in one dimension	52
III.2.7 Conclusion	53
III.3 Choix d'observations informatives	56
III.3.1 Introduction	57
III.3.2 Inferring CO ₂ surface fluxes	57
III.3.3 Data sources	58
III.3.4 Results	58
III.3.5 Conclusion	60
III.4 Impact des corrélations entre les erreurs	63
III.4.1 Introduction	63
III.4.2 Method	64

III.4.3 Results	67
III.4.4 Discussion and Conclusions	70
IV Opérateur d'observation	73
IV.1 Introduction	73
IV.2 RTTOV-CLD	74
IV.2.1 Introduction	74
IV.2.2 Description of the radiation scheme	75
IV.2.3 The data	76
IV.2.4 The variational approach	78
IV.2.5 Variational retrieval of cloud information	79
IV.2.6 Discussion	87
IV.3 Évaluation de l'adjoint du modèle direct	91
IV.3.1 Introduction	91
IV.3.2 Description of the radiation schemes	92
IV.3.3 Generalities about variational assimilation	94
IV.3.4 Validation of NeuroFlux for variational assimilation	96
IV.3.5 Comparison between RTTOV-5 and Synsatrad	103
IV.3.6 Conclusion	110
V Inversion	115
V.1 Introduction	115
V.2 Mise en œuvre	115
V.2.1 Introduction	116
V.2.2 The Inference Scheme	117
V.2.3 Observations and Prior Information	119
V.2.4 Transport Model	124
V.2.5 Results	125
V.2.6 Discussion	133
V.2.7 Conclusion	134
V.3 Diagnostics	138
V.3.1 Introduction	138
V.3.2 Method and Data	139
V.3.3 Results	144
V.3.4 Discussion and Conclusions	149
A Bibliographie	155
B Curriculum vitae	161
C Publications scientifiques	165

Résumé du mémoire et des travaux

On voit, par cet Essai, que la théorie des probabilités n'est, au fond,
que le bon sens réduit au calcul.

P. S. Laplace, Théorie analytique des probabilités, Introduction (1812)

Le théorème dit « de Bayes »¹ est un modèle mathématique de l'apprentissage. Il décrit comment l'apport d'une nouvelle information améliore la connaissance d'un phénomène. Découvert en 1774 par Pierre Simon Laplace, il fournit une solution générique aux problèmes inverses et est devenu une référence essentielle pour les méthodes d'estimation statistique. Son succès témoigne de sa flexibilité et de sa rigueur pour le traitement des observations. Son application pour l'étude d'un problème particulier fait appel à des savoirs variés, car chacune des composantes d'un système d'inversion requiert un travail spécialisé, sur le problème scientifique étudié, sur les observations, sur la modélisation, ou sur l'ingénierie informatique. Mais elle doit être guidée par une compétence spécifique liée à la théorie des probabilités.

Le présent mémoire explore plusieurs questions fondamentales autour du théorème de Bayes à travers une sélection de mes publications dans les dix dernières années : comment spécifier les statistiques d'erreur des différentes informations disponibles ? Toute observation est-elle utile ? Comment relier les variables observées et les variables d'étude ? Comment appliquer le théorème dans le cas de problèmes de grandes dimensions ? Les réponses à ces questions sont étayées dans le cadre de deux problèmes scientifiques.

Le premier problème est **l'assimilation des informations fournies par les satellites sur les nuages et la pluie dans les modèles numériques mis en œuvre pour la prévision météorologique** (application A). J'ai pu l'étudier lors de mon travail post-doctoral au CEPMMT² entre 1998 et 2003. En dehors de la prévision immédiate (à l'échelle de quelques heures), ce sujet était presque vierge lorsque mes collègues du CEPMMT et moi nous y sommes intéressés : de telles données étaient rejetées par les systèmes de prévision.

La résolution de ce problème par le théorème de Bayes inclut les éléments suivants :

- une estimation a priori des variables thermodynamiques de l'atmosphère que l'on souhaite optimiser (essentiellement des champs tri- ou quadri-dimensionnels de température, d'humidité et de pression) - elle est fournie par la prévision précédente,
- des observations de l'atmosphère, parmi lesquelles se trouvent les luminances mesurées

¹ $p(A|B) = p(B).p(B|A)/p(A)$, où A et B sont deux événements, $p(A)$ et $p(B)$ sont leurs probabilités respectives, $p(A|B)$ est la probabilité de A lorsque B est réalisé et $p(B|A)$ est la probabilité de B lorsque A est réalisé.

²Centre Européen pour les Prévisions Météorologiques à Moyen Terme (en anglais ECMWF)

- par les satellites en présence d'hydrométéores,
- un modèle numérique de l'évolution de l'atmosphère dans la fenêtre temporelle considérée,
 - des opérateurs d'observation (dont des codes de rayonnement) qui calculent les variables observées (parmi lesquelles les luminances reçues par les satellites) à partir des variables que l'on souhaite optimiser,
 - des modèles statistiques des erreurs des éléments précédents,
 - une méthode de calcul de l'équation de Bayes.

Le deuxième problème scientifique concerne **l'estimation des flux de dioxyde de carbone à la surface du globe** (application B), que je mets en œuvre au LSCE³ depuis la fin de l'année 2003. Il était exploré depuis une dizaine d'années lorsque j'ai rejoint le LSCE, mais les méthodes analytiques développées jusqu'alors ne permettaient que des estimations des flux à faible résolution spatiale et temporelle et utilisant moins de quelques milliers d'observations à la fois seulement.

L'application B du théorème de Bayes inclut les éléments suivants :

- une estimation a priori des variations spatiotemporelles des flux de CO₂ - elle est fournie par des climatologies ou des modèles,
- des observations directes ou par télédétection des concentrations de CO₂ dans l'atmosphère sur une fenêtre de temps (typiquement quelques mois),
- un modèle numérique du transport atmosphérique du CO₂ dans la fenêtre de temps considérée,
- des opérateurs d'observation qui calculent les variables observées (par exemple des concentrations moyennes pondérées sur la verticale) à partir des champs tridimensionnels des concentrations de CO₂,
- des modèles statistiques des erreurs des éléments précédents,
- une méthode de calcul de l'équation de Bayes.

Avec ces deux exemples d'application du théorème de Bayes, j'illustre la richesse du sujet et je montre que ce théorème recèle bien plus de subtilités que ne le suggère la concision de sa forme. Le titre du mémoire fait écho à l'ouvrage de Laplace *Théorie analytique des probabilités* (1812), qui a grandement diffusé l'approche bayésienne.

Le chapitre introductif présente le théorème de Bayes, le place dans son contexte historique et résume son application pour l'étude de l'atmosphère.

Le deuxième chapitre traite de l'information a priori dans le cadre de l'application B et s'appuie sur un article suscité par la préparation de ce mémoire (Chevallier et coll. 2006). Les statistiques de l'information fournie a priori par le modèle de la biosphère terrestre ORCHIDEE⁴ de l'IPSL⁵ y sont estimées par comparaison à des mesures *in situ*. Cette approche contraste avec l'empirisme des études précédentes. Les résultats de la comparaison indiquent que les erreurs de l'a priori ne suivent pas une distribution gaussienne multivariée : les erreurs du modèle ont une queue plus lourde. Les corrélations temporelles sont linéaires

³Laboratoire des Sciences du Climat et de l'Environnement

⁴ORganizing Carbon and Hydrology In Dynamic Ecosystems Environment

⁵Institut Pierre Simon Laplace

avec le temps après le premier jour et restent fortes même après un mois, signe de biais à l'échelle de la semaine. Les corrélations spatiales sont faibles ou inexistantes, ce qui limite la possibilité de propager spatialement les informations fournies par les observations : ce résultat contredit une hypothèse courante. Les écarts-types (2 gC.m^{-2} par jour) sont du même ordre de grandeur que les valeurs postulées dans les précédents travaux. Le prolongement de cette étude novatrice figure maintenant dans un projet européen⁶.

Le chapitre III aborde le sujet des observations en s'appuyant sur trois articles (Chevallier et coll. 2004, 2005, Chevallier 2007). Il invite à ne garder qu'un sous-ensemble des mesures disponibles. Trois critères d'utilité sont retenus : le contenu en information des observations, la linéarité (autour de l'état de base) de l'opérateur qui relie les variables estimées aux variables observées et la faiblesse des biais. Ces trois critères peuvent être redondants. En effet, pour l'application A, la non-linéarité de l'opérateur d'observation (un modèle diagnostique des nuages joint à un modèle de rayonnement) fait souvent dévier les erreurs hors des distributions Gaussiennes, induit des biais et diminue l'information exploitable des observations. Au contraire, l'application B repose sur un opérateur linéaire (représentant le transport d'un traceur passif dans l'atmosphère), mais incertain, donc souvent biaisé et réduisant ainsi aussi l'information disponible.

Pour l'application A, les simulations de 2 canaux infrarouge du radiomètre MVIRI⁷ embarqué sur les satellites Meteosat et de 324 canaux du radiomètre AIRS⁸ embarqué sur le satellite Aqua sont examinées. Seuls les canaux sondant la haute troposphère à 4,5, à 6,3 et à $14,3 \mu\text{m}$ semblent appropriés pour l'assimilation dans un modèle d'analyse variationnel quadri-dimensionnel (4D-Var) comme celui du CEPMMT. La pertinence des observations à $6,3 \mu\text{m}$, disponibles sur tous les satellites météorologiques en orbite géostationnaire est vérifiée sur des mesures satellitaires réelles par comparaison à des radiosondages.

Pour l'application B, l'analyse de concentrations de CO₂ simulées pour la haute troposphère par un modèle de transport indique que des biais supérieurs à quelques dizaines de ppm⁹ dans des produits satellitaux correspondants (comme ceux issus de AIRS) dégraderaient notablement l'estimation des flux de carbone.

Ces travaux, comme ceux du précédent chapitre sur les erreurs a priori ont contribué de manière originale aux discussions sur l'apport d'observations nouvelles au regard de l'information existante. Ils sont imprégnés d'orthodoxie bayésienne et certains aspects négatifs de leurs conclusions ont pu susciter des débats houleux.

Le chapitre III propose aussi un examen de l'effet de corrélations entre les erreurs des observations. Ce sujet a été peu traité jusqu'à présent et la préparation de ce mémoire m'a incité à l'étudier et à publier dessus. J'utilise une approche stochastique originale (la réalisation d'ensembles d'inversions cohérents avec les statistiques d'erreur assignées à l'information a priori et aux observations), mais rigoureuse, pour évaluer trois approximations usuelles des

⁶COCOS (*Coordination Action Carbon Observation System*), projet européen du 7^e programme cadre pour la recherche et le développement.

⁷Meteosat Visible and Infrared Imager

⁸Advanced Infrared Sounder

⁹parties par million

corrélations dans le cadre de l'application B : négliger les corrélations, diminuer la densité des observations et augmenter l'erreur spécifiée des observations. La troisième approximation produit les meilleurs résultats.

Le quatrième chapitre concerne l'opérateur d'observation et reprend deux articles (Chevallier et Mahfouf 2001, Chevallier et coll. 2002). Il décrit d'abord le développement d'un modèle de rayonnement appelé RTTOV-CLD et incorporant l'effet des nuages pour l'application A. Ce problème est caractérisé par l'importance de phénomènes dont l'échelle est inférieure à celle de la maille des modèles numériques de l'atmosphère. Des approximations ont été choisies afin de maintenir les temps de calcul du code à des niveaux réalistes dans un contexte de prévision opérationnelle, tout en préservant une précision a priori plus petite que l'erreur introduite par l'incertitude sur les variables atmosphériques du système de prévision. L'effort sur la précision du code n'a pu être étayé par des validations directes, car les données appropriées n'existent pas, mais les paramétrisations correspondaient à l'état de l'art au moment de leur développement.

RTTOV-CLD est une extension du modèle de rayonnement RTTOV¹⁰. RTTOV a été créé pour simuler les luminances mesurées par les radiomètres orbitaux en ciel clair (sans nuages) ou en présence d'une unique couche de nuages. RTTOV-CLD introduit la possibilité de nuages multi-couches semi-transparents et non-diffusifs, dans l'infrarouge et les micro-ondes. Sous l'approximation des corps gris, chaque couche est décrite par une couverture fractionnaire horizontale et une émissivité. Plusieurs paramétrisations de l'émissivité (en fonction du contenu en eau liquide et solide des couches nuageuses, de leur température, du type de surface et de la fréquence) et plusieurs types de recouvrement des couches (aléatoire, maximal et maximal-aléatoire) sont mises en place dans le code.

Un travail similaire a été réalisé pour prendre en compte l'effet de la pluie, avec un modèle appelé RTTOV-SCATT (Chevallier et Bauer 2003, Moreau et coll. 2003, Bauer et coll. 2006b). RTTOV-SCATT est une autre extension de RTTOV, dédiée au rayonnement dans les micro-ondes. Le profil vertical des hydrométéores (nuages d'eau et de glace, pluie et glace précipitante) est pris en compte avec un modèle de diffusion simple. Les couches d'hydrométéores se recouvrent de manière aléatoire et leurs propriétés optiques (coefficients d'extinction, albédo de diffusion simple et paramètre d'asymétrie) sont fournies au code par des tables de Mie précalculées. Seule la surface dépolarise le rayonnement.

Avant même de servir pour l'assimilation de données, ces nouveaux codes m'ont permis de réaliser une série de validations indirectes des nuages et des précipitations simulés par le modèle de prévision du CEPMMT. Elles ont permis d'établir que :

- malgré le réalisme de la distribution géographique des nuages simulés par le modèle de prévision et de leurs variations saisonnières, l'impact radiatif instantané des nuages est trop faible, probablement à cause d'un déficit de glace, la fréquence d'occurrence des nuages hauts est surestimée dans la zone de convergence intertropicale et les stratocumulus à l'Est des continents sont sous-estimés (Chevallier et coll. 2001, Chevallier et

¹⁰Radiative Transfer for Television and Infrared Observation Satellite (TIROS) Operational Vertical Sounder, code communautaire dont les développements et la distribution sont financés par EUMETSAT (*European Organisation for the Exploitation of Meteorological Satellites*) et plusieurs services de prévision météorologique en Europe.

Kelly 2002) ;

- la qualité des champs de nuages est stable entre les prévisions à 3 heures et celles à 24 heures (Chevallier et Kelly 2002) ;
- les structures spatiales des champs de nuages prédits ont des tailles supérieures à 100 km alors que des observations à la même résolution que le modèle (35 km) varient de plus de 10% d'un point de grille à l'autre (Chevallier et Kelly 2002) ;
- la trop grande taille des champs de nuages induit celle des champs de pluie (Chevallier et Bauer 2003) ;
- les contenus en eau liquide des nuages et la pluie sont surestimés par le modèle, en particulier dans les Tropiques, ce qui suggère que le modèle de convection contribue fortement à cette surestimation (Chevallier et Bauer 2003).
- la qualité des champs de nuages de la réanalyse de 45 ans (ERA-40) est nettement supérieure à celle de la réanalyse de 15 ans (ERA-15), même si les périodes et les régions où peu de mesures existent pour contraindre le système de prévision (c'est-à-dire avant 1979) manquent de réalisme (Chevallier et coll. 2005c).

Ces diagnostics constituent les préliminaires à l'assimilation d'information sur les hydrométéores dans le modèle de prévision du CEPMMT. L'assimilation des luminances de l'instrument spatial SSM/I en présence de pluie est opérationnelle au CEPMMT depuis juin 2005 et utilise RTTOV-SCATT (Bauer et coll. 2006a). Celle des luminances dans l'infrarouge avec RTTOV-CLD en présence de nuages est toujours à l'étude (Szyndel et coll. 2005). L'utilisation de ces modèles s'est étendue au-delà du CEPMMT (voir par exemple Keil et coll. 2007, Burlaud et coll. 2007). Afin de faciliter leur maintenance, ils ont été progressivement fondus dans la version officielle du modèle RTTOV (Moreau et coll. 2003, Bauer et coll. 2006b, Saunders et coll. 2006).

Le chapitre IV insiste aussi sur la nécessaire précision des dérivées premières de l'opérateur d'observation dans les systèmes d'inversion. En effet les dérivées interviennent dans la recherche du minimum de la fonction coût des systèmes Bayésiens de type variationnel, comme le 4D-Var. L'erreur de ces dérivées parasite l'inversion. Le chapitre montre une validation de ces dérivées pour RTTOV et pour le modèle de rayonnement fondé sur les réseaux de neurones artificiels (NeuroFlux, Chevallier et al. 2000) que j'ai développé durant ma thèse au LMD¹¹ et au début de mon séjour au CEPMMT. Dans les deux cas, la sensibilité à la vapeur d'eau n'est pas satisfaisante. Des améliorations ont été apportées au modèle RTTOV depuis cette étude avec mon concours (Matricardi et coll. 2004). Pour NeuroFlux, une paramétrisation avec des Jacobiens climatologiques est suggérée qui permet de bénéficier de la rapidité du code sans être pénalisé par l'erreur des Jacobiens natifs. NeuroFlux est utilisé dans le 4D-Var du système de prévision opérationnel du CEPMMT depuis juin 2003 (Janiskovà et coll. 2002). Un travail analogue au NCEP¹² s'y réfère explicitement (Krasnopolksy et coll. 2005).

La mise en place de systèmes d'inversion bayésiens de type « variationnel », aptes à traiter des problèmes de grandes dimensions, est le sujet du **cinqième chapitre**. Deux articles y sont présentés (Chevallier et coll. 2005, 2007). Un système complet, que j'ai créé, est

¹¹Laboratoire de Météorologie Dynamique

¹²National Centers for Environmental Prediction

décrit pour l'application B et son fonctionnement analysé. L'algorithme d'inversion provient du CEPMMT et le modèle de transport du CO₂, dont j'ai codé l'adjoint, est développé au LMD. Différents diagnostics du système sont exposés : linéarité du modèle de transport, conditionnement de la minimisation, fonction coût au minimum, nombre de degrés de liberté du signal et réduction d'erreur. La difficile estimation des erreurs de l'inversion pour des problèmes de grandes dimensions est réalisée de deux manières différentes. D'une part, les premiers vecteurs propres de la Hessienne de la fonction coût sont obtenus comme sous-produits de l'inversion et permettent une estimation de la qualité de l'inversion. D'autre part, une approche originale par tirages aléatoires est développée pour quantifier les erreurs.

Ce système d'inversion manifeste le pont que j'ai établi entre la communauté météorologique et le LSCE pour les problèmes d'inversion. Son utilisation sur des données satellitaires réelles (les concentrations restituées à partir des radiomètres TOVS¹³) et sur des observations simulées du futur radiomètre OCO¹⁴ est montrée. Il est l'un des quelques précurseurs d'une approche qui devrait se généraliser dans les prochaines années pour le CO₂ comme pour les autres constituants atmosphériques (Hakami et coll., 2005, Rödenbeck 2005, Meirink et coll. 2006, Baker et coll. 2006, Stavrakou et coll. 2006, Dubovik et coll. 2008). Il joue maintenant un rôle fort dans plusieurs projets de la Commission européenne (GEMS¹⁵ et son successeur MACC¹⁶, COCOS) et pour les agences spatiales (la préparation de OCO, GOSAT¹⁷, A-SCOPE¹⁸ et ASCENDS¹⁹).

Une prospective personnelle et des annexes sur mon parcours complètent ce mémoire.

¹³TIROS Operational Vertical Sounder

¹⁴Orbiting Carbon Observatory

¹⁵Global Earth-system Monitoring using Satellite and in-situ dat

¹⁶Monitoring of the Atmospheric Composition and Climate

¹⁷Greenhouse gases Observing Satellite, Japon

¹⁸Advanced Space Carbon and Climate Observation of Planet Earth, Europe

¹⁹Active Sensing of CO₂ Emissions over Nights, Days and Seasons, États-Unis

Prospective personnelle

You don't need a weatherman
to know which way the wind blows.

B. Dylan, Subterranean Homesick Blues, (1965)

A. Préambule

Dresser une prospective personnelle est osé. Je travaillais il y a dix ans sur la modélisation du rayonnement atmosphérique, il y a cinq ans sur la prévision météorologique, j'étudie aujourd'hui le cycle du carbone : puis-je honnêtement pronostiquer sur mon travail à l'horizon de cinq ans ? Les résultats du dépouillement à partir de 2009 des mesures de OCO²⁰ et GOSAT²¹, instruments pionniers pour l'observation satellitaire du CO₂, ne peuvent-ils pas par exemple m'amener à orienter mes recherches dans des directions que je ne soupçonne pas maintenant ? Le bénéfice d'un poste permanent au CEA rattaché au LSCE tempère l'incertitude de mon activité, mais le paysage actuel de la recherche incite aussi à la prudence. Les organismes français se réorganisent et leur mode de financement évolue. Face à des ressources moins pérennes, nous concourrons aujourd'hui dans des appels d'offre régionaux, nationaux ou internationaux. Les projets que je gère ne s'étalent pas sur plus de quatre ans. Autour de moi, le projet CARBOEUROPE-IP²², et ses cinq années de financement fait figure d'exception, mais le consortium ne sera même pas directement reconduit par la Commission européenne. Cette évolution vers des projets à courte échéance manifeste la réalisation de la prophétie faite par Alexis de Tocqueville dès 1840 d'une recherche délaissant progressivement les concepts abstraits pour se focaliser sur l'utilitaire²³. Même si l'exemple de quelques scientifiques visionnaires d'abord incompris et isolés (tel Charles D. Keeling, pionnier de la mesure du CO₂) invite au soupçon vis-à-vis des institutions, il est peu probable que je m'investisse demain fortement sur un sujet qui n'intéresse pas les agences de recherche. Je suppose en revanche que mon implication dans les structures de recherche va encore croître à l'avenir, que j'aurai la possibilité de promouvoir mes idées et d'influencer la rédaction des prochains appels d'offres.

²⁰Orbiting Carbon Observatory

²¹Greenhouse gases Observing Satellite

²²Assessment of the European terrestrial carbon balance, projet européen du 6^e programme cadre pour la recherche et le développement (PCRD)

²³« L'inégalité permanente des conditions porte les hommes à se renfermer dans la recherche orgueilleuse et stérile des vérités abstraites ; tandis que l'état social et les institutions démocratiques les disposent à ne demander aux sciences que leurs applications immédiates et utiles » (Tocqueville, 1840).

Dans le cadre de cet exercice prospectif, quelques tendances fortes se dégagent pour les prochaines années. Les questions scientifiques y côtoient des enjeux éthiques, techniques, économiques et de communication.

B. Contexte

Médiation

La question de la médiation scientifique se pose particulièrement dans le domaine de l'environnement où la communauté scientifique s'est imposée comme veilleur et prophète de la planète, par exemple par le GIEC. La société réserve depuis peu une place particulière au chercheur des sciences de l'environnement, dans un forum bigarré où s'affrontaient déjà économistes libéraux et écologistes politiques. La difficulté de communication favorise le mélange des genres, les malentendus et l'ambiguïté. Par exemple, la vérification de l'application du protocole de Kyoto a pu servir la promotion de méthodes pourtant inadaptées à cette question stratégique (voir la section V.3.4 de ce mémoire). Face à un avenir dont les dangers sont révélés par la connaissance scientifique, la tentation est aussi grande de fonder l'éthique sur la science et de substituer le scientifique au politique. Or, la science rend le monde intellligible mais ne définit pas les valeurs d'une société : privée de conscience, elle n'est pas plus bucolique qu'elle n'est prédatrice.

Plus généralement, le rapport de la science à la vérité est en général mal cerné. Les théoriciens peuvent être parfois particulièrement dogmatiques, mais la vérité scientifique, fruit de l'expérience, de la conjecture et de la logique, apparaît mouvante et flexible à l'échelle des décennies. Son évolution est d'ailleurs formalisée par le théorème de Bayes. Au niveau même du chercheur confronté au réel, le travail quotidien est école d'humilité, chaque expérience mettant le plus souvent en défaut son intuition première et l'obligeant à affiner constamment sa vision du monde. On notera aussi que depuis les travaux influents de l'épistémologue Karl Popper, une thèse n'est qualifiée de scientifique que, paradoxalement, dans son lien aux thèses contraires. La vérité scientifique, fille du Temps, pour reprendre l'adage de Francis Bacon, est toujours en chantier. Au-delà de ses résultats, la science implique donc une attitude d'ouverture face au monde qu'il importe de vulgariser, peut-être avant même ses résultats.

Dans ce domaine, je me suis limité jusqu'ici à défendre une certaine rigueur dans nos communications, à participer à de nombreuses discussions impromptues et à répondre à quelques interviews dans les médias. Je souhaite approfondir mon engagement, en particulier en direction des écoles : dans le contexte d'une diminution dramatique du nombre d'étudiants en sciences physiques²⁴, il est important que les chercheurs s'investissent pour assurer leur relève.

Réseaux

Des réseaux de scientifiques ont toujours existé, soutenus par l'amitié et l'émulation, dont témoigne une abondante littérature épistolaire, mais la structuration, parfois même juridique,

²⁴voir le rapport qu'a présenté Jean Dercourt à ce sujet à l'Académie des sciences en 2004

de ces liens internationaux est récente. Bien plus qu'auparavant, des consortiums se forment pour mettre en commun des ressources (comme au CEPMMT), comparer des outils (comme TRANSCOM²⁵ ou AEROCOM²⁶) ou répondre à des appels d'offres. Lauréat un jour, un consortium peut perdre l'appel d'offres suivant ou le soutien de ses membres et se dissoudre. Ces réseaux forts mais mouvants impliquent des efforts patients de diplomatie (en amont), de gestion administrative et financière (en aval). Ils dynamisent nos programmes de recherche et nous offrent l'occasion de contribuer à des efforts transnationaux ambitieux, comme les projets de GEOSS²⁷ ou le GIEC. En revanche, leur instabilité fragilise la cohérence de nos travaux et ne crée de l'emploi, par les appels d'offres, que précaire.

Ingénierie

Cette science en réseaux formels est renforcée, mais non générée, par la révolution informatique. D'une part, l'informatique en réseaux facilite la communication. D'autre part, l'augmentation des moyens de calcul, en termes de puissance comme en termes de stockage, suscite le développement de programmes de simulation informatique de plus en plus complexes. Elle impose l'association d'expertises larges encadrées par une solide ingénierie informatique, comme l'illustre le modèle du système Terre de l'IPSL. Un exemple plus modeste est donné par le système inverse décrit au chapitre V, dont j'ai importé la structure du CEPMMT, alors que le modèle direct vient du LMD, l'information a priori pour la biosphère terrestre d'une collaboration entre le LMD et le LSCE, et les observations de différents instituts à travers le monde.

La maintenance des grands codes informatiques nécessite une rigueur de programmation croissante et l'intégration de développements purement techniques dans le travail des chercheurs, comme la parallélisation ou la mise à niveau des codes. La chasse aux archaïsmes du Fortran 77, vieux de 30 ans, n'est pourtant pas terminée. La dérivation des modèles, la mise au point de leurs codes tangent-linéaires et de leurs codes adjoints prennent aussi une ampleur considérable dans les travaux d'inversion pour la géophysique. Dans ce domaine, j'ai appris au CEPMMT à coder à la main les modèles adjoints. J'ai repris cette stratégie fastidieuse pour le modèle de transport LMDZ. En revanche, nous avons fait le choix au LSCE d'utiliser un outil de différenciation automatique pour le modèle de végétation ORCHIDEE et ses dizaines de milliers de lignes. En particulier ce type d'outil convient bien à un modèle partagé en constante évolution. Malgré cette aide, le travail progresse difficilement et nécessite beaucoup d'attentions.

Paradoxalement, j'ai pu constater qu'un travail de recherche est souvent perçu à travers ses réalisations techniques. Ainsi, ma publication en tant que premier auteur la plus citée (Chevallier et coll. 1998, citée 74 fois) concerne la réalisation d'un « produit » : une base de données de profils atmosphériques échantillonnes. Certaines publications plus théoriques (par exemple Chevallier et coll. 2004, reproduite en section III.2, citée 12 fois) ont été peu remarquées. Le système d'inversion CarbonTracker (<http://www.esrl.noaa.gov/gmd/ccgg/carbontracker/>) bénéficie aussi d'une publicité considérable grâce à la qualité de son site Internet, malgré la faiblesse de certaines des

²⁵Atmospheric Tracer Transport Model Intercomparison Project

²⁶Aerosol Comparisons between Observations and Models

²⁷Global Earth Observation System of Systems, effort international d'observation de la Terre

hypothèses scientifiques sous-jacentes²⁸. Le succès du site ne doit pas laisser indifférent dans le contexte d'une diminution des ressources propres des laboratoires.

L'ingénierie informatique offre surtout un cadre de travail propice à la recherche. J'ai pu mesurer au CEPMMT le bénéfice de s'appuyer sur une structure opérationnelle pour disposer facilement de données et d'outils pour les traiter. À mon arrivée au LSCE, j'ai souhaité m'investir dans la mise en place de chaînes de traitement en temps réel pour les modèles OR-CHIDEE²⁹ (<http://www-lsceorchidee.cea.fr>) et LMDZ³⁰ -INCA³¹ (<http://www-lsceinca.cea.fr>) de l'IPSL. Nos contributions, que j'ai co-écrites, aux projets GEMS³² et à son successeur MACC³³ nous entraînent aussi vers la réalisation de systèmes d'inversion des flux de carbone et d'aérosols automatisés, avec une diffusion large de produits via un site Internet. Développés continuellement au LSCE, on peut imaginer que ceux-ci soient mis en œuvre un jour en parallèle dans un centre opérationnel dédié. Même si elles peuvent être stratégiques, de telles applications doivent rester subordonnées à une quête paradigmatic pour comprendre la nature. Elles doivent être d'abord inspirées par le goût du savoir, ne serait-ce que pour préserver la fécondité de la recherche scientifique et la possibilité de découvrir d'autres applications directement utiles à la société.

C. Thèmes

Mon arrivée au LSCE en 2003 a orienté mes activités vers l'étude des cycles biogéochimiques. Une méthode, l'approche bayésienne, et un milieu, l'atmosphère, sont les deux éléments de continuité avec mes travaux précédents. Je souhaite poursuivre l'exploration de mon environnement de travail actuel en m'appuyant sur ces deux axes. Plus précisément, l'utilisation des mesures atmosphériques pour estimer les flux de gaz à effet de serre et des aérosols à la surface du globe occupe l'essentiel de ma recherche. Ce problème scientifique s'inscrit dans le contexte plus large des changements climatiques générés par l'homme et est donc d'une actualité particulièrement forte : comment est réparti le puits de carbone de la biosphère terrestre ? Comment est-il affecté par des anomalies climatiques telle la sécheresse européenne en 2003 ? Le puits de carbone dans l'océan austral ou dans l'Atlantique Nord diminue-t-il ? Quelle est la part des zones innondées dans les émissions de méthane ? Quelle est la contribution des feux de biomasse à la chimie atmosphérique ? ... Puisqu'il n'existe pas aujourd'hui d'observations directes des flux d'échange entre l'atmosphère et la surface à l'échelle du globe, traiter ces questions nécessite de combiner une grande quantité d'observations indirectes et ambiguës dans des systèmes d'inversion de données de plus en plus évolués et rationnels.

Stratégie

Le système d'inversion variationnel quadridimensionnel que j'ai développé depuis mon arrivée au LSCE, dans la continuité d'un travail réalisé à une dimension pour EUMETSAT³⁴

²⁸Les statistiques d'erreurs définies sont contredites par les résultats de la section II.2.

²⁹ORganizing Carbon and Hydrology In Dynamic Ecosystems Environment

³⁰Modèle de circulation générale du Laboratoire de Météorologie Dynamique

³¹Interaction Chimie - Aérosols

³²Global Earth- system Monitoring using Satellite and in-situ data projet européen du 6^e PCRD

³³Monitoring of the Atmospheric Composition and Climate, projet européen du 7^e PCRD.

³⁴European Organisation for the Exploitation of Meteorological Satellites

(http://www.metu.gov.uk/research/interproj/nwpsaf/ecmwf_1dvar/index.html), représente un atout important dans la communauté scientifique. La rigueur de ses bases théoriques jointes à sa flexibilité offrent un cadre pertinent pour analyser les différentes bases de données d'observation sur les cycles biogéochimiques. Conçu initialement pour l'étude des concentrations de dioxyde de carbone dans l'atmosphère, il est progressivement étendu à d'autres espèces (gaz réactifs et aérosols) et à d'autres milieux (la biosphère terrestre et les océans). Il peut aussi servir de référence pour évaluer d'autres méthodes d'inversion moins précises, comme les méthodes d'ensembles. La variété des collaborations autour de cet outil (en France, au Royaume Uni, au Japon et aux États Unis) valident a posteriori la pertinence de sa méthode et témoignent de la richesse de ses applications possibles. Il est détaillé au chapitre V. Ma stratégie de recherche pour les prochaines années s'organise naturellement autour de ce système. Elle vise à continuer son développement pour extraire une information scientifique pertinente des flots continus de données hétérogènes générées par les ambitieux programmes d'observation de la Terre. Les flux inversés sont intéressants en eux-mêmes pour quantifier les échanges entre les surfaces et l'atmosphère. Ils servent aussi de référence, dans la limite de leurs incertitudes, pour la validation et le développement des modèles numériques qui simulent ces flux.

Dioxyde de carbone

La mise en orbite prévue pour début 2009 des instruments OCO et GOSAT donne un relief particulier au travail que j'ai réalisé pour développer le système d'inversion présenté au chapitre V. L'exploitation des données novatrices sur le dioxyde de carbone atmosphérique que ces appareils fourniront me mobilisera particulièrement dans les prochaines années. Des collaborations avec les équipes pilotes de ces projets aux États-Unis et au Japon sont en cours. En particulier, mon système d'inversion a été installé récemment au NIES³⁵ pour le traitement des données de GOSAT à la source. Cette collaboration s'étend au méthane (voir la section suivante). Je participe aussi aux études préliminaires de projets d'observation satellitaire par lidar en Europe et aux États-Unis qui pourraient succéder à la technologie de sondage passif de OCO et GOSAT.

La disponibilité prochaine de mesures par télédétection spatiale n'efface pas l'intérêt des mesures de surface. Des dizaines de sites ont été mis en place dans les dernières décennies et forment une archive unique sur les flux de carbone pour une période cruciale où les taux des émissions anthropiques s'emballent (Raupach et coll. 2007) et commencent à perturber le climat (Hegerl et coll. 2007). Le système d'inversion contribuera aussi aux activités de l'observatoire ICOS³⁶, l'un des 35 projets de Très Grand Instrument qui viennent d'être classés prioritaires par le forum Européen sur les infrastructures de recherche (ESFRI).

La quantification rigoureuse des incertitudes sur les produits inversés est un enjeu essentiel pour la communauté scientifique. Il n'est pas évident que les inversions publiées jusqu'ici avec les mesures de surface soient plus précises que leur information a priori : l'empirisme dominant pour la spécification des erreurs en entrée des systèmes d'inversion, jointe à la faible densité du réseau d'observations, imposent le doute, comme en témoigne par exemple la polémique récente sur la réalité de la saturation du puits de carbone de l'océan austral

³⁵National Institute for Environmental Studies, Tsukuba, Japon

³⁶Integrated Carbon Observation System

(Law et coll. 2008, Zickfeld et coll. 2008, Le Quéré et coll. 2008). Une fois ce préliminaire établi, l'amélioration par rapport à l'a priori doit être quantifiée et les produits documentés. L'actuelle augmentation de la diffusion des produits des inversions renforce encore cette nécessité. Un tel travail peut s'appuyer sur des outils théoriques (comme l'illustre la section V.3) mais doit aller plus loin. En effet, les chiffres publiés avec cette approche sont souvent très optimistes car les inventaires des sources d'erreur restent lacunaires. L'ensemble des mesures de concentrations (en particulier celles qui n'ont pas servi pour les inversions, comme les mesures aéroportées) et de flux (dans la lignée de la section II.2) doit aussi être exploitée à cet effet. Un tel enjeu englobe la difficile prise en compte des biais des mesures et des modèles de transport dans les systèmes d'inversion. À cet égard, l'instrument MOPITT³⁷ dédié au monoxyde de carbone, mais dont les algorithmes de traitement s'apparentent à ceux de OCO et GOSAT, fournit un exemple intéressant : les biais des produits sont mal connus mais varient manifestement en fonction de l'altitude, du type de surface et de l'heure locale (Emmons et coll. 2004). Des biais affectent aussi l'information a priori. Pour le CO₂, l'estimation de ces biais représente même l'enjeu scientifique principal car ils expriment justement les puits de carbone que l'on cherche à quantifier. Enfin, si l'objectif premier est la détection de biais plutôt que la réduction des erreurs aléatoires de l'a priori, les méthodes habituelles d'évaluation de la performance des systèmes d'inversion ne sont peut-être pas les plus appropriées et devraient alors être revisitées.

Même avec les instruments spatiaux, le problème inverse restera sous-constraint et il semble pertinent de combiner les observations des concentrations de CO₂ avec d'autres mesures. Celles des concentrations des isotopes du CO₂ (¹³CO₂ et ¹⁴CO₂) informeront par exemple sur la répartition des émissions entre océans et surfaces continentales et entre biosphère et énergies fossiles. Le cycle du carbone dans l'atmosphère est lié à celui de l'oxygène dont les concentrations sont aussi mesurées. Des mesures satellitaires renseignent sur l'état de la végétation et sur celui du sol (température et teneur en eau). Des mesures locales des flux de CO₂, des flux de chaleur latente et des flux de chaleur sensible peuvent aussi servir à l'inversion en améliorant l'information a priori. C'est l'une des motivations du volet « carbone » du projet GEOLAND³⁸. Dans le projet CAMELIA³⁹, nous considérerons l'intégration en synergie des différentes observations dans l'inversion, en couplant le modèle de transport atmosphérique avec le modèle de végétation ORCHIDEE. Dans ce cas, les paramètres d'ORCHIDEE sont directement inversés. Les flux sont aussi optimisés, mais de manière indirecte, fournis comme produit intermédiaire de l'inversion. Outre la possibilité d'intégrer dans l'inversion d'autres observations que celles des concentrations, cette stratégie facilite l'interprétation des résultats de l'inversion des flux (pour comprendre les processus impliqués dans leurs variations ou pour diagnostiquer les faiblesses des équations du modèle) et offre la possibilité d'extrapoler dans le temps (pour le passé et pour l'avenir) l'information des mesures (sous l'hypothèse forte de la robustesse des équations inscrites dans le modèle de surface). L'extrapolation dans le temps ne concerne pas que les valeurs optimisées mais englobe toute la densité de probabilité des paramètres, ce qui permet de décrire l'incertitude

³⁷Measurement Of Pollution In The Troposphere

³⁸GMES products & services, integrating EO monitoring capacities, to support the implementation of European directives and policies related to "land cover and vegetation", projet européen du 6^e et du 7^e programme cadre pour la recherche et le développement (PCRD)

³⁹Carbon flux Modelling using Earth observation Land products for Initiation and by Assimilation, projet de l'Agence Spatiale Européenne

des prédictions des concentrations (comme dans la prévision d'ensemble des centres de météorologie). La description des incertitudes sur les paramètres peut être complétée par l'incertitude sur les forçages atmosphériques des modèles de biosphères (cet aspect sera évoqué dans le cadre du projet AUTREMENT⁴⁰). Une stratégie similaire d'optimisation de paramètres de modèles doit être mise en place pour l'océan.

Le modèle de l'atmosphère LMDZ est un élément essentiel de ce projet. Je l'utilise avec une résolution relativement basse ($3,75^\circ$ en longitude et $2,75^\circ$ en latitude) pour limiter les temps de calcul du système d'inversion variationnelle. Il importe de préparer la transition vers des simulations à plus haute résolution (le degré), voire à méso-échelle (la dizaine de kilomètres) pour accroître la précision des simulations. Ce travail est en cours au LSCE à partir de la version zoomée de LMDZ et des modèles atmosphériques Chimère et Méso-NH. Je souhaite continuer à m'y impliquer. De plus, le couplage entre le modèle de climat LMDZ et les données des centres météorologiques est réalisé par un simple guidage des vents simulés. Le système de guidage occupe ainsi la place d'un 4D-Var et pourrait être repensé pour les applications inverses, où la qualité de la représentation des phénomènes synoptiques devient essentielle.

Gaz à effet de serre réactifs et aérosols

Au-delà de ce travail sur les puits et sources du CO₂, l'estimation en synergie des émissions de gaz et des aérosols à la surface du globe constitue un projet sur lequel je souhaite particulièrement m'investir. La stratégie que j'ai choisie consiste à étendre le système d'inversion variationnel décrit au chapitre V aux espèces réactives, comme CO, par l'adjonction d'un modèle numérique simplifié de la chimie atmosphérique. Le choix d'un modèle simplifié est motivé par le peu de composés directement observés actuellement. Deux branches de ce modèle ont été développées spécialement pour préparer ce projet.

La première branche représente la chaîne d'oxydation des hydrocarbures, qui fait intervenir les molécules de méthane, de formaldéhyde (CH₂O) et de monoxyde de carbone, toutes trois observées par satellite (en particulier par les instruments SCIAMACHY⁴¹, GOME⁴², MOPITT, IASI⁴³ et bientôt GOSAT). Elle inclut aussi des molécules mesurées uniquement par des moyens conventionnels : le méthylchloroforme (C₂H₃Cl₃), qui informe sur les concentrations de OH, et l'hydrogène. Les réactions intermédiaires, comme celles de production-destruction de CH₃O₂ et CH₃O, sont considérées comme très rapides par rapport aux réactions entre les cinq espèces résolues. De plus, les variations spatiales du radical hydroxyle (OH) sont prescrites par grandes bandes de latitude (à la différence des variations temporelles qui sont optimisées). Ce premier système simplifié non-linéaire a été progressivement mis en place au LSCE avec ma coordination. Il devra être raffiné et pourra être éventuellement complexifié, par exemple pour inclure la chimie de l'ozone.

La deuxième branche du modèle de chimie simplifié concerne les aérosols. Elle a été conçue et mise en place par Olivier Boucher (Hadley Centre, GB) et Nicolas Huneeus

⁴⁰Aménager l'Utilisation des Terres et des Ressources de l'Environnement en Modélisant les Écosystèmes aNTropiques, projet de l'Agence Nationale pour la Recherche

⁴¹SCanning Imaging Absorption spectrometry for Atmospheric CHartographY

⁴²Global Ozone Monitoring Experiment

⁴³Infrared Atmospheric Sounding Interferometer

(Laboratoire d'Optique Atmosphérique, LOA, Lille). Ce schéma regroupe les différents types d'aérosols sous la forme de quatre traceurs : Les précurseurs gaseux, les particules fines, les poussières et les sels marins. Le système d'inversion avec ce modèle d'aérosols permettra d'interpréter les observations d'épaisseurs optiques des instruments satellitaires MODIS⁴⁴, POLDER⁴⁵ et PARASOL⁴⁶. Il est déjà intégré au projet Européen MACC.

Les feux de biomasse (c'est-à-dire les brûlis associés à certaines pratiques agricoles, les feux de forêt et de savane, et l'utilisation du bois pour le chauffage) sont le point commun entre les deux branches du modèle de chimie car ils émettent de grandes quantités de matières gazeuses et solides. Un couplage des inversions pourrait être établi par les corrélations d'erreur sur la localisation et l'intensité des émissions a priori. La quantification des émissions pyrogéniques est un enjeu scientifique important pour comprendre la chimie atmosphérique et l'action de l'homme sur le climat, mais compliquent singulièrement le problème inverse car les événements extrêmes comme les feux font dériver les statistiques d'erreurs de l'information a priori hors des densités Gaussiennes. Là encore des avancées méthodologiques sont particulièrement attendues pour renforcer la crédibilité des émissions inversées.

Les inversions pour la chaîne d'oxydation des hydrocarbures peuvent aussi être utilement combinées avec celles pour le CO₂ et son isotope ¹⁴CO₂ pour l'étude des émissions des combustibles fossiles. Les inversions des émissions de CO et CO₂ des feux de biomasse peuvent aussi être étudiées en lien avec les mesures spatiales de l'activité de la végétation ou des surfaces brûlées. De même, les émissions de CH₄ peuvent être reliées aux mesures des surfaces des zones inondées. Le radon, informatif sur les caractéristiques du transport atmosphérique et observé par plusieurs réseaux conventionnels, peut être aussi incorporé au système d'inversion. Enfin, les mesures de température et de précipitation peuvent aider à l'interprétation des flux inversés. Le croisement des informations issues des mesures de surface et des différents sondeurs, comme MOPITT, OCO, GOSAT et MODIS ouvre un terrain presque vierge et manifestement fécond.

Méthodes d'inversion

La caractérisation des erreurs des différentes composantes des systèmes d'inversion retient mon attention depuis plusieurs années, comme l'illustrent les chapitres II et III. En effet, il est important de réduire l'arbitraire qui prévaut habituellement par manque de mesures indépendantes des systèmes d'inversion. Ce type d'étude s'inscrit maintenant formellement dans le projet COCOS⁴⁷ pour le CO₂ et doit être étendu aux autres versions du système d'inversion. Participant à l'engouement actuel pour les méthodes stochastiques, j'ai aussi introduit une approximation de ce type pour calculer l'erreur de l'a posteriori (voir la section V.3).

D'autres développements connexes pourraient être fructueux. C'est le cas de l'optimisation de quelques paramètres du modèle ORCHIDEE par une méthode d'ensembles, par exemple

⁴⁴MODerate-resolution Imaging Spectroradiometer

⁴⁵Polarization and Directionality of Earth Reflectances

⁴⁶Polarization and Anisotropy of Reflectances for Atmospheric Science coupled with Observations from a Lidar

⁴⁷Coordination Action Carbon Observation System, projet européen du 7^e PCRD.

un filtre à particules. Il est légitime de s'interroger sur l'intérêt d'étendre ce type d'approche à des problèmes de plus grandes dimensions, comme l'inversion des flux à l'échelle du globe. En effet, la propagation des statistiques d'erreurs dans un système d'inversion nécessite un nombre d'éléments dans les ensembles plus grand que le nombre effectif de variables à inverser : les méthodes d'ensembles appliquées à des problèmes de grandes dimensions ne peuvent donc être mises en œuvre que si les statistiques d'erreur sont fortement corrélées, ce qui est rarement le cas dans les domaines auxquels je m'intéresse. En revanche, l'inversion par ensembles stochastiques s'adapte idéalement aux moyens de calcul parallèles actuels. De plus, elle est relativement facile à mettre en œuvre, en comparaison des méthodes adjointes. Plusieurs équipes de premier plan ont donc beaucoup investi dans cette direction (p. ex. Zupanski et coll. 2007, Peters et coll. 2007). La comparaison de ces méthodes avec des méthodes plus précises, comme celle que j'utilise⁴⁸, pourrait quantifier utilement leur précision.

En amont de ces travaux appliqués, je souhaite étudier les méthodes d'inversion elles-mêmes. Nous avons souligné tout au long de ce mémoire que les systèmes d'inversion bayésiens, comme celui que j'ai développé, reposent en général sur les hypothèses d'un opérateur d'observation linéaire et d'erreurs gaussiennes. Les filtres à particules n'ont pas cette limitation mais souffrent de temps de calcul souvent prohibitifs. Le projet AssimilEx⁴⁹, auquel je participe, a pour ambition de développer une méthode d'assimilation de données optimale adaptée au densités de probabilité à queue lourde. Elle se place dans le cadre de la théorie des valeurs extrêmes. Ce travail prospectif me permettra de continuer à m'interroger sur la théorie des probabilités.

⁴⁸La méthode variationnelle est aussi simplifiée puisque peu d'itérations sont en fait réalisées, mais elle est plus efficace car elle est adaptative : les directions de minimisation sont déterminées pour chaque problème particulier, alors que les membres d'un ensemble sont nécessairement déterminés a priori.

⁴⁹*Theoretical developments of data ASSIMILation models for climate EXtremes*, projet de l'Agence Nationale pour la Recherche

Chapitre I

Introduction

Vérité de la science ?

Toute science de la nature repose sur la perception.

S. Weil, Cahier Ki1, ms 51 (1940)

I.1 Petite histoire de la théorie des probabilités

Les théories scientifiques naissent au confluent de l'expérience, des mathématiques et de la métaphysique. Jusqu'au XIX^e siècle, la négation du hasard et des phénomènes surnaturels a constitué une motivation fondamentale pour la recherche scientifique. Pourtant, une théorie des probabilités s'est formée au XVII^e siècle, afin de traiter rationnellement des phénomènes *apparemment* aléatoires. Après quelques prémisses isolées sous la plume de Gerolamo Cardano en 1565 ou de Galilée en 1620, elle éclot en 1654 de l'échange épistolaire entre deux amis mathématiciens, Blaise Pascal et Pierre Fermat, au sujet d'un problème de répartition de gains de jeu. Le Sort quitte alors la sphère du sacré pour devenir objet d'étude scientifique. Les jeux dits « de hasard », à partir de dés, de boules ou de pièces de monnaie, fournissent une multitude de problèmes mathématiques pour lesquels il est facile d'accumuler les observations. En quelques décennies, une dizaine de mathématiciens répartis entre la Hollande, la France, l'Angleterre, l'Allemagne et l'Écosse (principalement Christiaan Huygens, Jakob Bernoulli, Pierre Rémond de Montmort, Nicolaus Bernoulli, Abraham de Moivre et Thomas Bayes) bâtissent une « doctrine de la chance ». En parallèle, la notoriété de cette science naissante s'établit en démographie (pour l'étude des naissances, des décès et des épidémies), en économie (pour la quantification du risque et la détermination des primes d'assurance) et en métrologie (pour l'étude des erreurs d'observation). Même en théologie, Blaise Pascal développe, dans un célèbre pari, un étonnant argumentaire probabiliste sur la foi en Dieu.

L'essai de Pierre Simon Laplace sur la *Théorie analytique des probabilités*, dont la première version est publiée en 1812, marque la maturité de ce domaine. L'auteur y approfondit les résultats de ses prédécesseurs, ajoute les siens et en dégage une théorie générale du calcul des probabilités, puissant outil qu'il prétend applicable pour l'étude de n'importe quel phénomène physique. Le lecteur moderne y retrouve par exemple l'algèbre des probabilités composées et des probabilités conditionnelles, l'analyse combinatoire, la loi des grands nombres, la loi normale et le théorème de la limite centrale, la méthode des moindres carrés et, point focal du présent mémoire, le théorème de Bayes. Des applications variées illustrent la théorie. L'intro-

**THÉORIE
ANALYTIQUE
DES PROBABILITÉS;**

PAR M. LE MARQUIS DE LAPLACE,

Pair de France; Grand Officier de la Légion d'honneur; l'un des quarante de l'Académie française; de l'Académie des Sciences; membre du Bureau des Longitudes de France; des Sociétés royales de Londres et de Göttingue; des Académies des Sciences de Russie, de Danemark, de Suède, de Prusse, des Pays-Bas, d'Italie, etc.

TROISIÈME ÉDITION,

REVUE ET AUGMENTÉE PAR L'AUTEUR.

PARIS,

M^{me} V^e COURCIER, Imprimeur-Libraire pour les Mathématiques,
rue du Jardinet, n^o 12.

1820.

FIG. I.1 – Couverture de la troisième édition de l'ouvrage de Laplace (téléchargeable sur <http://math-doc.ujf-grenoble.fr/OEUVRES/>).

duction de cette somme ardue de plusieurs centaines de pages est aussi éditée séparément sous le titre *Essai philosophique sur les probabilités* et assure la promotion du sujet au-delà du cercle des spécialistes. Elle se présente d'abord comme une profession de foi affirmant le déterminisme du monde : le futur est contenu dans le passé et le scientifique peut potentiellement tout expliquer et tout prédire. Elle est ensuite un plaidoyer sur l'utilisation du calcul des probabilités pour palier la limitation, peut-être provisoire, de notre entendement.

L'ouvrage de Laplace domine la discipline pendant plus d'un demi-siècle. Ensuite, son influence s'efface devant des ouvrages de forme plus moderne, alors même que l'usage du calcul des probabilités s'étend et permet des avancées théoriques considérables, comme le montrent la création de la mécanique statistique vers 1870 et celle de la physique quantique dans les premières décennies du XX^e siècle. Plus encore, dans ces nouvelles théories scientifiques la notion de probabilité devient irréductible et participe aux lois de la nature, alors qu'elle n'était jusqu'ici utilisée que pour les approximer. Ainsi, le second principe de la thermodynamique affirme le comportement particulier d'un système statistique physique fermé. Un autre exemple est fourni par la physique quantique qui rejette la notion de localisation précise pour une particule subatomique au motif qu'elle est aussi un paquet d'ondes¹. La science s'éloigne alors, peut-être momentanément², de son fondement déterministe, renonce

¹Cette négation est exprimée par le principe d'indétermination d'Heisenberg

²« While we have thus shown that the wave function does not provide a complete description of the physical reality, we left open the question of whether or not such a description exists. We believe, however, that such a theory is possible » (Einstein et coll., 1935).

à l'ambition qu'elle avait de prédire tous les phénomènes physiques et se recentre sur sa capacité à transformer le monde.

En parallèle, des débats méthodologiques virulents animent aussi la communauté des statisticiens du XX^e siècle. La théorie des probabilités s'étoffe encore, avec une abstraction croissante, pour affirmer son socle théorique, mieux décrire les distributions, qu'elles soient univariées ou multivariées, et tester des hypothèses par la statistique. La révolution informatique des dernières décennies multiplie les applications possibles. Avec le calcul de masse, la science des probabilités parachève son emprise sur la vie moderne³.

I.2 Définition de la probabilité

La probabilité mathématique est une mesure de l'incertitude, nombre réel compris entre 0,0 (désignant, selon les auteurs, l'invraisemblance ou la quasi-invraisemblance) et 1,0 (certitude ou quasi-certitude). Au-delà de cette affirmation, la définition précise de la probabilité est... incertaine et a occasionné de vastes controverses scientifiques et philosophiques depuis le début du XX^e siècle. À minimâ, les fréquentistes définissent la probabilité p d'un événement comme la limite du rapport entre le nombre de ses réalisations n et le nombres d'expériences N , lorsque N croît vers l'infini : $p = \lim_{N \rightarrow \infty} \frac{n}{N}$. Ce concept ontologique restreint la probabilité aux événements reproductibles et réguliers. Il n'est apparu qu'au XX^e siècle, bien qu'il s'appuie sur la loi des grands nombres introduite par Jakob Bernoulli en 1713. Cette définition se distingue de la notion classique fondée sur l'épistémologie : la probabilité y est liée à l'état des connaissances de l'observateur. Prenons un exemple pour illustrer la différence entre les deux conceptions. L'auteur classique, comme Bernoulli ou Laplace, n'a aucun scrupule à définir la probabilité qu'il pleuvra demain. En revanche, le fréquentiste n'acceptera cette définition que parce qu'il existe une expérience de *demain* tous les jours. La probabilité appliquée à un jour précis du calendrier n'a pour lui aucun sens. Laplace s'appuie sur les mesures quand il le peut et sur son bon sens dans le cas contraire (comme dans le principe de la raison insuffisante, que nous abordons plus loin en II.1), alors que le fréquentiste ne s'appuie que sur les observations. Notons que le traitement de l'incertitude dans le quatrième rapport du GIEC⁴ rejoint la notion classique (IPCC, 2005). À côté de ces deux célèbres définitions de la probabilité, d'autres existent, par exemple celle d'Augustin Cournot fondée sur la géométrie (1843).

On appelle aujourd'hui *bayésienne* l'approche classique, du nom de Thomas Bayes, prêtre presbytérien anglais du XVIII^e siècle et auteur de la solution d'un problème inverse particulier publiée en 1763, quelques années après sa mort⁵. Ce vocabulaire est maladroit puisque la conception bayésienne des probabilités est antérieure à Bayes (elle apparaît au moins chez Bernoulli), et puisqu'un fréquentiste ne conteste pas le théorème éponyme énoncé dans la section suivante. Malgré cette réserve, nous suivons l'usage dans ce mémoire.

Même définie de manière fréquentiste, la probabilité d'un phénomène accède rarement au statut d'attribut objectif. La représentation d'un phénomène physique sous forme de

³Le lecteur intéressé par la courte, mais dense, histoire des probabilités pourra utilement se référer aux ouvrages d'histoire que nous avons consultés : Coumet (1970), Daston (1988), Fienberg (2006), Hacking (1975), Hahn (2004), Hald (1990), Krüger et coll. (1987, 2 vol.), Shafer et Vovk (2006) et Stigler (1986). D'autre part, la plupart des textes fondateurs de la théorie des probabilités sont disponibles sur la toile.

⁴Groupe d'Experts Intergouvernemental sur l'Évolution du Climat

⁵Il est en fait difficile de faire la distinction dans le texte de 1763 entre la contribution de Bayes et celle de son éditeur posthume, Richard Price (Bellhouse, 2002).

variables aléatoires repose en général sur une interprétation subjective de la réalité. Par exemple, la génération de nombres « aléatoires » par un ordinateur suit en fait un algorithme déterministe. La probabilité n'est donc pas une propriété physique comme peuvent l'être la masse ou la vitesse, sauf lorsqu'elle est calculée à partir de la fonction d'onde de la mécanique quantique⁶. Ainsi, la différence entre une probabilité estimée de 0,40 et une autre de 0,45 est-elle souvent trop faible pour être globalement significative. Pour sélectionner objectivement l'une plutôt que l'autre, il faudrait un nombre infini de la même expérience. Dans la réalité, on ne dispose que d'un nombre fini d'expériences, réalisées le plus souvent dans un contexte inconstant. Paradoxalement, seules les probabilités certaines (1,0 et 0,0) sont toujours vérifiables (c'est-à-dire réfutables au sens poppérien) par l'expérience et ont donc toujours un sens physique.

I.3 Compendium du théorème de Bayes

La méthode inverse introduite par Laplace en 1774 et passée à la postérité sous le nom d'un autre pionnier des statistiques⁷ est une méthode générique simple pour estimer la distribution de la probabilité⁸ de n'importe quelle variable en combinant des informations connexes de différentes natures. Elle fournit une méthode d'estimation quantitative aux sciences expérimentales, même dans le cas de problèmes mathématiquement mal posés ou dans le cas de mesures indirectes. Face aux anathèmes des fréquentistes, sa flexibilité, quelle que soit la taille du problème, et l'utilité de ses résultats ont été ses meilleurs promoteurs. Elle est une méthode de référence pour le traitement d'observations de l'atmosphère dans les sciences de l'environnement en général et en météorologie en particulier.

Dans l'inférence bayésienne, chaque information, ainsi que les variables estimées, sont décrites par des distributions de probabilité discrètes ou continues. Pour des distributions discrètes, on peut écrire le théorème de Bayes sous la forme suivante :

$$p(\mathbf{x} = \mathbf{x}_0 \mid \mathbf{y} = \mathbf{y}_0, \mathcal{C}) = p(\mathbf{x} = \mathbf{x}_0 \mid \mathcal{C}) \frac{p(\mathbf{y} = \mathbf{y}_0 \mid \mathbf{x} = \mathbf{x}_0, \mathcal{C})}{p(\mathbf{y} = \mathbf{y}_0 \mid \mathcal{C})} \quad (\text{I.1})$$

\mathbf{x} et \mathbf{y} sont respectivement les variables dont on estime la distribution de probabilité et les observations à intégrer. \mathbf{x}_0 et \mathbf{y}_0 sont des valeurs que celles-ci peuvent prendre. \mathcal{C} est l'ensemble des connaissances disponibles avant de traiter les observations, par exemple la description des erreurs ou des observations analysées précédemment. Les probabilités p mesurent le degré de vraisemblance des propositions qu'elles ont en argument. Une barre verticale est le signe d'une probabilité conditionnelle. Elle indique que la probabilité se réfère à l'événement situé à gauche du symbole sous la condition de l'événement situé à droite.

$p(\mathbf{x} = \mathbf{x}_0 \mid \mathbf{y} = \mathbf{y}_0, \mathcal{C})$ est la probabilité *a posteriori*⁹ c'est-à-dire l'état de notre connaissance

⁶La réductibilité du hasard à l'échelle macroscopique reste le sujet d'un débat passionné. Le lecteur notera par exemple les conclusions contradictoires sur la prédictibilité du simple tirage d'une pièce de monnaie entre I. Prigogine (1996) d'une part, et B. Diu et B. Leclerc (2005) d'autre part. Pour le premier, l'incertitude sur le tirage est irréductible, alors que les seconds pensent la réduire par une meilleure connaissance des conditions du lancer de la pièce.

⁷Augustin Cournot mentionne « la règle attribuée à Bayes » dans son essai de 1843 (p. 158).

⁸Une distribution de probabilité est une fonction qui associe une probabilité à tout intervalle de l'espace des nombres réels.

⁹La locution « *a posteriori* » est empruntée du latin scolaire. Sa graphie et sa typographie varient encore. On la trouve dans les textes français en un ou deux mots, avec ou sans trait d'union, en romain, en gras ou en italique, avec ou sans accent. Le dictionnaire de l'Académie française l'écrit « *à postérieur* » dans sa 6^e édition (1835), « *à posteriori* » dans ses 7^e (1878) et 8^e (1935) éditions. Tout accent disparaît dans la 9^e édition en cours que nous suivons ici, malgré l'ambiguité de lecture du *a* non accentué en français.

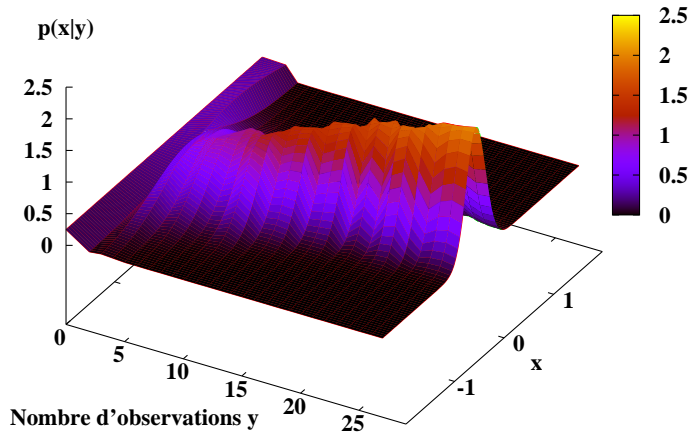


FIG. I.2 – Évolution de la densité de probabilité d'une variable x . Partant d'une densité $p(x)$ uniforme sur l'intervalle $[-2, 2]$, un nombre croissant d'observations y affine progressivement la fonction $p(x | y)$.

sur x après l'analyse des observations. La fonction $p(x | y = y_0, \mathcal{C})$, pour tous les x possibles, est la solution complète de l'inversion.

$p(x = x_0 | \mathcal{C})$ est la probabilité a priori, c'est-à-dire notre préjugé, l'état de notre connaissance sur x avant l'analyse des observations.

$p(y = y_0 | x = x_0, \mathcal{C})$ est la probabilité des observations lorsque les variables x égalent x_0 . On l'appelle *fonction de vraisemblance*. Les observations ne renseignent pas nécessairement directement sur les variables à estimer : son calcul fait alors intervenir un opérateur d'observation, qui modélise le lien entre les variables et les observations. Dans la notation utilisée ici, cet opérateur fait partie de la connaissance \mathcal{C} .

$p(y = y_0 | \mathcal{C})$ est la probabilité des observations. Comme elle ne dépend pas de x , elle se comporte comme une constante de normalisation pour le problème d'inférence.

L'équation I.1 est une conséquence directe de la formule des probabilités composées de De Moivre (1718)¹⁰. Elle exprime une mise à jour de la connaissance. Typiquement, partant de l'ignorance complète de la valeur d'une variable, l'application successive de I.1 à chaque fois qu'une nouvelle série d'observations est disponible affine la distribution de probabilité et rapproche progressivement de la certitude. Ce modèle de l'apprentissage est illustré par la figure I.2. Notons son aspect totalitaire : il absorbe potentiellement toute information disponible et n'en laisse alors aucune indépendante, pour valider ou réfuter (au sens poppérien) son résultat. Remarquons aussi que les variables observées y ne sont pas nécessairement les

¹⁰ « The Probability of the happening of two Events dependent, is the product of the Probability of the happening of one of them, by the Probability which the other will have of happening, when the first is considered as having happened » (de Moivre, 1718). Sous forme mathématique, la probabilité que deux événements A et B se produisent conjointement est $p(A \cap B) = p(A)p(B|A)$. Par symétrie on a aussi $p(A \cap B) = p(B)p(A|B)$ et donc $p(A)p(B|A) = p(B)p(A|B)$, d'où $p(B|A) = p(B)p(A|B)/p(A)$, le théorème de Bayes.

variables étudiées x . En ce sens, le théorème de Bayes formalise l'adage antique selon lequel ce qui apparaît manifeste ce qui est caché¹¹.

On parle en général d'inversion pour une application unique de la règle de Bayes et d'assimilation de données dans le cas d'applications successives. Cette distinction est en fait floue car une séquence d'applications (comme dans le filtre de Kalman) peut être reformulée sous la forme d'une inversion strictement équivalente.

La règle de Bayes s'applique à n'importe quelle distribution de probabilité discrète et est généralisable aux distributions continues. Parmi les distributions continues, les lois gaussiennes (ou normales) sont souvent préférées. En effet, le théorème de la limite centrale établit que si une somme de variables aléatoires possède une variance finie, elle converge vers une distribution gaussienne. Ainsi, l'accumulation de petites causes d'erreur conduit à une distribution d'erreur proche d'une gaussienne. De plus, le théorème de Bayes conserve la loi gaussienne (l'équation I.1 fournit des lois de probabilité a posteriori gaussiennes si les lois de probabilité a priori et celles des observations sont gaussiennes). Enfin, comme indiqué dès 1809 par Carl Friedrich Gauss, dans le cas de lois gaussiennes, le maximum de la densité de probabilité a posteriori correspond à la solution donnée par la méthode des moindres carrés¹², ce qui a ouvert des perspectives considérables pour l'application de cette équation dans le cas de problèmes de grandes dimensions, comme nous le verrons au chapitre V.

Il existe plusieurs approches pour appliquer le théorème de Bayes. Premièrement, il peut exister une expression analytique exacte de la distribution a posteriori. C'est le cas si les erreurs de l'information a priori et celles des observations suivent des lois gaussiennes. On peut aussi ne reconstituer la distribution a posteriori que pour un ensemble de points judicieusement choisis dans l'espace de x , par exemple par une approche de Monte Carlo. Enfin, on peut se contenter d'estimer la valeur de x la plus probable, qui correspond au maximum de la distribution a posteriori. On notera que ce dernier cas ne permet pas d'intégrer de nouvelles observations par une application supplémentaire de I.1.

I.4 Théorème de Bayes et étude de l'atmosphère

Les problèmes inverses en sciences atmosphériques recouvrent traditionnellement deux types d'applications. La première est la télédétection, c'est-à-dire l'estimation locale de variables atmosphériques à partir d'observations indirectes, souvent depuis l'espace. La seconde est l'estimation de l'état complet tridimensionnel de l'atmosphère qui permet d'initialiser les modèles de prévision météorologique. Dans les deux cas, les méthodes inverses se sont d'abord développées de manière empirique (p. ex. Kaplan, 1959, pour la télédétection et Bjerknes, 1904, pour la prévision météorologique). Elles se sont ensuite affinées essentiellement avec l'apport de la méthode d'estimation par moindres carrés. En particulier, les travaux sur le filtrage de Rudolph E. Kalman (1960) à partir des idées de Andrei N. Kolmogorov (1941) et Norbert Wiener (1949) ont eu une influence considérable. Ce n'est qu'a posteriori que le théorème de Bayes est devenu pour beaucoup le paradigme du domaine, l'étalon d'évaluation des techniques d'inversion (p. ex. Lee et Ho, 1964, et Lorenc, 1986). À

¹¹sur cet adage, voir par exemple l'ouvrage de Pierre Hadot (2004)

¹²Plus précisément, Gauss remarque cette propriété dans le cas de densités de probabilité gaussiennes pour les observations, et uniformes pour l'information a priori. Alors, seuls les termes d'écart aux observations est présent dans la fonction quadratique. L'extension au cas de densités de probabilité a priori gaussiennes est triviale car alors l'information a priori et les observations jouent le même rôle dans l'équation I.1.

côté de ces applications majeures, l'inférence Bayésienne intervient aussi dans certains traitements d'observations atmosphériques : pour la détection de nuages (English et coll., 1999), de biais (Haimberger, 2005), ou de changements climatiques (*The International Ad Hoc Detection and Attribution Group*, 2005).

L'application du théorème de Bayes est particulièrement délicate pour des problèmes de grandes dimensions, comme dans le cas de l'initialisation de modèles de prévision. Les centres météorologiques convergent actuellement vers le développement de systèmes variationnels à trois ou quatre dimensions (Lewis et Derber, 1985 ; Le Dimet et Talagrand, 1986). La formule de Bayes y est appliquée sous les hypothèses de densités de probabilité gaussiennes et d'un opérateur d'observation linéaire. Chaque application combine l'ensemble des observations récoltées sur une fenêtre de six ou douze heures avec la prévision a priori, issue de l'analyse faite dans la fenêtre temporelle précédente. À minimâ, l'opérateur d'observation \mathcal{H} est un opérateur d'interpolation spatial entre les variables d'analyse et les observations. Suivant la sophistication du système, \mathcal{H} peut aussi inclure un modèle numérique de la circulation générale de l'atmosphère et un modèle de rayonnement adapté aux mesures satellitaires. L'hypothèse de linéarité pour cet opérateur est satisfaite par un développement de Taylor au premier ordre, éventuellement simplifié, autour d'un état de base \mathbf{x}_o . Dans les systèmes quadri-dimensionnels (4D-Var), $\mathcal{H}(\mathbf{x}_o + \delta\mathbf{x}, t)$ est approximé par $\mathcal{H}(\mathbf{x}_o, t) + \frac{\partial\mathcal{H}(\mathbf{x}_o, t)}{\partial\mathbf{x}}\delta\mathbf{x}$, t désignant le temps et \mathbf{x} le vecteur des variables atmosphériques à estimer (température, humidité, pression, etc.). Un système tri-dimensionnel (3D-Var) utilise l'expression plus simple $\mathcal{H}(\mathbf{x}_o, t_o) + \frac{\partial\mathcal{H}(\mathbf{x}_o, t_o)}{\partial\mathbf{x}}\delta\mathbf{x}$, avec t_o l'heure de l'analyse. L'état de l'atmosphère qui correspond au maximum de la densité de probabilité a posteriori est estimé par la minimisation d'une fonction, dite *fonction coût* ou *fonction écart*. Actuellement, la principale limitation de ces systèmes est le manque de communication entre des fenêtres d'analyse successives : alors que les erreurs de l'a priori dans une fenêtre donnée devraient tenir compte des erreurs de l'analyse de la fenêtre précédente, elles restent partiellement ou totalement statiques.

L'extension à la chimie atmosphérique est une innovation récente. Elle concerne l'estimation des concentrations (Fisher et Larry, 1995), éventuellement jointe à celle des flux aux interfaces entre l'atmosphère et la surface (Enting et coll., 1995). Les techniques sont en général similaires à celles utilisées pour l'initialisation des modèles de prévision, mais dans certains cas, la faible dimension du problème permet l'application du théorème de Bayes sous forme analytique, par une suite d'opérations algébriques (Enting et coll., 1995). Importée du monde de la recherche, l'estimation de la composition chimique de l'atmosphère semble rejoindre progressivement le monde de la météorologie opérationnelle (Peuch et coll., 2000).

I.5 Présentation du mémoire

Ce mémoire s'appuie sur les travaux scientifiques que l'auteur a menés successivement au Laboratoire de Météorologie Dynamique (LMD, Palaiseau) de mars 1994 à janvier 1998, puis au Centre Européen pour les Prévisions Météorologiques à Moyen Terme (CEPMMT, Reading, GB) jusqu'en décembre 2003 et enfin au Laboratoire des Sciences du Climat et de l'Environnement (LSCE, Gif-sur-Yvette). Ils débutèrent par la modélisation du rayonnement atmosphérique par réseau de neurones artificiels, sujet de sa thèse au LMD et de son premier contrat au CEPMMT, pour évoluer ensuite vers les méthodes inverses appliquées aux hydrométéores (au CEPMMT) puis au cycle du carbone et aux aérosols (au LSCE).

Le titre du mémoire est une référence explicite à l'essai de Pierre Simon Laplace qui a créé et

popularisé la méthode d'inférence bayésienne. Pour l'anecdote, le nom de Laplace a été donné à la fédération des instituts de recherche d'Île-de-France qui travaillent sur l'environnement de la Terre¹³, dont font partie le LMD et le LSCE. Le plan du mémoire est organisé autour du théorème de Bayes plutôt que suivant un ordre chronologique. Les premiers chapitres discutent de ses composantes : l'information a priori (chapitre II), les observations (chapitre III), l'opérateur d'observation (chapitre IV). L'application de la règle de Bayes pour un problème de grandes dimensions, celui de l'estimation de la distribution spatio-temporelle des flux de dioxyde de carbone à la surface du globe, est décrite au chapitre V. Le matériau de chaque chapitre est constitué par une sélection d'un ou plusieurs articles dont l'auteur du mémoire a dirigé le travail et l'écriture. Chaque sélection est précédée d'une introduction. Des annexes sur le parcours de l'auteur le complètent.

¹³Il s'agit de l'Institut Pierre Simon Laplace (IPSL). Le nom de l'IPSL est un hommage à l'œuvre pluridisciplinaire de Laplace, mathématicien, astronome, physicien et vulgarisateur.

Chapitre II

Information a priori

S'il y a de la raison dans ces sciences,
il faut aussi qu'il y ait quelque connaissance a priori.
E. Kant, Critique de la raison pure, préface (1787)

II.1 Introduction

L'information a priori est l'atout de l'inférence bayésienne, car elle induit l'unicité de la solution du problème inverse. Cependant la difficulté éprouvée pour la caractériser a suscité de vives critiques. Ces reproches nous semblent injustes car son arbitraire éventuel n'est que le reflet d'un problème mal défini : le théorème de Bayes fournit une méthode pour le résoudre mais n'y ajoute pas d'information.

Bien sûr, le nombre et la qualité des observations peuvent rendre négligeable l'influence de l'a priori. Le problème est alors mathématiquement bien posé (c'est le cas par exemple chez Fisher et coll., 2006). Dans d'autres cas, l'information a priori peut être comparée à des observations afin de déduire ses statistiques de probabilité. Le débat concerne le cas fréquent où l'a priori influence notablement le résultat sans qu'il puisse être directement validé. Ainsi, plusieurs auteurs ont pointé l'arbitraire de la définition de l'ignorance a priori. Pourtant, depuis Jakob Bernoulli ou Pierre Simon Laplace, un principe, celui de la « raison insuffisante¹ », conduit au choix de l'équiprobabilité de tous les états du système étudié dans ce cas. Malheureusement, la distribution uniforme n'est pas nécessairement conservée lors d'un changement de variable. Par exemple, si l'on ne connaît rien sur une variable x , on ne connaît rien non plus sur son carré x^2 . Mais la constance de $p(x)$ est exclusive de celle de $p(x^2)$. On ne peut donc pas définir l'ignorance de manière univoque. D'autre part, la distribution uniforme n'est pas bornée : son intégrale n'est donc pas l'unité, contrairement à la définition d'une probabilité (on parle alors d'a priori impropres).

Plusieurs autres stratégies ont été proposées depuis Laplace pour définir la distribution de probabilité a priori (voir par exemple la synthèse de Jaynes, 2003). Une approche consiste à déduire de la physique du problème étudié les propriétés d'invariance que satisfait la connaissance a priori, et de formaliser celle-ci en conséquence. Une autre consiste à contrôler l'infor-

¹Le « principe de la raison insuffisante » est un jeu de mot à partir du « principe de la raison suffisante » de Leibniz, qui conduit au déterminisme.

mation contenue dans la distribution de probabilité a priori en utilisant l'entropie de Shannon². Par ailleurs, dans certains cas favorables, la forme de la distribution est connue (par exemple, on sait, ou on suppose, que c'est une gaussienne), mais pas ses paramètres. On marginalise alors les paramètres en intégrant la solution I.1 sur toutes les valeurs possibles des paramètres³. Enfin, les statistiques de l'a priori peuvent être déduites par analogie ou par comparaison avec des phénomènes mieux connus⁴ (de Finetti, 1937).

Malgré ces travaux, l'a priori est souvent considéré comme un simple terme de régularisation et est alors paradoxalement défini de manière empirique en fonction des observations. C'est se priver d'une partie de la richesse du cadre bayésien et risquer que l'analyse soit en fait moins bonne que l'information préexistante.

L'exemple présenté ici concerne l'inversion des flux de dioxyde de carbone à la surface du globe à partir d'observations de la concentration atmosphérique du CO₂. Le problème est clairement mal posé et l'a priori importe. L'approche que nous proposons consiste à exploiter les quelques mesures de flux de CO₂ disponibles pour rechercher les caractéristiques de la distribution de probabilité a priori. Malgré le faible nombre de stations de mesure, cette approche innove par rapport à l'empirisme utilisé précédemment. Notre étude tend à indiquer l'absence de corrélation spatiale de l'erreur a priori, alors que les résultats d'inversion publiés jusqu'alors supposaient de fortes corrélations.

II.2 Caractérisation des erreurs

Cette section reprend l'article de Chevallier et coll. (2006) publié au *Geophysical Research Letters*. Cet article a été directement suscité par la préparation du présent mémoire.

On the Assignment of Prior Errors in Bayesian Inversions of CO₂ Surface Fluxes

Frédéric Chevallier^a, Nicolas Viovy^a, Markus Reichstein^b, Philippe Ciais^a

^aLaboratoire des Sciences du Climat et de l'Environnement
Institut Pierre-Simon Laplace
Gif-sur-Yvette, France

^bMax-Planck Institute for Biogeochemistry
Jena, Germany

Abstract. For the estimation of surface CO₂ fluxes from atmospheric concentration measurements, most often Bayesian approaches have been adopted. As with all Bayesian techniques the definition of prior probability distributions is a critical step in the analysis. However, practical considerations usually guide the definition of prior information rather than objective criterions. In this paper, in situ CO₂ flux pointwise measurements made by the eddy-covariance

²Un exemple d'application pour les sciences de l'environnement est donné par Bocquet (2005).

³Un exemple simplifié d'application pour les sciences de l'environnement est donné par Michalak et coll. (2005).

⁴Par exemple en météorologie les statistiques de l'a priori sont souvent prises d'ensembles de prévisions ou d'ensembles d'analyses météorologiques (Parish et Derber 1992, Fisher et Andersson 2003).

technique are used to estimate the errors of prior fluxes provided by the prognostic carbon-water-energy model ORCHIDEE. The results contradict the usual convenient assumption of a multivariate Gaussian distribution. The errors of ORCHIDEE have a heavier-tail distribution with a linear temporal dependency after the second lag day and no particular spatial structure. Such error distribution significantly complicates the inversion of CO₂ surface fluxes.

II.2.1 Introduction

Quantifying the spatio-temporal variations of CO₂ surface fluxes over continents has been a scientific target of primary importance since the end of the 1980s (Keeling et al., 1989; Tans et al., 1990). Several bottom-up methods have been developed, based on local observations (e.g., Baldocchi et al., 2001), on ecosystem modelling (e.g., Krinner et al., 2005), or on a combination of both. Despite dramatic improvements, the uncertainty of each estimate is still too large for these estimates to be reliably used for detailed regional estimates of carbon fluxes. One alternative and complementary approach consists in inferring the fluxes from the atmospheric concentration measurements, knowing how the movement of air parcels link the former to the latter (the top-down approach implemented by, e.g., Enting et al., 1995, Gurney et al., 2002, Rdenbeck et al., 2003). The diffusive nature of atmospheric transport makes such an inversion problem mathematically ill-posed : the measurements have to be combined with some other information to regularize it, usually through the Bayes' formula. This essential extra information consists of what one knows about the CO₂ surface fluxes prior to the examination of the concentration measurements. If one knew nothing, one should choose uniform prior distribution probabilities for the fluxes (i.e., any flux state is all equally likely). There actually exists some (limited) knowledge of the biogeochemical processes that govern the fluxes and which are gathered in numerical models of the terrestrial carbon cycle. In situ pointwise measurements of the ecosystem fluxes at flux towers, large scale inventories of fossil fuel emissions, of carbon stocks changes, and satellite-based

observations of vegetation activity and disturbances also provide some prior information about the fluxes.

Empiricism has dominated the assignment of prior flux errors in Bayesian inversions so far, which bears consequences on the reliability of the inferred fluxes. For convenience, errors are usually modelled by tuneable multivariate (space-time) normal (Gaussian) distributions. Two different strategies could improve on the current situation. The first one, called "marginalization", consists in treating the unknown characteristics of the prior errors, like the standard deviations, as unknown variables in the Bayes' rule. Michalak et al. (2005) developed a simplified approach along this path. This method is still difficult to implement for large dimension problems. Another strategy, which is favoured here, consists in estimating the prior error characteristics based on actual flux observations.

In this paper, surface flux measurements made by the eddy-covariance technique (Aubinet et al., 2000; Baldocchi et al., 2001) on a continuous basis are used to investigate the errors of prior fluxes of the terrestrial biosphere. Prior CO₂ fluxes (i.e. fluxes prior to the analysis of any concentration observation) are provided here by a numerical carbon cycle model : the Organizing Carbon and Hydrology In Dynamic EcosystEms model (ORCHIDEE) described by Krinner et al. (2005). The model and the observations are presented in the next section. Section II.2.3 shows the results, which are discussed in the last section.

II.2.2 Model and Data

Developed at Institut Pierre-Simon Laplace (IPSL), the carbon-water-energy model OR-

CHIDEE explicitly simulates the principal processes of the continental biosphere influencing the global carbon cycle and the fluxes of CO₂ exchanged with the atmosphere, like photosynthesis and respiration of plants and soils. The model handles short-term (half-hourly) to long-term (yearly and beyond) flux and pool variations. It is fully described by Krinner et al. (2005). We focus here on the configuration of the model which is being used as prior information for flux inversions at Laboratoire des Sciences du Climat et de l'Environnement (LSCE). It relies on prescribed atmospheric conditions, a static land-cover distribution, a prognostic observation-independent phenology and a simple two-layer hydrology module.

The direct measurement of CO₂ surface fluxes is provided by the eddy covariance method. This method deduces fluxes from the covariance between fluctuations in anomalous vertical wind velocity and CO₂ mixing ratio (e.g., Aubinet et al., 2000). Some limitations of the method in unsteady atmospheric conditions and over complex landscapes induce substantial uncertainty in the fluxes. Random errors are about 0.4 gC.m⁻² for daily totals, based on Hollinger and Richardson (2005), i.e. of smaller amplitude than the departures between the ORCHIDEE simulations and the measurements presented below. Biases occur in some atmospheric conditions and are difficult to quantify. Despite their uncertainties, the flux towers are considered as the reference standard for CO₂ flux measurement and a network of them has been developed across representative ecosystems (Baldocchi et al. 2001). We use quality-controlled records obtained at 34 flux tower stations located in the Northern hemisphere, for which we assume negligible errors for daily (24-hour) averages in comparison to those of ORCHIDEE. These sites data were from the Flux-Net archive at Oak Ridge (Baldocchi et al., 2001) and from a separate collection of European forest sites recently used in Ciais et al.

(2005). Each record spans several years between 1994 and 2004, and consists of observations of 2-meter temperature, 10-meter wind, precipitation and radiation fluxes in addition to the CO₂ fluxes, with a time step of 30 minutes. Incomplete records of the CO₂ fluxes have not been gap-filled whereas meteorological variables have been interpolated when needed. These meteorological variables have been used as a boundary condition for ORCHIDEE simulations at each site. Vegetation is distributed in the simulations according to the site characteristics. Note that most sites include more than one vegetation type. The initial plant and soil carbon reservoirs are not known and, following the common practice, have been set at the initial time step of each simulation so that the simulated ecosystems are carbon-neutral on a yearly basis.

The eddy-covariance flux observations make it possible to investigate the errors of the simulated fluxes at various temporal resolutions. Most inversion studies up to now have inferred monthly fluxes (Gurney et al. 2002 and references therein). However, the specification of fixed temporal flux patterns within a month necessarily induces spatial and temporal correlations of the model errors at the observation locations that are difficult to take into account, and are usually not. The technical limitations (i.e. computer memory and power) that prevented to infer fluxes at higher temporal resolutions are being circumvented thanks to the introduction of new formulations of the Bayesian inference problem (e.g., Chevallier et al., 2005; Peters et al., 2005). Consequently, we focus here on 24-hour flux averages.

II.2.3 Results

Altogether, the database of daily-mean eddy-covariance fluxes consists of 31,500 quality controlled samples. Figure II.1 displays the correlation between the modelled and the observed daily fluxes as a function of the dominant plant functional type (PFT) on

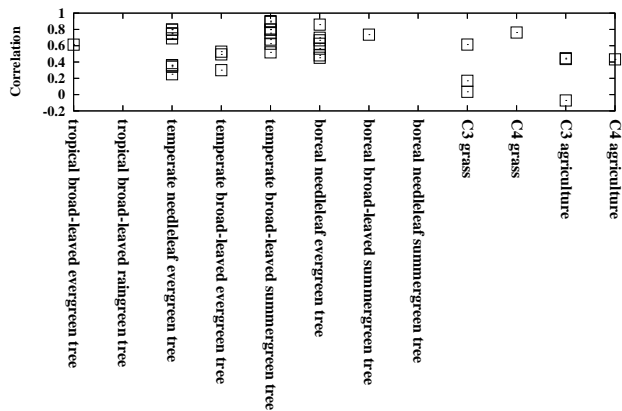


FIG. II.1 – Correlations between the modelled and the observed daily fluxes as a function of the dominant plant functional type on each measurement site. The 12 plant functional types of ORCHIDEE are used. Note that a plant functional type may relatively dominate a site even though it only covers 40% of the site.

each site. The 12-PFT classification of ORCHIDEE is used. The scatter of the points illustrates the diversity of processes that are involved and that are reproduced in ORCHIDEE with various skills, with correlations ranging from about 90% for some forest sites to about zero for some crop sites.

Figure II.2 shows the distribution of the model-minus-observation differences after combining the data from all sites. The negative bias of the distribution (0.6 gC.m^{-2} per day) was expected because vegetation at most eddy covariance sites is in growing phase, and therefore acts as sink for carbon whereas the model has been initialized to be carbon-neutral on the long-term mean. However, a mean 0.6 gC.m^{-2} per day sink over the whole vegetated land surface of the Earth, which is about 10^{14} m^2 , would translate into a global sink of 22 GtC per year. This excessive figure (IPCC 2001) indicates that the database of flux measurements over-represents productive vegetation stands and that different stages of ecosystem disturbance regimes are not covered by the Fluxnet network well enough. This is consistent with the fact that most sites are affected by human activities, like cutting, planting and nitrogen fertilisa-

tion.

The differences spread around the mean with a 2 gC.m^{-2} per day standard deviation. Note that such random errors translate to much less than 22 Gt C per year because uncorrelated random errors evolve as the square root of the time and space scales of the aggregation whereas the bias have a linear behaviour. The actual value of the impact of random errors depends on the time and space correlations. As a corollary, the much-looked-for land biospheric sink (IPCC, 2001) may be negligible compared to the daily 24-hours flux at the scale of a model grid point, even though it dominates the uncertainty of the global annual budget.

In Figure II.2, two theoretical distributions have been superimposed to the one of the model-data flux differences. The first one is the Gaussian distribution with the same mean and standard deviation. The second one is the Cauchy distribution (also called Lorentz distribution) with location parameter 0.3 and scale parameter 1. Obviously, approximating the ORCHIDEE errors by the Gaussian distribution is a poor approximation whereas the Cauchy distribution would be more appropriate. This is because the daily fluxes are well

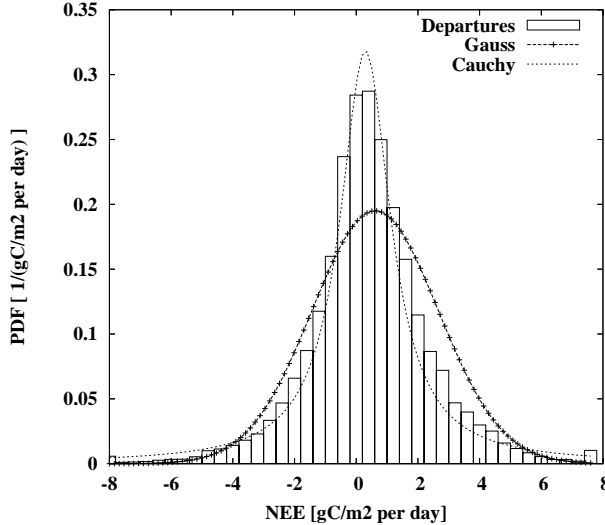


FIG. II.2 – Probability Density Function (PDF) of the ORCHIDEE-minus-observation departures for daily CO₂ fluxes. The Gaussian distribution with the same mean and standard deviation, as well as the Cauchy distribution with location parameter 0.3 and scale factor 1.0, are also reported on the graph.

simulated at some sites during some periods but poorly in other cases (as seen in Fig. II.1). Errors at individual sites are more normally distributed (not shown). In other words, the simulation error is not purely random but depends on nuisance variables (in the statistical sense), like the start of the growing season or the plant hydric stress. Therefore a Cauchy distribution, with a relatively narrow peak compared to the tails, better fits the error distribution than a normal distribution. In order to keep Gaussian errors for individual fluxes, one would have to use different widths of the Gaussian distribution, depending on sites or periods.

Correlations of the differences between the simulations and the measurements of the in situ daily fluxes are shown in Figure II.3 as a function of time and space. Time correlations drop down to about 70% at lag-day 2 and behave rather linearly afterwards, which is far from a Gaussian decay. The correlations at lag-day 30 are about 30%. Spatially, the correlation between the differences at distinct sites is below 50% in absolute value

even when considering nearby sites. Given the large spread of the space correlations at any distance, no obvious spatial coherence can be identified.

II.2.4 Discussion and Conclusions

Assuming normally-distributed prior errors is common practice for Bayesian inversions for several reasons. First, this approximation makes the problem analytically solvable, either by matrix operations or by the minimization of a cost function (e.g., Lorenz, 1986). Second, it is the least committal choice when one only knows the mean and the standard deviation of the actual distribution (Jaynes 1957). Third, under certain conditions, the distribution of the sum of a large number of independent variables is indeed approximately Gaussian, as stated by the central limit theorem. None of these reasons justifies a systematic use of Gaussian error distributions and there is a need to investigate the properties of the prior errors, at least to estimate the mean and the variance of their distribution. In this study, pointwise

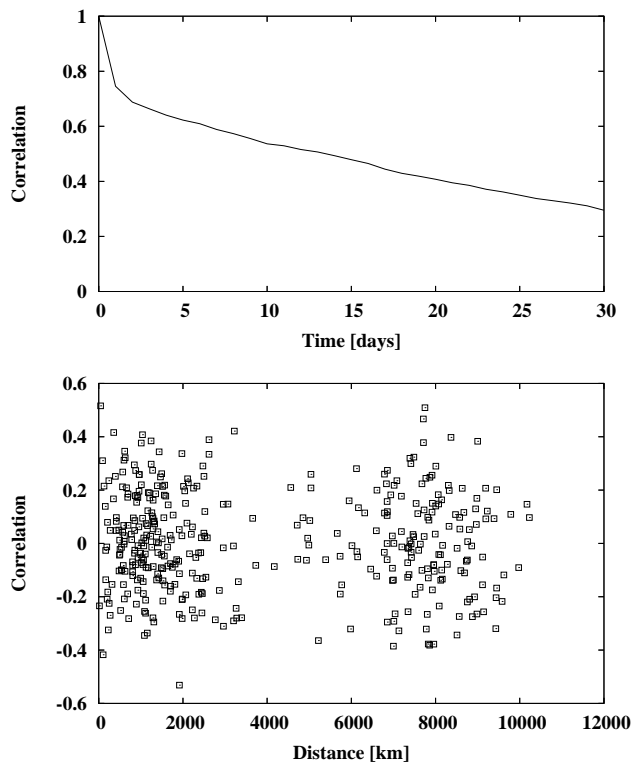


FIG. II.3 – Time (top) and space (bottom) correlations of the differences between the ORCHIDEE simulations and the observations.

continuous measurements made by the eddy covariance technique have been used to estimate the characteristics of the prior errors for CO₂ flux inversions. The prior is provided by the model of the terrestrial biosphere ORCHIDEE. This strategy is not fully exhaustive. First, the eddy covariance measurements are affected by some errors. Second, the observation towers consider areas of size typically about 1 km², whereas ORCHIDEE is used at a lower spatial resolution to provide flux maps, typically about 100x100 km² (see for instance <http://www.lsce-orchidee.cea.fr>). Furthermore, for large areas, the atmospheric forcing needed to run the model cannot be obtained from local observations but is provided by short-range weather forecasts of lower accuracy. Last, our flux database is biased towards temperate middle-aged forest ecosystems. However, in spite of these limitations, local observations by the eddy-covariance technique may be the only reliable benchmark and only they can currently provide some evidence about the structure of the simulation errors. The present study focuses on the daily CO₂ fluxes simulated by ORCHIDEE and its results may not be valid for other time scales or other models, that require specific attention based on a similar methodology.

This study indicates an error standard deviation of 2 gC.m⁻² per day when considering all ecosystems together. Combined with the temporal correlations of Fig. II.3, this number corresponds to a monthly error budget (i.e. the square root of the sum of the covariances within a month) of about 60 gC.m⁻² and a yearly one of about 200 gC.mm⁻² at one site (without any respect to the nature of its vegetation). As a comparison, Rödenbeck et al. (2003) guessed errors to be of similar or smaller amplitude (depending on latitude) for the prior information in their flux inversion (their Figs. 9D and 9E) whereas Houweling et al. (2004) supposed twice as large values. These studies included biomass burning in addition to the biosphere photosynthesis and

respiration CO₂ fluxes, and hypothesised perfect knowledge of fossil fuel emissions. Both types of processes deserve a specific investigation. Our study also shows that the temporal correlations of the ORCHIDEE errors slowly decrease in a linear way after lag-day 2. No particular spatial structure could be identified. The absence of spatial correlation emphasizes the importance to perform flux inversions at horizontal resolutions as high as possible, since subgrid scale errors are correlated by construction. Obviously, the sparse eddy-covariance network may not reveal some correlation structure that may actually exist. In particular, the fact that each site contains a mixture of vegetation types prevented us to analyze the arguably-larger correlations within a given vegetation type. Nevertheless, there seems to be less justification in introducing spatial correlations than to ignore them. If the results hold for other models of the biosphere and other sites, one would wonder whether surface measurements of CO₂ concentrations actually contain much information about the spatial distribution of biospheric fluxes. Indeed, in the absence of spatial correlations, inversion increments generated by the surface observations are mainly confined to the vicinity of the measurements (e.g., Bocquet, 2005). Such issue highlights the importance of the forthcoming spatial instruments dedicated to the observation of atmospheric CO₂, because they will provide measurements well above the surface and a much denser coverage of the globe.

Finally, our results seem to indicate that there is no ground for choosing Gaussian prior error distributions in atmospheric inversion, at least when using daily fluxes from ORCHIDEE. Gaussian distributions can still be justified by their analytical properties from a pragmatic point of view. Indeed a distribution with heavier tails makes the Bayesian cost function non-quadratic and therefore increases the computational burden of the inversion. Further, there is no closed-form

solution to the inversion problem any more. However, properly assigning the prior errors in flux inversions would make the flux inversions closer to what they are supposed to be : the best solutions given the evidence provided.

Acknowledgments. Authors wish to thank F.-M. Bréon, P. Naveau, P. Peylin and P. Rayner (LSCE) for fruitful discussions about the topic. C. Rödenbeck (MPI-Jena) and two anonymous reviewers made useful comments on an earlier version of the paper. This study was made possible by the work of numerous scientists, students and technicians involved in data collection and analysis at the various Fluxnet sites. Most data have been downloaded from <http://www.daac.ornl.gov/FLUXNET/> fluxnet.html. The other ones have been kindly provided by M. Aubinet, J. Banza, C. Bernhofer, A. Carrara, A. Granier, W. Kutsch, D. Loustau, D. Papale, J. S. Pereira, K. Pilegaard, M. J. Sanz, G. Seufert, J.-F. Soussana and T. Vesala. This study was co-funded by the European Union under projects GEMS and GEOLAND.

References

- Aubinet, M., et al. (2000), Estimates of the annual net carbon and water exchange of forests : The EUROFLUX methodology, *Advances in Ecological Research* 30 : 113-175.
- Baldocchi, D., et al. (2001), FLUXNET : A new tool to study the temporal and spatial variability of ecosystem-scale carbon dioxide, water vapor, and energy flux densities, *Bull. Am. Meteor. Soc.*, 82 : 2415-2434
- Bocquet, M. (2005), Grid resolution dependence in the reconstruction of an atmospheric tracer source, *Nonlinear processes in Geophysics*, 2, 219-233.
- Chevallier, F., M. Fisher, P. Peylin, S. Serrar, P. Bousquet, F.-M. Bréon, A. Chédin, and P. Ciais, 2005b : Inferring CO₂ sources and sinks from satellite observations : method and application to TOVS data, *J. Geophys. Res.*, 110, D24309, doi :10.1029/2005JD006390.
- Ciais, P., et al. (2005), Europe-wide reduction in primary productivity caused by the heat and drought in 2003, *Nature*, 437, 529-533.
- Enting, I.G., C.M. Trudinger and R.J. Francey (1995), A synthesis inversion of the concentration and ¹³C atmospheric CO₂, *Tellus*, 47B, 35-52.
- Gurney, K. R., et al. (2002), Towards robust regional estimates of CO₂ sources and sinks using atmospheric transport models, *Nature*, 415 :6872, 626-630.
- Hollinger, D.Y., and A.D. Richardson (2005), Uncertainty in eddy covariance measurements and its application to physiological models, *Tree Physiology*, 25, 873- 885
- Houweling, S., F.-M. Bréon, I. Aben, C. Rödenbeck, M. Gloor, M. Heimann, and P. Ciais (2004), Inverse modeling of CO₂ sources and sinks using satellite data : a synthetic inter-comparison of measurement techniques and their performance as a function of space and time, *Atmos. Chem. Phys.*, 4, 523-538.
- IPCC (2001), Climate Change 2001 : The Scientific Basis. Contribution of Working Group I to the Third Assessment Report of the Intergovernmental Panel on Climate Change, 881 pp, Cambridge University Press, Cambridge, UK.
- Jaynes, E. T. (1957), Information theory and statistical mechanics, *Phys. Rev.*, 106, 620-630.

- Keeling, C.D., R.B. Bacastow, A.F. Carter, S.C. Piper, T.P. Whorf, M. Heimann, W.G. Mook, and H. Roeloffzen (1989), A three-dimensional model of atmospheric CO₂ transport based on observed winds : 1. Analysis of observational data, in *Aspects of Climate Variability in the Pacific and the Western Americas*, Geophysical Monograph ser., vol. 55, edited by D.H. Peterson, pp. 165-236, AGU, Washington, DC.
- Krinner G., N. Viovy, N. de Noblet-Ducoudre, J. Oge, J. Polcher, P. Friedlingstein, P. Ciais, S. Sitch, and I. C. Prentice (2005), A dynamic global vegetation model for studies of the coupled atmosphere-biosphere system, *Global Biogeochem. Cycles*, 19, GB1015, doi :10.1029/2003GB002199.
- Lorenc, A. C. (1986), Analysis methods for numerical weather prediction, *Quart. J. Roy. Meteorol. Soc.*, 112, 1177-1194.
- Michalak, A. M., A. Hirsch, L. Bruhwiler, K. R. Gurney, W. Peters, and P. P. Tans (2005), Maximum likelihood estimation of covariance parameters for Bayesian atmospheric trace gas surface flux inversions, *J. Geophys. Res.*, 110, D24107, doi :10.1029/2005JD005970.
- Peters, W., J. B. Miller, J. Whitaker, A. S. Denning, A. Hirsch, M. C. Krol, D. Zupanski, L. Bruhwiler, and P. P. Tans (2005), An ensemble data assimilation system to estimate CO₂ surface fluxes from atmospheric trace gas observations, *J. Geophys. Res.*, 110, D24304, doi :10.1029/2005JD006157.
- Rödenbeck, C., S. Houweling, M. Glooer, and M. Heimann (2003), CO₂ flux history 1982-2001 inferred from atmospheric data using a global inversion of atmospheric transport, *Atmos. Chem. Phys.*, 3, 1919-1964.
- Tans, P.P., I.Y. Fung and T. Takahashi (1990) Observational constraints on the global atmospheric CO₂ budget, *Science*, 247, 1431-1438.

Chapitre III

Observations

Nous savons tous qu'il y a de bonnes expériences et qu'il y en a de mauvaises.

Celles-ci s'accumuleront en vain ; qu'on en ait fait cent, qu'on en ait fait mille, un seul travail d'un vrai maître, d'un Pasteur par exemple, suffira pour les faire tomber dans l'oubli.

H. Poincaré, La science et l'hypothèse, chap. 9 (1904)

III.1 Introduction

Le traitement des observations dans l'inférence bayésienne semble plus aisé que celui de l'information a priori. En effet, approximer les densités de probabilité des erreurs d'observation par des gaussiennes est communément admis. Cependant une gaussienne est définie par deux paramètres : la moyenne et l'écart-type. Or, si l'écart-type d'erreur des observations est souvent bien connu, les biais le sont rarement. De plus, des corrélations peuvent exister entre les erreurs des observations : il faut alors aussi les estimer. Le problème se complique encore si un opérateur d'observation est utilisé dans l'inversion. Dans ce cas, l'erreur de l'opérateur se combine avec celle de la mesure et la densité de probabilité résultante n'est plus nécessairement gaussienne. En particulier, si l'opérateur est non-linéaire, il y a peu de chances que ses erreurs soient symétriques, et par extension, gaussiennes.

Les deux premiers articles présentés ici insistent sur la sélection des observations. Nous y scrutons différents types d'observations, d'une part pour vérifier qu'elles contiennent une information significative sur les variables que nous souhaitons optimiser, d'autre part pour étudier la capacité de l'opérateur à les décrire correctement. Dans les deux cas, nous recommandons de n'utiliser qu'un sous-ensemble des observations disponibles.

Le troisième article considère la possibilité de corrélations entre les erreurs des observations. Cet aspect est rarement pris en compte directement et la pertinence d'approximations courantes y est étudiée.

En complément de ce chapitre, on pourra utilement consulter le paragraphe *The Observation Error Covariance Matrix* de la section V.2.3 qui traite de l'estimation des erreurs de données satellitaires.

III.2 Choix d'observations interprétables

Cette section reprend l'article de Chevallier et coll. (2004) paru dans *Quarterly Journal of the Royal Meteorological Society*.

The capability of 4D-Var systems to assimilate cloud-affected satellite infrared radiances

Frédéric Chevallier, Philippe Lopez, Adrian M. Tompkins, Marta Janisková and Emmanuel Moreau

European Centre for Medium-Range Weather Forecasts
Reading, UK

Abstract. Four-dimensional variational (4D-Var) assimilation schemes assume the linearity of their forward model in the vicinity of prior information and usually do not properly handle variables that have finer temporal and spatial scales in the real world than in the forward model. Hence cloud-affected satellite infrared radiances are discarded from numerical weather prediction 4D-Var systems despite the critical need of observations within the cloudy regions. This paper suggests the reappraisal of that choice, subject to achieving improvements in the numerical simulation of cloudiness.

A new observation operator, that computes cloud-affected infrared radiances from 4D-Var control variables, namely atmospheric temperature, humidity, ozone, surface temperature and surface pressure, is presented. The vertical distributions of cloud cover and of cloud condensate are diagnosed in the operator itself. The goal of this paper is to assess the feasibility of using it to assimilate cloud-affected infrared radiances such as those from the narrow-band Advanced Infrared Sounder on-board the Aqua platform or those from the broad-band Meteosat Visible and Infrared Imager. It is shown that there is a potential benefit in assimilating some of the upper tropospheric channels at 4.5, 6.3 and 14.3 μm in the presence of clouds directly in 4D-Var, for instance the 6.3 μm channel on-board all the geostationary satellites. The approach is illustrated with one-dimensional variational retrievals collocated with radiosonde observations.

III.2.1 Introduction

The improvement of weather forecast skill in recent years owes much to the development of Bayesian estimation techniques for atmospheric data assimilation. In particular, an in-

creasing number of numerical weather prediction (NWP) centres opt for three- and four-dimensional variational assimilation systems (respectively 3D-Var and 4D-Var) to perform their atmospheric analyses (e.g. Rabier et al. 2000, Lorenc et al. 2000). 3D- and 4D-Var es-

timate the atmospheric variables from a background state (usually based on an earlier forecast) and from available observations. They perform best when background and observation error statistics are Gaussian, unbiased and perfectly known, and when the forward model, that relates the background variables to the observed variables, is linear. Linearity is actually only needed in the vicinity of the background for perturbations whose magnitude is of the same order as the background errors. Yet observations for which significant non-linearities affect the forward model are discarded from 3D- and 4D-Var systems. Consequently, infrared satellite radiances are currently not assimilated in the presence of clouds, even though they would inform the NWP systems about regions of the atmosphere which strongly influence the forecasts (McNally 2002).

At the European Centre for Medium-Range Weather Forecasts (ECMWF) an observation operator that computes cloud-affected radiances from some of the ECMWF 4D-Var control variables (temperature, humidity and ozone profiles, surface temperature and surface pressure) has been developed for data assimilation. The operator diagnoses the vertical distributions of cloud cover and of cloud condensate by taking both large-scale and convective processes into consideration. The goal of this paper is to assess the possibility of its use for assimilating cloud-affected radiances within a 4D-Var system. The assessment is based on the examination of the accuracy and of the linearity of this new observation operator for the simulation of the narrow-band channels from the Advanced Infrared Sounder (AIRS) on-board the Aqua platform and of the broad-band channels from the Meteosat Visible and Infrared Imager (MVIRI).

The plan of the paper is as follows. Section III.2.2 outlines the 4D-Var method and discusses the implications for the selection of observations. Section III.2.3 describes the data and the observation operator. Accuracy and

linearity of the observation operator are estimated in sections III.2.4 and III.2.5 respectively. A one-dimensional variational (1D-Var) scheme is used in section III.2.6 to illustrate the previous results. Concluding discussion follows in section III.2.7.

III.2.2 Theoretical framework of 4D-Var

General formalism

4D-Var systems are a practical formulation of Bayesian estimation theory for the particular case of a linear problem with un-biased Gaussian errors. They seek a model trajectory $\mathbf{x}(t)$ that is statistically consistent with the information provided by the observations \mathbf{y} available during a given time period $[t_0, t_n]$ and that provided by an *a priori* model state \mathbf{x}^b called the background state. The background \mathbf{x}^b is usually based on a short-range forecast. The model trajectory $\mathbf{x}(t)$ is completely defined by the initial state \mathbf{x}_0 at time t_0 .

The balance of the model initial state \mathbf{x}_0 between the observations \mathbf{y} and the background \mathbf{x}^b is measured by an objective cost-function defined as follows :

$$\begin{aligned} J(\mathbf{x}_0) = & \frac{1}{2}(\mathbf{x}_0 - \mathbf{x}_0^b)^T \mathbf{B}^{-1} (\mathbf{x}_0 - \mathbf{x}_0^b) \quad (\text{III.1}) \\ & + \frac{1}{2} \sum_i (\psi_i[\mathbf{x}_0] - \mathbf{y}_i)^T \mathbf{R}_i^{-1} (\psi_i[\mathbf{x}_0] - \mathbf{y}_i) \end{aligned}$$

where at any time t_i , \mathbf{y}_i is the vector of observations, ψ_i is the forward operator providing the equivalent of the observations from the model initial state \mathbf{x}_0 , \mathbf{R}_i is the observation error covariance matrix and \mathbf{B} is the background error covariance matrix of the state \mathbf{x}^b . Superscripts -1 and T denote respectively inverse and transpose matrix. Subscript i denotes the time index.

ψ_i is the combination of a dynamic *model operator*, usually called M_i , and of a static *observation operator*, usually called H_i (Ide et al. 1997). Observation errors described by \mathbf{R}_i are assumed to be uncorrelated from one time

step i to another. It is important to understand that they are defined with respect to the forward model ψ_i which is assumed to be perfect. Consequently, \mathbf{R}_i actually contains the errors of ψ_i in addition to the measurement errors.

The control vector \mathbf{x}_0 includes the prognostic variables to be initialized in the forecast model : vorticity, divergence, temperature, humidity, ozone, surface temperature and surface pressure in the case of the ECMWF 4D-Var. Surface temperature is actually defined at satellite observation points only since soil variables are specifically analysed in a separate Optimal Interpolation system. In theory, cloud cover and cloud condensate could be 4D-Var control variables as well, but the definition of their background errors and of their coupling with temperature and humidity background errors would be particularly challenging, for instance when cloud cover is zero or unity.

The minimization uses a descent algorithm which requires several computations of the gradient of J with respect to the initial state \mathbf{x}_0 . Given the dimension of the state vector the adjoint technique is used to provide an efficient estimate of ∇J :

$$\begin{aligned} \nabla J(\mathbf{x}_0) &= \mathbf{B}^{-1}(\mathbf{x}_0 - \mathbf{x}_0^b) \\ &+ \sum_i \Psi_i^T \mathbf{R}_i^{-1} (\psi_i[\mathbf{x}_0] - \mathbf{y}_i) \end{aligned} \quad (\text{III.2})$$

where Ψ_i^T is the adjoint of the forward operator (i.e. the derivative or Jacobian matrix).

Additionally, an incremental formulation of the variational system is used at ECMWF (Courtier et al. 1994) : departures $\psi_i[\mathbf{x}_0] - \mathbf{y}_i$ are computed at resolution 40 km, the analysis increments are computed at the lower resolution of 125 km. The system copes with weak non-linearities through an “inner-loop/outer-loop algorithm”, where the cost function is minimised in the inner loop based on a linearisation of ψ_i in the vicinity of the initial state which is updated in the outer loop. A simplified version of the derivatives of

ψ_i are used both for the linearisation (tangent-linear model Ψ_i) and for the adjoint model Ψ_i^T . In the following, cycle 25r5 of the ECMWF forecasting system that became operational in March 2003 is used.

Implications for the selection of cloud-affected observations

The variational formulation of the inverse problem outlined above, together with currently available computer power allows the operational handling of large numbers of control variables (about 5 million currently at ECMWF) and of observations (about 1.5 million per 12-hour analysis cycle). It would provide statistically optimal analyses if the errors statistics \mathbf{B} and \mathbf{R}_i were un-biased, Gaussian and perfectly known and if the problem was linear. For instance significant non-linearities may exist in a 4D-Var system, but they degrade the realism of the corresponding analyses and tend to limit the impact in the subsequent forecasts to short ranges. As a consequence, attempts are made to bring the 4D-Var systems as close as possible to optimality by removal of biases (e.g. Harris and Kelly 2001), by choosing Gaussian error control variables (e.g. Dee and da Silva 2003), by a careful estimation of the error statistics (e.g. Derber and Bouttier 1999), by the improvement of the parameterizations of the forward operator and by avoiding observations for which ψ_i is significantly non-linear with respect to the analysis increments $\mathbf{x}_0 - \mathbf{x}_0^b$.

To account for cloud processes in such a framework is obviously a challenge. Indeed, fine-scale atmospheric processes significantly impact the cloud fields and result in significant non-linearities at the spatial and temporal scales of the NWP models. Further, they make cloud parameterizations particularly difficult to formulate. Conversely, cloud observations also contain large-scale information, through the dynamics, which allows a realistic representation of cloud systems in NWP (e.g. Chevallier and Kelly 2002). In the

next sections the accuracy of the recently-developed observation operator and its linearity with respect to perturbations of the order of the expected size of analysis increments will be estimated in order to select cloud-affected channels for assimilation within 4D-Var.

III.2.3 Data and model

The satellite data

The present study exploits the observations from two space-borne instruments, MVIRI and AIRS.

MVIRI has been flown on-board the Meteosat 1 to 7 geostationary satellites, operated by the European Organisation for the Exploitation of Meteorological Satellites (EU-METSAT). It includes three spectrally-broad measurement channels : two infrared ones (from 10.5 to 12.5 μm and from 5.7 to 7.1 μm respectively) and one visible (0.45 to 1 μm). An image of the earth disc as seen from the geostationary orbit is generated at 30 minute intervals in each channel. It consists of 2500×2500 pixels for the infrared channels ($5 \times 5 \text{ km}^2$ resolution at the subsatellite point) and 5000×5000 pixels ($2.5 \times 2.5 \text{ km}^2$) for the visible one. One Meteosat satellite is normally stationed close to zero degree longitude, but depending on operational choice, an additional one may be positioned above the Atlantic or the Indian Ocean.

For the present study, the radiances from the two infrared Meteosat channels are extracted from the EUMETSAT Radiance Data from Clouds (RDC) product in the form of mean brightness temperatures in 16×16 pixel quadrants. This averaging results in a resolution (80 km at the subsatellite point) similar to the ECMWF analysis (currently about 125 km). It is useful to note that data from a related EUMETSAT product, the Clear Sky Radiances (CSR), are operationally assimilated at ECMWF (Köpken et al. 2003). Those radiances result from averages for the pixels not affected by clouds in each quadrant. Only

data from the quadrants where more than 70% of the pixels are judged clear are actually assimilated. Consistently, quadrants will be considered cloudy in the following when more than 30% of the pixels are not classified as clear.

The AIRS instrument, operated by the National Aeronautic and Space Agency (NASA), provides significantly different measurements of the infrared spectrum. On-board the Aqua sun-synchronous polar orbiter, it observes nearly all points of the globe twice a day, moving northward across the equator at about 01 :30 PM local time. It samples the infrared spectrum between 3.7 and 15.4 μm with 2378 channels. Additionally 4 channels are located in the visible (from 0.4 to 1.0 μm). Horizontal resolution reaches 13.5 km and 2.3 km at nadir for the infrared and the visible channels respectively. No attempt is made to average the data. As a starting point, a subset of 324 channels for one satellite spot in eighteen has been made operationally available to ECMWF by the National Environment Satellite Data and Information Service (NESDIS). Data from cloud-free channels are currently assimilated in a research mode, with a cloud detection method described by McNally and Watts (2003).

AIRS observations for wave numbers below 2000 cm^{-1} and MVRI ones are bias-corrected using a constant offset in each channel in order to account for possible erroneous knowledge of the instrument characteristics. The offset is estimated independently from cloud-free departure statistics (Köpken and McNally 2003, personal communication).

Observation operator

Diagnostic and prognostic models. A prognostic model implies a scheme that computes the tendencies $\partial\eta/\partial t$ of some cloud quantity η with respect to time t , therefore retaining cloud information from previous time-steps of the integration. A diagnostic model alternatively diagnoses the state of η at time t

from other variables, thus precluding a memory of cloud variables and thus implying that cloud mass is not necessarily conserved.

The ECMWF forecast model includes a prognostic cloud scheme (Tiedtke 1989, 1993) which could in principle be used in the 4D-Var physics for the assimilation of cloud information, provided that cloud variables are added in the 4D-Var control vector. Such a strategy would pose the acute problem of defining background error statistics for the new variables, as mentioned in section III.2.2. As a consequence, a diagnostic approach has been preferred. A model has been developed and is described hereafter. It uses only the existing 4D-Var control variables as input and was kept relatively simple so that thresholds and strong non-linearities do not make the 4D-Var minimization stop before reaching the absolute minimum of the cost function.

The present study does not cover the full 4D-Var forward model. It focuses mainly on its static part, or observation operator H (see section III.2.2), that computes satellite radiances from the relevant 4D-Var control variables, namely atmospheric temperature, humidity, ozone, surface temperature and surface pressure. Indeed the dynamic part, or model operator M , computes the time evolution of all the control variables and is not specific to the assimilation of radiances in the presence of clouds. The reader is referred to Janisková et al. (2002) for the impact of the introduction of cloud-radiation interaction within the model operator.

Convection model. The convection model of the observation operator is based on the ECMWF operational mass-flux scheme, initiated by Tiedtke (1989), but uses a simplified algorithm. All types of convection (shallow, mid-level, and deep) are treated in a similar way. In particular, the link between the model control variables and the subgrid-scale convective quantities (the so-called closure assumption) is expressed through a single formulation that depends on the release of

convective available potential energy in time. The equations that describe the vertical evolution of the updraught mass-flux M_u and of the updraught thermodynamic variables Φ_u are un-coupled :

$$\frac{\partial M_u}{\partial z} = -(\epsilon - \delta) M_u \quad (\text{III.3})$$

$$\frac{\partial \Phi_u}{\partial z} = -\epsilon(\Phi_u - \bar{\Phi}) \quad (\text{III.4})$$

where $\bar{\Phi}$ denotes field values in the environment, and ϵ and δ are the entrainment and detrainment fractional rates respectively. The bulk convective updraught is assumed to originate from the surface only if its initial vertical velocity as calculated from the surface heat fluxes is positive. The departures of the updraught from the environment are also assumed to be dependent on the surface heat fluxes. If convection cannot be initiated from the surface, the convective ascent may originate from higher levels provided relative humidity exceeds 80%. In this case, the initial vertical velocity of the bulk updraught is set equal to 1 m s^{-1} . Regardless of whether the updraught originates from the surface or higher up, the vertical evolution of its kinetic energy is computed following Simpson and Wiggert (1969) which involves the entrainment of environmental air into the updraught. Convection is assumed to be active only if the updraught vertical velocity remains positive at cloud base. Simplified calculations of downdraughts and convective momentum transport, based on the operational scheme, are also included in the modified parameterization. The calculation of the precipitation formation rate from the updraught cloud condensate specific content is inspired from Tiedtke (1989). Further details of the convection scheme are given by Moreau et al. (2003).

Large-scale cloud model. As described by Tompkins and Janisková (2003), the stratiform part of the diagnostic cloud scheme assumes that the subgrid-scale fluctuations of total water are uniformly distributed. Two parameters only are therefore needed to describe

the corresponding probability density function (PDF) in any model layer i , hereafter RH_i^c and κ_i . RH_i^c is the critical relative humidity above which clouds are allowed to form, κ_i sets the total water variance, or equivalently the distribution width. Stratiform cloud cover in layer i is consequently expressed as :

$$C_i^{strat} = 1 - \sqrt{\frac{1 - RH_i}{1 - RH_i^c - \kappa_i(RH_i - RH_i^c)}} \quad (\text{III.5})$$

where RH_i is the relative humidity in layer i . RH_i^c and κ_i are empirically defined in each layer once for all. Initially the RH_i^c 's were estimated using $\kappa_i = 0.7$ so that the diagnostic model fits the prognostic scheme (Tiedtke 1993) well. Values of RH_i^c between 0.55 in the middle troposphere up to about 0.9 at the tropopause and at the surface were obtained. The coefficients κ_i were then adjusted to agree with top-of-the-atmosphere radiation observations. In addition, precipitation fluxes are estimated in a manner close to the prognostic scheme, in order to pave the way for the assimilation of rain-affected microwave radiances, but this aspect is not exploited here.

The radiance model. The radiative transfer model to compute satellite radiances has already been documented within previous studies (Chevallier et al. 2001, Chevallier and Kelly 2002, Chevallier et al. 2002) and only its salient features are recalled here. The scheme applies in the infrared as in the microwave spectrum, but does not take scattering into account. Cloud absorption is computed in each model layer using parameterizations similar to those used in the ECMWF forecast model for the broad-band radiative fluxes. Cloud layers are assumed to overlap according to the maximum-random scheme of Raäsänen (1998). The Radiative Transfer for Television and Infrared Observation Satellite (TIROS) Operational Vertical Sounder (RT-TOV : Eyre 1991, Saunders et al 2002) computes the gaseous absorption. The model has been used since 2000 for the routine monitoring of the clouds modelled by the ECMWF

forecasting system in operations and in the 40-year re-analysis program.

III.2.4 Accuracy of the observation operator

MVIRI

The accuracy of the observation operator is illustrated for the Meteosat-7 data for 30 November 2002 at 12 UTC. The atmospheric circulation is very similar to that described in Chevallier and Kelly (2002) for December 2000. Various cloud systems are present in the $11\ \mu\text{m}$ full resolution image (Figure III.1) : several frontal systems spread in the mid-latitudes and tropical convection is very active over the oceans as over land. Inputs to the observation operator are extracted from the 12-hour forecast initialized from the 00 UTC analysis. Cloud variables are diagnosed by the moist physics described above but can also be simply extracted from the forecast archive. In the latter case, the cloud variables are computed by the prognostic cloud scheme. The same radiation model is used in both cases. Although the forecast resolution reaches $40\ km$, a reduced grid of $80\ km$ is used here for better compatibility with the 4D-Var system.

Statistics of the model vs. the observations are presented in Table III.1 for the two infrared channels in the Meteosat cloudy quadrants. From this simple test, the diagnostic and the prognostic physics appear to perform similarly with respect to observations, despite significant standard deviations ($9.6\ K$ at $11\ \mu\text{m}$) of the differences between each other. This result is particularly important for 4D-Var applications, where the diagnostic model would be used in place of the prognostic one (see section III.2.3). The largest departures from the observations occur around $11\ \mu\text{m}$. Indeed in this atmospheric spectral window little gaseous absorption takes place so that any cloud above the boundary layer has a strong impact on this channel. Comparatively, the $6.3\ \mu\text{m}$ channel is very sensitive

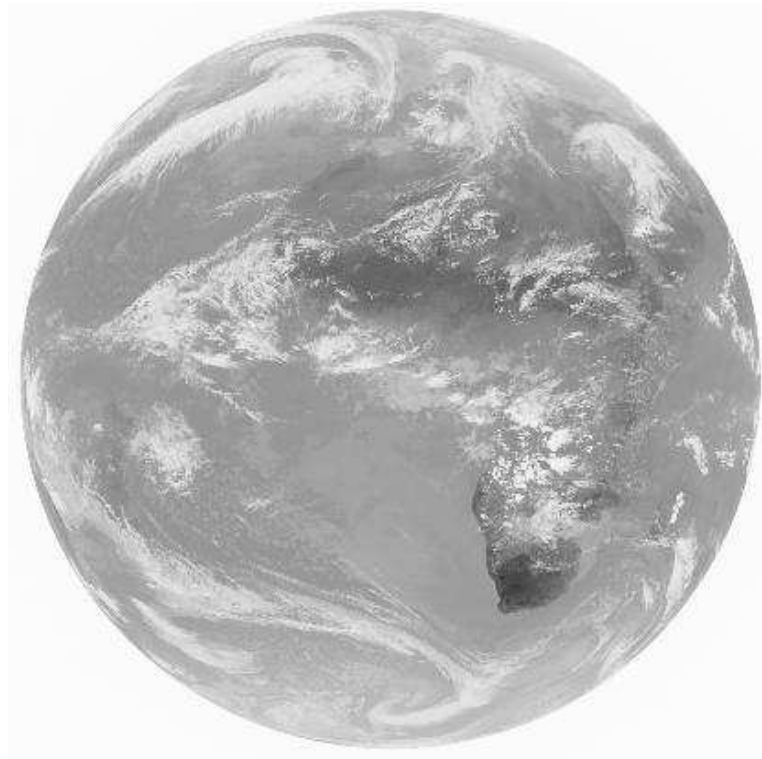


FIG. III.1 – Observed Meteosat-7 $11 \mu m$ image on 30 November 2002 at 12 UTC.

MVIRI channel	O		D - P		D - O		P - O	
	Mean	Std.	Mean	Std.	Mean	Std.	Mean	Std.
$6.3 \mu m$	234.1	7.9	0.2	2.6	-1.9	5.8	-2.0	5.7
$11 \mu m$	260.9	18.4	-1.5	9.6	8.2	18.0	9.7	16.5

TAB. III.1 – Mean and standard deviation of the observations (O) and of the differences between the two model brightness temperatures or between modelled and observed brightness temperatures, in degrees Kelvin. The model cloud variables are either prognosticated (P) or diagnosed (D). Statistics are presented for the two MVIRI infrared channels and are restricted to the Meteosat quadrants where less than 70% of the pixels are judged clear (10770 quadrants out of 22718).

to upper tropospheric humidity (e.g. Schmetz and Turpeinen 1988). It is therefore hardly affected by low level clouds and less affected by upper- and mid-level clouds. Table III.1 also indicates the existence of biases between the model and the observations, that should be removed before those observations are assimilated.

The fraction of observed variance explained by the model is defined as $f = (Var[y] - Var[H[x] - y]) / Var[y]$, where $Var[y]$ is the variance of the observation and $Var[H[x] - y]$ is the variance of the departures ($f = 1$ if the model is perfect and $f = 0$ if the model does not correlate with the observations). This fraction f is 0.48 and 0.20 respectively at 6.3 and $11 \mu m$ for the prognostic model and 0.46 and 0.04 respectively for the diagnostic model. This means that both models have some similar significant skill in predicting 80 km-resolution $6.3 \mu m$ cloud optical thickness, but have nearly none at $11 \mu m$, at least on an average in the Meteosat disk. The deficiencies at $11 \mu m$ can be caused by the cloud scheme, the radiation model or by the temperature and humidity fields. One may note that the prognostic scheme is used in dynamic mode and is combined with other parameterizations in the forecast model to predict the temperature and humidity variations.

It would be interesting to investigate the PDF of the observation operator errors, because they would dominate the observation error covariances R (time index i has been dropped and model operator is ignored) and would consequently be assumed to be Gaussian within 4D-Var (see section III.2.2). Two methods could be used to infer R . The first one would directly measure it with accurate validation data, including both the inputs and the outputs of the observation operator. Such data, for instance from the Atmospheric Radiation Measurement program (ARM, Stokes and Schwartz 1994), do not exist in sufficient number to build reliable error statistics. The second method would infer R indirectly from

the PDF of the departures of the model from the observations, that include both observation and background errors, and from accurate estimation of the background error statistics B . Rough estimates of B exist and are used below, but do not reach a sufficient accuracy for this task. Therefore the PDF of the departures in the cloudy quadrants is used here as a poor surrogate. They are shown in Figure III.2 for the cloudy quadrants, together with the Gaussian distributions that have the same mean and standard deviation. There is no indication in the figure that the assumption of Gaussian shape for the observation errors is a significant issue in comparison to the accuracy and to the linearity properties.

AIRS

The model evaluation for the 324 available AIRS channels is less straightforward than for Meteosat because the AIRS spectrometer provides only few observations for a specific time. Model fields from several time steps are needed in order to accumulate a significant amount of collocated data. As a consequence, AIRS data are being passively monitored in the forecasting system (with ranges from 3 to 15 hours and at resolution 40 km), which takes the model data at observation time. Figure III.3 presents the corresponding global statistics of the differences between the prognostic model and the observation for the cloud-affected AIRS channels on 30 November 2002. Other periods have been investigated and very similar results to those from Figure III.3 have been obtained. For comparison, the wave-numbers covered by the MVIRI infrared filter functions are indicated in the legend of the figure. In addition Figure III.4 displays the fraction of the cloud-affected observed variance explained by the model.

For technical reasons, the diagnostic model cannot be used yet for passive monitoring in the forecasting system. As a consequence, diagnostic and prognostic brightness temperature are compared independently to

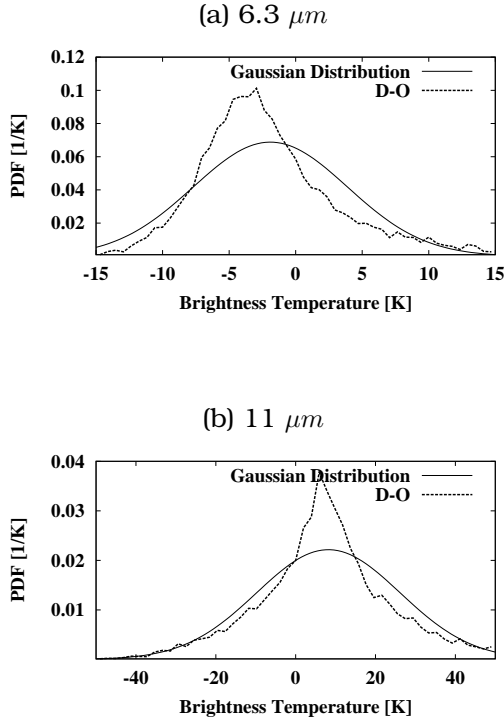


FIG. III.2 – Probability density function (PDF) of the departures between diagnostic-model (D) and observed (O) MVIRI 6.3 and 11 μm brightness temperatures in the Meteosat-7 cloudy quadrants of 30 November 2002 at 12 UTC. The Gaussian distributions with the same means and standard deviations are also reported on the graphs.

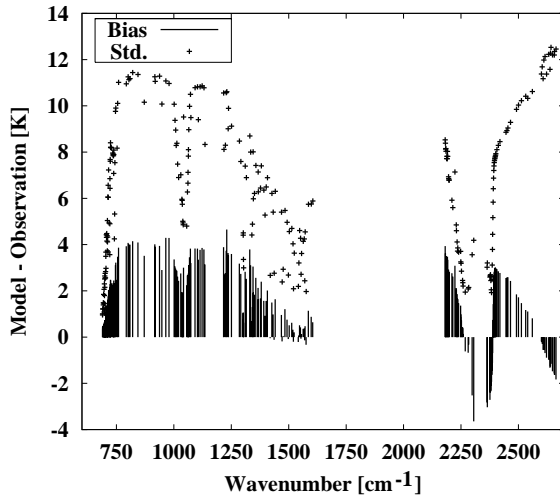


FIG. III.3 – Bias and standard deviation of the differences between the model and the cloud-affected observed AIRS brightness temperatures on 30 November 2002. The model uses the prognostic cloud scheme. Above 2000 cm^{-1} day-time pixels are discarded. For comparison, the filter functions of the infrared MVIRI channel cover wavenumbers between 1351 and 1818 cm^{-1} around 6.3 μm and those between 770 and 976 cm^{-1} around 11 μm .

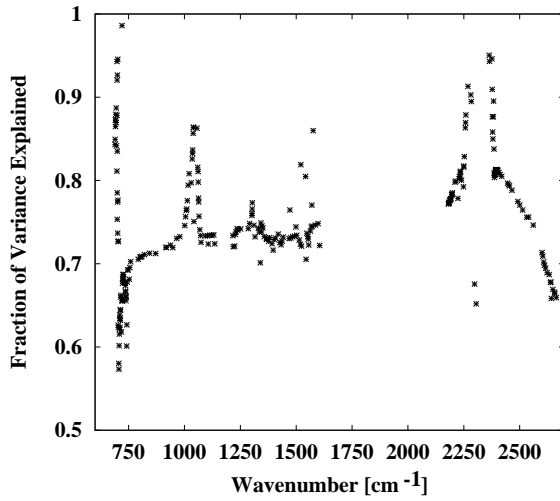


FIG. III.4 – Fraction of observation variance explained by the model for the cloud-affected AIRS data on 30 November 2002. The model uses the prognostic cloud scheme.

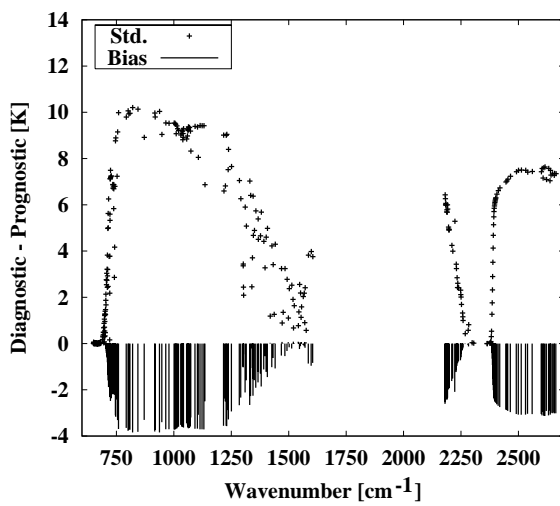


FIG. III.5 – Bias and standard deviation of the differences between the model diagnostic and prognostic AIRS brightness temperatures. Model data correspond the Meteosat-7 disk on 30 November 2002 at 12 UTC. Clear points are removed using the Meteosat-7 cloud detection. In contrast to Figure III.3, stratospheric channels are not removed.

the real AIRS data, using the Meteosat-7 $6.3 \mu\text{m}$ cloud mask for 30 November 2002 at 12 UTC. For each cloud-affected quadrant, equivalent AIRS brightness temperatures are computed using the diagnostic and the prognostic scheme. Rather than using a constant zenith angle, the Meteosat-7 angle is used. Corresponding statistics are presented in Figure III.5.

From Figure III.3, it is obvious that the model statistics are the best in the channels least affected by clouds. Biases are mainly positive, showing that the model underestimates the cloud radiative forcing, consistent with the Meteosat validation and with previous studies (e.g. Chevallier et al. 2001). A different behaviour occurs for the near-infrared channels above 2500 cm^{-1} . Although they are window channels, the bias reduces with increasing wavenumber and finally changes sign. This is likely caused by the absence of cloud scattering and/or of cloud reflection in the radiation model. Large negative values occur around 2300 cm^{-1} for cloud-affected and for clear channels (McNally 2003, personal communication) and are being investigated. The fraction of variance explained by the model is much higher than for the Meteosat comparison (mentioned in Section III.2.4) despite the discrepancy between the observation and the model resolutions (respectively 13 km at nadir and 40 km), which did not happen with Meteosat RDC. This apparent contradiction actually reflects the different orbits of the two instruments. Indeed mid-latitudes are better modelled than the Tropics, in particular over land, which favours the AIRS-based statistics. For instance, if the latitudes within 30° of the Equator are removed from the Meteosat statistics, the fraction of variance explained by the prognostic model reaches 0.66 and 0.89 at $6.3 \mu\text{m}$ and $11 \mu\text{m}$ respectively.

Since the diagnostic model has been tuned to radiation observations, the biases between diagnostic and prognostic brightness temperatures nearly cancel the biases between pro-

gnostic ones and observations (Figure III.5). Standard deviations are slightly smaller between the two models than with observations, but are here much smaller than the observation “random” variations (not shown).

III.2.5 Linearity of the observation operator

The linearity assumption is tested here for perturbations $\delta\mathbf{x} = \mathbf{x} - \mathbf{x}^b$, that are of the order of magnitude expected in 4D-Var, i.e. comparable to the background errors. Consequently, the perturbations are defined based on the principal components of the ECMWF operational background error matrix \mathbf{B} (Rabier et al. 1998, Derber and Bouttier 1999). Temperature errors vary with latitude and humidity error statistics are a function of relative humidity. Temperature and humidity errors are un-coupled. One $\delta\mathbf{x}$ is then a Gaussian perturbation applied to all principal components at once. This ensures that \mathbf{B} is the covariance matrix of the perturbations.

The choice is made here to use the atmospheric profiles within the Meteosat-7 disk on 30 November 2002 at 12 UTC as a dataset sampling very diverse atmospheric conditions. For each cloud-affected quadrant, the correlation between the tangent-linear perturbations $\mathbf{H}\delta\mathbf{x}$ (where \mathbf{H} is the adjoint of the observation operator) to the AIRS brightness temperatures and the non-linear ones $\mathbf{H}[\mathbf{x}^b + \delta\mathbf{x}] - \mathbf{H}[\mathbf{x}^b]$ is computed using an ensemble of 100 perturbations. The zenith angle is set to that of Meteosat-7. The PDF of the correlations is shown for each channel in Figure III.6a. Stratospheric channels are easily identified because they correspond to the narrow PDFs close to unity, around wavenumbers 500 cm^{-1} and 2300 cm^{-1} . Channels that both have a sensitivity in the troposphere and systematically correspond to high correlations (e.g. above 0.85) can be found in the $H_2O \nu_2$ band (around 1500 cm^{-1}) and next to the stratospheric channels (in the lower-

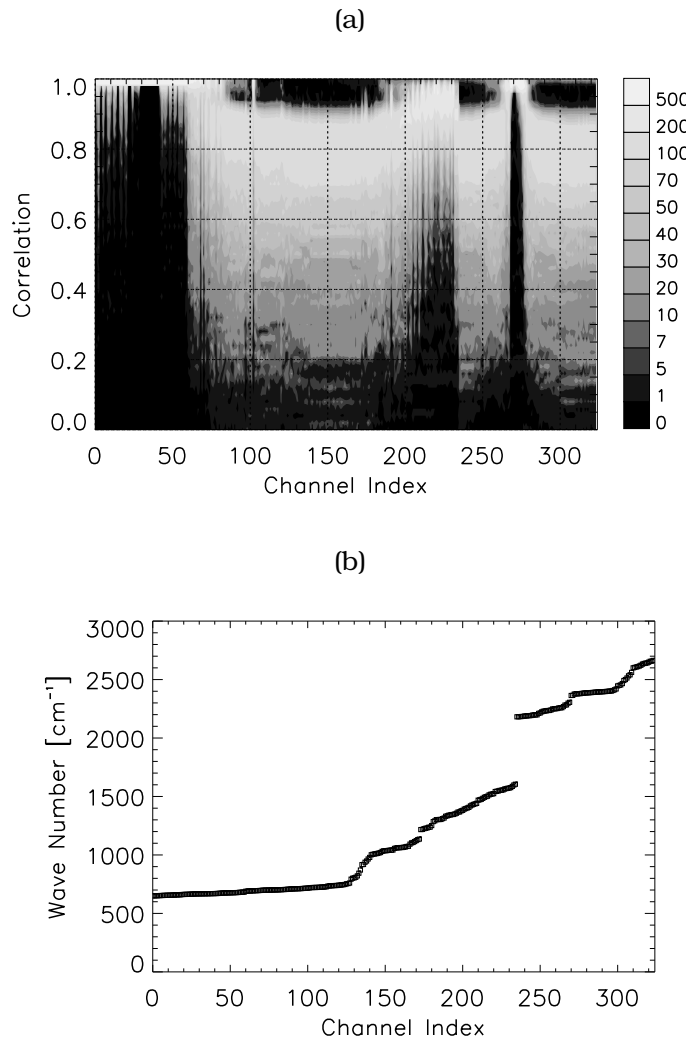


FIG. III.6 – Figure (a) presents the bi-dimensional histogram of the correlation between linear and non-linear brightness temperature perturbations for each one of the 324 AIRS channel subset. The input temperature and humidity perturbations follow the statistics of the ECMWF background error. Negative correlations are not represented. The correspondence between channel index and wave number is shown in Figure (b).

wavenumber part of the $CO_2 \nu_2$ band -around 700 cm^{-1} - and around 2250 cm^{-1}) only. Those few channels sound the upper troposphere only and are less affected by clouds. Channels with sensitivities lower down in the troposphere show high non-linear behaviours. Reducing the humidity perturbations by a factor of two only slightly increases the correlations (not shown). This indicates that improvements in the quality of the background in the forthcoming years are not likely to change the status of those channels with respect to linearity. Results for MVIRI, with high correlations at $6.3\text{ }\mu\text{m}$ and low at $11\text{ }\mu\text{m}$, do not bring additional information and are not reported here.

III.2.6 Application in one dimension

A 1D-Var scheme is used to illustrate the previous findings about the accuracy and the linearity of the infrared satellite radiances. The principle of the 1D-Var is similar to that of 4D-Var, but the control vector \mathbf{x} in Eq. III.1 represents only a single column and there is no time dimension. In the present case, the background \mathbf{x}_0^b comes from the ECMWF short-range forecasts, the observations \mathbf{y} are either the MVIRI $6.3\text{ }\mu\text{m}$ channel or 35 near-linear AIRS channels at 6.3 and $14.3\text{ }\mu\text{m}$ described below. Consistent with the present discussion, the forward operator is linearised around the background state \mathbf{x}_0^b during the 1D-Var minimisation. Background error statistics \mathbf{B} for the control variables (temperature and humidity) are the ones used in the ECMWF operational model. Observation error standard deviations in \mathbf{R} are defined conservatively from the departure statistics presented in Table III.1 for MVIRI and Figure III.3 for AIRS, as in section III.2.4. Error correlations of 0.8 are arbitrarily specified between AIRS channels. Observations are bias-corrected with respect to the background by removing the biases shown in Table III.1 for

Meteosat and Figures III.3 and III.5 for AIRS.

The 35 near-linear AIRS channels are selected among the subset of 324 from the following three quantitative criteria : the cloud impact on the brightness temperature (estimated from the model simulations) must be more than 0.5 K on an average, the correlations between linear and non-linear increments must exceed 0.85 (from Figure III.6), and the standard deviations of the differences between diagnosed and observed brightness temperatures (computed from the numbers in Figures III.3 and III.5 and simply assuming uncorrelation between each other) must be below 6 K . Further, $4.5\text{ }\mu\text{m}$ AIRS channels are not used here because of the solar radiation, but could be used during night-time. Among the 35, 13 channels are located about $14.3\text{ }\mu\text{m}$ and 22 channels are located about $6.3\text{ }\mu\text{m}$. At $6.3\text{ }\mu\text{m}$ water vapour absorption impedes cloud absorption and accurate linear channels can be found with lower weighting functions (i.e. which peak as low as about 400 hPa) than at $14.3\text{ }\mu\text{m}$.

The 1D-Var is applied to satellite radiances for November 2002 and February 2003, that have been collocated with 00 and 12 UTC operational radiosondes. AIRS radiances are processed only when cloudiness is detected in 22 channels at least among the 35 and MVIRI is used in cloudy quadrants only. Results are presented for collocations in the northern hemisphere mid-latitudes (between 30 and 70°N) and for $1.5\text{ hour} \times 80\text{ km}$ time-space windows. They actually mainly represent Europe because of the orbital characteristics of the satellites and of the location of the operational radiosondes. Inputs and outputs of the 1D-Var are compared with the collocated radiosondes in terms of relative humidity. For atmospheric temperatures below 243 K , only Vaisala RS90 radiosondes are used (Nash 2002).

1D-Var relative humidity increments reach a maximum at 350 and 400 hPa for MVIRI and AIRS respectively, with root mean square

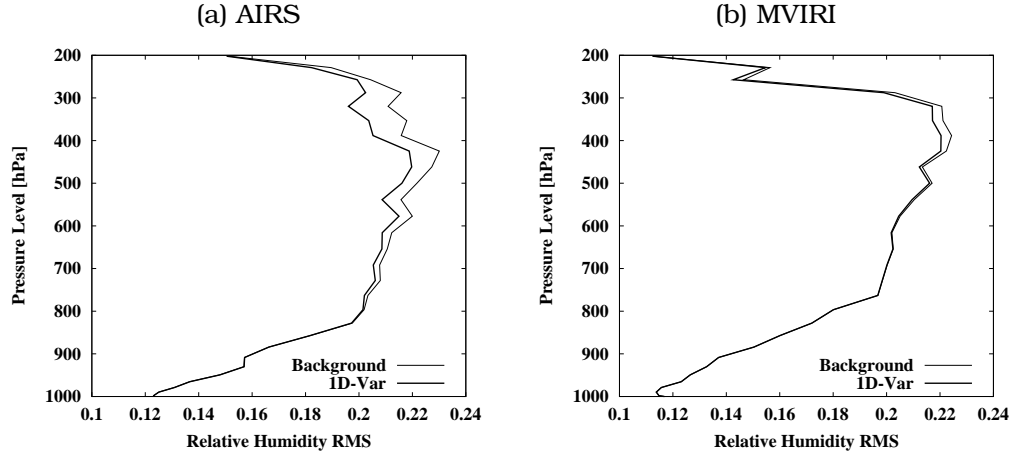


FIG. III.7 – Root mean square (RMS) difference between the model relative humidity and collocated radiosonde measurements for November 2002 and February 2003 in the northern hemisphere mid-latitudes. Relative humidity is defined between zero and one. The model profile is either the background or the 1D-Var retrieval. Assimilated observations are either 35 AIRS channels (a) or the MVIRI $6.3 \mu\text{m}$ (b). For AIRS, data are processed when cloudiness is detected in 22 channels at least among the 35. Cloudy MVIRI quadrants only are used in (b). In both cases, statistics include about 250 cases in the upper troposphere and about 1500 in the lower troposphere.

values of 0.017 and 0.10 respectively (not shown). Smaller increments are obtained from MVIRI since a single channel is used. Figure III.7 indicates that the 1D-Var method reduces the differences between the model upper tropospheric relative humidity and the radiosondes measurements by up to 0.005 for MVIRI and by up to 0.015 for AIRS. Interestingly, the difference reduction is about the same when cloud-free observations are processed with clear-sky R statistics and no cloud processes in the observation operator \mathbf{H} (not shown). Obviously, no perfect fit between the model and the observations can be achieved because of significant measurement and collocation errors. Most importantly, the high temporal frequency of the MVIRI images is not exploited by the 1D-Var but impacts the 4D-Var wind analysis significantly, as was demonstrated by the 4D-Var assimilation of MVIRI in the clear-sky quadrants (Köpken et al. 2003).

III.2.7 Conclusion

An observation operator has been developed, that computes cloud-affected satellite brightness temperatures from some of the ECMWF 4D-Var control variables : temperature, humidity and ozone profiles, surface temperature and surface pressure. It comprises a diagnostic cloud scheme with a representation of large-scale and convective processes and a radiation model. In order to evaluate the capability of 4D-Var systems to handle satellite infrared observations in the presence of clouds, its accuracy and its linearity have been assessed. Results have been illustrated within a 1D-Var framework.

A first important result of the present study concerns the diagnostic cloud scheme. It is expected not to perform as well as the prognostic scheme in dynamic mode for long integrations, but in static mode the comparison between model and observations was not qualitatively sensitive to whether the diagnostic model or the reference prognostic cloud scheme is used. Both explain a significant

portion of the observation variance, except, for both, in the Tropics at $11\ \mu m$. The diagnostic scheme explains a slightly lower portion of the variance, but has smaller biases due to different tuning. Further, the two schemes should have similar sensitivities, since one of them is a simplified version of the other one (this aspect will be documented elsewhere). As a consequence, it seems that the diagnostic model could be used in the 4D-Var observation operator in lieu of the prognostic model, which would avoid the introduction of cloud variables in the 4D-Var control vector.

Secondly, it is clear that the channels that are the most impacted by clouds are very non-linear for perturbations of the order of the current background errors in global NWP. They cannot be processed directly within the current ECMWF 4D-Var system, where only weak non-linearities are tolerated. In addition large errors were shown for these channels, both in terms of bias (which could be removed) and of standard deviations. Non-linearities actually reveal the deficiency of the NWP background in resolving the ambiguity of the cloud-affected radiances in terms of temperature and humidity information. These observations can be pre-processed by a local non-linear retrieval method, as is done for the geostationary atmospheric motion vectors (e.g. Schmetz et al. 1993).

In contrast, the observation operator showed much more linear and accurate behaviour for some of the upper tropospheric channels, at 4.5 , 6.3 and $14.3\ \mu m$. It is worth emphasising two features of the approach. First, accuracy is achieved in these channels despite a lower spatial resolution compared to the observations, which seems to indicate that the representativeness error is not a significant issue here. Second, the focus is on temperature and humidity fields and not on cloud variables, since the latter are diagnosed from the former. An obvious advantage is that temperature and humidity analysis increments are likely to improve the forecast

far away from the analysis (e.g. Marécal and Mahfouf 2002). On the other hand, the accuracy of the present observation operator is still limited and only part of the information of the observations can be extracted.

The conclusion of our assessment is that there is a potential benefit in assimilating cloud-affected satellite radiances at 4.5 , 6.3 and $14.3\ \mu m$, for instance the $6.3\ \mu m$ channel on-board all the geostationary satellites, *directly in 4D-Var*. This would avoid blending 4D-Var and local retrieval methods to exploit these channels in the presence of cirriform clouds. Scientific developments to the current 4D-Var systems may still be needed, for instance to improve the estimation of background error statistics, or to harmonize the resolution of the observations and the variable model resolutions within the incremental formulation. This is a concern for all types of assimilated observations.

A similar study will be performed for a selection of microwave channels in the presence of clouds and rain (Moreau et al. 2003). Channels in strong water vapour absorption bands, for instance at $22.235\ GHz$ or $183.31\ GHz$, are well modelled (Chevallier and Bauer 2003) and may be sufficiently linear for direct 3D- or 4D-Var assimilation.

Acknowledgments. This work was done in the context of the Satellite Application Facility on Numerical Weather prediction which is co-sponsored by EUMETSAT. M. Doutriaux-Boucher at EUMETSAT coordinated the set-up of the Radiance Data from Clouds product. The kind help from P. Watts and A. McNally (ECMWF) in dealing with the AIRS data was very much appreciated. Comments from E. Andersson, A. Hollingsworth, A. Simmons and J.-N. Thépaut at ECMWF, from R. W. Saunders at the Met Office and from one anonymous reviewer helped to improve the discussion.

References

- Chevallier, F., Bauer, P., Kelly, G., Jakob, C. and McNally, T., 2001 : Model clouds over oceans as seen from space : Comparison with HIRS/2 and MSU radiances. *J. Climate*, **14**, 4216–4229
- Chevallier, F. and Kelly, G., 2002 : Model clouds as seen from space : comparison with geostationary imagery in the 11 μm channel. *Mon. Wea. Rev.*, **130**, 712–722
- Chevallier, F., Bauer, P., Mahfouf, J.-F. and Morcrette, J.-J., 2002 : Variational retrieval of cloud profile from ATOVS observations. *Q. J. R. Meteor. Soc.*, **128**, 2511–2526
- Chevallier, F. and Bauer, P., 2003 : Model rain and clouds over oceans : comparison with SSM/I observations. *Mon. Wea. Rev.*, **131**, 1240–1255
- Courtier, P., Thépaut, J.-N. and Hollingsworth, A., 1994 : A strategy for operational implementation of 4D-Var, using an incremental approach. *Q. J. Roy. Meteor. Soc.*, **120**, 1367–1388
- Dee, D. P. and da Silva, A. M., 2003 : The choice of variable for atmospheric moisture analysis. *Mon. Wea. Rev.*, **131**, 155–171
- Derber, J. and Bouttier, F., 1999 : A reformulation of the background error covariance in the ECMWF global data assimilation system. *Tellus*, **40A**, 1–25
- Eyre, J. R., 1991 : A fast radiative transfer model for satellite sounding systems'. ECMWF Technical Memorandum, 176
- Harris, B. A. and Kelly, G., 2001 : A Satellite Radiance Bias Correction Scheme for Radiance Assimilation. *Q. J. Roy. Meteor. Soc.*, **127**, 1453–1468
- Ide, K., Courtier, P., Ghil, M. and Lorenc, A., 1997 : Unified notation for data assimilation : Operational, sequential and variational. *J. Met. Soc. Japan*, **75**, 181–189
- Janisková, M., Mahfouf, J.-F., Morcrette, J.-J. and Chevallier, F., 2002 : Linearized radiation and cloud schemes in the ECMWF model : development and evaluation. *Q. J. R. Meteor. Soc.*, **128**, 1505–1528
- Köpken, C., Thépaut, J.-N. and Kelly, G. A., 2003 : Assimilation of Geostationary WV Radiances from GOES and Meteosat at ECMWF. EUMETSAT/ECMWF Fellowship Programme Research Report, 14.
- Lorenc, A. C., Ballard, S. P., Bell, R.S., Ingleby, N. B., Andrews, P. L. F., Barker, D. M., Bray, J. R., Clayton, A. M., Dalby, T., Li, D., Payne, T. J. and F. W. Saunders, 2000 : The Met. Office global three-dimensional variational data assimilation scheme. *Q. J. R. Meteor. Soc.*, **126**, 2991–3012
- Marécal, V. and Mahfouf, J.-F., 2002 : Four dimensional variational assimilation of total column water vapor in rainy areas. *Mon. Wea. Rev.*, **130**, 43–58
- McNally, A. P., 2002 : A note on the occurrence of cloud in meteorologically sensitive areas and the implications for advanced infrared sounders. *Q. J. Roy. Meteor. Soc.*, **585**, 2551–2556
- McNally, A. P. and Watts, P. D., 2003 : A cloud detection algorithm for high spectral resolution infrared sounders. *Q. J. Roy. Meteor. Soc.*, in press
- Moreau, E., Bauer, P. and Chevallier, F., 2003 : Variational retrieval of rain profiles from spaceborne passive microwave radiance observations. *J. Geophys. Res.*, **108(D16)**, 4521, doi :10.1029/2002JD003315
- Moreau, E., Lopez, P., Bauer, P., Tompkins, A. M., Janisková, M. and Chevallier, F., 2003 : Variational retrieval of temperature and humidity profiles using rain rates versus microwave brightness temperatures'. ECMWF Technical Memorandum, 412, submitted to *Q. J. R. Meteor. Soc.*
- Nash, J., 2003 : Review of test results on the accuracy of radiosonde relative humidity sensors. ECMWF/GEWEX workshop on humidity analysis, 8-11 July 2002, ECMWF, 117–123.'
- Rabier, F., McNally, A. P., Andersson, E., Courtier, P., Undén, P., Eyre, J., Hollingsworth, A., and Bouttier, F., 1998 : The ECMWF implementation of three dimensional variational assimilation (3D-Var). Part II : Structure functions. *Q. J. Roy. Meteor. Soc.*, **124**, 1809–1829
- Rabier, F., Järvinen, H., Klinker, E., Mahfouf, J.-F. and Simmons, A., 2000 : The ECMWF operational implementation of four dimensional variational assimilation. Part I : Experimental results with simplified physics. *Q. J. Roy. Meteor. Soc.*, 1143–1170
- Räisänen, P., 1998 : Effective longwave cloud fraction and maximum-random overlap clouds - a problem and a solution. *Mon. Wea. Rev.*, **126**, 3336–3340

- Saunders, R. W., Brunel, P., Chevallier, F., Deblonde, G., English, S. J., Matriardi, M. and Rayer, P. J., 2002 : RTTOV-7 - Science and validation report'. The Met Office, Forecasting Research Technical Report, 387, available from URL http://www.metoffice.com/research/nwp/publications/papers/technical_reports/sa.html
- Schmetz, J. and Turpenheim, O., 1988 : Estimation of the upper-tropospheric relative humidity field from METEOSAT water vapor image data. *J. Appl. Meteor.*, **27**, 889–899
- Schmetz, J., Holmlund, K., Hoffman, J., Strauss, B., Mason, B., Gaertner, V., Koch, A. and Van De Berg, L., 1993 : Operational cloud-motion winds from Meteosat infrared images. *J. Appl. Meteor.*, **32**, 1206–1225
- Simpson, J. and Wiggert, V., 1969 : Models of precipitating cumulus towers. *Mon. Weather Rev.*, **97**, 471–489
- Stokes, G. M., and Schwartz, S. E., 1994 : The Atmospheric Radiation Measurement (ARM) Program : programmatic background and design of the cloud and radiation testbed. *Bull. Amer. Meteo. Soc.*, **75**, 1201–1221
- Tiedtke, M., 1989 : A comprehensive massflux scheme for cumulus parametrization in large-scale models. *Mon. Wea. Rev.*, **117**, 1779–1800
- Tiedtke, M., 1993 : Representation of clouds in large-scale models. *Mon. Wea. Rev.*, **121**, 3040–3061
- Tompkins, A. M. and Janisková, M., 2003 : A cloud scheme for data assimilation : description and initial tests'. ECMWF Technical Memorandum, 410, submitted to *Q. J. R. Meteor. Soc.*

III.3 Choix d'observations informatives

Cette section reprend l'article de Chevallier et coll. (2005a) paru dans *Geophysical Research Letters*.

The Contribution of AIRS Data to the Estimation of CO₂ Sources and Sinks

Frédéric Chevallier
Laboratoire des Sciences du Climat et de l'Environnement
CEA-CNRS, IPSL, Gif-sur-Yvette, France

Richard J. Engelen
European Centre for Medium-Range Weather Forecasts
Reading, UK

Philippe Peylin
Laboratoire de Biogochimie des Milieux Continentaux
INRA-CNRS-UPMC, INRA-INAPG, Thivernal-Grignon, France

Abstract. The analysis of radiance measurements from the Atmospheric Infra-Red Sounder (AIRS) has been providing the first global maps of CO₂ concentrations in the cloud-free upper troposphere. This paper explores the usefulness of this data for the estimation of CO₂ surface

fluxes. It appears that atmospheric mixing makes the upper tropospheric CO₂ concentrations rather zonal, which indicates that AIRS data inform about very broad features of the surface fluxes only. Further, such a small variability imposes a stringent constraint on the size of retrieval biases and of transport model biases for the estimation of CO₂ surface fluxes. We show that latitude-dependent biases larger than a few tenths of a particle per million (ppm), at least south of 25°N, would harm the inversions. Significant improvements to the concentration retrieval algorithms and to the transport models are a prerequisite for the inversion of surface fluxes from AIRS.

III.3.1 Introduction

Satellite data play an outstanding role in the monitoring of the Earth atmosphere, not only for numerical weather prediction, but also for the study of chemical compounds, like ozone or carbon monoxide. However, no satellite instrument is yet operational, that was designed for the observation of CO₂. The CO₂-dedicated Orbiting Carbon Observatory (OCO) and the Greenhouse gases Observing Satellite (GOSAT) will not be launched until 2008. In the mean time, expectations have risen based on theoretical studies (Rayner and O'Brien 2001, Houweling et al. 2004) and on the retrieval of CO₂ concentrations from existing instruments built for other purposes than CO₂ mapping (e.g. Chedin et al. 2003) despite the entanglement of many signals in the satellite radiances (e.g., Houweling et al. 2005). In particular, the high spectral resolution of the Atmospheric Infra-Red Sounder (AIRS) flown on-board the National Aeronautics and Space Administration's (NASA) Aqua platform provides significant information about the CO₂ concentration in the upper troposphere (Engelen and Stephens 2004). This instrument has been operated since 2002 and CO₂ retrieval algorithms have been developed at several institutes (Crevoisier et al. 2004, Engelen et al. 2004, Chahine et al. 2005). This study is the first one to consider the potential utility of such retrievals to infer surface fluxes based on real data. Our analysis is based on the comparison between the AIRS retrievals produced at the European Centre for Medium-Range Weather Forecasts (ECMWF) and the

CO₂ concentrations simulated by the global climate model of the Laboratoire de M^{eteorologie Dynamique} (LMDZ, Sadourny and Laval 1984, Hourdin and Armengaud 1999) using surface fluxes from a climatology.

III.3.2 Inferring CO₂ surface fluxes

Up to now, Bayesian inference has guided the works on the estimation of CO₂ surface fluxes at the global scale (e.g., Gurney et al. 2002). Let x be a vector of discretized CO₂ surface fluxes. Under the assumptions of unbiased Gaussian error statistics, theory indicates that the most probable values of x 's components, given some prior fluxes (or background) x^b and some measurements of CO₂ concentrations y , can be expressed as (e.g. Rodgers 2000) :

$$x^a = x^b + BH^T(HBH^T + R)^{-1}(y - Hx^b) \quad (\text{III.6})$$

where R and B are the error covariance matrices of the observations and of the background respectively, and H is the transport model that simulates the observations from the surface fluxes x . Expressions equivalent to Equation III.6 also exist, that provide alternate numerical approaches to compute the same optimal solution. In this study, the LMDZ model, guided by ECMWF meteorological analyses, is the H operator. A detailed evaluation of the realism of the LMDZ model for the simulation of atmospheric chemistry is given by Hauglustaine and coauthors (2004). For the present application of LMDZ, tracer large-scale advection and subgrid-scale

transport is solved on a regular $3.75^\circ \times 2.5^\circ$ (longitude-latitude) grid with 19 sigma-pressure layers in the vertical.

III.3.3 Data sources

The data assimilation system at ECMWF has been primarily designed to analyze atmospheric variables of direct meteorological significance, like temperature and winds. CO₂ has been recently added to the list of the analysis variables, as described by Engelen and coauthors (2004, 2005). The CO₂ analysis is directly controlled by the radiances from the AIRS instrument and benefits from the quality of the other analyzed variables, like temperature, ozone and humidity, that also affect the AIRS measurements. The CO₂ analysis is currently restricted to the ECMWF model grid points collocated with the AIRS observations during the assimilation window. For each one of these grid points, a limited set of 18 channels is used to estimate one column value for the upper troposphere above about 600hPa. In the presence of a cloud in the upper or in the middle troposphere, less channels are used and the retrieval only covers the tropospheric column above the cloud top. The horizontal resolution of the CO₂ retrievals is about that of the instrument : 13.5 km at nadir and $41 \times 23 \text{ km}^2$ at the end of the scans. The data processed here include the 16 million retrievals from year 2003 for which all 18 channels were available (i.e. no cloud above the boundary layer). Note that ECMWF receives one AIRS spot every nine only and in principle more retrievals could be obtained.

For background information, we use a climatology of carbon fluxes, that include anthropogenic and natural components. Fossil fuel CO₂ emissions are from the EDGAR3.0 emission database (Olivier et al. 1996). Air-sea CO₂ exchange is prescribed from the climatology by Takahashi and colleagues (2002) with a sink of 1.8 Gt C per year. The biosphere-atmosphere exchange of CO₂ is estimated by the Terrestrial Uptake and Release

of Carbon (TURC) model (Lafont et al. 2002), which is annually balanced. The daily fluxes calculated by TURC have been redistributed throughout the day to account for the diurnal cycle of the fluxes. The CO₂ concentrations at the initial time step of the time window are defined from a simulation using optimized fluxes (Bousquet et al. 2000).

In order to remove the global bias from the inference system (that may come from the observations or from the background), we calculate an offset of the atmospheric CO₂ concentrations by subtracting the mean of the departure statistics ($y - Hx^b$) from the prior concentrations at the initial step of the time window.

III.3.4 Results

To compare the LMDZ simulations with the individual AIRS observations, the modelled concentration profiles are first extracted at the same date, time and location as the retrievals. LMDZ upper tropospheric CO₂ columns are then defined by convolving the profiles using a typical AIRS weighting function. It peaks at about 200hPa, with a negligible contribution from the atmosphere below 500hPa. For consistency with the definition of the ECMWF retrieval, which excludes the stratosphere, the stratospheric part of the weighting function is set to zero individually for each situation. Last, in order to take the influence of the prior information on the retrievals into account, the model values and the prior value are combined using the averaging kernel of each retrieval (e.g. Rodgers and Connor 2003).

Figures III.8 and III.9 illustrate the comparison between the simulation using the prior fluxes and the AIRS observations. They condense the information in terms of seasonal cycles (Figure III.8) and of zonal means (Figure III.9). They show that the datasets share some common features in the tropics, where they both describe a similar seasonal cycle. Large systematic differences (i.e. up to a few ppm) appear at higher latitudes, with a signi-

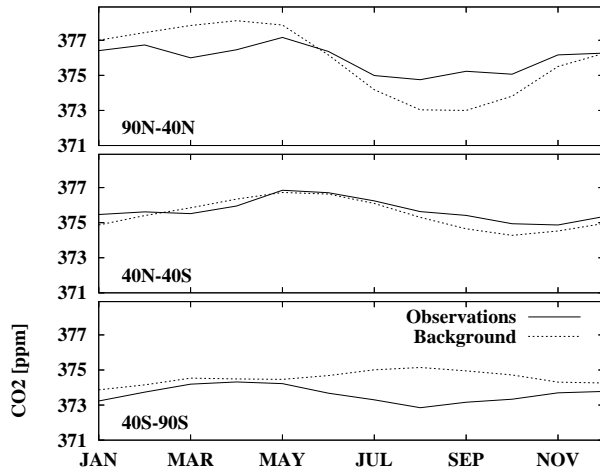


FIG. III.8 – Monthly mean of the upper tropospheric CO₂ concentrations in the background and in the AIRS observations in three latitude bands. Note that individual estimates have been averaged unweighted, although the density of the observations increases towards the poles.

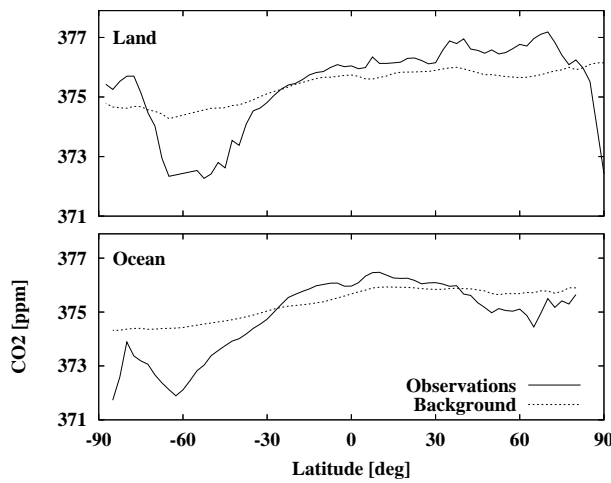


FIG. III.9 – Zonal annual mean of the upper tropospheric CO₂ concentrations in the background and in the AIRS observations over land and ocean.

ficant land vs. sea contrast in the observations, that does not exist in the model. The differences out of the tropics are not surprising, since lower tropopause heights and smaller temperature lapse rates make the retrievals less reliable there (Engelen et al. 2004). The simplicity of the weighting function with which the model is convolved may also contribute to the biases. This aspect is currently under investigation.

The analysis of the variability of the individual estimates from the two datasets is particularly informative for flux inversions. This study focusses on the data variability as a function of latitude. Regional variability could be discussed similarly. As shown in Figure III.10, the model displays a north-south gradient of variability with a standard deviation less than 3ppm. The AIRS estimates behave differently. Their standard deviation is about 3.7ppm within 25° from the equator and rises above 6ppm at high latitudes, similarly in both hemispheres. This standard deviation actually results from the retrieval error superposed upon the natural variations of CO₂. As for the model, its relatively coarse resolution is expected to smooth the simulated variability, but there are good reasons to trust its latitudinal variations, that are based on known differences in vegetation, fossil fuel emission and transport. For the observations, the retrieval accuracy diminishes from the equator to the poles (Engelen et al. 2004). The bowl-shaped curve in Figure III.10 seems to indicate that the retrieval variability is dominated by the retrieval error and that the natural variability of CO₂ does not exceed a couple of ppm, at least south of 25° N. For comparison, the model variability at the surface in the tropics is five times larger than in the upper troposphere. The reduced upper tropospheric variability improves the representativeness of measurements there. On the other hand, such measurements can only constrain the broad scales of the surface fluxes.

From Equation III.6, one may notice that

the Bayesian analysis increments $x^a - x^b$ simply equal the observation-minus-background departures $d = (y - Hx^b)$ weighted by the gain matrix $K = BH^T(HBH^T + R)^{-1}$. The linear dependency of the increments as a function of the departures means that observations harm the inversion (i.e. the analysis x^a is worse than the background x^b) if they are fraught with biases of the order of these departures. A poor estimate of the gain matrix K or a biased background x^b degrades the analysis as well, but this is a separate issue. Owing to the small values of the model variability versus the AIRS one, the standard deviation of the departures d is about that of the observations. With departures standard deviations about 4ppm in the tropics, biases should be less than about 0.4ppm (i.e. one order of magnitude less than the departures) to have negligible impact on the flux inversion. Larger biases can be tolerated at higher latitudes only due to larger departures there. Now, in Equation III.6 the observation error is measured with respect to the forward model H , which is assumed to be perfect. It therefore combines the actual forward model errors, the representativeness errors of the measurements and the retrieval errors. Ensuring its biases to be not larger than a few tenth of ppm in a latitude band is particularly challenging. On the retrieval side, this may be achieved by processing the AIRS channels with more complementary information about temperature, aerosols and clouds. On the model side, the quality of the subgrid parameterization (boundary layer turbulence and moist convection) is essential. The bias requirement needs to be re-evaluated when more retrieval datasets are available, but improvements to the retrieval algorithms usually reduce the variability of the products together with their errors.

III.3.5 Conclusion

The prominent role of carbon dioxide in the energy balance of the Earth system makes it

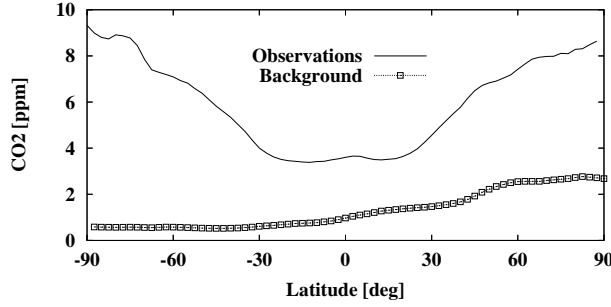


FIG. III.10 – Standard deviations of the individual AIRS observations and of the individual background concentrations, per latitude band.

important to monitor the temporal and the spatial variations of its concentration in the atmosphere. For the first time, global maps of CO₂ in the upper troposphere are available from remote sensing. They are of direct relevance for the evaluation of transport models, in addition to the high quality but sparse aircraft measurements. The comparison between the AIRS retrievals and a simulation using the LMDZ transport model shows some agreement in terms of broad geographical and temporal features in the tropics only. A more detailed analysis will be reported elsewhere (Tiwari et al., manuscript in preparation). Together with the retrievals of carbon monoxide (McMillan et al. 2004) and of methane, the AIRS data may also contribute to the understanding of extreme events, like plumes from biomass-burning. However, from the current version of the AIRS retrievals at ECMWF, CO₂ concentrations in the upper troposphere appear to follow a rather zonal structure with variations usually less than 2 ppm at any given latitude south of 25°N. This weak variability makes it fundamental that latitude-dependent biases are kept within a few tenths of ppm in this portion of the world for quantitative use of the concentration retrievals, in particular for assimilation in a transport model. Upper bounds for the regional biases could be investigated in a similar way. The small variability highlights the limited information brought by high altitude concentrations on surface fluxes and

indicates that only the very broad scales can be constrained. From the previous analysis, it is not surprising that the surface fluxes inverted with the AIRS data have not proved to be of particularly good quality so far (result not shown). A better situation is expected when accurate estimates of CO₂ that include the boundary layer are available, for instance from OCO and GOSAT (e.g. Rayner and O'Brien 2001).

Acknowledgments. Authors wish to thank P. Bousquet, F.-M. Bréon, P. Ciais and P. Rayner for fruitful interactions, and F. Marabelle for computer support. This study was co-funded by the European Union under the project GEMS. C. Barnet (NOAA/NESDIS) and one anonymous reviewer provided constructive comments on an earlier version of this paper.

References

- Bousquet, P., P. Peylin, P. Ciais, C. Quere, P. Friedlingstein, and P. Tans (2000), Regional changes in carbon dioxide fluxes of land and oceans since 1980, *Science*, 290, 1342-1346.
- Chahine, M., C. Barnet, E.T. Olson, L. Chen, and E. Maddy (2005) On the determination of atmospheric minor gases by the method of vanishing partial derivatives with application to CO₂. *Geophys. Res. Lett.*, in press.
- Chédin, A., S. Serrar, N. A. Scott, C. Crevoisier, and R. Armante (2003), First global measurement of midtropospheric CO₂ from NOAA polar satellites : Tropical zone, *J. Geophys. Res.*, 108, doi :10.1029/2003JD003439.
- Crevoisier C., S. Heilliette, A. Chédin, S. Serrar, R. Armante, and N. A. Scott (2004), Midtropospheric CO₂ concentration retrieval from AIRS observations in the tropics, *Geophys. Res. Lett.*, 31, doi :10.1029/2004GL020141.
- Engelen, R. J., E. Andersson, F. Chevallier, A. Hollingsworth, M. Matricardi, A. P. McNally, J.-N. Thpaut, and P. D. Watts (2004), Estimating atmospheric CO₂ from advanced infrared satellite radiances within an operational 4D-Var data assimilation system : methodology and first results. *J. Geophys. Res.*, 109, D19309, doi :10.1029/2004JD004777.
- Engelen, R. J., and G. L. Stephens (2004), Information content of infrared satellite sounding measurements with respect to CO₂. *J. Appl. Meteor.*, 43, 373-378.
- Engelen, R. J. and A. P. McNally (2005), Estimating atmospheric CO₂ from advanced infrared satellite radiances within an operational 4D-Var data assimilation system : results and validation, *J. Geophys. Res.*, in press.
- Gurney, K. R., R. M. Law, A. S. Denning, P. J. Rayner, D. Baker, P. Bousquet, L. Bruhwiler, Y. H. Chen, P. Ciais, S. Fan, I. Fung, M. Gloor, M. Heimann, K. Higuchi, J. John, T. Maki, S. Maksyutov, K. Masarie, P. Peylin, M. Prather, B. C. Pak, J. Randerson, J. Sarmiento, J., S. Taguchi, T. Takahashi, and C. W. Yuen (2002), Towards robust regional estimates of CO₂ sources and sinks using atmospheric transport models, *Nature*, 415 :6872, 626-630.
- Hauglustaine, D.A., F. Hourdin, L. Jourdain, M.-A. Filiberti, S. Walters, J.-F. Lamarque and E.A. Holland (2004). Interactive chemistry in the Laboratoire de Mtorologie Dynamique general circulation model : Description and background tropospheric chemistry evaluation. *Journal of Geophysical Research* 109(D4), doi :10.1029/2003JD003957.
- Hourdin, F., and A. Armengaud (1999), Test of a hierarchy of finite-volume schemes for transport of trace species in an atmospheric general circulation model. *Mon. Wea. Rev.*, 127, 822-837.
- Houweling, S., F.-M. Bréon, I. Aben, C. Rödenbeck, M. Gloor, M. Heimann, and P. Ciais (2004), Inverse modeling of CO₂ sources and sinks using satellite data : a synthetic inter-comparison of measurement techniques and their performance as a function of space and time. *Atmos. Chem. Phys.*, 4, 523-538.
- Houweling, S., W. Hartmann, I. Aben, H. Schrijver, J. Skidmore, G.-J. Roelofs, and F.-M. Bron (2005), Evidence of systematic errors in SCIAMACHY-observed CO₂ due to aerosols. *Atmos. Chem. Phys. Disc.*, 5, 3313-3340.
- Lafont, S., L. Kergoat, G. Dedieu, A. Chevillard, E. Kjellstrm, U. Karstens, and O. Kolle (2002), Spatial and temporal variability of land CO₂ fluxes estimated with remote sensing and analysis data over western Eurasia, *Tellus*, 54B, 820-833.
- McMillan, W. W., C. Barnet, L. Strow, M. T. Chahine, M. L. McCourt, J. X. Warner, P. C. Novelli, S. Korontzi, E. S. Maddy, and S. Datta (2005), Daily global maps of carbon monoxide from NASA's Atmospheric Infrared Sounder, *Geophys. Res. Lett.*, 32, L11801, doi :10.1029/2004GL021821.
- Olivier, J. G. J., A. F. Bouwman, C. W. M. Van der Maas, J. J. M. Berdowski, C. Veldt, J. P. J. Bloos, A. J. H. Visschedijk, P. Y. J. Zandyelt, and J. L. Haverlag (1996), Description of EDGAR Version 2.0. A set of global emission inventories of greenhouse gases and ozone-depleting substances for all anthropogenic and most natural sources on a per country basis and on 1x1 grid, RIVM/TNO report, December 1996. RIVM, Bilthoven, RIVM report nr. 771060 002. [TNO MEP report nr. R96/119].

- Rayner, P. J., and D. M. O'Brien (2001), The utility of remotely sensed CO₂ concentration data in surface source inversions, *Geophys. Res. Lett.*, 28, 175-178.
- Rodgers, C. D. (2000) : Inverse methods for atmospheric sounding : theory and practice, World Scientific, 238 pp.
- Rodgers, C. D., and B. J. Connor (2003), Intercomparison of remote sounding instruments, *J. Geophys. Res.*, 108(D3), 4116, doi :10.1029/2002JD002299.
- Sadourny, R., and K. Laval (1984), January and July performance of the LMD general circulation model, In *New Perspectives in Climate Modeling*, A.L. Bergerand C. Nicolis (eds.), Elsevier Press, Amsterdam, 173-197.
- Takahashi, T., S. C. Sutherland, C. Sweeney, A. Poisson, N. Metzl, B. Tilbrook, N. Bates, R. Wanninkhof, R. A. Feely, C. Sabine, J. Olafsson and Y. Nojiri (2002), Global Sea-Air CO₂ Flux Based on Climatological Surface Ocean pCO₂, and Seasonal Biological and Temperature Effect, *Deep Sea Res. II*, 49, 1601-1622.

III.4 Impact des corrélations entre les erreurs

Cette section reprend l'article de Chevallier (2007) paru dans *Geophysical Research Letters*.

Impact of Correlated Observation Errors on Inverted CO₂ Surface Fluxes from OCO Measurements

Frédéric Chevallier

Laboratoire des Sciences du Climat et de l'Environnement
Institut Pierre-Simon Laplace
Gif-sur-Yvette, France

Abstract. Proper assignment of error statistics is essential in the field of Bayesian inference. This paper studies the impact of correlated observation errors in the case of the estimation of CO₂ surface fluxes from NASA's forthcoming Orbiting Carbon Observatory (OCO). Using a series of observation simulation system experiments, it is shown that hypothetical observation error correlations of 0.5 in neighbouring observations have a rather limited impact on the accuracy of the inverted fluxes when they are correctly taken into account. The information loss induced by commonly-used approximate treatments of the observation error correlations (neglecting, observation thinning and error inflating), that are computationally more efficient, is quantified. Error inflation has the least detrimental impact among the suboptimal set-ups and limits the loss in uncertainty reduction to a few per cent, in spite of its very low reduced chi-squared.

III.4.1 Introduction

Statistical inference systems are vulnerable to any structure in their random variables that is not well accounted for. Systematic errors, or biases, are a prominent example of such structures and receive much attention. Error correlations are another ex-

pression of organized patterns in the inference systems. A proper inference system should link correlated information pieces and weight them properly. For instance, correlated errors in the prior information reduce the effective dimension of the inversion problem and therefore theoretically should in-

duce more accurate solutions. Correlated observation errors have a similar beneficial effect when each observation corresponds to a different variable to estimate. However, for a series of observations of a single variable x , the final uncertainty on x is larger for positively-correlated than for uncorrelated errors (the effect is opposite for negative correlations). In practice, correlations are often ignored, both because there are difficult to detect and quantify, and because properly taking them into account slows down the inversion systems to a large extent. A prominent illustration is given by the numerical weather prediction systems, since most of them assume uncorrelated observation errors (but correlated prior errors). To attenuate the effects of such a rough simplification, these systems include two empirical adjustments (e.g., Liu and Rabier, 2003, and references therein) : the observation density is thinned (i.e., only a subset of all possible remotely-sensed weather data is assimilated) and the errors assigned to the assimilated ones are usually inflated. For the estimation of CO₂ surface fluxes from measurements of atmospheric concentrations, diagonal error matrices have been empirically used until recently (e.g., Gurney et al., 2002). Prior error correlations have been introduced in some studies (e.g., Rdenbeck et al., 2003), but observation errors are still assumed to be uncorrelated, even though all components of the observation errors can be affected by correlations. For instance, error correlations in remote sensing measurements are generated by misinterpreted features in the electromagnetic spectrum and by the ancillary data used in retrieval (see, e.g., Fig. 2 of Chevallier et al., 2005). Since the observations are interpreted in the inversion system with the help of an atmospheric transport model (that links the fluxes to the measurements), such models also contribute to the observation error budget and induce space-time correlations between observation errors (e.g., Kaminski et al., 2001).

Before the end of the decade, two ground-breaking CO₂-dedicated instruments will be launched to monitor CO₂ concentrations from space : Orbiting Carbon Observatory (OCO, Crisp et al. 2004) and Greenhouse Gases Observing Satellite (GOSAT, Inoue and the GOSAT team, 2006). Several articles (e.g., Rayner and OBrien, 2001; Pak and Prather, 2001; Houweling et al., 2004; Chevallier et al., 2007) have highlighted the potential of such data to significantly reduce the uncertainties related to flux variations. These successive studies describe observing system simulation experiments (OSSEs) with increasing realism, but all of them made the assumption of null observation error correlations. At best, the observation density was preliminarily thinned.

This paper aims at investigating the impact of correlated errors in inverse modelling. OCO serves as a case study, with hypothetical error correlations of +0.5 introduced for observations 280 km apart. Such correlation errors could be induced by the remote sensing product and/or by the transport model. Despite the large number of observations, an analytical form of the covariance matrix inverse is found, given the instrument measurement configuration. This form serves us as a rigorous reference to assess the impact of commonly-used simplified treatments of the correlations : neglecting, observation thinning and error inflating. The set-up of our OSSEs is described in the next section. Results are shown in section III.4.3, followed by a conclusion in section III.4.4.

III.4.2 Method

The simulation of the observing system impact on flux estimation closely follows the method of Chevallier et al. (2007). We recall here its successive steps : - use a climatology of CO₂ surface fluxes as boundary conditions to a transport model and generate a set of pseudo observations accounting for the satellite orbit and cloud cover, - perturb the pseudo-observations consistently with as-

sumed observation error statistics, - perturb the surface flux climatology consistently with assumed error statistics, - perform a Bayesian inversion of the surface fluxes using the perturbed pseudo-observations as data and the perturbed climatology as the prior field, - compare the estimate of the inversion to the flux climatology to get the errors in the estimate.

The method is actually applied several times with different perturbations each time, in order to compute the inversion error statistics. The present study relies on an ensemble of four one-year inversions of surface fluxes in eight-day segments. Doing that, a series of 180 fluxes is available at each location of the world that provides stable statistics. In the case of large-dimensional systems, like the present one, the errors in the estimate can also be computed with the Lanczos algorithm (Chevallier et al., 2005), but only in the case of optimal systems. The Monte Carlo approach used here does not have such a limitation.

The atmospheric transport is simulated by the general circulation model of the Laboratoire de Mtorologie Dynamique (LMDZ, Hourdin et al., 2007) at $3.75^\circ \times 2.5^\circ$ (longitude-latitude) resolution, nudged to winds from weather analyses. Atmospheric conditions correspond to year 2003. The CO_2 flux climatology includes 3-hourly biospheric fluxes, monthly oceanic fluxes and yearly fossil fuel emissions, but, by construction of our OSSEs, the results presented here are not sensitive to their definition (but rather to the definition of their errors, which is given later in this section).

The observations are individual column-averaged dry air mole fractions of CO_2 , denoted X_{CO_2} , in clear spots and in the sunlit hemisphere, like those of the forthcoming OCO instrument (Crisp et al. 2004). Their time-space sampling emulates the OCO planned orbitography and accounts for cloud cover statistics. It is assumed that the instrument is in the glint observing mode. Before being pro-

cessed, the observations are binned per orbit at the $3.75^\circ \times 2.5^\circ$ model resolution. This preliminary thinning is motivated by the large observation error correlations that the transport model may induce at short distances. In this study, we investigate the impact of hypothetical mid-range correlations (+0.5) between neighboring model grid boxes. The simulated OCO orbit and cloud cover give about 243,500 observations at the horizontal resolution of the LMDZ transport model for the whole year 2003.

The Bayesian inversion is achieved by the variational scheme of Chevallier et al. (2005). This system finds the optimal fluxes x_a that fit both the observations y with their specified error covariance matrix R and the prior fluxes x_b with their specified error covariance matrix B , by iteratively minimizing the cost function J defined by :

$$\begin{aligned} J(x) = & (x - x_b)^T B^{-1} (x - x_b) \\ & + (H(x) - y)^T R^{-1} (H(x) - y) \end{aligned} \quad (\text{III.7})$$

H is the transport model convolved with a uniform vertical weighting function.

The control variables x are the CO_2 surface fluxes both at daytime and night-time, at each point of the $3.75^\circ \times 2.5^\circ$ model grid every eight days. The inversion also retrieves the CO_2 concentrations at the initial time step of the LMDZ simulation, but this has a negligible impact on the surface flux results presented here. Spatial correlations of the individual flux errors are specified as a function of distance, with correlation e-folding lengths of 500 and 1000 km over land and ocean respectively. No temporal correlations are considered for these fluxes at eight-day resolution. The square root of the sum of the error covariances in B is set to 0.8 and 2.0 Gt C per year for ocean and land respectively. The errors are spread in space proportionally to grid size over ocean and to an annual-mean heterotrophic respiration flux pattern over land. Error standard deviations at the grid point level

correspond to about 0.4 gC.m^{-2} per day over ocean and 4 gC.m^{-2} per day over vegetated areas. This configuration, detailed and discussed in Chevallier et al. (2007), expresses the current uncertainty of the carbon budget at the Earth surface in a simple, but rather realistic manner. However, it is subjective and the absolute values of the figures presented in the result section should be interpreted with caution.

The observation error statistics of the 243,500 independent X_{CO_2} observations are the focus of the present study and five configurations (C1 to C5) are considered. They differ in the definition of the covariance matrix R for the generation of the simulated observations and for the inversion formulation (Eq. (III.7)).

The first two cases are statistically optimal, i.e. the inversion finds the most likely value of the fluxes given the information provided by the prior fluxes and by the observations. Consistent with the theory, the covariance matrix R used to generate the observations is also used in the minimisation (Eq. (III.7)).

- C1 corresponds to the set-up of Chevallier et al. (2007), with uniform observation error standard deviations of 2 ppm (accounting for the combination of expected measurement and transport errors) and no observation error correlations. Observations are simply generated from the Gaussian distribution centered on the true X_{CO_2} values and a 2 ppm standard deviation.

- In C2, the standard deviations have the same values (2 ppm), but the observation error correlations are arbitrarily set to +0.5 from one observation to the next along the satellite track, which corresponds to a distance of about 280 km. Distant correlations are set accordingly (e.g., 0.25 between two observations separated by one). Correlated observation errors are generated with a Markov chain. Note that, at the model resolution, the OCO sub-tracks follow a mostly South-North line from

and to the high-latitudes of the two hemispheres, with about 14 orbits per day separated by about 25 degrees of longitude (measurements are made in the sunlit part of the orbits) : the linear correlation pattern defined here may not be appropriate for instruments with large swaths. Technically, this configuration involves inverting the non-diagonal R matrix for the computation of the cost function (Eq. (III.7)). This is made possible by the simple form of the exact inverse in our case : without any approximation R^{-1} is simply a tridiagonal matrix with about 1.67 ppm^{-2} in the main diagonal, and about -0.67 ppm^{-2} in the two sub-diagonals.

The third, fourth and fifth inversion configurations are approximate (and suboptimal) treatments of the error-correlated observations (configuration C2), using an ad hoc diagonal R matrix in the inversion, rather than the non-diagonal one used to generate the observations. Those three configurations are borrowed from the usual practice in variational data assimilation :

- Configuration C3 simply ignores the existence of correlations : the off-diagonal terms of R are suppressed for the inversion (Eq. (III.7)) without any further adaptation.

- In C4, the observation density is thinned in order to remove the largest correlations from the system. Keeping one observation out of every two, the remaining correlations are less than 0.25 and are neglected. Note that a correlation threshold of 0.2 gave an optimal thinning interval in the study by Liu and Rabier (2003), in the context of numerical weather prediction.

- The last configuration (C5) inflates the observation errors of the 243,500 X_{CO_2} observations in the inversion, so that the system trusts them less : variances in R are arbitrarily multiplied by 2 for the inversion (i.e., the assigned standard deviations are about 2.8 ppm) and the off-diagonal terms are neglected. The twofold factor was chosen by trial-and-error so as to make the standard devia-

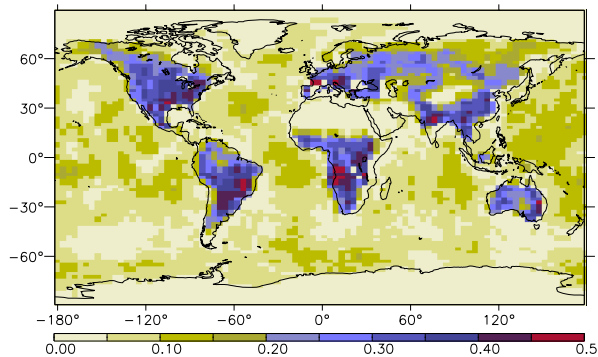


FIG. III.11 – Fractional error reduction of the eight-day mean grid point CO₂ surface fluxes for configuration C1 (no observation error correlations). The error reduction is defined as $(1 - \sigma_a/\sigma_b)$, with σ_a the posterior error standard deviation and σ_b the prior error standard deviation.

tion of the flux increments ($x_a - x_b$) in this configuration about that of the optimal configuration C1.

III.4.3 Results

Fig. III.4.3 presents the maps of the uncertainty reduction from the prior to the analysis for the eight-day fluxes, in the case of configuration C1. This optimal set-up without observation error correlations corresponds to the results of Chevallier et al. (2007) (see their Fig. 2), the main difference being that four years instead of six are used in the statistics (which are, therefore, slightly less representative). The uncertainty reduction is defined as one minus the ratio of the posterior error standard deviation to the prior error standard deviations. A value of zero indicates that the observations have not provided any information to the prior. A value of one would be reached if the observations gave a perfect knowledge about the fluxes. Negative values occur when the analysis is worse than the prior and happen only in suboptimal configurations (see configuration C3 hereafter). Fig. III.4.3 shows that the OCO-type observing system should significantly reduce the flux uncertainty over the vegetated areas (by up to about 45% with our set-up). The reduction is smaller over the oceans, but still

exceeds 10% in some regions, like the Western Pacific.

The impact of observation error correlations is displayed in Fig. III.4.3 for the optimal scenario C2. The error correlations slightly degrade the analysis and correspondingly diminish the fractional error reduction, mainly over ocean, by up to 0.06. The largest impact over ocean may be explained by the length of the prior error structures which is smaller over land (500 km vs. 1000 km, see section III.4.2) : there are fewer observations for a given flux error structure over land than over ocean and therefore the impact is less. The different a priori uncertainties assigned to the land and to the ocean may also play a role. An indication of our proper treatment of the off-diagonal terms in R is given by the value of the cost function J (Eq. (III.7)) at its minimum : as expected for an optimal system (e.g., Chevallier et al. 2007), it is very close to the number of observations (243,500) and the reduced chi-squared (J divided by the number of observations) is one.

Ignoring the observation error correlations (configuration C3) further degrades the results by up to about 0.1 over both land and ocean (upper part of Fig. III.4.3). Since the error reduction in the reference set-up C2 is usually less than 0.10 over sea (Fig. III.4.3), the results indicate that the suboptimal flux

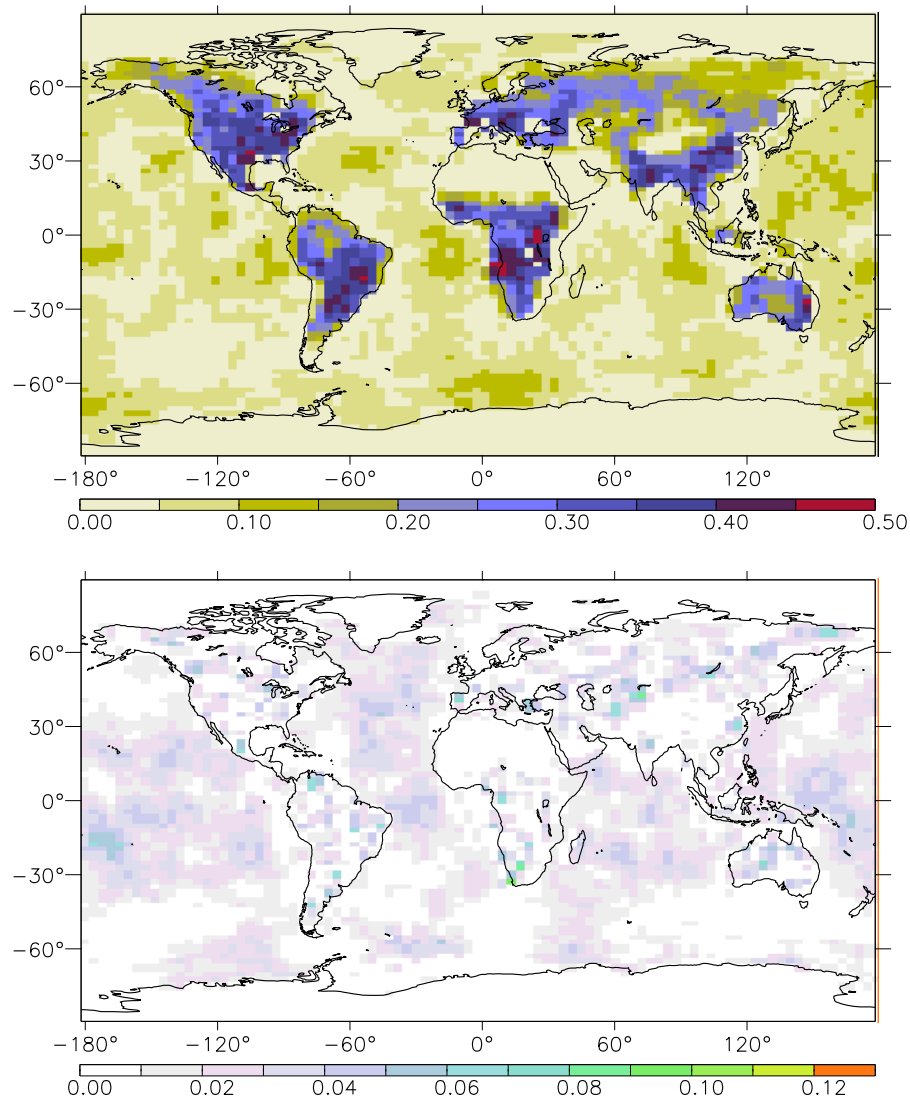


FIG. III.12 – The upper part is the same as Fig. III.4.3, but for the optimal configuration C2, where observation error correlations exist and are properly taken into account. The difference between Fig. III.4.3 and the top panel (Fig. III.4.3 minus the top panel) is shown in the lower part of the figure.

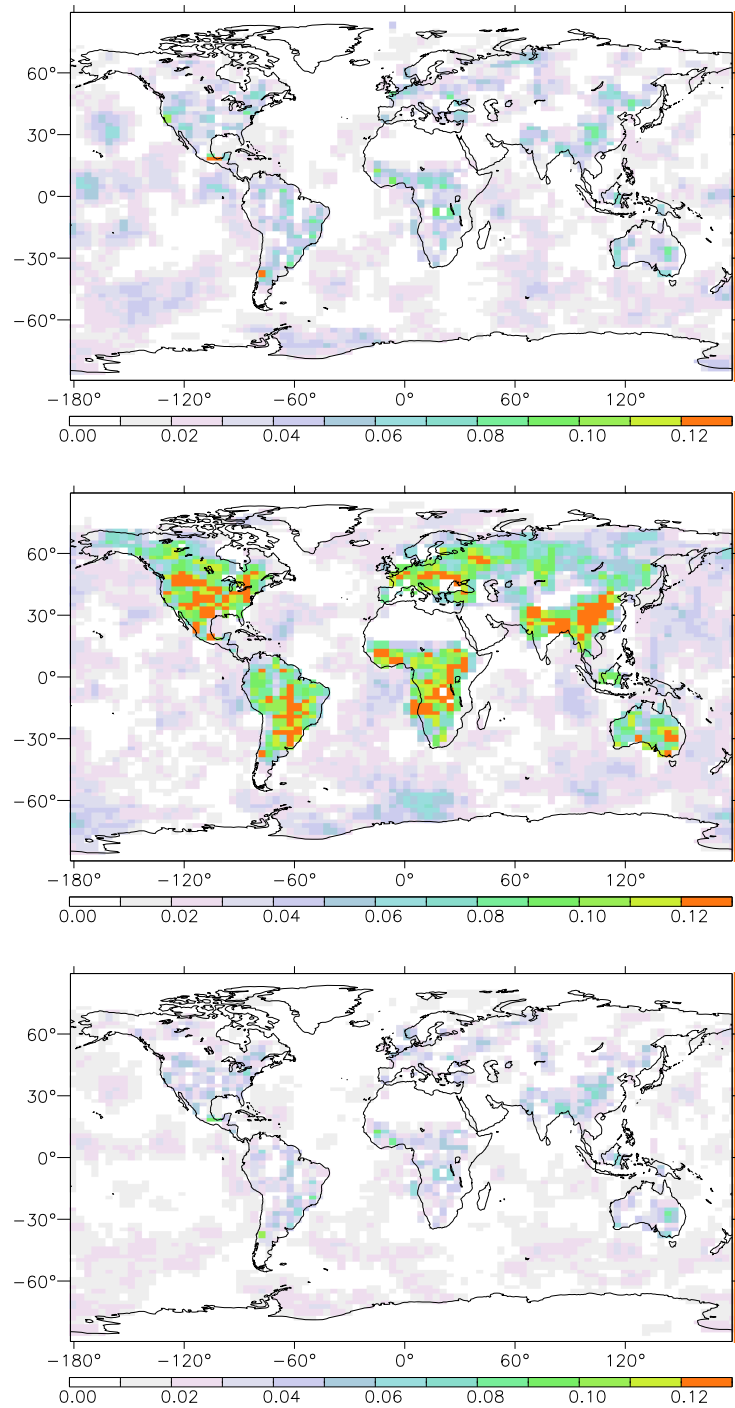


FIG. III.13 – Degradation of the fractional error reduction (FER) shown in the upper part of Fig. III.4.3 (configuration C2), induced by the suboptimal configurations C3 (top), C4 (middle) and C5 (bottom). The degradation is expressed as the FER of configuration C2 minus the suboptimal FER.

analysis provides little information in those parts of the globe. It is even slightly worse than the prior fluxes in some oceanic regions (e.g., in the Pacific about French Polynesia and about latitude 50S, or off the coasts of Somalia and of the Arabic Peninsula). The standard deviation of the inversion flux increments is about 30% larger than for the optimal configuration C2 over ocean and about 10% larger over land (not shown). The cost function minimum is not close to the number of observations, as expected from a suboptimal system. It reduces to about 238,500 vs. 243,500 because the system trusts the observations too much. The reduced chi-squared is about 0.98.

Configuration C4 relies on data thinning to perform the inversion without dealing with the off-diagonal terms of \mathbf{R} . In this case (middle part of Fig. III.4.3), while the observations never drive the estimate further from the truth than the prior (as happens in some places in C3), they generally only correct it by two-thirds of the way as in C2, resulting in larger errors than in C3. The twofold-reduced number of observations makes the cost function about 121,000 and therefore a reduced chi-squared about 0.99.

The alternative of inflating the observation error variances (configuration C5) appears to be the least detrimental among the three approximate (and computationally-simple) solutions, with degradations usually less than 0.03 over ocean and 0.06 over land. Note that this confirms the strategy chosen for the Atmospheric Tracer Transport Model Intercomparison Project (Gurney et al. 2002). In contrast with C3 and C4, the relatively small spatial scale of the difference patterns implies that the quality of the inverted carbon fluxes is hardly affected by the approximate C5 set-up when integrated over continental-size regions. The standard deviation of the inversion flux increments are within 10% of those of the optimal configuration C2 over both land and ocean (not shown). The twofold-inflated ob-

servation error variances make J about half the number of observations at its minimum and induce a chi-squared about 0.5. This very low value despite the rather good performance of the suboptimal configuration emphasises the ambiguity of the chi-squared diagnostic. In particular, it cannot be used alone to tune prior or observation errors safely.

III.4.4 Discussion and Conclusions

Performing Bayesian inversion involves modelling the statistical characteristics of the errors. The chosen models potentially include a huge number of monovariate and multivariate moments. Multivariate moments, like covariances, are even more difficult to assign than univariate ones, like biases and variances. Further, technical considerations may cause one to neglect some of them. Based on the Monte Carlo approach of Chevallier et al. (2007), this paper quantifies the detrimental impact of unaccounted observation error correlations in the inversion of CO₂ surface fluxes for a particular set-up of the inference problem : in some (limited) cases, the inverted fluxes are of lesser quality than the prior ones. Observation thinning and error inflation are safer alternatives, but leave out some of the observation information content, as illustrated with our inversion configurations C4 and, to a lesser extent, C5. The practical consequence is the importance of rigorous knowledge of spatial error correlations not only for the prior (Chevallier et al., 2006), but also for the observations. Such task is particularly challenging for observation errors since they combine measurement, model and representativeness errors. Multi-sensor observing systems (with, e.g., OCO, GOSAT and in situ measurements together) would be less sensitive to inadequate specification of the measurement errors of the individual instruments because independent biases would partially cancel out. Representativeness and transport error correlations should be studied, e.g., along the lines of the

methods described by Gerbig et al. (2003) and Lin and Gerbig (2005) for standard deviations. The present paper focussed on spatial error correlations in the context of a satellite instrument with a sampling repeat cycle of several days (16 for OCO). Temporal correlations of the transport model errors are an important issue for the processing of in situ high-frequency measurements and should be carefully studied as well.

Acknowledgments. The author would like to thank F.-M Bréon, P. Peylin and three anonymous reviewers for their constructive comments on an earlier version of this paper, and F. Marabelle for computer support. This study was co-funded by the European Commission under the project GEMS, contract number SIP4-CT-2004-516099.

References

- Chevallier, F., M. Fisher, P. Peylin, S. Serrar, P. Bousquet, F.-M. Bréon, A. Chédin, et P. Ciais (2005), Inferring CO₂ sources and sinks from satellite observations : method and application to TOVS data. *J. Geophys. Res.*, 110, D24309, doi :10.1029/2005JD006390.
- Chevallier, F., N. Viovy, M. Reichstein, and P. Ciais (2006), On the assignment of prior errors in Bayesian inversions of CO₂ surface fluxes, *Geophys. Res. Lett.*, 33, L13802, doi :10.1029/2006GL026496.
- Chevallier, F., F.-M. Bréon, and P. J. Rayner (2007), The contribution of the Orbiting Carbon Observatory to the estimation of CO₂ sources and sinks : theoretical study in a variational data assimilation framework. *J. Geophys. Res.*, 112, D09307, doi :10.1029/2006JD007375..
- Crisp, D., et al. (2004), The Orbiting Carbon Observatory (OCO) Mission, *Advances in Space Research*, 34(4), 700-709.
- Gerbig, C., J. C. Lin, S. C. Wofsy, B. C. Daube, A. E. Andrews, B. B. Stephens, P. S. Bakwin, and C. A. Grainger (2003), Toward constraining regional-scale fluxes of CO₂ with atmospheric observations over a continent : 1. Observed spatial variability from airborne platforms, *J. Geophys. Res.*, 108(D24), 4756, doi :10.1029/2002JD003018.
- Gurney, K.R. et al. (2002), Towards robust regional estimates of CO₂ sources and sinks using atmospheric transport models, *Nature*, 415 :6872, 626-630.
- Hourdin, F., et al. (2007), The LMDZ4 general circulation model : climate performance and sensitivity to parametrized physics with emphasis on tropical convection, *Climate Dynamics*, 27, 787-813, doi :10.1007/s00382-006-0158-0
- Houweling, S., F.-M. Bréon, I. Aben, C. Rödenbeck, M. Gloor, M. Heimann, and P. Ciais (2004), Inverse modeling of CO₂ sources and sinks using satellite data : a synthetic intercomparison of measurement techniques and their performance as a function of space and time. *Atmos. Chem. Phys.*, 4, 523-538.
- Inoue, G., and the GOSAT team (2006), Global carbon dioxide and methane column observation by GOSAT (Greenhouse gases observing satellite), *Geophysical Research Abstracts*, 8, 10624.
- Kaminski, T., P. J. Rayner, M. Heimann, and I.G. Enting (2001), On aggregation errors in atmospheric transport inversions. *J. Geophys. Res.*, 106(D5), 4703-4716.
- Lin, J.C. and C. Gerbig (2005), Accounting for the effect of transport errors on tracer inversions, *Geophysical Research Letters*, 32 (L01802), doi :10.1029/2004GL021127.
- Liu and Rabier (2003), The potential of high-density observations on Numeric Weather prediction : a study with simulated observations .*Quart. J. Roy. Meteor. Soc.*, 129, 3013-3035.
- Pak, B.C., and M.J. Prather (2001), CO₂ source inversions using satellite observations of the upper troposphere, *Geophys. Res. Lett.*, 28, 4571-4574.
- Rayner, P. J., and D. M. O'Brien (2001), The utility of remotely sensed CO₂ concentration data in surface source inversions, *Geophys. Res. Lett.*, 28, 175-178.
- Rödenbeck, C., S. Houweling, M. Gloor, and M. Heimann (2003), CO₂ flux history 1982-2001 inferred from atmospheric data using a global inversion of atmospheric transport. *Atmos. Chem. Phys.*, 3, 1919-1964.

Chapitre IV

Opérateur d'observation

Il n'est pas bon que le pouvoir d'observer se développe plus vite que l'art d'interpréter.

É. Chartier, dit Alain, *Propos sur l'éducation* (1932)

IV.1 Introduction

L'opérateur d'observation établit le lien entre les variables d'intérêt et les variables observées. Mais, lors de l'inversion bayésienne, ses erreurs se combinent aux erreurs des observations et réduisent l'information disponible, comme nous l'avons vu au chapitre précédent. De plus, même si la précision des dérivées partielles de l'opérateur est peu regardée, elle affecte aussi la qualité du résultat. Enfin, le modèle direct est soumis aux limitations de la puissance de calcul et de la taille de la mémoire informatique disponibles. Le travail sur la modélisation directe pour l'inversion est donc particulièrement exigeant.

Nous présentons ici deux articles. Le premier concerne la modélisation directe pour l'assimilation des mesures des radiomètres orbitaux travaillant dans l'infrarouge et les micro-ondes, lorsque la scène visée contient des nuages. Le deuxième article se focalise sur la précision des dérivées partielles de deux modèles pour l'assimilation de données. Une alternative est proposée pour palier le manque de précision des dérivées partielles de l'un d'eux.

IV.2 RTTOV-CLD

Cette section reprend l'article de Chevallier et coll. (2002) paru dans *Quarterly Journal of the Royal Meteorological Society*.

Variational retrieval of cloud profile from ATOVS observations

F. Chevallier, P. Bauer, J.-F. Mahfouf and J.-J. Morcrette

European Centre for Medium-Range Weather Forecasts
Reading, UK

Abstract. Radiation observations such as those from the Advanced Tiros Operational Vertical Sounder (ATOVS) on-board the National Oceanic and Atmospheric Administration (NOAA) satellites provide information about cloud systems. However, like the other cloud observations they are not used in global data assimilation systems.

As an essential step towards the assimilation of such data, a fast infrared and microwave radiation model and its linearised version (tangent linear and adjoint operators) have been developed for the computation of model-equivalent cloud-affected satellite radiances. They are used in a global one-dimensional variational (1D-Var) analysis of ATOVS radiances over open oceans. In non-precipitating areas, it is shown that the 1D-Var can remove, create and modify the cloud variables in each model layer to fit the observed radiances. The retrieved profiles have a degree of realism that will improve with better background constraint. This study is a first step toward the assimilation of clouds by variational analysis of clouds and dynamics at once, and will be further continued.

IV.2.1 Introduction

Numerical Weather Prediction (NWP) models require accurate initial conditions and therefore rely heavily on the quality of the assimilation schemes. Pressure, temperature, water vapour, and wind information from conventional and satellite observations have been operationally assimilated at global NWP centres for a long time. Despite the major influence of clouds on the atmosphere water and energy balance, there is still no explicit cloud analysis in global systems. The cloud contribution to the satellite radiances is removed from the assimilation systems either by some partition method that separates it from the direct temperature and humidity contributions (e.g., McMillin and Dean 1982; Eyre 1989; Phalippou 1996) or by filtering out the corresponding radiances. Studies have shown

that the cloud areas may correspond to regions where key analysis errors are located, and therefore are crucial for the quality of the forecasts (McNally 2002). In meso-scale models only, cloud analyses based on nudging techniques have been introduced (e.g. Lipton 1993; MacPherson *et al.* 1996; Bayler *et al.* 2000).

The main reason why global analysis systems do not include cloud information is that cloud processes contain small spatial and temporal scales not explicitly described by NWP models. These makes it difficult to observe and model cloud 4D variability. However, even though surface precipitation has similar features, positive impact of assimilating Special Sensor Microwave/Imager (SSM/I) or Tropical Rainfall Measuring Mission (TRMM)-derived surface rainfall rates has been observed (e.g., Hou *et al.* 2000, Marécal and

Mahfouf 2002). These authors use a one-dimensional retrieval scheme to extract the model-resolved-scale information on moisture from the surface rainfall rates. Similar prospects are being studied for the assimilation of cloud information. Such information is available on a global scale from the operational ATOVS radiometer on-board the NOAA polar-orbiting spacecrafs. ATOVS measures infrared and microwave radiation in 40 narrow channels and is sensitive to the vertical structure of clouds. An essential step towards the use of this data is the set-up of an accurate, fast and linearisable radiation scheme for the computation of model-equivalent cloud-affected satellite brightness temperatures. The linearisation in the vicinity of model profiles stems from the application to the variational framework. This paper presents such a model for the infrared and the microwave parts of the atmospheric spectrum, based on the Radiative Transfer for Tiros Operational Vertical Sounder (RTTOV : Eyre, 1991; Saunders *et al.*, 1999). To demonstrate its potential for cloud variational assimilation, the model, described in section IV.2.2, is used in 1D-Var analyses of cloud-affected ATOVS observations on-board the NOAA-15 satellite. Qualitative evaluation of the 1D-Var analyses is done by comparison with independent Cloud and the Earth's Radiant Energy System (CERES) observations from the Terra spacecraft operated by the National Aeronautics and Space Administration. The data and the 1D-Var scheme are presented in sections IV.2.3 and IV.2.4 respectively. The results are shown in section IV.2.5. The conclusions are outlined in section IV.2.6.

IV.2.2 Description of the radiation scheme

The direct model

The RTTOV radiation model is used operationally at several NWP centres. It handles instruments like ATOVS or SSM/I. Even

though it is mainly used for clear-sky satellite radiance simulations, its current version (RTTOV-6) is able to take cloud-radiation interaction into account. In the infrared, cloudiness is treated as a single semi-transparent layer, which is defined by two parameters only : the cloud top pressure and its effective amount (i.e. the cloud layer emissivity times the cloud fraction). In the microwave though, cloud absorption is computed in each of the RTTOV 43 fixed layers from the (interpolated) liquid water profile (English *et al.* 1999).

In the present study, this capacity is extended to vertical profiles of cloud cover, liquid water and ice water described on any vertical pressure grid in a way similar to the ECMWF operational broad-band infrared radiation scheme (Morcrette 1991, Morcrette *et al.* 2001). Similar work in the infrared only was done on a previous version of the system but was never used operationally (Rizzi 1994).

Following Washington and Williamson (1977), clouds are introduced as multi-layer grey bodies. Their contribution to the radiances is determined by their horizontal coverage n^i and their emissivity ϵ_ν^i in each vertical layer i of the model. This approach enables the radiances in the presence of semi-transparent cloud layers to be expressed as a linear combination of the clear sky radiance, and of the radiances in the presence of single layered clouds treated as black bodies. The coefficients of the linear combination are functions of the n^i 's and of the ϵ_ν^i 's and depend on the way the cloudy layers overlap. Specular reflection of the cloud downward emission at the surface is taken into account because it has a strong impact over sea for microwaves. Even though the gas absorption computation is performed on 43 fixed levels with RTTOV, the cloud computation is carried out on the original model levels (60 in the following) so that no interpolation of cloud variables is needed.

Various overlapping hypotheses can be used according to the vertical structure of the

clouds (e.g., Morcrette and Jakob 2000). The maximum-random formulation of Raïsänen (1998) that explicitly distinguishes between the horizontal coverage and the emissivity of the cloud layers is used here.

Cloud absorption is taken into account in the infrared spectrum following Ebert and Curry (1992) for ice water and Smith and Shi (1992) for liquid water. The single scattering albedo is usually small for the infrared wavelengths above $5 \mu\text{m}$ at the top of the atmosphere and is neglected. Consistently with the broadband radiation model, ice particle radii vary between 30 and $60 \mu\text{m}$ with a temperature dependency from Ou and Liou (1995). Liquid particle radius is set to $10 \mu\text{m}$ over land and $13 \mu\text{m}$ over sea.

Cloud absorption is introduced in the microwave spectrum in the range from 1-200 GHz as a direct function of frequency and liquid water/ice content. Comparison to full Mie-calculations using modified Gamma-distributions adjusted to water contents for particle size indicated that : (1) scattering by droplets can be neglected for all currently used microwave channels (i.e. the single scattering albedo is less than 0.002) while scattering by ice particles may become significant for $\nu > 60 \text{ GHz}$ (i.e. the single scattering albedo may be more than 0.01); (2) the shape of droplet size spectra is negligible. Ice and water dielectric properties were calculated following Hufford (1991) and Liebe *et al.* (1989), respectively. Precipitation-radiation interaction in the microwave is important but is not considered here since its scattering properties do not fit within the multi-layer grey body framework. More elaborated, and therefore more computationally-expensive, parameterisations are needed.

Tangent linear and adjoint operators

Even with a fast model like the one described here, further developments are needed in order to make a model computationally efficient in the framework of variational

assimilation. In particular, the tangent-linear and adjoint technique allows to avoid the explicit computation of Jacobians in the assimilation model. The tangent-linear operator of a direct model analytically computes output perturbations corresponding to input perturbations, with a computational cost that is typically only about twice as much as that of the direct model. A first order Taylor series approximation is used. The adjoint of the tangent-linear operator analytically computes sensitivities with respect to the inputs from sensitivities with respect to the outputs (e.g., Rabier *et al.* 1992; Errico 1997). The adjoint operator is about two to three times only slower than the direct model. The tangent-linear and adjoint operators of the radiation model described here have been developed without a priori modifications.

IV.2.3 The data

The satellite data

This study uses data from two instruments on-board the NOAA-15 satellite, the High-resolution Infrared Radiation Sounder/3 (HIRS/3) and the Advanced Microwave Sounding Unit-A (AMSU-A), and data from the CERES instrument on-board the Terra satellite. NOAA-15 and Terra were launched in May 1998 and December 1999 respectively and operate in close near-polar, sun-synchronous orbits : when moving Southward, the spacecrafts cross the Equator at 07 :30 and 10 :30 LST respectively.

HIRS/3 and AMSU-A are two of the ATOVS radiometers. The HIRS/3 instrument measures radiation in 20 channels covering both the long-wave and the short-wave parts of the spectrum. Use is made here of the $11 \mu\text{m}$ window channel, and of the four 13 to $15 \mu\text{m}$ channels in the main CO_2 -absorption band, the weighting-function peaks of which are regularly spread in the troposphere. Those channels are very sensitive to ice clouds. The AMSU-A radiometer comprises 15 channels

for making passive measurements in the 5.5 millimetre wavelength oxygen region and in three window channels at 23.8, 31.4 and 89.0 GHz. Among the channels covered by the radiation model (mainly those below 60 GHz), only six channels, at 23.8, 31.4, 50.3, 52.8, 53.6 and 54.4 GHz, are affected by (water) clouds. All six are used here. The ground instantaneous field of view of HIRS/3 and AMSU-A is typically a circle of about 20 km and 50 km diameter respectively at nadir. The infrared and microwave radiances are bias-corrected here along the lines of the method described by Harris and Kelly (2001).

The CERES instrument is an improved version of the Earth radiation Budget Experiment (ERBE) scanner instruments, which operated from 1984 through 1990 (Barksstrom 1984). It consists of a three-channel broadband radiometer. The channels respectively measure the short-wave (0.2-5 μm), the total (0.2-100 μm) and the 8-12 μm "window" broadband radiation with a resolution of about 20 km for the instrument on-board Terra (Wielicki *et al.* 1995). A set of algorithms similar to those for ERBE has been designed to convert the measurements of these channels into broadband long-wave and short-wave fluxes using spectral and angular corrections. The uncertainty of the instantaneous fluxes (CERES Terra FM1 Edition1 ES8 product) has been estimated to 12.7 W.m^{-2} for the long-wave, and to 38 W.m^{-2} for the short-wave (Wielicki *et al.* 1995). In the near future, these uncertainties are expected to be reduced with the combined use of the data from an imager flown with CERES.

The model data

The atmospheric model data come from the ECMWF operational forecast system. 4D-Var analyses are produced at nominal times of 00 and 12 UTC, with an assimilation window of 12 hours. The forecast model is a global spectral model and includes a semi-Lagrangian advection scheme together with a

linear Gaussian grid (Hortal 2000). The reduced horizontal grid associated with the triangular truncation $T_L 511$ corresponds to a regular grid size of about 40 km from the equator to the poles. In the vertical, a hybrid coordinate of 60 levels between the surface and the top of the atmosphere is used. The physics package is based on Gregory *et al.* (2000). In particular, two prognostic equations describe the time evolution of cloud condensate and cloud cover (Tiedtke 1993), while rain and snow are separate diagnostic quantities. Clouds are formed by moist convection, diabatic cooling and boundary-layer turbulence. The scheme links their dissipation to adiabatic and diabatic heating, turbulent mixing of cloud air with unsaturated environmental air, and precipitation processes. The modifications to the original formulation from Tiedtke (1993) are given in Jakob (2000). The broadband radiation scheme includes the Rapid Radiative Transfer Model (RRTM : Mlawer *et al.*, 1997) for the infrared and the Fouquart and Bonnel (1980) scheme (with four spectral bands) for the short-wave. The sea surface temperature is prescribed from the National Center for Environmental Prediction analyses.

Previous validations of the model clouds

The documentation of the first-guess error is a prerequisite to the development of an assimilation scheme. This has been done on a global scale in the case of the cloud fields simulated by the ECMWF model within several surveys (Chevallier *et al.* 2001 and references therein ; Chevallier and Kelly 2002), in particular by comparison to TOVS radiances (Rizzi 1994 ; Chevallier *et al.* 2001), and CERES fluxes (Chevallier and Morcrette 2000). The model dynamics was shown to distribute the clouds well, but some important deficiencies have been identified : - the radiative impact of the ice clouds appears to be too low in the mid-latitudes, - the opposite characteristic is seen for the liquid water clouds, - the fre-

quency of occurrence of high clouds is overestimated in the Inter-Tropical Convergence Zone, - the stratocumulus off the West coast of the continents is underestimated. Work is underway to remedy some of those problems in parallel to the preparation of cloud assimilation.

IV.2.4 The variational approach

Generalities about variational data assimilation

The present ECMWF assimilation scheme is a four-dimensional variational system (4D-Var) described by Courtier *et al.* (1994). The 4D-Var system seeks an optimal balance between observations and the dynamics of the atmosphere by finding a model trajectory $\mathbf{x}(t)$ which is as close as possible to the observations available during a given time period $[t_0, t_n]$. The model trajectory $\mathbf{x}(t)$ is completely defined by the initial state \mathbf{x}_0 at time t_0 . The misfit to observations \mathbf{y} and to background (or first-guess) model state \mathbf{x}^b is measured by an objective cost-function, that is being minimised during the assimilation process. Observation and model errors are assumed to be unbiased and mutually uncorrelated.

1D-Var systems may be used for preliminary studies on the 4D-Var (e.g., Marécal and Mahfouf 2000). The principle of the 1D-Var is similar to that of 4D-Var, but the control vector \mathbf{x} represents only a single column and the time dimension is not included. The cost function reduces to :

$$\begin{aligned} J(\mathbf{x}) = & \frac{1}{2}(\mathbf{x} - \mathbf{x}^b)^T \mathbf{B}^{-1} (\mathbf{x} - \mathbf{x}^b) \\ & + \frac{1}{2}(\mathbf{H}(\mathbf{x}) - \mathbf{y})^T \mathbf{R}^{-1} (\mathbf{H}(\mathbf{x}) - \mathbf{y}) \end{aligned} \quad (\text{IV.1})$$

where \mathbf{y} is the vector of observations, \mathbf{H} is the operator simulating the observed data from the model variable \mathbf{x} , \mathbf{R} is the observation error covariance matrix (measurement errors and representativeness errors, including errors in H), and \mathbf{B} is the background error covariance matrix of the state \mathbf{x}^b . Supercripts -1 and T denote respectively inverse

and transpose matrix. In the following, H is the radiative transfer model. The control vector \mathbf{x} contains vertical profiles of cloud cover, cloud liquid and ice water. The temperature, gas concentrations and surface characteristics also could be control variables.

If \mathbf{H}^T is the adjoint operator mentioned in section 2(b) (i.e. the Jacobian matrix $\{\partial y_k / \partial x_l\}_{k,l}$, \mathbf{H} being the linearised version of H), the gradient of the cost function is :

$$\nabla J(\mathbf{x}) = \mathbf{B}^{-1}(\mathbf{x} - \mathbf{x}^b) + \mathbf{H}^T \mathbf{R}^{-1} (\mathbf{H}(\mathbf{x}) - \mathbf{y}) \quad (\text{IV.2})$$

The 1D-Var scheme

In the present study, the 1D-Var observations \mathbf{y} are the available channels among the 11 above-mentioned ATOVS ones (section 3(a)). In practice, infrared radiances are always available when AMSU data exist but the opposite is not true, mainly because rain-affected microwave data are removed consistently with the radiation model specifications. Rain detection is performed following Zhao *et al.* (2000). The liquid water profile is obviously less constrained when no AMSU data can be used.

The control variables \mathbf{x} consist of profiles of cloud cover, liquid and ice water contents from the top of the atmosphere to the surface (60 levels). The temperature and gas profiles, and the surface characteristics are kept constant.

A particular case occurs when there is no cloud in an atmospheric layer of the background \mathbf{x}^b . Indeed the corresponding derivatives (i.e. sensitivity) of the radiances with respect to cloud variables are then zero and the 1D-Var cannot create any cloudiness. In order to avoid this limitation, the zero values of cloud cover, liquid and ice water profiles in \mathbf{x}^b are replaced by very small ones : 10^{-4} for cloud cover and $2.10^{-10} \text{ kg.kg}^{-1}$ for cloud condensate.

The non-linear variation of cloud variables, in particular the on/off nature of the cloud layers, makes it difficult to estimate the back-

ground error covariance matrix B and leads to a scale-dependency of the results. Cloud misplacements would likely dominate errors that would be estimated globally and at model resolution (40 km here in the horizontal, between 20 meters and one kilometre in the vertical and in the troposphere), whereas at much lower spatial resolution (averaged from high resolution simulations) it would describe rather an average error inside the cloud systems, since the model locates them well, at least in the extra-tropics. Linking B to the model dynamical variables, like divergence, may reduce the non-linearity of the problem but is still difficult to implement. In any case the model biases, that are known to be large for liquid water and ice water in the case of the ECMWF model, remain an important issue, firstly because they violate the theoretical 1D-Var framework, secondly because they hamper the usual estimation of B based on forecast comparisons (e.g., Parrish and Derber 1992). Our choice for the present study is to perform the variational retrieval at model resolution using an empirically specified B with loose standard deviations that are much larger than the model biases and that do not restrain the creation and removal of tropospheric cloud layers by the 1D-Var. One may notice that this choice would make the introduction of temperature and gas profiles among the control variables x ineffective, since it enhances the sensitivity of infrared observations to cloud variables within the 1D-Var.

B 's standard deviations are set to very large values in the troposphere : 1.0 for cloud cover, $10^{-3} \text{ kg.kg}^{-1}$ for liquid and $5.10^{-4} \text{ kg.kg}^{-1}$ for ice water. For temperatures below 260 K (respectively above 274 K), the liquid (respectively ice) water error standard deviations are set to zero. Null values are also used above the tropopause for both liquid and ice water.

Even with large standard deviations, the vertical correlations of B exert a strong influence on the shape of the 1D-Var incre-

ments. A Gaussian shape of standard deviation 100 hPa is defined when there is no cloud in the first-guess. If a cloud already exists, the standard deviation is increased to 200 hPa so that the 1D-Var little changes the cloud shape provided by the first-guess. The Gaussian values that are less than 0.01 are set to zero. Even though we believe that correlations exist between cloud cover errors, liquid water errors and ice water errors, no cross-correlation between these quantities were introduced, given the degree of empiricism of B .

A simple observation error covariance matrix R is used. The standard deviation is set to 1.0 and 2.0 K respectively in the infrared and in the microwave channels, with no correlation between the channels.

The minimiser of the present 1D-Var code is a limited memory quasi-Newton method, the M1QN3 software developed at Institut National de Recherche en Informatique et en Automatique (INRIA) (Gilbert and Lemaréchal, 1989).

IV.2.5 Variational retrieval of cloud information

Application to synthetic observations

Preliminary tests are performed on individual profiles with synthetic observations. The extreme case where cloud is present in the observation and not in the background is shown here as an example.

The cloud cover, liquid and ice water profiles of a series of model situations are used to compute synthetic HIRS/3 and AMSU-A observations, but are suppressed in the 1D-Var background x^b . Other variables, like temperature and surface characteristics are used similarly in the synthetic observation computation and in the background. The result of two of the 1D-Var experiments is shown in Figures IV.1 and IV.2. The cases are extracted respectively from a front in the Northern Atlantic and from a tropical deep-convective system. The issue of precipitation impact in the

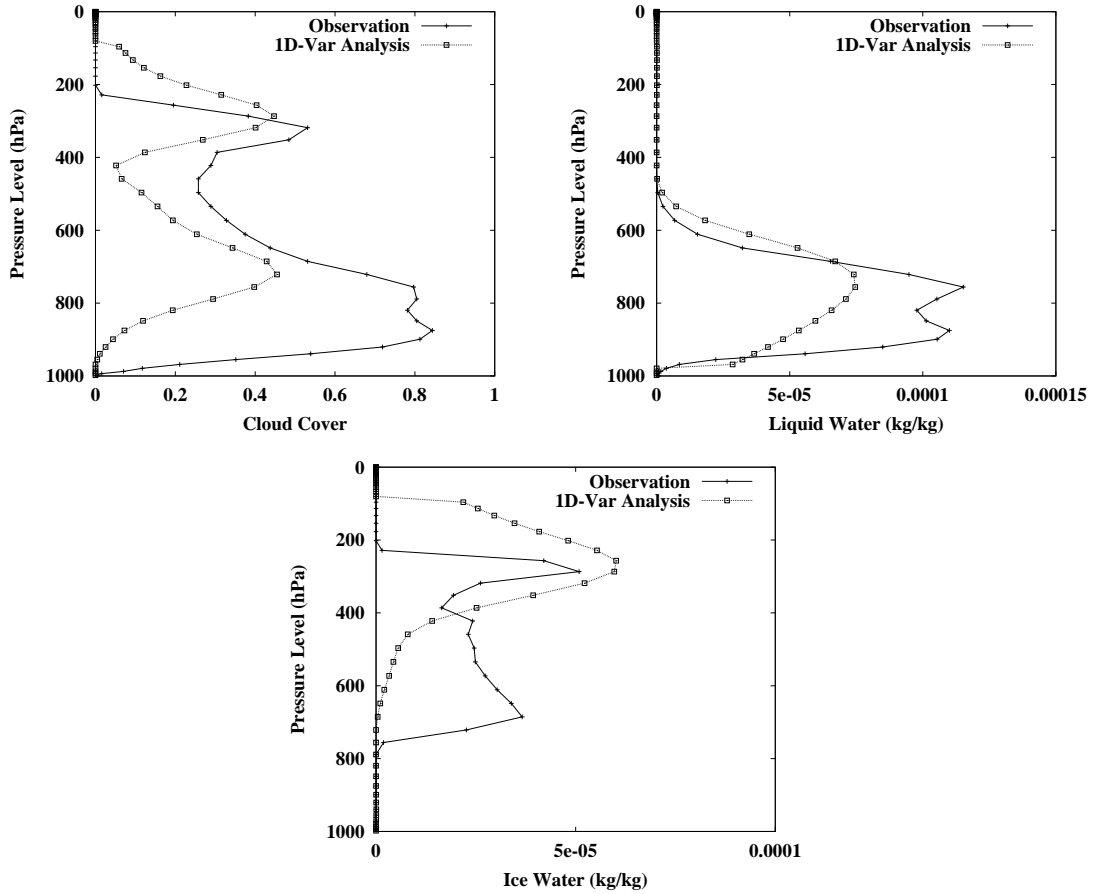


FIG. IV.1 – 1D-Var output and desired output profiles using synthetic observations. Case from a Northern Atlantic front. The background profiles does not have any cloudiness.

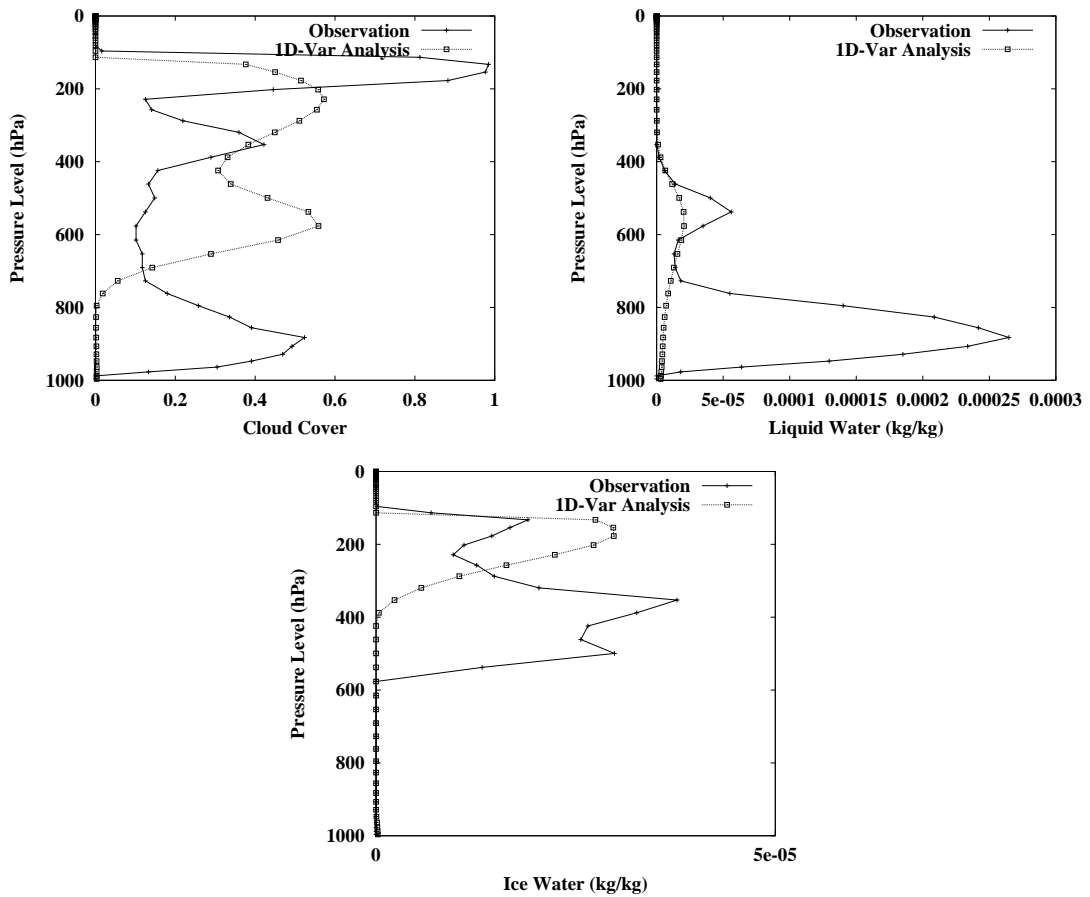


FIG. IV.2 – Same as previous but for a deep convection case.

microwave is not considered here since this experiment relies on simulations only. Therefore all AMSU-A channels are used (section 3(a)). The brightness temperature background departures are more than 30 K for the lowest infrared channels and about 10 K for the microwave channel. The retrieved cloud cover profiles have a double-peak structure. The highest peak corresponds to ice water and the lowest one to liquid water. The retrieved condensate profiles have a Gaussian shape, consistent with the specified error covariance matrix, with a width about the specified one or larger.

The retrieved shapes of the cloud profiles do not accurately reproduce the “truth” (i.e. the profiles of the synthetic observations) and therefore already show some limitations of the approach. However they have some degree of realism, despite the lack of information contained in the background profiles, as specified by B. Moreover, the brightness temperature departures with the observations are reduced by about 80% compared to the initial departures. Similarly, the 1D-Var can modify the shape of existing cloudiness in the background and even remove the clouds so as to fit the observations (not shown).

Application to real data

The 1D-Var scheme described above is applied to cloud retrieval from real ATOVS observations on 15 March 2001. All morning orbits (07 :30 LST at the Equator) from NOAA-15 are used. 3, 6, 9 and 12-hour forecasts, starting from the global analyses at 00 and 12 UTC, are taken from the ECMWF operational archives. This allows to collocate the model data with the satellite observations within 1.5 hours. The model profiles are extracted from the archive on a regular $60\times 60\text{ km}^2$ grid. The observations are used at the nearest grid point. Open sea points, for which surface temperature and emissivity are accurately known, between latitudes 60°N and 60°S only are considered, which makes 154780

points, of which 115465 correspond to non-rain-affected AMSU observations. For each one of them, a 1D-Var analysis is performed. In most cases, about ten iterations are needed by the 1D-Var to converge.

The fit of background and analysis to assimilated HIRS $11\text{ }\mu\text{m}$ and AMSU-A 50.3 GHz observations is presented in Figure IV.3.

Consistent with previous validations of the ECMWF model, the background bi-dimensional histogram for HIRS $11\text{ }\mu\text{m}$ is asymmetrical (Figure IV.3a), with much larger number of points occurring above the diagonal than below. This feature is explained by an underestimation of the cloud radiative forcing by the ECMWF model, possibly due to a lack of ice clouds (Jakob and Rizzi 1997; Chevallier *et al.* 2001). From Figure IV.3b, the 1D-Var analysis dramatically improves the fit to the observations. The points that remain distant from the diagonal are cases where the 1D-Var minimisation ends in a secondary minimum of the cost function (equation (1)). For instance, some warm observations (about 290 K) are still associated to cold model values (below 240 K), which shows that the 1D-Var is not always able to remove the cloudiness. For those profiles the cloud emissivity ($1 - e^{-u}$, with u the layer cloud optical depth) is unity in several atmospheric layers and its derivative ($u.e^{-u}$) is close to zero. The examination of the probability density functions of the cloud variables (see Figure IV.4 for liquid and ice water) indicates that the 1D-Var overall increased the cloud ice content. High cloud cover is overall not much affected but the occurrence of high clouds (i.e. clouds above 450 hPa) increases from 50% of the first-guess profiles up to 66% of the analysed ones. All the generated clouds are not radiatively very active, but this value is too high by comparison to cloud climatologies (e.g., Wylie *et al.* 1994) and underlines the limitation of the top-of-the-atmosphere passive infrared and microwave radiations as sole constraints on the cloud profile retrieval.

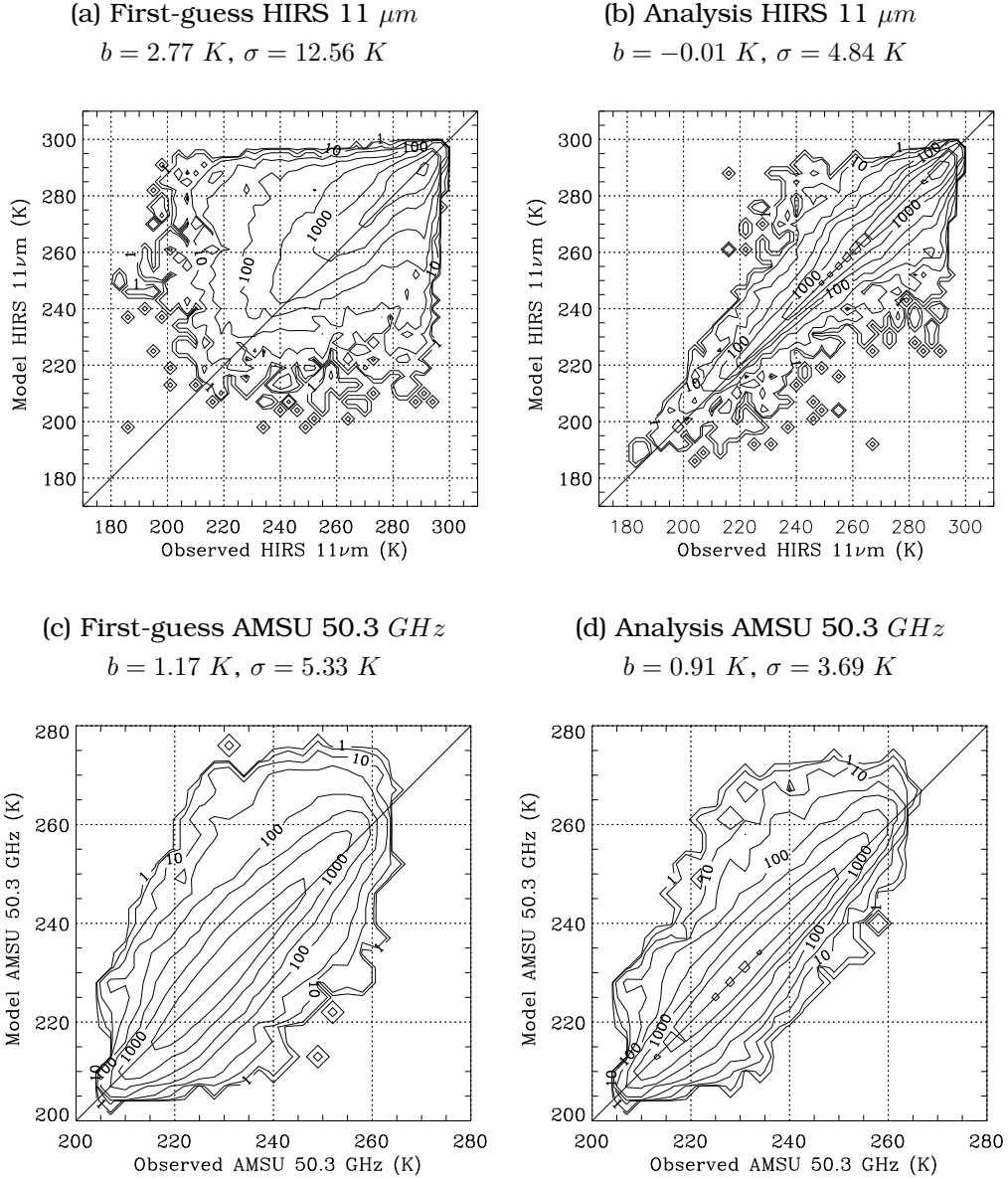


FIG. IV.3 – Bi-dimensional probability density function (PDF) of top-of-the-atmosphere HIRS 11 μm and AMSU 50.3 GHz brightness temperatures of the first-guess (left panel) or of the analysis (right panel) versus the NOAA-15 observation. The PDF is in $10^6/K$. The contours are drawn at 1, 3, 10, 30, 100, 300, 1000, 3000 $\times 10^6/K$. The mean (b) and the standard deviation (σ) of the differences (model minus observation) are indicated on top of each plot.

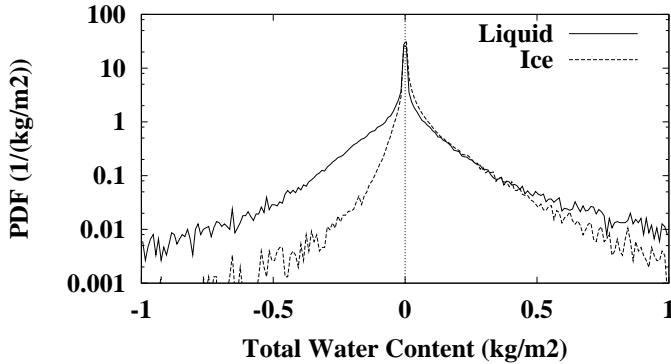


FIG. IV.4 – Probability density functions (PDF) of the 1D-Var increments of total liquid or ice water (analysis minus first-guess). The PDFs are not significantly changed when considering only the points where AMSU-A was assimilated.

The background bi-dimensional histogram for AMSU-A 50.3 GHz of Figure IV.3c shows a large spread around the diagonal, with more points above the diagonal than above consequently to an overestimation of the liquid water. The 1D-Var retrieval illustrated in Figure IV.3d notably increases the concentration of points around the histogram diagonal, by a slight decrease of cloud water content (Figure IV.4) and by cloud removal. Nevertheless the remaining positive bias suggests that the 1D-Var is not efficient enough in removing cloud layers.

Comparison with independent observations

As an independent validation of the 1D-Var retrievals, the ECMWF operational long-wave and short-wave operational broad-band models presented in section 3(b) are used to compute top-of-the-atmosphere fluxes for comparison with CERES observations. However, it must be kept in mind that the CERES observations lag three hours behind the ATOVS ones (see section 3(a)). During this period, cloud developments may significantly affect the comparison. Also the broad-band fluxes are sensitive to quantities that are not control variables in the 1D-Var, like specific humidity.

The statistics (bias and standard deviation) of model vs. observed outgoing long-wave

radiation (OLR) are displayed in Figure IV.5 as a function of the observed OLR and in tropical (20°S - 20°N) and mid-latitudes. Similarly to the brightness temperature results, a very large bias occurs for the cold observed OLRs, with the model first-guess being about 80 W.m^{-2} warmer. It can be seen that the 1D-Var reduces it to about 40 W.m^{-2} in the mid-latitudes and to less than 60 W.m^{-2} in the tropics. A remaining bias (also one of opposite sign for the high OLRs) was expected since clouds may have moved in-between the CERES and the ATOVS observations, in particular in the tropical convective areas. The observation time difference is also likely to explain the increase of the standard deviations in the mid-latitudes (by about 10 W.m^{-2}), because the 1D-Var systematically enhances the cloud radiative forcing.

The top-of-the-atmosphere short-wave radiation is more impacted by liquid water clouds than the infrared. The corresponding results are presented in Figure IV.6 with the total planetary albedo, which is the ratio between outgoing and incoming radiation at the top of the atmosphere. In the model computation, the local time is set to that of the CERES observation. The first-guess bias (model minus observation) goes from positive for small CERES albedos to negative for large CERES values. In addition to the observation time dif-

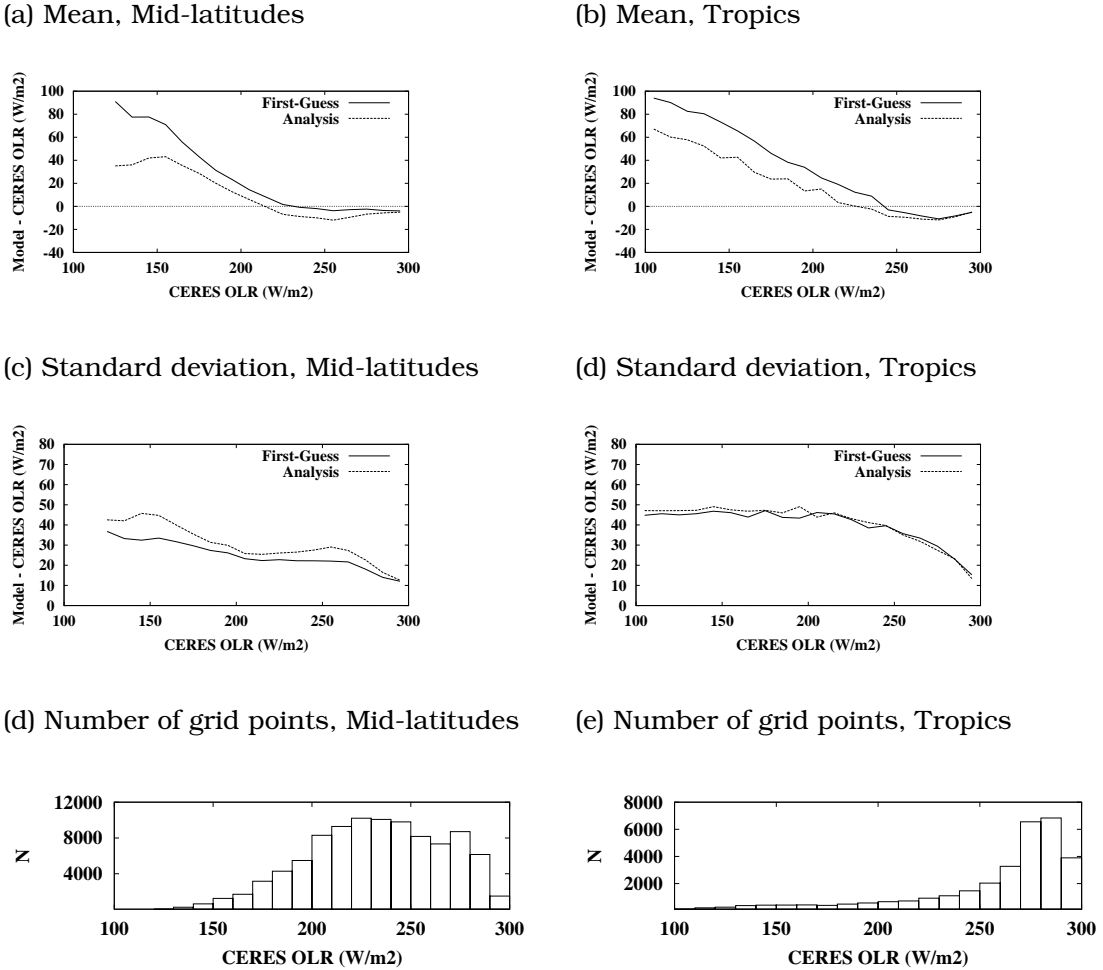


FIG. IV.5 – Mean and standard deviation of the difference between the top-of-the-atmosphere long-wave radiation (OLR) of the first-guess or of the analysis and the corresponding CERES measurements, as a function of CERES observation. The number of points used in the statistics (N) appears in the lower row. Distinction is made between tropical (20°S - 20°N) and mid-latitudes. The fluxes are in $\text{W} \cdot \text{m}^{-2}$.

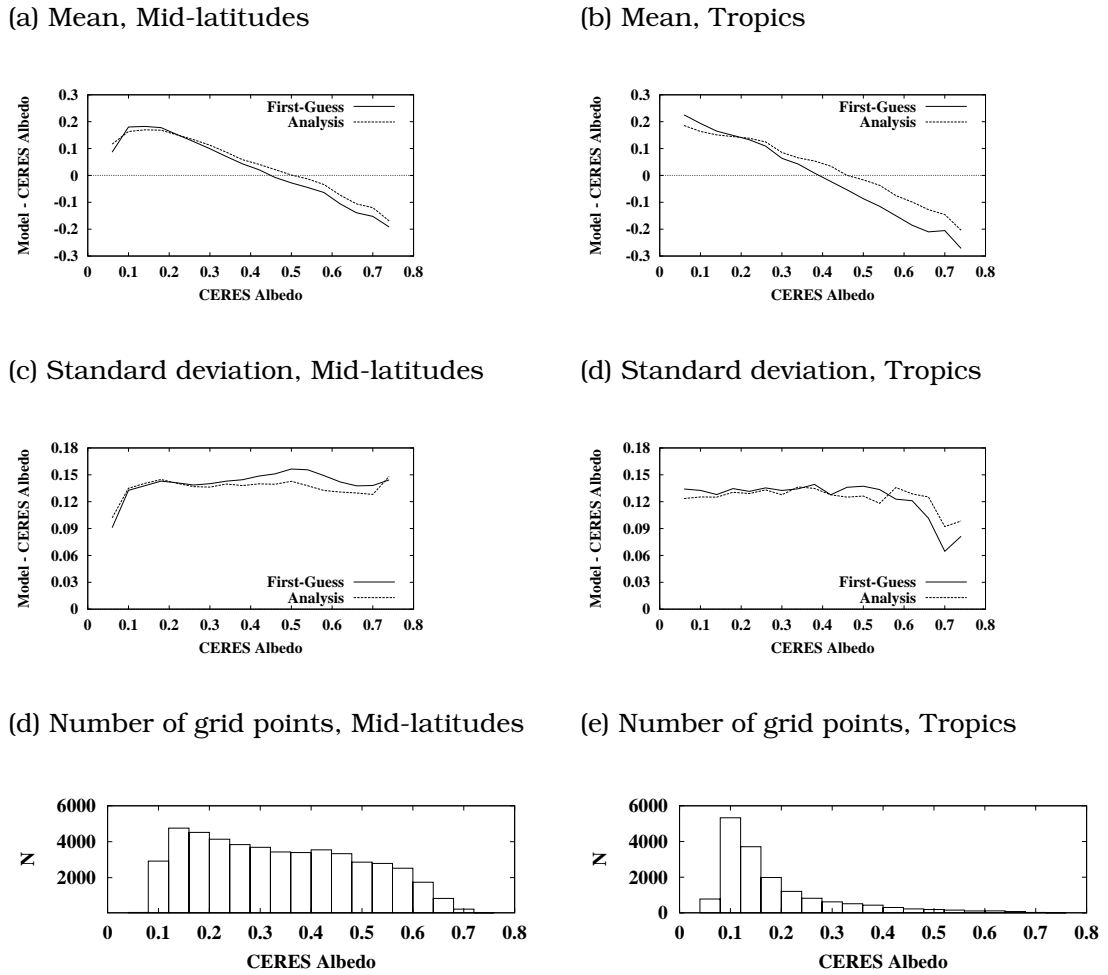


FIG. IV.6 – Same as previous but for the short-wave total planetary albedo.

ference, the bias for small CERES albedos is likely to be caused by excessive frequency of low clouds in the ECMWF model. The underestimation of ice water suggested by the infrared results mainly influences the bias for large CERES albedos, but thick liquid clouds may also induce such albedos. The 1D-Var retrieval reduces the bias at both ends, in particular for large CERES albedos (the reduction is of about 0.7 in the tropics). The standard deviation is overall reduced as well.

As a conclusion, the comparison with the CERES data highlights the improvement of the model ice clouds representation by the 1D-Var retrieval. A small positive impact is found for low clouds, that are controlled in the 1D-Var mostly by the broad microwave information.

IV.2.6 Discussion

A fast radiation model for the computation of cloud-affected brightness temperatures and its linearised versions (tangent-linear and adjoint) are presented. Their application in a 1D-Var scheme shows that information about liquid and ice water that is contained in the ATOVS radiances can be extracted by the 1D-Var. In non-precipitating areas over open oceans, where the surface properties are rather well known, clouds can be suppressed, created or modified to fit the observed radiances. In precipitating areas, which cover about 5% of the oceans, microwave radiances are significantly affected but no rain/snow absorption and scattering parametrisation has been introduced yet in the radiation model. This will be investigated in a further study with more complex parameterisations.

The coarse vertical resolution of cloud information in (A)TOVS radiances drove previous surveys towards the retrieval of single layer cloud properties (e.g., Eyre 1989; Wyllie *et al.* 1994; Stubenrauch *et al.* 1999) or of integrated contents (Zhao *et al.* 2000). The present study aims at an improved exploita-

tion of that information through profile retrieval, that uses a first-guess and an overlap hypothesis from a forecast model. This approach may be even more valuable when high spectral resolution measurements of Atmospheric Infrared Radiometric Sounder and Infrared Atmospheric Sounder Interferometer are available, that will provide higher vertical resolution of semi-transparent clouds. However the necessary specification of the first-guess error through a covariance matrix is made particularly difficult by the non-linearity of the cloud variables and by the model biases. This problem was solved here empirically. Furthermore top-of-the-atmosphere radiation is a weak constraint on profile retrieval and the retrieved profiles have a moderate degree of realism only. For instance, it was shown that excessive high clouds were generated by the method, even though the radiative impact of some of these may be small at the satellite height.

A particularly interesting prospect of the present study is the possibility of introducing the radiation model together with a diagnostic cloud scheme within the 4D-Var observation operator for the assimilation of cloud-affected ATOVS observations. In that case temperature, humidity and wind are control variables in place of cloud cover, liquid water and ice water, that become intermediary variables. By construction, the 4D-Var analysis achieves then a consistency between cloud parameters and dynamics, which is essential for forecast models. Indeed experiments have shown that a dynamics that is inconsistent with the cloud profiles loses the analysed cloud information within a few model time steps (Chevallier *et al.* 2000). This approach moves part of the non-linearities and thresholds from the control variable space to the observation operator, making the estimation of background error matrix easier and the minimisation more complex. Moreover the physics of a diagnostic scheme brings a supplementary constraint on cloud increments (e.g., correlations between

cloud cover, liquid water and ice water errors), that should improve them. This important issue is being investigated at ECMWF by Janisková (2001). The 4D-Var assimilation of cloud information is a large and complex project, of which the present study is only an aspect.

The validation of the present 1D-Var puts into evidence the limits of the sensitivity of infrared and passive microwave radiation to cloud properties. Up-coming international missions, like Cloudsat (Stephens *et al.* 2000) will allow a dramatic improvement in the vertical and horizontal resolution of cloud information compared to ATOVS, and may bring even more appropriate data for cloud assimilation. Nonetheless it is essential that a proper link is made between observed or retrieved data and the lower-resolution model variables.

Acknowledgments. This work was done at the Satellite Application Facility on Numerical Weather prediction which is co-sponsored by Eumetsat. The help of M. Janisková for the development of the tangent-linear and adjoint operators was much appreciated. Authors also thank J.-N. Thépaut, J. R. Eyre and R. Saunders for kind support and fruitful discussions, and two anonymous reviewers for helpful comments on the paper. The INRIA (Institut National de Recherche en Informatique et Automatique) provided the M1QN3 minimisation code.

References

- Barkstrom, B. R., 1984 : The Earth Radiation Budget Experiment (ERBE). *Bull. Amer. Meteo. Soc.*, 65, 1170-1185.
- Bayler, G. M., R. M. Aune, and W. H. Raymond, 2000 : NWP initialization using GOES sounder data and improved modeling of non-precipitating clouds. *Mon. Wea. Rev.*, 128, 3911-3920.
- Chevallier, F., P. Bauer, G. Kelly, C. Jakob, and T. McNally, 2001 : Model clouds over oceans as seen from space : comparison with HIRS/2 and MSU radiances. *J. Climate*, 14, 4216-4229.
- Chevallier, F., P. Bauer, G. Kelly, J.-F. Mahfouf, C. Jakob, and T. McNally, 2000 : Requirements for the assimilation of cloudy radiances. *ECMWF/ EuroTRMM Workshop on Assimilation of Clouds and Precipitation, Reading, UK, 6-9 November 2000*, 205-233.
- Chevallier, F., and G. Kelly, 2002 : Model clouds as seen from space : comparison with geostationary imagery in the 11- μm window channel. *Mon. Wea. Rev.*, 130, 712-722.
- Chevallier, F., and J.-J. Morcrette, 2000 : Comparison of model fluxes with surface and top-of-the-atmosphere observations. *Mon. Wea. Rev.*, 128, 3839-3852.
- Courtier, P., J.-N. Thépaut, and A. Hollingsworth, 1994 : A strategy for operational implementation of 4D-Var, using an incremental approach. *Q. J. Roy. Meteor. Soc.*, 120, 1367-1388.
- Ebert, E. E. and J. A. Curry, 1992 : A parameterization of cirrus cloud optical properties for climate models. *J. Geophys. Res.*, 97D, 3831-3836.
- English, S., C. Poulsen, and A. J. Smith, 1999 : Forward modelling for liquid water cloud and land surface emissivity. In *Proceedings of the ECMWF/EUMETSAT Workshop on use of ATOVS data for NWP assimilation, ECMWF, Reading, 2-5 November 1999*, 91-96.
- Errico, R. M., 1997 : What is an adjoint model ? *Bull. Amer. Meteo. Soc.*, 78, 2577-2591.
- Eyre, J. R., 1989 : Inversion of cloudy satellite sounding radiances by non-linear optimal estimation. I : Theory and simulation for TOVS. *Q. J. Roy. Meteor. Soc.*, 115, 1001-1037.

- Eyre, J. R., 1991 : A fast radiative transfer model for satellite sounding systems. *ECMWF Technical Memorandum No. 176*, 28 pp. [available from ECMWF, Shinfield Park, Reading RG2 9AX, UK].
- Fouquart, Y. and B. Bonnel, 1980 : Computation of solar heating of the Earth's atmosphere : a new parameterization. *Beitr. Phys. Atmosph.*, 53, 35-62.
- Gilbert, J. C., and C. Lemaréchal, 1989 : Some numerical experiments with variable-storage quasi-Newton algorithms. *Mathematical Programming*, 45, 407-435.
- Gregory, D., J.-J. Morcrette, C. Jakob, A. C. M. Beljaars, and T. Stockdale, 2000 : Revision of convection, radiation and cloud schemes in the ECMWF Integrated Forecasting System. *Q. J. Roy. Meteor. Soc.*, 126, 1685-1710.
- Harris, B. A., and G. Kelly, 2001 : A Satellite Radiance Bias Correction Scheme for Radiance Assimilation. *Q. J. Roy. Meteor. Soc.*, 127, 1453-1468.
- Hortal, M., 2000 : The development and testing of a new two-time-level semi-Lagrangian scheme (SETTLS) in the ECMWF forecast model. *Q. J. Roy. Meteor. Soc.*, in press.
- Hou, A. Y., D. V. Ledvina, A. M. da Silva, S. Q. Zhang, J. Joiner, R. M. Atlas, G. J. Huffman and C. D. Kummerow, 2000 : Assimilation of SSM/I-Derived Surface Rainfall and Total Precipitable Water for Improving the GEOS Analysis for Climate Studies. *Mon. Wea. Rev.*, 128, 509-537.
- Hufford, G., 1991 : A model for the complex permittivity of ice. *Int. J. Infrared Millimeter Waves*, 12, 677-681.
- Jakob, C., 2000 : The representation of cloud cover in atmospheric general circulation models. *PhD thesis*, Ludwig-Maximilians-Universität München, 193 pp.
- Jakob, C., and R. Rizzi, 1997 : Evaluation of model OLR in cloudy regions using TOVS-1B data. *Proc. of the Int. TOVS Study Conference, Igls, Austria, 20-26 February 1997*, 197-206.
- Janisková, M., 2001 : Preparatory studies for the use of observations from the Earth Radiation Mission in numerical weather prediction. European Space Agency contract report. ESA contract No. 13151/98/NL/GD, 79 pp [available from ECMWF, Shinfield Park, Reading RG2 9AX, UK].
- Liebe, H. J., T. Manabe, and G. A. Hufford, 1989 : Millimeter wave attenuation and delay rates due to fog/ cloud conditions. *IEEE Trans. Antennas Propag.*, 37, 1617-1623.
- Lipton, A. E., 1993 : Cloud shading retrieval and assimilation in a satellite-model coupled mesoscale analysis system. *Mon. Wea. Rev.*, 115, 3062-3080.
- Marécal, V., and J.-F. Mahfouf, 2000 : Variational retrieval of temperature and humidity profiles from TRMM precipitation data. *Mon. Wea. Rev.*, 128, 3853-3866.
- Marécal, V., and J.-F. Mahfouf, 2002 : Four dimensional variational assimilation of total column water vapor in rainy areas. *Mon. Wea. Rev.*, 130, 43-58.
- McMillin, L. M., and C. Dean, 1982 : Evaluation of a new operational technique for producing clear radiances. *J. Appl. Meteor.*, 21, 1005-1014.
- McNally, A. P., 2002 : A note on the occurrence of cloud in meteorologically sensitive areas and the implications for advanced infrared sounders. *Q. J. Roy. Meteor. Soc.*, in press.
- MacPherson, B., B. J. Wright, W. H. Hand and A. J. Maycock, 1996 : The impact of MOPS moisture data in the UK Meteorological Office mesoscale data assimilation scheme *Mon. Wea. Rev.*, 124, 1746-1766.
- Mlawer, E. J., S. J. Taubman, P. D. Brown, M. J. Iacono, and S. A. Clough, 1997 : Radiative transfer for inhomogeneous atmospheres : RRTM, a validated correlated-k model for the longwave. *J. Geophys. Res.*, 102, 16663-16682.
- Morcrette, J.-J., 1991 : Radiation and Cloud Radiative Properties in the European Centre for Medium Range Weather Forecasts forecasting system. *J. Geophys. Res.*, 96 :D5, 121-9132.
- Morcrette, J.-J., E. J. Mlawer, M. J. Iacono, and S. A. Clough, 2001 : Impact of the radiation-transfer scheme RRTM in the ECMWF forecasting system. *ECMWF Newsletter*, 91, 2-9.
- Morcrette, J.-J., and C. Jakob, 2000 : The response of the ECMWF model to changes in cloud overlap assumption. *Mon. Wea. Rev.*, 128, 1707-1732.
- Ou, S.-C., and K.-N. Liou, 1995 : Ice microphysics and climatic temperature feedback. *Atmos. Res.*, 35, 127-138.

- Parrish, D. F. and J. C. Derber, 1992 : The National Meteorological Center's Spectral Statistical Interpolation Analysis System. *Mon. Wea. Rev.*, 120, 1747-1763.
- Phalippou, L., 1996 : Variational retrieval of humidity profile, wind speed and cloud liquid-water path with the SSM/I : Potential for numerical weather prediction. *Q. J. Roy. Meteor. Soc.*, 122, 327-355.
- Rabier, F., P. Courtier, and O. Talagrand, 1992 : An application of adjoint models to sensitivity analysis. *Beitr. Phys. Atmos.*, 65, 177-192.
- Räisänen, P., 1998 : Effective longwave cloud fraction and maximum-random overlap clouds - a problem and a solution. *Mon. Wea. Rev.*, 126, 3336-3340.
- Rizzi, 1994 : Raw HIRS/2 radiances and model simulations in the presence of clouds. ECMWF Technical Memorandum No. 73, 29 pp. [available from ECMWF, Shinfield Park, Reading RG2 9AX, UK].
- Saunders, R., M. Matricardi, and P. Brunel, 1999 : An improved fast radiative transfer model for assimilation of satellite radiance observations. *Quart. J. Roy. Meteor. Soc.*, 125, 1407-1425.
- Smith, E. A., and L. Shi, 1992 : Surface forcing of the infrared cooling profile over the Tibetan plateau. Part I : Influence of relative longwave radiative heating at high altitude. *J. Atmos. Sci.*, 49, 805-822.
- Stephens, G., D. Vane, and S. Walter, 2000 : CloudSat : a new dimension in the satellite observation of global cloudiness. In *Proc. of the GCSS-WGNE-ECMWF Workshop on cloud processes and cloud feedbacks in large-scale models*, ECMWF, Reading, UK, 9-13 Nov. 1998, WMO/World Climate Research Programme, WMO/TD No. 993, 143-160.
- Stubenrauch, C.J., R. Holz, A. Chédin, D. Mitchell, and A.J. Baran : 1999 Retrieval of Cirrus ice crystal sizes from 8.3 and 11.1 μm emissivities determined by the Improved Initialization Inversion of TIROS-N Operational Vertical Sounder observations. *J. Geophys. Res.*, 104 :D24, 31793-31808.
- Tiedtke, M., 1993 : Representation of clouds in large-scale models. *Mon. Wea. rev.*, 121, 3040-3061.
- Washington, W. M. and D. L. Williamson, 1977 : A description of the NCAR GCM. In *Methods in Computational Physics*, 17, J. Chang. (Ed.), Academic Press, New York, 111-172.
- Wielicki, B. A., R. D. Cess, M. D. King, D. A. Randall, and E. F. Harrison, 1995 : Mission to Planet Earth : role of clouds and radiation in climate. *Bull. Amer. Meteo. Soc.*, 76, 2125-2153.
- Wylie, D. P., W. P. Menzel, H. M. Woolf, and K. I. Strabala, 1994 : Four years of global cirrus cloud statistics using HIRS. *J. Climate*, 7, 1972-1986.
- Zhao, L. R., N. C. Grody, R. R. Ferraro, C.-Z. Zou and F. Weng, 2000 : The new NOAA AMSU hydrological product suite : validation of AMSU-A TPW and CLW. In *Proc. of the American Meteorological Society 10th conference on satellite meteorology and oceanography*, Long Beach, CA, 9-14 January 2000, 196-199.

IV.3 Évaluation de l'adjoint du modèle direct

Cette section reprend l'article de Chevallier et Mahfouf (2001) paru dans *Journal of Applied Meteorology*.

Evaluation of the Jacobians of infrared radiation models for variational data assimilation

Frédéric Chevallier and Jean-François Mahfouf

European Centre for Medium-Range Weather Forecasts
Reading, UK.

Abstract. In this paper, linearised versions of fast infrared radiative transfer schemes for variational data assimilation are studied. A neural network-based infrared broad-band radiation model (NeuroFlux) is compared to the European Centre for Medium-Range Weather Forecasts operational radiation model. Also, a scheme for satellite brightness temperature computation (RTTOV) is compared to a more physically-based scheme : the narrow-band model Synstrad developed at European Organization for the Exploitation of Meteorological satellites. The Jacobians are examined. They are converted into flux perturbations with the tangent-linear approximation, and into atmospheric variable increments with a one-dimensional variational assimilation system. For NeuroFlux as well as for RTTOV, despite accurate flux and radiance computation, the sensitivity with respect to water vapour needs to be improved. However the random structure of the neural-network derivative error allows to use NeuroFlux with a single mean Jacobian in the variational context. Also, further improvements to RTTOV are expected from on-going work on the regression data-set and on the choice of the regression predictors.

IV.3.1 Introduction

A variational algorithm adjusts a set of control variables in order to minimise a function of these variables. Variational algorithms have been increasingly used in data assimilation for numerical weather prediction. They are particularly suitable to derive statistically optimal descriptions of the atmospheric state (the so-called *analyses* of the operational weather centres) used to provide initial conditions for forecast models. In this case the function, called *cost function*, essentially consists of two terms : the first one quantifies the fit of the model state to available observations, and the second one quantifies its fit to a prior estimate (usually a short-range forecast from a previous analysis), given statistics of ob-

servation and background errors. The principle of variational data assimilation has been known for several decades (e.g., Sasaki, 1958; Lewis and Derber, 1985; Le Dimet and Talagrand, 1986). However, its high computational cost has made it operationally available only recently. At European Centre for Medium-Range Weather Forecasts (ECMWF), a three-dimensional variational assimilation system (3D-Var : Courtier *et al.*, 1998) replaced a previous scheme based on optimal interpolation (Hollingsworth, 1987) in 1996. The inclusion of the time dimension of observations in the analyses was achieved in 1997 with a four-dimensional variational assimilation system (4D-Var) as described by Courtier *et al.* (1994). An important consequence of

the recent introduction of variational data assimilation in the operational weather centres is the necessity of accurate parametrisations in the analysis procedure not only in terms of atmospheric fluxes but also in terms of partial derivatives of the fluxes with respect to atmospheric variables (i.e. the Jacobians). These derivatives are needed to estimate the gradient of the cost function during the minimisation. This is placing an extra demand on modellers since it increases the requirements for the validation of physical parametrisation schemes. Moreover, a minimisation process is time-consuming when the description of the control variables is global. Therefore only fast physical parametrisations can be linearised for global variational analyses of the atmosphere. Examples of physical parametrisations for 4D-Var can be found in Janisková *et al.* (1999) and in Mahfouf (1999).

The present study examines two infrared radiation schemes for application in 4D-Var. They use different parametrisations because developments have been performed independently. The first model is a fast scheme for radiative flux computation that has been developed by Chéruy *et al.* (1996) and Chevalier *et al.* (1998). This scheme is based on artificial neural networks. The second one is the Radiative Transfer for Tiros Operational Vertical Sounder (RTTOV : Eyre, 1991; Saunders *et al.*, 1999) for satellite radiance computation. Each scheme is validated here for variational assimilation by comprehensive comparison with a more physically-based scheme : respectively the ECMWF operational wide-band model developed by Morcrette (1991) and the narrow-band model Synsatrad (Tjemkes and Schmetz, 1997). Estimating the quality of their Jacobians is not trivial. For a better understanding of the differences, they are converted into flux perturbations with the tangent-linear approximation, and into atmospheric variable increments with a one-dimensional variational assimilation system (1D-Var), where radiation is

the only physical process represented.

The plan of the paper is as follows. A description of the four infrared radiation models is given in section IV.3.2. Section IV.3.3 presents the general formalism of 4D-Var and 1D-Var. Section IV.3.4 shows the validation of the neural network-based scheme with the ECMWF operational wide-band model in a variational framework. Similarly, the comparison between RTTOV-5 and Synsatrad is detailed in section IV.3.5. Section IV.3.6 provides an overall summary.

IV.3.2 Description of the radiation schemes

Two schemes for infrared broad-band flux computation

The ECMWF operational infrared broad-band radiation model (hereafter EC-OPE) computes the atmospheric fluxes and cooling rates. The cooling rates are the vertical derivatives of the net fluxes at each pressure level. As described by Morcrette (1991), the long-wave spectrum from 0 to 2820 cm^{-1} is divided in EC-OPE into six spectral regions. The integration over wavenumber is performed using a band emissivity method. The transmission functions for water vapour and carbon dioxide over the six spectral intervals of the scheme are fitted using Padé approximants on narrow-band transmissions obtained with statistical band models. Clouds are represented by multi-layer grey bodies (Washington and Williamson, 1977). Recent improvements to the scheme affect the description of the water vapour continuum and of the ice cloud optical properties, as stated by Gregory *et al.* (1998). In the ECMWF operational forecast model, radiative fluxes are currently updated once every three hours and at sample points only, in order to save time in the rather expensive radiation computations (Morcrette, 2000). However, the code is still too slow for use in the variational analysis. Therefore a very simple long-wave radiation model

is used in 4D-Var. As described in Mahfouf (1999), it allows perturbations of fluxes and cooling rates to be computed with respect to temperature variations only.

In order to increase the time-space sampling, a faster version of EC-OPE, called NeuroFlux, has been derived using a statistical approach, the *multi-layer perceptron* defined by Rumelhart *et al.* (1986), together with the same cloud representation than in EC-OPE : the *multi-layer grey body model*. Consistently with the latter, upward and downward fluxes are computed in NeuroFlux as :

$$F(P_i) = \sum_k a_k F_k(P_i) \quad (\text{IV.3})$$

where P_i is the pressure level, F_k is the flux in the presence of a single layered black cloud in layer k or the clear sky flux (with the convention $k = 0$ for clear sky), and a_k is a weight. The a_k 's are functions of the layered cloud characteristics (cloud cover, liquid and ice water contents, particle size, ...; e.g., Ebert and Curry, 1992) and depend on the way cloudy layers overlap (e.g., Geleyn and Hollingsworth, 1979). In EC-OPE, the F_k 's are computed by the method summarised at the beginning of this section, whereas artificial neural networks are used in NeuroFlux. The parameters of the neural networks are derived from EC-OPE using a non-linear regression. The set of atmospheric profiles used to define the neural network (the learning dataset) is described by Chevallier *et al.* (2000a). The validation of NeuroFlux showed that it is seven times faster than the original code while its accuracy is comparable to the accuracy of the ECMWF operational scheme, with a negligible impact on numerical simulations (Chevallier *et al.*, 2000b).

Two schemes for satellite radiance computation

The RTTOV scheme is used operationally at ECMWF for the simulation of satellite brightness temperatures. It can handle instruments like Advanced TIROS Operational

Vertical Sounder (ATOVS), Special Sensor Microwave Imager (SSM/I) or Meteosat. Version 5 of this code (Saunders *et al.*, 1999) is used here. The method, originally derived from the work of McMillin *et al.* (1979), is single-band. It is based on two main approximations. The first one is that the Planck function does not vary significantly on the spectral interval considered (the spectral band of the satellite channel), so that a mean value of the Planck function can be introduced for each temperature. The second approximation is the use of a regression fitting to reference convolved line-by-line layer optical depths from the temperature and absorbing gas profiles. The reference line-by-line computations for RTTOV-5 come from GENLN2 version 4 (Edwards, 1992), with a water vapour continuum from the Clough *et al.* (1989) model, version 2.1. The temperature and absorbing gas profiles as inputs to the code are described on a fixed 43-level pressure grid.

RTTOV is compared here to Synsatrad, the narrow-band scheme developed at European Organization for the Exploitation of Meteorological satellites (EUMETSAT). This method, after Sneden *et al.* (1975), solves the monochromatic radiative transfer equation at uniformly sampled wave numbers (Tjemkes and Schmetz, 1997). The water vapour continuum refers to the Clough *et al.* (1989) model, version 2.2. The spectral resolution of the scheme depends on the channel. As an example, 750 wave numbers are used for the $6.3 \mu\text{m}$ channel on the Meteosat-7 platform, and 500 wave numbers are used for the $6.3 \mu\text{m}$ channel on High resolution Infrared Radiation Sounder (HIRS), second generation, on-board the NOAA-14 space-craft. This corresponds to resolutions of respectively 0.67 and 0.28 cm^{-1} .

The present study focuses on five channels that are of particular interest for operational weather forecasting : the water vapour sounding channels of HIRS on-board NOAA-14 at $12.5 \mu\text{m}$ (HIRS-10), $7.3 \mu\text{m}$ (HIRS-

11) and $6.3 \mu m$ (HIRS-12), the water vapour sounding channel of Meteosat-7 at $6.3 \mu m$ (Meteosat-WV), and the ozone sounding channel of HIRS on-board NOAA-14 at $9.7 \mu m$ (HIRS-09). Restriction is made here to clear-sky modelling. Carbon dioxide and minor absorbing gas concentrations are set to the estimated mean level for year 2005. The surface emissivity is set to one.

IV.3.3 Generalities about variational assimilation

General formalism of 4D-Var

The 4D-Var system seeks an optimal balance between observations and the dynamics of the atmosphere by finding a model trajectory $\mathbf{x}(t)$ which is as close as possible to the observations available during a given time period $[t_0, t_n]$. The model trajectory $\mathbf{x}(t)$ is completely defined by the initial state \mathbf{x}_0 at time t_0 .

The misfit to given observations \mathbf{y}^o and to an *a priori* model state \mathbf{x}^b called background is measured by an objective cost-function defined as follows :

$$\begin{aligned} J(\mathbf{x}_0) = & \frac{1}{2} (\mathbf{x}_0 - \mathbf{x}_0^b)^T \mathbf{B}^{-1} (\mathbf{x}_0 - \mathbf{x}_0^b) \\ & + \frac{1}{2} \sum_{i=0}^n (\mathbf{H}_i[\mathbf{x}(t_i)] - \mathbf{y}_i)^T \mathbf{R}_i^{-1} (\mathbf{H}_i[\mathbf{x}(t_i)] - \mathbf{y}_i) \end{aligned} \quad (\text{IV.4})$$

where at any time t_i , \mathbf{y}_i is the vector of observations, \mathbf{H}_i is the operator providing the equivalent of the data from the model variable $\mathbf{x}(t_i)$, \mathbf{R}_i is the observation error covariance matrix (measurement errors and representativeness errors, including H_i errors), and \mathbf{B} is the background error covariance matrix of the state \mathbf{x}^b . The background \mathbf{x}^b is usually provided by a short-range forecast. Superscripts -1 and T denote respectively inverse and transpose matrix. The subscript i denotes the time index.

In equation IV.4, the observation operator H_i includes a radiative transfer model for the computation of model-equivalent satellite

brightness temperatures, like RTTOV, if such quantities are assimilated.

The model state $\mathbf{x}(t_i)$ is defined as :

$$\mathbf{x}(t_i) = M(t_i, t_0)[\mathbf{x}_0] \quad (\text{IV.5})$$

where M is the non-linear forecast model integrated from time t_0 to time t_i . M may include an infrared radiative transfer model for the computation of fluxes and cooling rates, like the one described in Mahfouf (1999).

The control vector \mathbf{x}_0 includes the prognostic variables to be initialised in the forecast model : vorticity, divergence, temperature, specific humidity and surface pressure. The minimisation uses a descent algorithm which requires several computations of the gradient of J with respect to the initial state \mathbf{x}_0 . Given the dimension of the state vector the adjoint technique is used to provide an efficient estimate of ∇J (Le Dimet and Talagrand, 1986) :

$$\begin{aligned} \nabla J(\mathbf{x}_0) = & \mathbf{B}^{-1} (\mathbf{x}_0 - \mathbf{x}_0^b) \\ & + \sum_{i=0}^n \mathbf{M}_i^T \mathbf{H}_i^T \mathbf{R}_i^{-1} (\mathbf{H}_i[\mathbf{x}(t_i)] - \mathbf{y}_i) \end{aligned} \quad (\text{IV.6})$$

where \mathbf{H}_i^T is the adjoint of the observation operator and \mathbf{M}_i^T is the adjoint of the forecast model.

General formalism of 1D-Var

The principle of the 1D-Var is similar to that of 4D-Var, but the control vector \mathbf{x} represents only a single-column and the time dimension is not included. The cost-function reduces to :

$$\begin{aligned} J(\mathbf{x}) = & \frac{1}{2} (\mathbf{x} - \mathbf{x}^b)^T \mathbf{B}^{-1} (\mathbf{x} - \mathbf{x}^b) \\ & + \frac{1}{2} (\mathbf{H}(\mathbf{x}) - \mathbf{y})^T \mathbf{R}^{-1} (\mathbf{H}(\mathbf{x}) - \mathbf{y}) \end{aligned} \quad (\text{IV.7})$$

In the following, H is a radiation model, for instance RTTOV or EC-OPE. The control vector \mathbf{x} contains vertical profiles of temperature, specific humidity, and ozone. Given the low dimension of the control vector, a perturbation method is used to compute the Jacobian

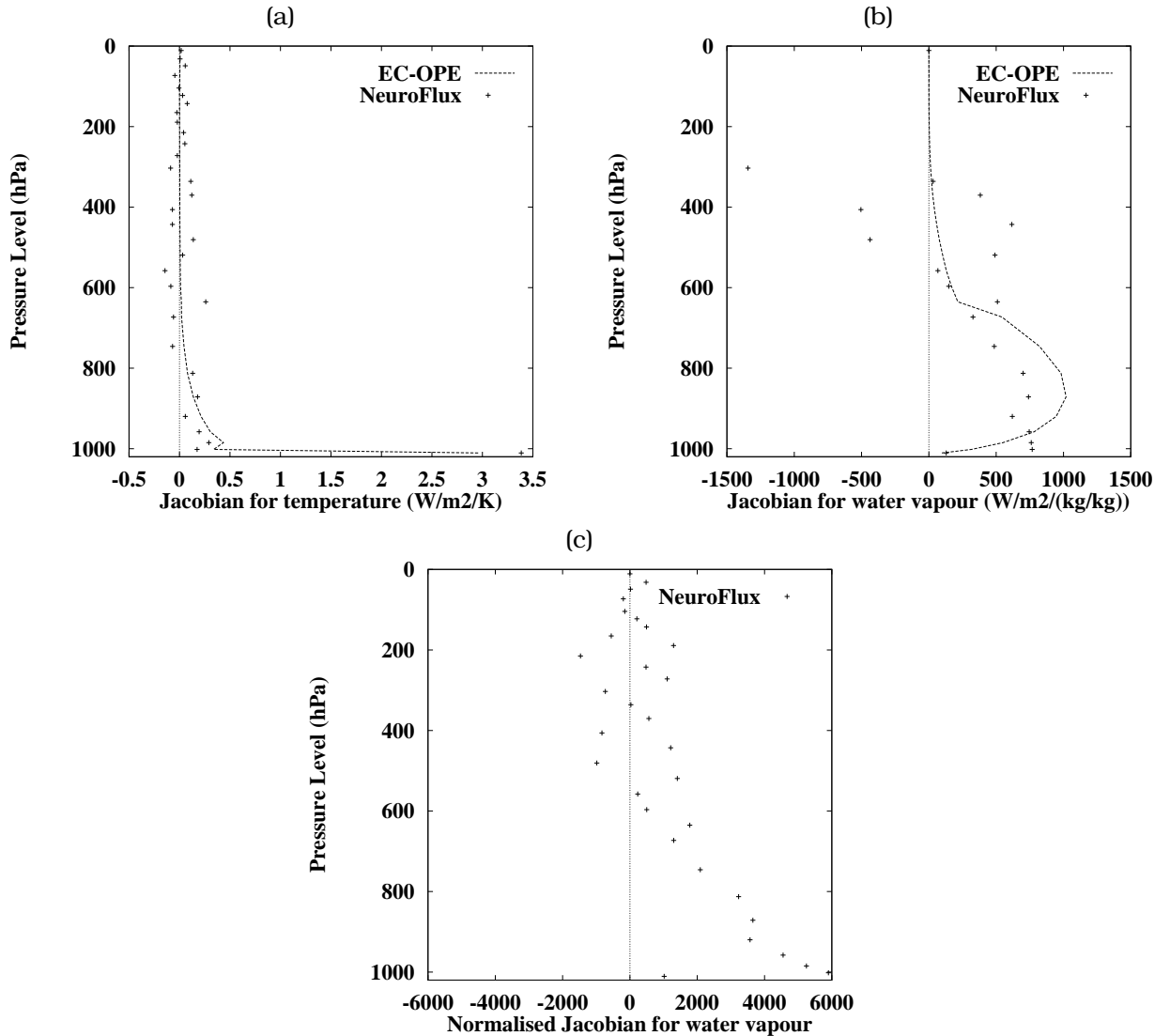


FIG. IV.7 – Jacobians of surface downward flux for temperature (a) and water vapour (b) as calculated by EC-OPE and NeuroFlux for the standard tropical atmosphere. The higher part of the neural network Jacobian for water vapour does not appear because NeuroFlux provides values above 300 hPa that are higher than those of EC-OPE by several orders of magnitude. The neural network Jacobian for water vapour, normalised in the neural network space, is shown in (c).

elements of the adjoint operator \mathbf{H}^T (i.e. the Jacobian matrix $\{\partial y_k / \partial x_l\}_{k,l}$). \mathbf{H}^T is required to compute the gradient of the cost function :

$$\nabla J(\mathbf{x}) = \mathbf{B}^{-1}(\mathbf{x} - \mathbf{x}^b) + \mathbf{H}^T \mathbf{R}^{-1}(\mathbf{H}(\mathbf{x}) - \mathbf{y}) \quad (\text{IV.8})$$

The minimiser of the present 1D-Var code is a limited memory quasi-Newton method, the M1QN3 software developed at Institut National de Recherche en Informatique et en Automatique (INRIA) (Gilbert and Lemaréchal, 1989). Examples of applications of the 1D-Var code can be found in Marécal and Mahfouf (1999) and in Fillion and Mahfouf (2000).

The background error covariance matrix

As shown in equations IV.4 and IV.7, the error covariance matrix \mathbf{B} plays an essential role in 1D- and 4D-Var by determining the spatial distribution of the information on the model variables (McNally, 2000). The matrices that are used in the ECMWF 4D-Var are described by Rabier *et al.* (1998) and by Derber and Bouttier (1999). The correlations are estimated by assuming that the difference between forecasts at different ranges valid at the same time are representative of short-range forecast error statistics, as is done by Parrish and Derber (1992). Specific humidity and ozone correlations are sharp on the vertical, whereas atmospheric temperature correlations are broad in the troposphere and in the lower stratosphere with negative correlations between the two regions. No cross-correlation between the background error of temperature, specific humidity and ozone is used. Mass and wind are coupled through a linear balance operator. The standard deviations of forecast errors for temperature and ozone have been derived with the same approach, whereas the water vapour standard deviations are computed from an empirical formula (Rabier *et al.*, 1998). An example of standard deviations of temperature and humidity is given in Figure 2 of Fillion and Mahfouf (2000). For temperature, they are

about one degree in the troposphere with higher values in the stratosphere, up to 4.5 K. The ozone standard deviations for unbalanced quantities (i.e. the fraction of the ozone errors not coupled with wind errors) are shown in Figure IV.8.

In the following, \mathbf{B} is specified according to the operational 4D-Var for unbalanced quantities at the corresponding vertical resolutions. Two vertical resolutions are used here : the 31- and 50-level grids that have been used operationally at ECMWF respectively between 1991 and 1998, and in 1999. For ozone, standard deviations are taken from the more recent 60-level model and vertical correlations are set to zero.

IV.3.4 Validation of NeuroFlux for variational assimilation

The multi-layer grey body approach in NeuroFlux

As explained in section IV.3.2, NeuroFlux has been derived from a non-linear regression to the ECMWF operational wide-band model (EC-OPE). In the ideal case, its computations would be identical to those of EC-OPE. In fact, the neural network parametrisation introduces some uncertainty in the fluxes and cooling rates, as well as in the Jacobians. As shown by Chevallier *et al.* (2000b), the accuracy of the method in terms of fluxes and cooling rates is high enough in the context of a numerical model of the atmosphere. For assimilation purposes, it is also important to have accurate Jacobians.

The Jacobians of NeuroFlux with respect to cloud characteristics are very similar to those of EC-OPE, because both schemes rely on the multi-layer grey body approach to treat cloudiness. Indeed, by differentiating Equation IV.3, it can be written :

$$dF(P_i) = \sum_k a_k.dF_k(P_i) + F_k(P_i).da_k \quad (\text{IV.9})$$

The da_k 's can be computed from the multi-layer grey body algorithm, with the same ac-

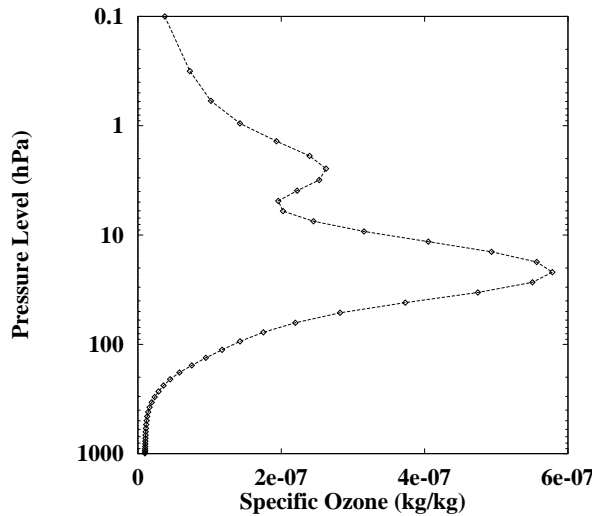


FIG. IV.8 – Profile of background error standard deviations for unbalanced ozone.

curacy in NeuroFlux and in EC-OPE. This requires little computing time compared to the F_k 's and dF_k 's computation. As a consequence the uncertainty of the dF 's computed by NeuroFlux lies in the F_k 's and dF_k 's. In NeuroFlux, they are computed by neural networks with comparable accuracy for each value of k .

Validation of the Jacobians

As an example of F_k , the clear-sky surface downward long-wave flux (SDLF) is considered here. The comparison between the Jacobians of the clear-sky SDLF for temperature and water vapour (i.e. the partial derivative of the flux with respect to temperature or water vapour) computed by NeuroFlux and EC-OPE is shown in Figures IV.7a and IV.7b in the case of a tropical standard atmosphere (McClatchey *et al.*, 1971). All the Jacobian elements for EC-OPE are positive which means that an increase in water vapour or temperature will increase the SDLF. Sensitivity of the SDLF to temperature is only significant near the surface and then decreases exponentially with height. Its sensitivity to specific humidity is important over a deeper layer of the lower troposphere up to 600 hPa. The decrease of the Jacobian near the surface comes from the dominance of water vapour absorption.

Compared to EC-OPE, the Jacobian of NeuroFlux for temperature appears irregular, though still close to the reference computation. The wiggles originate from the statistical approach of NeuroFlux. Indeed in a formal neural network, the information is propagated from its inputs to its outputs by non-linear projections on successive spaces, that transform and filter it. The localisation of the information, as on a pressure level grid, is partially lost. This has been already observed by Aires *et al.* (1999) for the modelling of HIRS brightness temperatures. The shape of the Jacobian for water vapour brings more concern. Not only the magnitude of the Jacobian below 600 hPa is underestimated, but NeuroFlux provides derivative values above 600 hPa that are higher than those of EC-OPE by several orders of magnitude. The reason of such irregularities is that, as explained by Chevalier (1998), the variables in input to the neural networks are normalised by dividing each variable by its spread in the learning dataset. The normalised Jacobians, as illustrated on Figure IV.7c, have limited oscillations. When projected on the physical space, using specific humidity as the water vapour variable, they convert into a chaotic profile in the upper atmosphere, where the values of specific humidity are very low.

Use of a single mean Jacobian in conjunction with NeuroFlux

The Jacobian weaknesses of NeuroFlux make it difficult to use them in variational data assimilation if significant water vapour increments are allowed by the B matrix (Equation IV.4) above 600 hPa. However, the accurate computation of finite-size perturbations of fluxes by NeuroFlux (Chevallier *et al.*, 2000b) suggests that NeuroFlux could be used to update the fluxes at each iteration of the minimisation, if a suitable Jacobian is provided by another way for the gradient computation. Such a configuration may solve the problem of computing time posed by EC-OPE.

A single mean Jacobian matrix is built as follows. The global archive of ECMWF 6-hour forecast from 1 March 1998 at 00 UTC is used to compute a mean temperature and water vapour profile, on the 31-level vertical pressure grid. The single mean Jacobian matrix is the Jacobian of this mean profile.

The association of NeuroFlux with the single mean Jacobian matrix is tested for variational assimilation. Two experiments are performed. First perturbations of cooling rates are computed. Then a 1D-Var scheme for the assimilation of surface fluxes is evaluated.

Impact on the computation of cooling rate perturbations.

Perturbations of atmospheric temperature, specific humidity, liquid and ice water, cloud cover and surface temperature, are estimated from the difference between the 6-hour and the 12-hour ECMWF forecasts valid for the first of July 1998 at 00 UTC. The resolution is of $2.5^\circ \times 2.5^\circ$ (10,300 grid points). For instance, the typical size of temperature perturbations is about one degree. Perturbations of long-wave cooling rates $\delta_1 C$ are then computed from the model variable perturbations δx : $\delta_1 C(\delta x) = C(x + \delta x) - C(x)$. Figure IV.9 presents the mean and standard deviation of the non-linear cooling rate perturbations computed with EC-OPE,

with and without cloud-radiation interaction. Three latitude classes are considered : tropical, mid-latitude and polar. Without cloud perturbations, standard deviations are below $0.5 K.d^{-1}$, except near the surface, where they reach $1.5 K.d^{-1}$ in average. Mean values are large only near the surface where they reach $0.3 K.d^{-1}$ in average for tropical and mid-latitude regions. With cloud perturbations, standard deviations increase up to $3.5 K.d^{-1}$, with some perturbations reaching up to $40 K.d^{-1}$ (not shown).

This dataset is used to validate the single mean Jacobian approach. For the single mean Jacobian approach, as for NeuroFlux, only the accuracy of clear-sky Jacobians matters if the multi-layer grey body algorithm is used to parametrise cloud effects. Indeed, from equation IV.9 it appears that :

$$\delta F(P_i) \simeq \sum_k a_k \cdot \delta F_k(P_i) + F_k(P_i) \cdot \delta a_k \quad (\text{IV.10})$$

Equation IV.10 is a good approximation when the perturbations δF_k and δa_k are small ($|\delta F_k| \ll F_k$ and $|\delta a_k| \ll a_k$). For analysis increments, this approximation is valid for δF_k but not for δa_k . Indeed δa_k can reach the size of a_k . But in this case $F_k(P_i) \cdot \delta a_k$ is the dominant term in equation IV.10, as seen by the comparison between Figures IV.9c and IV.9d, which makes the approximation still accurate.

To estimate qualitatively the variations of the clear sky Jacobians, cooling rate perturbations $\delta_2 C$ are computed from the temperature, specific humidity and surface temperature perturbations of the dataset, using a first-order Taylor development : $\delta_2 C(\delta x) = J \delta x$, where J is the single mean Jacobian matrix defined above. Figure IV.10 compares the clear-sky non-linear cooling rate perturbations from EC-OPE, $\delta_1 C$, and the linear perturbations $\delta_2 C$. The differences between the two computations originate both from the tangent-linear hypothesis and from the use of a single mean Jacobian matrix. They appear to be comparable to the signal (i.e. the non-

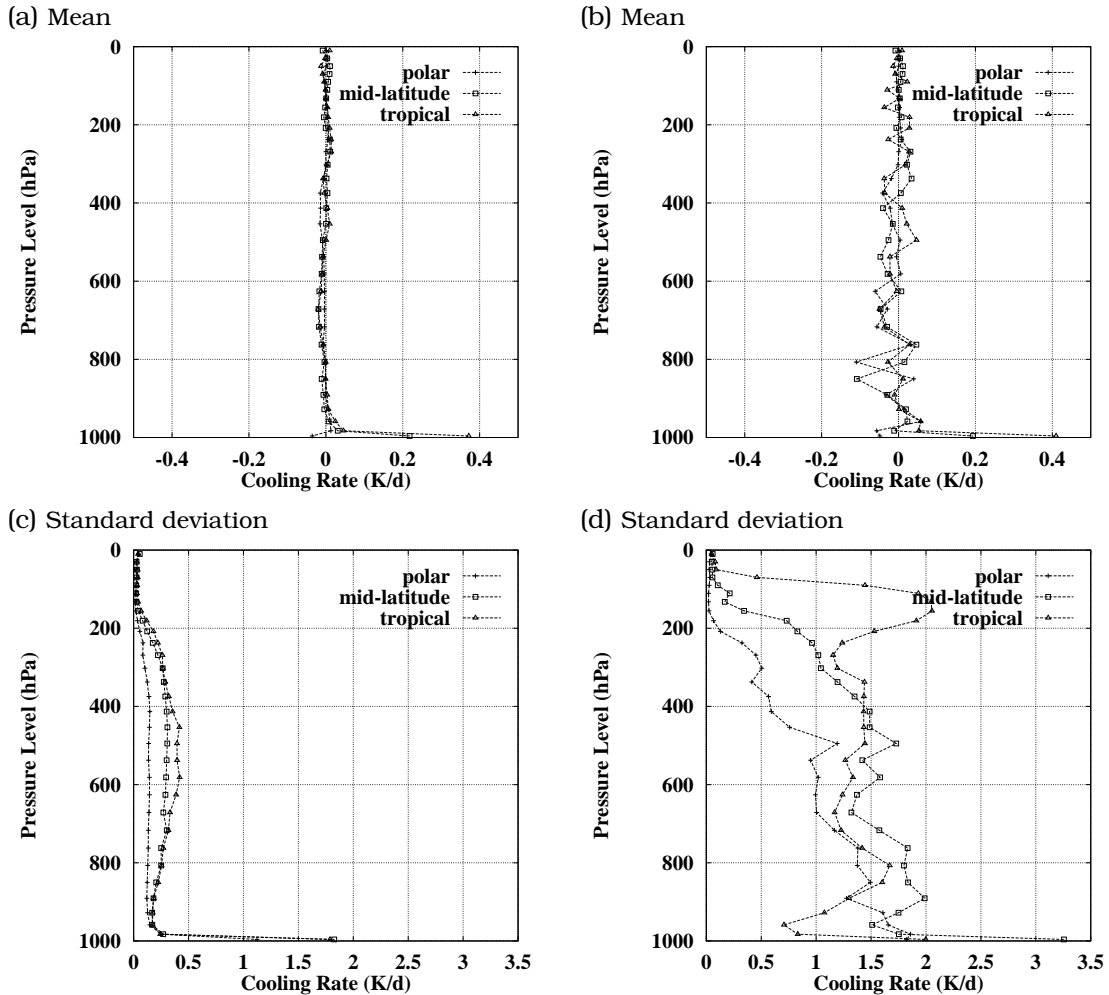


FIG. IV.9 – Mean (top row) and standard deviation (bottom row) of the clear sky (left column) and the total sky (right column) non-linear cooling rate perturbations, in $K.d^{-1}$. The perturbations are taken from the difference between the ECMWF 6- and 12- hour forecasts for 1 July 1998 at 00 UTC. Results are shown in three latitude classes.

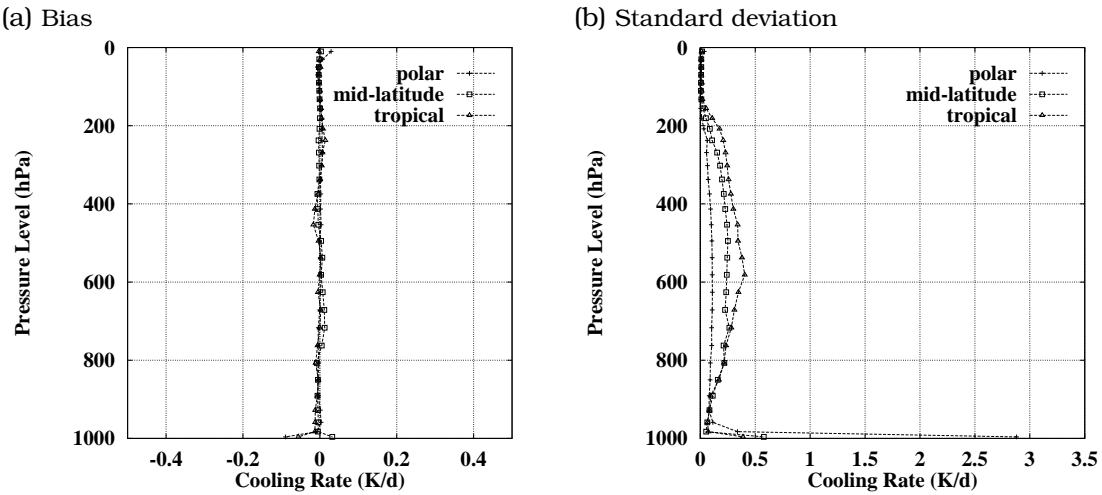


FIG. IV.10 – Mean (a) and standard deviation (b) of the comparisons between tangent linear and non-linear clear sky cooling rates, in $K.d^{-1}$. The tangent linear approach uses a single mean Jacobian. The perturbations are taken from the difference between the ECMWF 6- and 12-hour forecasts for 1 July 1998 at 00 UTC. Results are shown in three latitude classes. On (b), the standard deviation of the error in the polar class reaches $3 K.d^{-1}$ at the surface, whereas they are below $0.6 K.d^{-1}$ in the other latitudes.

linear perturbations shown in Figure IV.9), except below 900 hPa in the tropical and mid-latitudes, where the standard deviation of the differences, as well as the bias, are significantly smaller than the signal. Improvement in the polar class could be obtained with a standard polar Jacobian. Because the comparison takes the tangent-linear hypothesis into account, the performance of the single mean Jacobian is underestimated. As illustrated below, the existence of a clear-sky Jacobian is important from the top of the atmosphere to the surface.

Table IV.1 completes this study with the statistics of the corresponding boundary fluxes : the outgoing long-wave radiation and the surface net fluxes. The error of the tangent-linear computation appears to be significantly below the signal. Indeed the error standard deviation is less than 60% of the standard deviation of the clear-sky non-linear computation in every latitude classes, with negligible biases (less than $0.2 W.m^{-2}$).

The variability of the clear sky Jacobians does not appear to play an essential role when

computing all sky flux and cooling rate perturbations. As stated in the beginning of this section, the error of NeuroFlux compared to EC-OPE only concerns clear-sky modelling. This may allow to use a single mean Jacobian with NeuroFlux for variational data assimilation. This is further investigated in the next section.

Impact on variational assimilation. The single mean Jacobian approach is further tested in a 1D-Var data assimilation, where only its contribution determines the increments. Use is made of observations that were collected at Billings (Oklahoma, U. S. A.) as part of the Atmospheric Radiation Measurement (ARM) program (Stokes and Schwartz, 1994). A series of five clear-sky days in December 1997 is selected to evaluate a 1D-Var assimilation of SDLF. Observations of SDLF (from a pyrgeometer) were available on a two-minute basis and were processed to get hourly averages. Corresponding hourly atmospheric profiles for temperature and specific humidity are taken from ECMWF operatio-

(a) Outgoing long-wave radiation

	polar		mid-latitude		tropical	
	M	σ	M	σ	M	σ
TL - NL clear sky	-0.02	0.70	0.03	1.20	-0.14	1.46
NL clear sky	-0.13	1.49	-0.19	2.36	0.11	2.84
NL total sky	0.11	5.71	-0.19	11.78	0.74	17.27

(b) Surface net long-wave flux

	polar		mid-latitude		tropical	
	M	σ	M	σ	M	σ
TL - NL clear sky	-0.04	1.75	0.01	0.64	0.15	1.00
NL clear sky	0.16	2.94	0.04	4.52	-0.19	3.86
NL total sky	1.36	10.57	0.39	13.69	0.39	9.57

TAB. IV.1 – First row of each table shows the mean (M) and standard deviation (σ) of the comparisons between tangent-linear (TL) and non-linear (NL) clear sky outgoing long-wave radiation and clear sky surface net flux perturbations. Middle row shows the mean and standard deviation of the NL clear sky flux perturbations. Bottom row shows the mean and standard deviation of the NL total sky flux perturbations. The perturbations are taken from the difference between the ECMWF 6- and 12- hour forecasts for 1 July 1998 at 00 UTC. The fluxes are in $W.m^{-2}$. Results are shown in three latitude classes.

nal short-range forecasts. The profiles as well as the background statistics (the matrix \mathbf{B} of Equations IV.4 and IV.7) are described on a 31-layer vertical grid. The standard deviation of error for the SDLF is set to $10 W.m^{-2}$ as suggested by the standard for measurements set by the Baseline Surface Radiation Network (Heimo *et al.*, 1993).

The time series of model SDLF and of SDLF from ARM observation are shown in Figure IV.11c for the selected five days. The model systematically underestimates the observation fluxes up to $20 W.m^{-2}$. The reader is referred to Chevallier and Morcrette (2000) for a discussion about these differences. In this context, the 1D-Var iteratively modifies the temperature and water vapour profiles in order to better match the observed SDLF within a range of background errors given by the covariance matrix \mathbf{B} .

The result of the 1D-Var assimilation using the EC-OPE radiation scheme produces a series of long-wave fluxes in better agreement with the observations as expected (Figure

IV.11c). In agreement with the vertical structure of the Jacobians (Figure IV.7), the increase in long-wave flux has been done mostly through an increase of water vapour in the atmospheric column. The time series of the total column water vapour is shown in Figure IV.11d.

In the single mean Jacobian approach, NeuroFlux is used in the 1D-Var to update the SDLF at each iteration of the minimisation, whereas the single mean Jacobian matrix is used to compute the gradient of the cost function. Figures IV.11a and IV.11b show that the increments of SDLF and of total column water vapour computed by the single mean Jacobian approach are in good agreement with those computed by EC-OPE. A similar agreement is found for the vertical variation of the water vapour increments (not shown). Also, the number of iterations that is needed by the 1D-Var scheme to converge is about 25% smaller with the single mean Jacobian approach than with EC-OPE. This clearly indicates that the association of Neu-

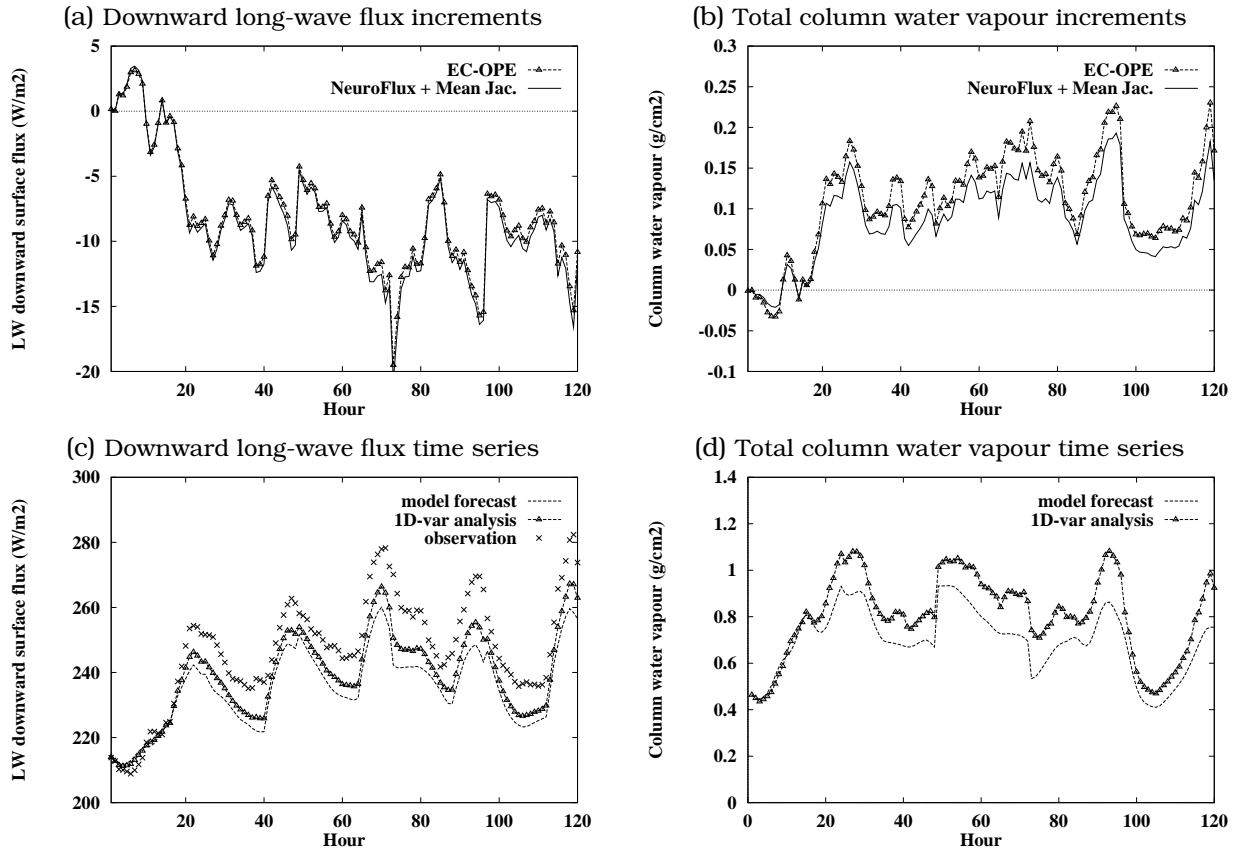


FIG. IV.11 – (a) shows the difference between the downward long-wave flux from a 1D-Var analysis using either EC-OPE or the single mean Jacobian approach, and the flux measured at ARM-SGP site by a pyrgeometer. The corresponding time series of total column water vapour increments are shown in (b). Flux and total column water vapour values are presented for EC-OPE on (c) and (d) respectively. In the single mean Jacobian approach, NeuroFlux is used to update the trajectory. The gradient computations are performed with a single mean Jacobian matrix.

roFlux and of the single mean Jacobian is reasonably consistent. Moreover, the use of a pre-computed Jacobian is obviously faster than an explicit computation.

Summary

The neural network-based Jacobians contain features that are considered not to be realistic. During the learning phase of the neural networks, a non-linear regression is performed to produce accurate fluxes and cooling rates. The inclusion of the Jacobians in the non-linear regression would increase the number of constraints by two orders of magnitude. This can be achieved with more complex neural networks, but the model would then be computationally less efficient. Now, the computational burden prevents EC-OPE to be introduced in the variational analysis and faster solutions are studied. An approach is proposed for variational assimilation, in which NeuroFlux only updates the fluxes in the minimisation, or re-computes the initial ones if the incremental 4D-Var is used. The gradient computation is performed with a single mean Jacobian. Both results from 1D-Var assimilation and tangent-linear approximation show that this approach is able to provide fast computations with good accuracy.

IV.3.5 Comparison between RTTOV-5 and Synsatrad

General

RTTOV and Synsatrad have been already compared for brightness temperature and Jacobian computation in the GEWEX Water Vapor Project (GVaP) where 23 models have been analysed with respect to the $6.3 \mu\text{m}$ channel on-board NOAA-14 (Soden *et al.*, 2000). It was confirmed that Synsatrad is in better agreement with line-by-line models than RTTOV. In particular, the behaviour of RTTOV Jacobians for water vapour was shown to be significantly different from that of the other mo-

dels. A comparison of some 19 models in the framework of the International ATOVS Working Group (ITWG) is enlarging the comparison to seven channels of HIRS (L. Garand, personal communication 2000). The present study completes these previous results. In addition to Eyre *et al.* (1993), who showed the positive impact of using RTTOV in the ECMWF analysis system through a 1D-Var retrieval, the present study compares its Jacobians to those from a more accurate scheme : Synsatrad. Compared to the previous Jacobian inter-comparisons, an interpretation of the Jacobians in terms of increments of geophysical quantities, *via* the 1D-Var, is provided here.

Comparison of brightness temperatures

To compare RTTOV and Synsatrad, a representative set of atmospheric profiles is used (Chevallier, 1999). It has been obtained by a random selection of 150 situations among a large set of 13,700 carefully sampled ECMWF global 6-hour forecasts. 28 extreme profiles have been added. Unlike temperature and specific humidity, ozone comes from a climatology dependent on season and latitude (Fortuin and Langematz, 1994). In order to avoid any artefact due to orography, only profiles with a surface pressure higher than 950 hPa are used here : 103 cases. 49 of them are taken from high- and mid- latitude situations (i.e. latitudes higher than 30° in absolute value), and 54 are located in the tropical band. These profiles, defined on a 50-level vertical grid, are interpolated on the RTTOV fixed 43-level grid. Therefore, the radiation computations are performed at the same resolution for both RTTOV and Synsatrad.

Table IV.2 presents the comparison between RTTOV and Synsatrad for the computation of the brightness temperatures in channels HIRS-09, -10, -11, -12 and Meteosat-WV. In the high- and mid- latitude situations, mean differences are below 0.4 K with standard deviations up to 0.7 K . Differences

(a) High and mid-latitudes

	HIRS-09		HIRS-10		HIRS-11		HIRS-12		MET. WV	
	M	σ								
RTTOV-5 - Synsatrad	-0.3	0.4	-0.1	0.2	0.4	0.4	0.3	0.7	0.0	0.7
Synsatrad	249.9	13.3	267.5	14.6	251.3	7.4	239.3	6.3	239.1	6.3

(b) Tropical latitudes

	HIRS-09		HIRS-10		HIRS-11		HIRS-12		MET. WV	
	M	σ								
RTTOV-5 - Synsatrad	-0.6	0.1	-0.5	0.3	-0.1	0.5	-0.2	0.9	-0.9	1.0
Synsatrad	274.3	3.0	287.4	3.1	261.2	4.5	245.5	6.1	245.5	6.0

TAB. IV.2 – Statistics of the comparison of Synsatrad and RTTOV-5 for the computation of brightness temperatures, in K.

are slightly higher for tropical latitudes, with biases and standard deviations up to 0.9 K. These numbers are comparable to the validation statistics of RTTOV-5 shown by Saunders *et al.* (1999), even if the sign of the biases may differ. Indeed, as explained in section IV.3.2, Synsatrad solves the monochromatic radiative transfer equation, and therefore is more accurate in principle than RTTOV-5, but is still not a line-by-line model. Differences in the reference line-by-line computations of the two schemes, like the water vapour continuum versions used (versions 2.1 and 2.2 of the Clough *et al.* -1989- parametrisation), are not likely to affect the results to a significant extent. The higher bias occurs for Meteosat-WV in the tropics : 0.9 K. It is associated with a standard deviation of 1 K. This bias is further investigated in section IV.3.5.

Comparison of 1D-Var increments

The 1D-Var scheme described in section IV.3.3 allows for a further comparison between RTTOV-5 and Synsatrad. The global 103 profile set is used. 1D-Var increments are computed on the 50-level grid, so that the corresponding ECMWF error statistics can be applied. A vertical interpolation scheme is provided between the minimiser and the radiation models, that are both applied on the RTTOV fixed 43-level grid.

Simulated observations are constructed by adding 1 K to the 1D-Var first-guess brightness temperature, with respect to each code. A 1 K standard deviation for the observation uncertainty is specified for each channel. Tests with a 0.5 K standard deviation show similar results, differing only in the amplitude of the signals. Resulting 1D-Var increments of temperature, water vapour and ozone for each channel are examined. The conclusions for channels HIRS-11, -12 and Meteosat-WV are very similar. Therefore results for HIRS-11 and Meteosat-WV are not presented.

HIRS-09. As seen in table IV.3, the 1D-Var brightness temperature increments are small for HIRS-09, in particular in the high- and mid-latitude regions where the mean increment reaches 0.1 K only. Higher increments (0.3 K in the high- and mid-latitude regions) can be obtained if surface temperature is introduced in the 1D-Var control variables. Note that the increments would reach 1 K if no background term was specified in the cost function (equation IV.7). Of course, they would be zero if the observation term was omitted. The corresponding Jacobians for ozone, shown in Figure IV.12, peak at about 350 hPa, with higher values in the tropics than in other latitudes, whereas the maximum values of the ozone pro-

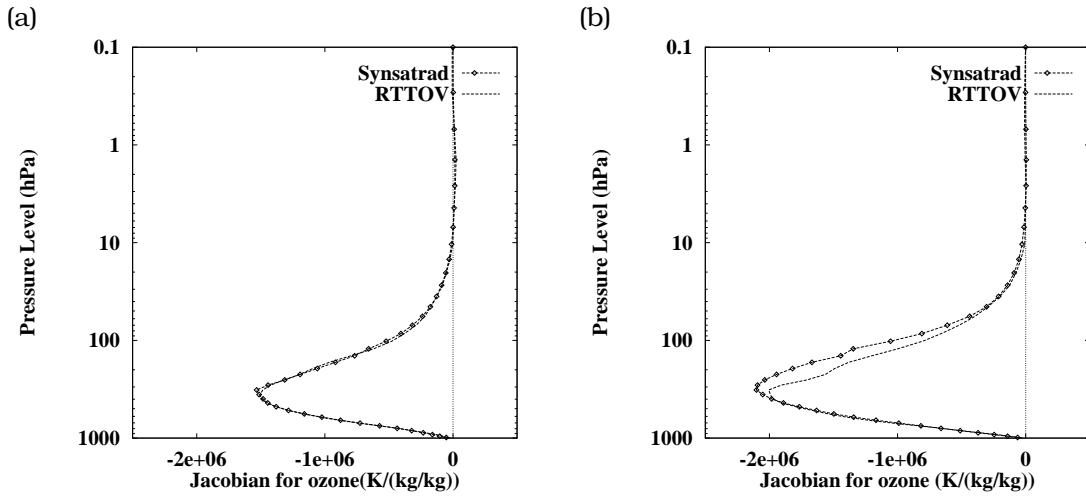


FIG. IV.12 – Mean Jacobian for ozone from Synsatrad and RTTOV for the high and mid latitudes (a) and for tropical latitudes (b) at the first iteration of 1D-Var. HIRS-09, tropical latitudes.

(a) High and mid-latitudes

	HIRS-09	HIRS-10	HIRS-11	HIRS-12	MET. WV
Mean δT_b RTTOV-5	0.10	0.29	0.64	0.80	0.81
Mean δT_b Synsatrad	0.11	0.30	0.62	0.75	0.75

(b) Tropical latitudes

	HIRS-09	HIRS-10	HIRS-11	HIRS-12	MET. WV
Mean δT_b RTTOV-5	0.28	0.66	0.78	0.84	0.84
Mean δT_b Synsatrad	0.31	0.63	0.77	0.83	0.83

TAB. IV.3 – Mean brightness temperature increment (δT_b) of the 1D-Var using either RTTOV-5 or Synsatrad.

files, in $kg.kg^{-1}$, occur at about 10 hPa . As a consequence, HIRS-09 is mostly sensitive to a region of the atmosphere in between, about 200 hPa , where only low increments of ozone, in $kg.kg^{-1}$, are allowed in the 1D-Var because of the background term, as shown in Figure IV.8. As shown in Figure IV.12, the RTTOV derivative values above 400 hPa are smaller than those of Synsatrad in the tropical regions. In the other regions, they are in good agreement.

The Jacobians for temperature, not shown, have their maximum higher in altitude, about 25 hPa , with a second local maximum at about 900 hPa . The corresponding temperature increments in the 1D-Var are very small in the tropical regions, less than 0.04 K , and are higher in the other latitudes, up to 0.2 K in average, with a good agreement between RTTOV and Synsatrad (not shown).

The ozone increments are shown in Figure IV.13. Consistently with the previous comment, the specific ozone increments peak at about 30 hPa , whereas the relative change of ozone mostly occurs at 200 hPa . As the gradient of the specified ozone error standard deviations (Figure IV.8) is sharp at 200 hPa , the reduction of the Jacobian values above 400 hPa from Synsatrad to RTTOV makes the ozone increments smaller for RTTOV.

HIRS-10. The brightness temperature increments are larger for HIRS-10 than for HIRS-09 : respectively about 0.30 and 0.65 K in the high and mid-latitude regions and in the tropical ones (table IV.3). Jacobians have their maximum in the low troposphere for the temperature and around 450 hPa for the water vapour (see figure IV.14 for the high and mid-latitude regions). There is no ozone absorption in this channel. Compared to Synsatrad, RTTOV-5 has smaller temperature Jacobians, and larger, somewhat irregular, water vapour ones.

The 1D-Var temperature and water vapour increments are shown in figures IV.16 and

IV.15 for the high and mid-latitude regions. The shape of the temperature increments reflects the specified background error covariance matrix, that includes negative correlations between temperature errors in the lower stratosphere and those in the troposphere (section IV.3.3). Temperature and water vapour increments are similar for both models in value as well as in shape. The Jacobian differences shown in figure IV.14 do not seem to be significant for variational data assimilation applications.

In the tropics, the brightness temperature increments are mainly due to specific humidity. Water vapour increments are similar for both schemes (not shown).

HIRS-12. The brightness temperature increments for HIRS-12 are similar with RTTOV and Synsatrad : between 0.75 and 0.85 K (Table IV.3). Jacobians have their maximum at about 500 hPa for temperature and at about 250 hPa for water vapour (Figure IV.17). If those for temperature are similar between the two models, the water vapour Jacobians have a clear distinct behaviour. RTTOV values are more than twice as high than for Synsatrad. Also, the maximum is higher in altitude with RTTOV. As expected the increment difference appears more for water vapour than for temperature (Figures IV.18 and IV.19). Indeed mean relative changes of water vapour reach 40% with RTTOV at 200 hPa while not exceeding 20% with Synsatrad. Of course, these relative changes at 200 hPa correspond to small absolute amounts of water vapour (Figure IV.19c).

Discussion

For the five channels studied (HIRS-09, -10, -11, -12 and Meteosat-WV), differences in computed brightness temperatures between the RTTOV and Synsatrad have usually less than half a degree bias and standard deviation. Jacobians for temperature appear to be in good agreement, while the width of HIRS-

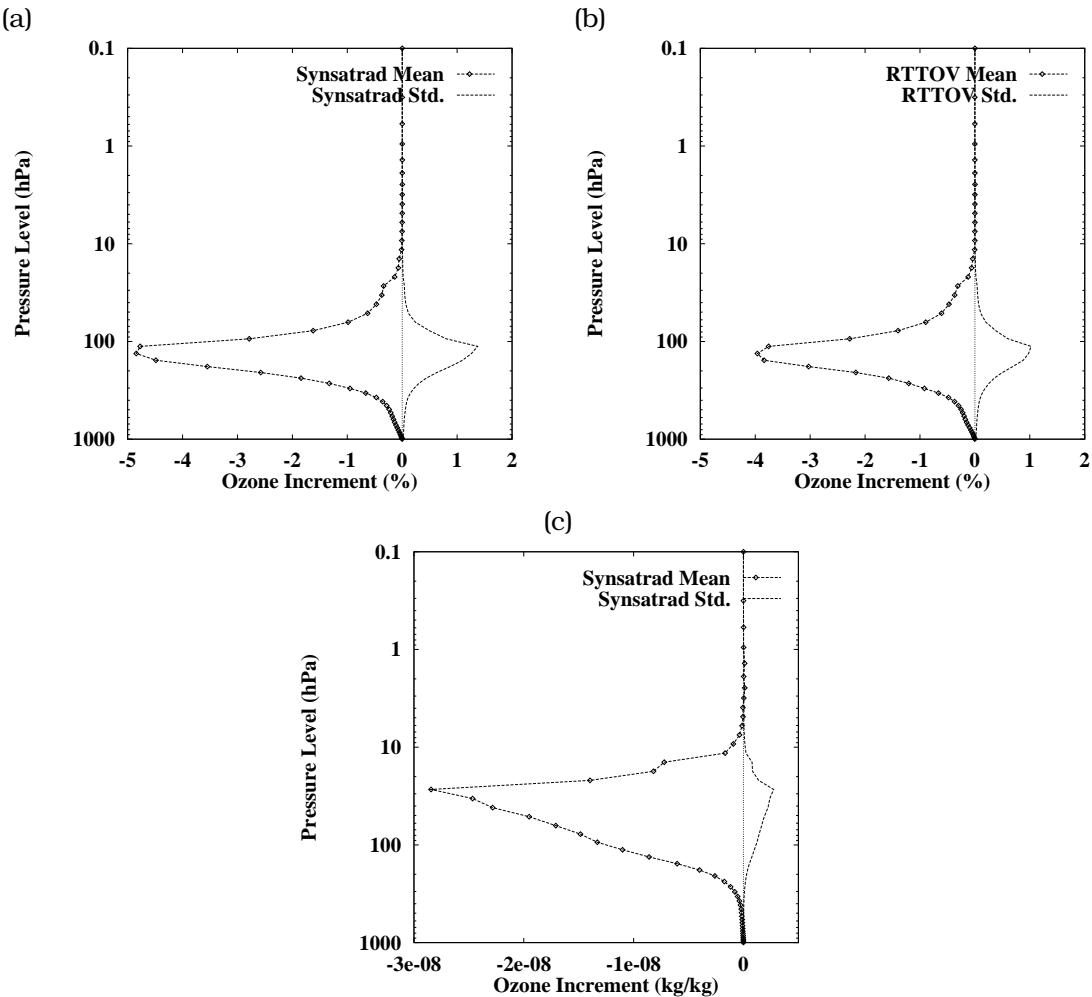


FIG. IV.13 – Statistics of ozone increments, in %, of Synsatrad (a) and RTTOV (b). The statistics expressed in terms of specific ozone values, in $\text{kg} \cdot \text{kg}^{-1}$, are shown in (c) for Synsatrad.

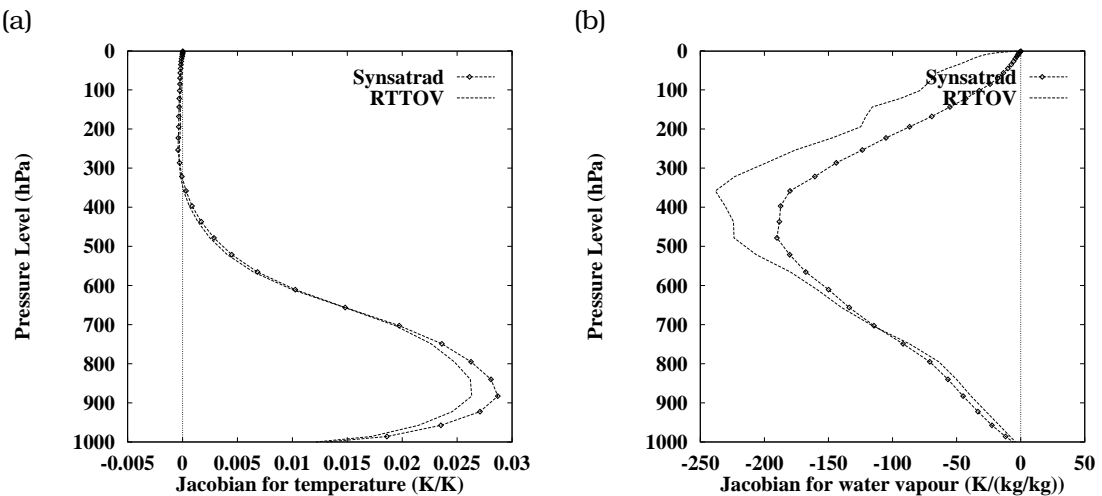


FIG. IV.14 – HIRS-10, high and mid-latitudes. Mean Jacobians for temperature and water vapour from Synsatrad and RTTOV at the first iteration of 1D-Var.

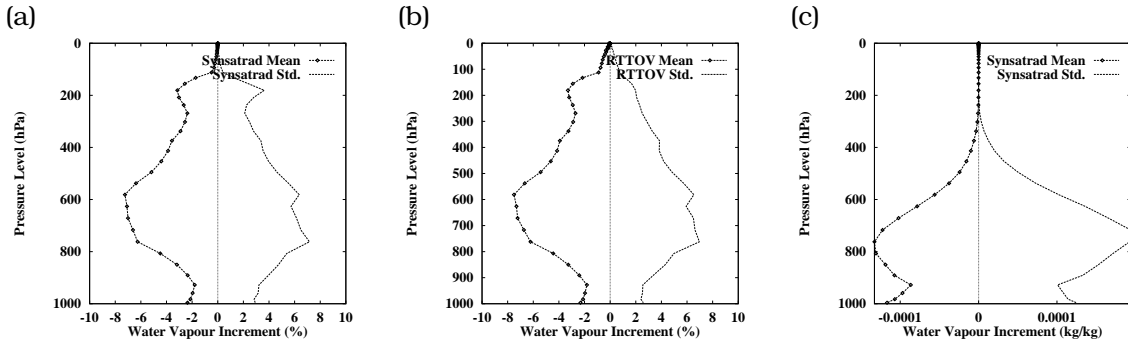


FIG. IV.15 – HIRS-10, high and mid-latitudes. Statistics of the water vapour increments from Synsatrad (a) and RTTOV-5 (b), in terms of relative change of specific humidity. The statistics in terms of specific humidity are shown in (c) for Synsatrad.

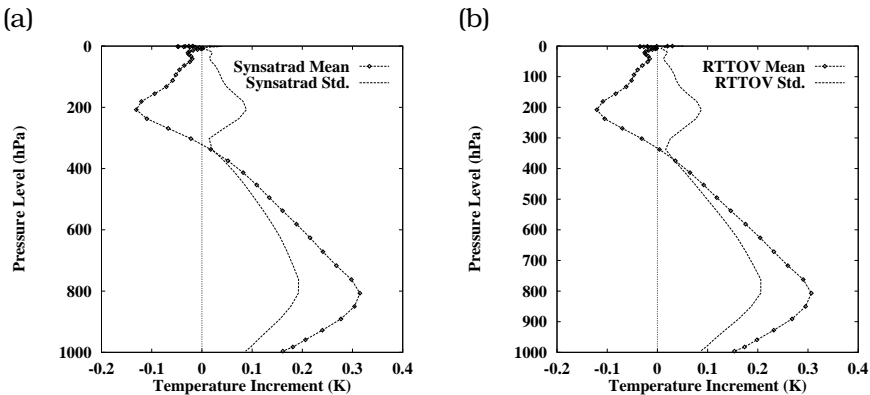


FIG. IV.16 – HIRS-10, high and mid-latitudes. Statistics of the temperature increments from Synsatrad (a) and RTTOV (b).

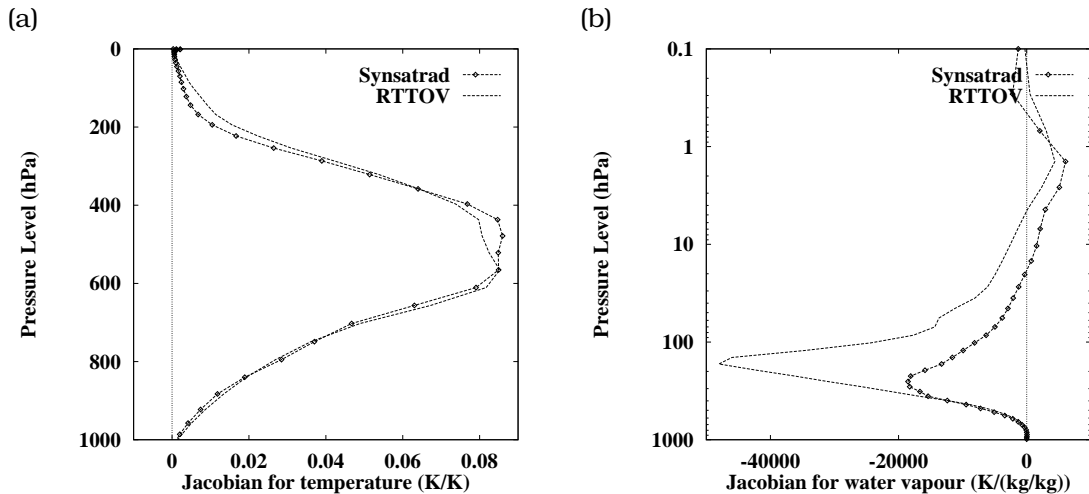


FIG. IV.17 – HIRS-12, high and mid-latitudes. Mean Jacobians for temperature and water vapour from Synsatrad and RTTOV at the first iteration of 1D-Var.

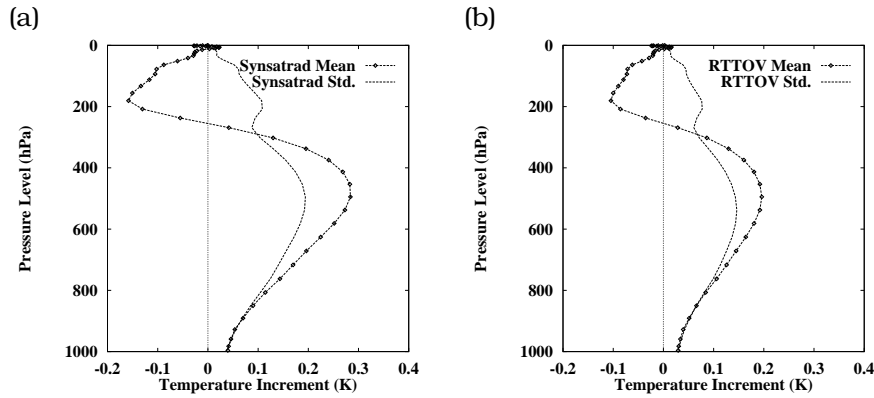


FIG. IV.18 – HIRS-12, high and mid-latitudes. Statistics of the temperature increments from Synsatrad (a) and RTTOV (b). HIRS-12, high and mid-latitudes.

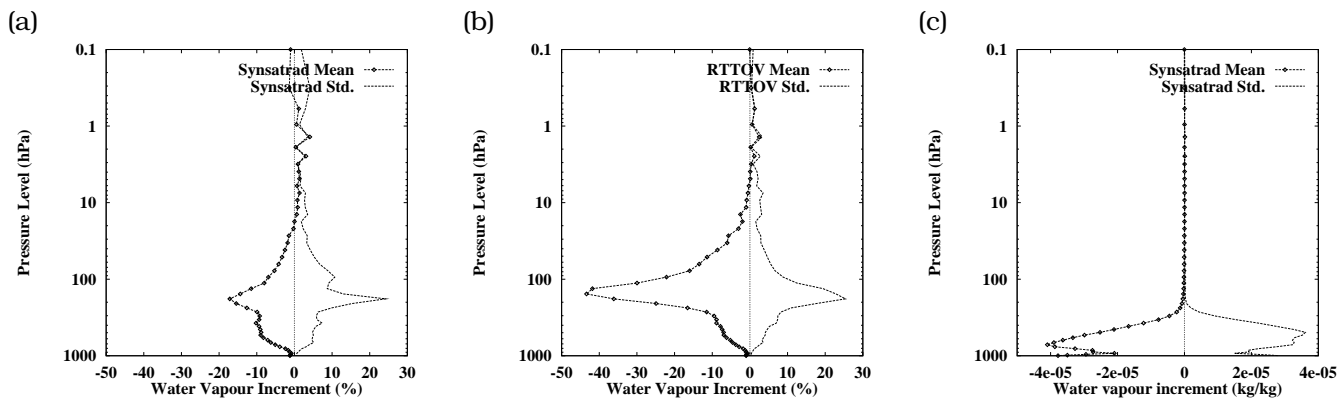


FIG. IV.19 – Statistics of the water vapour increments from Synsatrad (a) and RTTOV-5 (b), in terms of relative change of specific humidity. The statistics in terms of specific humidity are shown in (c) for Synsatrad.

09 Jacobian for ozone in the tropical regions appears to be higher with Synsatrad. HIRS-11, HIRS-12 and Meteosat-WV Jacobians for water vapour are significantly different between the two codes, in shape as well as in the vertical location of the maximum. Differences reduce for HIRS-10 that peaks lower in altitude.

These differences in Jacobians translate into differences in 1D-Var increments controlled by the specified background error statistics. As a consequence, the previous increment differences are mainly specific to ECMWF, from which system these statistics were taken. In the present study, only water vapour increments for HIRS-11, HIRS-12 and Meteosat-WV significantly differ between the two models.

Due to a more physical computation method, Jacobians of Synsatrad are expected to be closer to the truth than RTTOV. Soden *et al.* (2000) also show a deficiency of HIRS-12 RTTOV Jacobians for water vapour. As described in section IV.3.2, RTTOV is based on two approximations : the invariance of the Planck function on the channel width and the computation of optical depths through a linear regression.

The first approximation is explored with Synsatrad as follows. Single-band convolved transmissions are computed with the narrow-band model for the five channels considered here. They are used to calculate the radiance L_i in a channel i in a way that is consistent with RTTOV-5 :

$$\begin{aligned} L_i &= B_i(T_{N+1})\tau_i(N+1) \\ &+ \sum_{k=1}^N B_i(T_k)(\tau_i(k) - \tau_i(k+1)) \end{aligned} \quad (\text{IV.11})$$

N is the number of vertical layers, $B_i(T)$ is the mean Planck function in channel i for temperature T , $\tau_i(k)$ is the convolved transmittance in channel i from the top of the atmosphere (level 1) to level k , T_k is mean temperature in layer k .

Statistics of the difference between the ap-

proximate brightness temperatures and the full Synsatrad computation on the 103 profile dataset are shown in Table IV.4. Biases and standard deviations are below 0.1 K in absolute value for all channels, except for Meteosat-WV, where a bias of 0.5 K is found. This bias carries the same sign as the one between RTTOV and Synsatrad, but is not latitude-dependent as the latter (see Table IV.2). Indeed different sources of error add or compensate between RTTOV and Synsatrad. Table IV.4 suggests that the invariant-Planck-function approximation is important to explain the differences observed for Meteosat-WV. This is not surprising given the Meteosat-WV spectral width, ranging from 1350 to 1850 cm^{-1} , to be compared with HIRS-12 ranging between 1420 to 1560 cm^{-1} only. The low associated standard deviation (0.1 K) suggests that a simple bias correction is able to remove that particular problem. As far as the Jacobians are concerned, only small impact is found on Meteosat-WV as well as on HIRS-12 (not shown).

Therefore the second approximation on which RTTOV relies, namely the use of a linear regression to derive the optical depths, is likely to be responsible for the low accuracy of RTTOV $6.3\mu\text{m}$ and $7.3\mu\text{m}$ water vapour Jacobians. Improvements of RTTOV are expected from a better quality of the regression dataset (e.g., Chevallier, 1999) and from more adequate predictors (e.g., Matricardi and Saunders, 1999). The interpolation of the water vapour profiles of the current regression dataset between 100 and 300 hPa (as explained by Saunders *et al.*, 1999) may be the main reason for the bad Jacobians (R. Saunders, personal communication, 2000; see also Figure IV.17b).

IV.3.6 Conclusion

Variational methods are increasingly used for data assimilation in operational weather centres. They provide statistically optimal analyses of the atmosphere when error statis-

	High and mid-lat.		Tropical latitudes	
	M	σ	M	σ
HIRS-09	-0.1	0.0	-0.1	0.0
HIRS-10	0.0	0.0	0.0	0.0
HIRS-11	0.1	0.0	0.1	0.0
HIRS-12	-0.2	0.1	-0.1	0.1
Meteosat WV	-0.5	0.1	-0.5	0.1

TAB. IV.4 – Test of the impact of the spectral integration approximation used in RTTOV. Difference between the computation of brightness temperature with Synsatrad in the narrow-band mode and that with Synsatrad using the approximation (approximation minus narrow-band, in K).

tics and Jacobians are correctly specified. The evaluation of Jacobians for variational data assimilation has to be related to the complete framework including the specified error statistics. As an example, the differences between RTTOV and Synsatrad Jacobians were shown to be strongly influenced by these statistics when they are converted into 1D-Var increments.

Neural network-based Jacobians for broad-band infrared radiation were shown to be deficient for water vapour. However, the random structure of the derivative error allows to use NeuroFlux with a single mean Jacobian in the variational context. Errors produced by this approach are small. Clouds are the major modulator of fluxes and cooling rates and are accounted for in the framework of the multi-layer grey body approach. Therefore, accurate and fast long-wave broad-band radiation computations can be introduced in 4D-Var with the single mean Jacobian approach to compute increments and derivatives, and NeuroFlux to re-compute the trajectory around which the linearisation is performed.

For satellite brightness temperature modelling, RTTOV Jacobians were also shown to be deficient for water vapour for the $6.3\ \mu m$ and $7.3\ \mu m$ channels with a significant impact on the 1D-Var retrievals. The mean shape of the increments is similar to those of Synsatrad, but the signal amplitude differs. Be-

cause the RTTOV increment shape is good, the inclusion of RTTOV in variational data analysis for the assimilation of such channels positively impacts the quality of the operational analyses and forecasts, particularly in the southern hemisphere and tropics (McNally and Vespérini, 1996). Smaller weaknesses for temperature and ozone, as well as for water vapour in the $12.5\ \mu m$ channel (HIRS-10) do not significantly impact the increments. Further improvements to RTTOV are expected from on-going work in the framework of the Numerical Weather Prediction Satellite Application Facility (NWP/SAF) funded by Eumetsat, where both the regression data-set and the choice of the predictors are being revised.

Acknowledgments. This work was done at the Satellite Application Facility on Numerical Weather prediction which is co-sponsored by Eumetsat. Authors would like to thank F. Aires and A. Chédin for fruitful discussions about the neural-network-based Jacobians. For the comparison between RTTOV and Synsatrad, special thanks go to R. Saunders and S. Tjemkes. The kind help of G. Kelly, R. Munro, and E. Holm at various stages of the work was appreciated. F. Bouttier provided the statistics of forecast errors from the ECMWF operational data assimilation system. The INRIA (Institut National de Recherche en Informatique et Automatique) provided the M1QN3 minimisation code. M.

Janisková, T. McNally, J.-J. Morcrette, and R. Saunders helped to improve the initial manuscript.

References

- Aires, F., M. Schmitt, A. Chédin, and N. A. Scott, 1999 : The “weight smoothing” regularization of MLP for Jacobian stabilization. *IEEE Trans. Neural Networks*, 10 :6, 1502 :1510.
- Chéruy, F., F. Chevallier, J.-J. Morcrette, N. A. Scott, A. Chédin, 1996 : Une méthode utilisant les techniques neuronales pour le calcul rapide de la distribution verticale du bilan radiatif thermique terrestre. *C. R. Acad. Sci. Paris*, 322 :IIb, 665-672, in French.
- Chevallier, F., 1998 : La modélisation du transfert radiatif à des fins climatiques : une nouvelle approche fondée sur les réseaux de neurones artificiels. PhD thesis, University Paris VII, 230 pp. [Available from LMD, Ecole Polytechnique, 91128 Palaiseau cedex, France].
- Chevallier, F., 1999 : TIGR-like sampled databases of atmospheric profiles from the ECMWF 50-level forecast model. *ECMWF/Eumetsat NWP SAF Research Report No. 1*, 18 pp.
- Chevallier, F., F. Chéruy, N. A. Scott, and A. Chédin, 1998 : A neural network approach for a fast and accurate computation of longwave radiative budget. *J. Appl. Meteor.*, 37, 1385-1397.
- Chevallier, F., and J.-J Morcrette, 2000 : Comparison of model fluxes with surface and top-of-the-atmosphere observations. *Mon. Wea. Rev.*, in press.
- Chevallier, F., A. Chédin, F. Chéruy, J.-J. Morcrette, 2000a : TIGR-like atmospheric situation databases for accurate radiative flux computation. *Quart. J. Roy. Meteor. Soc.*, 126, 777-785.
- Chevallier, F., J.-J Morcrette, F. Chéruy, and N. A. Scott, 2000b : Use of a neural network-based longwave radiative transfer scheme in the ECMWF atmospheric model. *Quart. J. Roy. Meteor. Soc.*, 126, 761-776.
- Clough, S. A., F. X. Kneizys, and R. Davies, 1989 : Line shape and the water vapor continuum. *Atmos. Res.*, 23, 229-241.
- Courtier, P., J.-N. Thépaut, and A. Hollingsworth, 1994 : A strategy for operational implementation of 4D-Var, using an incremental approach. *Q. J. Roy. Meteor. Soc.*, 120, 1367-1388.

- Courtier, P., E. Andersson, W. Heckley, J. Pailleux, D. Vasiljević, M. Hamrud, A. Hollingsworth, F. Rabier, and M. Fisher, 1998 : The ECMWF implementation of three dimensional variational assimilation (3D-Var). Part I. : formulation. *Q. J. Roy. Meteor. Soc.*, 124, 1783-1808.
- Derber, J. and F. Bouttier, 1999 : A reformulation of the background error covariance in the ECMWF global data assimilation system. *Tellus*, 51A, 195-221.
- Ebert, E. E. and J. A. Curry, 1992 : A parameterization of ice optical properties for climate models. *J. Geophys. Res.*, 97D, 3831-3836.
- Edwards, D. P., 1992 : GENLN2. A general line-by-line atmospheric transmittance and radiance model. Technical note NCAR/TN-367+STR, 157pp. National Center for Atmospheric Research, Boulder, Co.
- Eyre, J. R., 1991 : A fast radiative transfer model for satellite sounding systems. *ECMWF Technical Memorandum No. 176*, 28 pp.
- Eyre, J. R., G. A. Kelly, A. P. McNally, E. Andersson, and A. Persson, 1993 : Assimilation of TOVS radiance information through one-dimensional variational analysis. *Q. J. Roy. Meteor. Soc.*, 119, 1427-1463.
- Fillion, L., and J.-F. Mahfouf, 2000 : Coupling of moist-convective and stratiform precipitation processes for variational data assimilation. *Mon. Wea. Rev.*, 128, 109-124.
- Fortuin, J. P. F. and Langematz, U., 1994 : An update on the global ozone climatology and on concurrent ozone and temperature trends. Proceedings of the International Society for Optical Engineering (SPIE) on *Atmospheric Sensing and Modeling*, Rome, Italy, September 29-30, SPIE Proceedings, Vol. 2311, 207-216.
- Geleyn, J.-F. and A. Hollingsworth, 1979 : An economical analytical method for the computation of the interaction between scattering and line absorption in radiation. *Beitr. Phys. Atmosph.*, 52, 1-16.
- Gilbert, J. C., and C. Lemaréchal, 1989 : Some numerical experiments with variable-storage quasi-Newton algorithms. *Mathematical Programming*, 45, 407-435.
- Gregory, D., J.-J. Morcrette, C. Jakob, and A. Beljaars, 1998 : Introduction of revised radiation, convection, cloud and vertical diffusion schemes into Cy18r3 of the ECMWF integrated forecasting system. ECMWF Technical Memorandum No. 254, 39 pp.
- Heimo, A., A. Vernez, and P. Wasserfallen, 1993 : Baseline Surface Radiation Network (BSRN). Concept and implementation of a BSRN station. WMO/TD No. 579, WCRP/WMO, Geneva.
- Hollingsworth, A., 1987 : Objective analysis for numerical weather prediction. *Short and medium range numerical weather prediction, Special Volume J. Met. Soc. Jap.*, Matsumo, T., Ed., 11-60.
- Janisková, M., J.-N. Thépaut and J.-F. Geleyn, 1999 : Simplified and regular physical parameterizations for incremental four-dimensional variational assimilation. *Mon. Wea. Rev.*, 127, 26-45.
- Le Dimet, F.-X. and O. Talagrand, 1986 : Variational algorithms for analysis and assimilation of meteorological observations. *Tellus*, 38A, 97-110
- Lewis, J. M. and J. C. Derber, 1985 : The use of adjoint equations to solve a variational adjustment problem with advective constraints. *Tellus*, 37A, 309-322.
- Mahfouf, 1999 : Influence of physical processes on the tangent-linear approximation. *Tellus*, 51A, 147-166.
- Marécal, V., and J.-F. Mahfouf, 1999 : Variational retrieval of temperature and humidity profiles from TRMM precipitation data. *ECMWF Technical Memorandum No. 293*, 28 pp.
- Matricardi, M., and R. Saunders, 1999 : Fast radiative transfer model for simulation of infrared atmospheric sounding interferometer radiances. *Appl. Opt.*, 38 :27, 5679 :5691.
- McClatchey, R. A., R. W. Fenn, J. E. A. Selby, F. E. Volz, and J. S., Garing, 1971 : Optical properties of the atmosphere. Technical Note No. AFCRL-TR-73-0096, 94 pp., Air Force Cambridge Res. Lab., Bedford, Mass.
- McMillin, L. M., H. E. Fleming, M. L. Hill, 1979 : Atmospheric transmittance of an absorbing gas. 3 : a computationally fast and accurate transmittance model for absorbing gases with variable mixing ratios. *Appl. Opt.*, 18, 1600-1606.

- McNally, A. P., 2000 : Estimates of short-range forecast-temperature error correlations and the implications for radiance-data assimilation. *Q. J. Roy. Meteor. Soc.*, 126, 361-373.
- McNally, A. P., and M. Vesperini, 1996 : Variational analysis of humidity information from TOVS radiances. *Q. J. Roy. Meteor. Soc.*, 122, 1521-1544.
- Morcrette, J.-J., 1991 : Radiation and Cloud Radiative Properties in the European Center for Medium Range Weather Forecasts forecasting system. *J. Geophys. Res.*, 96 :D5, 9121-9132.
- Morcrette, J.-J., 2000 : On the effects of the temporal and spatial sampling of radiation fields on the ECMWF forecasts and analyses. *Mon. Wea. Rev.*, 128, 876-887.
- Parrish, D. F. and J. C. Derber, 1992 : The National Meteorological Center's Spectral Statistical Interpolation Analysis System. *Mon. Wea. Rev.*, 120, 1747-1763.
- Rabier, F., A. McNally, E. Andersson, P. Courtier, P. Uden, J. Eyre, A. Hollingsworth and F. Bouttier, 1998 : The ECMWF implementation of three dimensional variational assimilation (3D-Var). Part II : Structure functions. *Q. J. Roy. Meteor. Soc.*, 124, 1809-1829.
- Rumelhart, D. E., G. E. Hinton, and R. J., Williams, 1986 : Learning internal representations by error propagation. *Parallel distributed processing : Explorations in the macrostructure of cognition 1*, D. E. Rumelhart and McClelland, Eds., MIT Press, 318-362.
- Sasaki, Y., 1958 : An objective analysis based on the variational method. *J. Meteor. Soc. Japan*, 36, 738-742.
- Saunders, R., M. Matricardi, and P. Brunel, 1999 : An improved fast radiative transfer model for assimilation of satellite radiance observations. *Quart. J. Roy. Meteor. Soc.*, 125, 1407-1425.
- Sneden, C., H. Johnson, and B. Krupp, 1975 : A statistical method for treating molecular line opacities. *Astrophys. J.*, 204, 281-289.
- Soden, B. and co-authors, 2000 : An intercomparison of radiation codes for retrieving upper tropospheric humidity in the 6.3 micron band : a report from the 1st GVAP workshop. *Bull. Amer. Meteo. Soc.*, 81, 797-808.
- Stockes, G. M., and S. E. Schwartz, 1994 : The Atmospheric Radiation Measurement (ARM) Program : programmatic background and design of the cloud and radiation testbed. *Bull. Amer. Meteo. Soc.*, 75, 1201-1221.
- Tjemkes, S. A. and J. Schmetz, 1997 : Synthetic satellite radiances using the radiance sampling method. *J. Geophys. Res.*, 102D, 1807-1818.
- Washington, W. M. and D. L. Williamson, 1977 : A description of the NCAR GCM's in General circulation models of the atmosphere. *Methods in Computational Physics*, J. Chang. Ed., 17, Academic Press, 111-172.

Chapitre V

Inversion

I wish to God these calculations had been performed
by steam!

C. Babbage (1812)

Rapporté par H. Eves, In Mathematical Circles (1969).

V.1 Introduction

L'inférence bayésienne repose essentiellement sur une seule formule : la règle de Bayes. Pourtant, certains problèmes peuvent atteindre des dimensions telles que son application en soi est problématique. Deux articles sont présentés ici pour illustrer la mise en place d'un système d'inversion de grandes dimensions. Ils concernent l'inversion des flux de dioxyde de carbone à la surface du globe à partir d'observations par satellite de la concentration atmosphérique du CO₂. On cherche à optimiser plusieurs centaines de milliers de variables en analysant plusieurs centaines de milliers d'observations. Le premier article décrit le système variationnel que nous avons constitué pour trouver la valeur la plus probable de la densité de probabilité a posteriori. Le deuxième le prolonge et décrit comment obtenir d'autres informations complémentaires, comme la largeur de la distribution a posteriori, à partir d'un tel système.

V.2 Mise en œuvre

Cette section reprend l'article de Chevallier et coll. (2005b) paru dans *Journal of Geophysical Research*.

Inferring CO₂ Sources and Sinks From Satellite Observations : Method and Application to TOVS Data

F. Chevallier¹, M. Fisher², P. Peylin³, S. Serrar^{1,4}, P. Bousquet, F.-M. Bréon¹, A. Chédin⁴, P. Ciais¹

¹Laboratoire des Sciences du Climat et de l'Environnement
Institut Pierre-Simon Laplace
Gif-sur-Yvette, France

²European Centre for Medium-Range Weather Forecasts
Reading, UK

³Laboratoire de Biogéochimie des Milieux Continentaux
INRA-CNRS-UPMC, INRA-INAPG, Thivernal-Grignon, France

⁴Laboratoire de Météorologie Dynamique
Institut Pierre-Simon Laplace
Palaiseau, France

Abstract. Properly handling satellite data to constrain the inversion of CO₂ sources and sinks at the Earth surface is a challenge motivated by the limitations of the current surface observation network. In this paper, we present a Bayesian inference scheme to tackle this issue. It is based on the same theoretical principles as most inversions of the flask network, but uses a variational formulation rather than a pure matrix-based one in order to cope with the large amount of satellite data. The minimization algorithm iteratively computes the optimum solution to the inference problem as well as an estimation of its error characteristics and some quantitative measures of the observation information content. A global climate model, guided by analyzed winds, provides information about the atmospheric transport to the inversion scheme. A surface flux climatology regularizes the inference problem.

This new system has been applied to one year's worth of retrievals of vertically-integrated CO₂ concentrations from the Television Infrared Observation Satellite Operational Vertical Sounder (TOVS). Consistent with a recent study that identified regional biases in the TOVS retrievals, the inferred fluxes are not useful for biogeochemical analyses. In addition to the detrimental impact of these biases, we find a sensitivity of the results to the formulation of the prior uncertainty and to the accuracy of the transport model. Notwithstanding these difficulties, four-dimensional inversion schemes of the type presented here could form the basis of multisensor data assimilation systems for the estimation of the surface fluxes of key atmospheric compounds.

V.2.1 Introduction

The monitoring of carbon dioxide fluxes at the Earth's surface has become a major scientific challenge over the last few decades. It has progressed mainly through the exploitation of in situ measurements of CO₂ concentration at a network of ground stations. With the help of atmospheric transport information, inverse methods have been applied to deduce the patterns and amplitude of surface fluxes that ge-

nerated the observed concentrations. However, with about 100 stations, the current network of surface stations provides scant information about the global-scale spatial and temporal variations of CO₂ fluxes, most particularly over land (e.g., Gurney et al. 2002). This situation is likely to improve : the surface observation network is being augmented, and efforts are being made to measure atmospheric CO₂ from space.

The impact of CO₂ variations on some satellite records has been noticed for a long time (e.g., Turner 1993, 1994), but CO₂ concentrations have been estimated from radiance measurements only recently. Retrieval methods were first applied to TOVS (Chédin et al. 2003b) then to the Atmospheric Infra-Red Sounder (AIRS) (Crévoisier et al. 2004, Engelen et al. 2004). Within the coming years, CO₂ retrievals are expected from the Infrared Atmospheric Sounding Interferometer (IASI) and the CO₂-dedicated Orbiting Carbon Observatory (OCO) and the Greenhouse gases Observing Satellite (GOSAT).

Such data contrast with the existing in situ measurements, and their nature will lead to a revolution in the methods of CO₂ flux estimation. First, they correspond to vertically-integrated concentrations rather than point-wise observations. Second, the radiance information is ambiguous and the accuracy of instantaneous retrievals of column integrated CO₂ is not expected to be better than a couple of particles per million (ppm) (Chédin et al. 2003, Dufour and Bréon 2003, Engelen and Stephens 2004). Third, the spatial density of the satellite data, which makes them attractive, increases the dimension of the observation vector by several orders of magnitude. Spatial and temporal averaging can reduce the dimension of the problem, but if one wants to use the information without degrading it, one faces new numerical problems.

The goal of this paper is to define a methodology to estimate CO₂ surface fluxes using the combination of raw satellite retrievals and any prior information, like a flux climatology. This methodology follows the bayesian framework, which has been widely used for the in situ network in a matrix form, but a variational formulation is chosen here, since it can cope with the dramatic increase of the number of data. The inference scheme is outlined in section V.2.2. It is applied to the first CO₂ retrieval dataset that has been compiled : the one from TOVS. Large regional biases

have been identified in this product so that it barely agrees with forward model simulations using optimized surface fluxes (Peylin et al., manuscript in preparation). Therefore we focus here on the illustration of the method, in preparation for the analysis of forthcoming retrieval data, of potentially improved quality. The TOVS product and the prior information about the surface fluxes are described in section V.2.3. Information about the atmospheric transport is provided by the global climate model of the Laboratoire de Météorologie Dynamique (LMD), which is called LMDZ (the last letter stands for ‘zoom capacity’). We nudge LMDZ towards the winds of the European Centre for Medium-Range Weather Forecasts (ECMWF), as discussed in section V.2.4. Section V.2.5 analyses the behaviour of the inference scheme in terms of 1) error reduction, 2) information content of the satellite data, 3) CO₂ flux and concentration increments, and 4) fit to ground measurements. Results are discussed in section V.2.6 and conclusion follows in section V.2.7.

V.2.2 The Inference Scheme

Theoretical Framework

In the following, the notations follow the convention defined by Ide et al. (1997). Observation values are represented as a vector y and their error statistics are assumed to be unbiased and Gaussian with covariance matrix R . Similarly, the prior information (or background) about the variables x to be optimized (here the CO₂ fluxes) is given by a vector x^b with unbiased Gaussian error statistics, described by the covariance matrix B . A model H (here a transport model and a convolution operator) provides the equivalent of the observations y (here satellite CO₂ retrievals, but they could be in situ measurements as well) from the control variables x . Errors of the forward model H can be taken into account in matrix R .

From the theory of Bayesian inference, it is

well known that if H is a linear operator \mathbf{H} , the information about the variables x , given the observations and the prior information, has Gaussian statistics as well, with mean x^a and covariance error matrix A .

x^a and A can be computed in different ways (e.g., Rodgers 2000). One of them is :

$$\mathbf{x}^a = \mathbf{x}^b - \quad (V.1)$$

$$\mathbf{B}\mathbf{H}^T(\mathbf{H}\mathbf{B}\mathbf{H}^T + \mathbf{R})^{-1}(\mathbf{H}\mathbf{x}^b - \mathbf{y})$$

$$\mathbf{A} = \mathbf{B} - \mathbf{B}\mathbf{H}^T(\mathbf{H}\mathbf{B}\mathbf{H}^T + \mathbf{R})^{-1}\mathbf{H}\mathbf{B} \quad (V.2)$$

After some algebra, equations V.1 and V.2 can be rewritten as follows, in order to change some of the dimensions of the matrices to invert :

$$\mathbf{x}^a = \mathbf{x}^b - \quad (V.3)$$

$$(\mathbf{H}^T\mathbf{R}^{-1}\mathbf{H} + \mathbf{B}^{-1})^{-1}\mathbf{H}^T\mathbf{R}^{-1}(\mathbf{H}\mathbf{x}^b - \mathbf{y})$$

$$\mathbf{A} = (\mathbf{H}^T\mathbf{R}^{-1}\mathbf{H} + \mathbf{B}^{-1})^{-1} \quad (V.4)$$

Alternatively, it can be shown that x^a is the minimum of the following quadratic cost function :

$$\begin{aligned} J(\mathbf{x}) &= \frac{1}{2}(\mathbf{x} - \mathbf{x}^b)^T\mathbf{B}^{-1}(\mathbf{x} - \mathbf{x}^b) \\ &+ \frac{1}{2}(\mathbf{H}\mathbf{x} - \mathbf{y})^T\mathbf{R}^{-1}(\mathbf{H}\mathbf{x} - \mathbf{y}) \end{aligned} \quad (V.5)$$

The minimum can be reached iteratively with a descent algorithm which requires several computations of the gradient of J with respect to the control variables x :

$$\nabla J(\mathbf{x}) = \mathbf{B}^{-1}(\mathbf{x} - \mathbf{x}^b) + \mathbf{H}^T\mathbf{R}^{-1}(\mathbf{H}\mathbf{x} - \mathbf{y}) \quad (V.6)$$

In this variational formulation of the inference problem, A is the inverse of the Hessian of J :

$$\mathbf{A} = (\nabla^2 J(\mathbf{x}))^{-1} \quad (V.7)$$

To summarize, the inference problem can be equivalently solved by matrix operations (equations V.1-V.2 or V.3-V.4) or as the solution to a variational optimization problem (equations V.5-V.7).

Practical Implementation

Practical considerations guide the choice between the matrix-based formulations and

the variational approach. If the number of observations does not exceed a few thousands, and if all elements of the matrix \mathbf{H} are directly known, equations V.1 and V.2 provide the most straight-forward solution. Conversely, equations V.3 and V.4 are more convenient to use when the number of control variables is small and R is easy to invert (e.g., R is diagonal). For large problems in both the observation space and the control variable space, the inversion of $(\mathbf{H}\mathbf{B}\mathbf{H}^T + \mathbf{R})$ or of $(\mathbf{H}^T\mathbf{R}^{-1}\mathbf{H} + \mathbf{B}^{-1})$ may be prohibitive. The variational framework still implies the inversion of B and R , but in many applications these matrices are sparse, if not diagonal. More generally, it is simpler to make convenient assumptions about B and R to make them easy to invert than it is for $(\mathbf{H}\mathbf{B}\mathbf{H}^T + \mathbf{R})$ and $(\mathbf{H}^T\mathbf{R}^{-1}\mathbf{H} + \mathbf{B}^{-1})$. Still, the implementation of the variational approach for large problems would stumble on the multiplication of \mathbf{H}^T by $\mathbf{R}^{-1}(\mathbf{H}\mathbf{x} - \mathbf{y})$ in the expression of ∇J (equation V.6) without the adjoint technique (e.g., Errico 1997). This approach avoids the explicit calculation of all the elements of \mathbf{H} by decomposing \mathbf{H}^T into a product of elementary operations $\mathbf{H}^T = \prod_{i=n}^1 \mathbf{H}_i$, with \mathbf{H}_i being the Jacobian matrix of the i^{th} line among n of the computer code of H . A single pass of the adjoint model computes $\mathbf{H}^T\mathbf{R}^{-1}(\mathbf{H}\mathbf{x} - \mathbf{y})$, which is added to $\mathbf{B}^{-1}(\mathbf{x} - \mathbf{x}^b)$ to give ∇J (equation V.6).

Up to now the estimation of CO₂ surface fluxes at the global scale has relied on the matrix formulation (e.g., Bousquet et al 2000, Gurney et al. 2002, Rödenbeck 2003). This paper reports on the implementation of the variational approach in order to deal with large numbers of observations and control vector dimensions of several hundred thousands. The minimization strategy follows the one chosen for the ECMWF 4-dimensional variational analysis system (4D-Var). The ECMWF 4D-Var minimization algorithm is based on the Lanczos version of the conjugate gradient algorithm (Lanczos 1950)

that advantageously provides the leading eigenvectors of the Hessian $\nabla^2 J(\mathbf{x})$ as a by-product of the minimization (Fisher and Courtier 1995). For efficiency, the minimization is preconditioned by defining the variable to optimize as

$$\chi = \mathbf{B}^{-1/2} \mathbf{x} \quad (\text{V.8})$$

The reader is referred to Trémolo et al. (2004) and references therein for a description of other features of the ECMWF 4D-Var. The ECMWF minimization algorithm has also been implemented for data assimilation in an ocean model (Weaver et al. 2003).

The Inferred Variables

In this study, the control vector \mathbf{x} contains the CO₂ surface fluxes to be inferred. Most inversions performed in the past have used monthly or even annual fluxes. Very few attempts have been made towards subdiurnal fluxes so far (Law et al. 2004). In the method described here, most of the computational burden (CPU and memory) is caused by the transport model, the performance of which is not affected by a change of the time discretization. However, the choice of the time resolution may affect the number of iterations of the minimization. It also bears consequences on the definition of the prior errors, because these are likely to be temporally correlated if the resolution is high. In the results presented here, fluxes are arbitrarily inverted as monthly averages, but a major sub-monthly variation is accounted for by defining day-time (i.e., from local sunset to sun-down) and night-time monthly fluxes separately. This allows a simple optimization of the biosphere diurnal cycle amplitude, some features of which are noticeable in the TOVS observations (Chédin et al. 2005). Note that it partly addresses the issue raised by Rayner et al. (2002) of biases caused by a poor sampling of the diurnal cycle by measurements.

Conversely, the spatial resolution of the fluxes in the control vector is a compromise. It

seems important to give some freedom to the inference system to adjust small-scale patterns, by specifying fluxes at the highest possible horizontal resolution (i.e., that of the transport model) (e.g., Kaminski et al. 2001). On the other hand, prior flux errors are more likely to be correlated from one cell to another at high horizontal resolution than at low. In the past, fluxes have been inferred over large regions, mainly for computational reasons that are not relevant here. Therefore, fluxes are defined in this study on the horizontal grid of the transport model, which is regular with 96 points in longitude and 72 in latitude (i.e., a $3.75^\circ \times 2.5^\circ$ longitude-latitude grid).

It is also important to give some freedom to the analysis system to adjust the CO₂ concentration field at the initial time step of the assimilation window in order not to alias its errors into flux errors. To do so, the 3D concentration field of CO₂ concentrations at the initial time step could be included in the control vector \mathbf{x} . Since we do not focus here on the analysis of this field, and in order not to unnecessarily increase the array dimension, only the initial total CO₂ atmospheric columns at each grid point of the $3.75^\circ \times 2.5^\circ$ grid are introduced in the control vector.

The dimension of the control vector for an assimilation window covering a whole year is about 200,000 (i.e., two times the number of grid points for the day and night fluxes, times the number of months, plus the number of grid points for the concentration field at initial time).

V.2.3 Observations and Prior Information

The TOVS CO₂ Retrievals

TOVS instruments have been operating since 1979 on board the polar-orbiting satellites of the National Oceanic and Atmospheric Administration (NOAA). Some of its channels at infrared wavelengths are noticea-

bly impacted by CO₂ variations, in particular in the upper troposphere. Upper tropospheric CO₂ retrievals from the NOAA-10 spacecraft have recently been produced for the tropical region (25°S-25°N). Further away from the Equator, the lower position of the tropopause, its warmer temperature and the larger variability of the temperature profile in the vertical prevent the extraction of the CO₂ signals. Clouds impede the inversion and the method is restricted to clear-sky spots. Even so, more than 100,000 retrievals at spatial resolution of about 100×100 km² are gathered per month of NOAA-10 observation. NOAA-10 is a sun-synchronous polar satellite. Its archive covers the period between November 1986 and September 1991, but only year 1990 is processed here. During that year NOAA-10 orbits crossed the equator at about 7:40 and 19:40 local solar time, which allows two samples of the diurnal cycle.

The column-CO₂ inversion algorithm is an artificial neural network of the type defined by Rumelhart et al. (1986). This non-linear regression has been trained from the Thermodynamical Initial Guess Retrieval (TIGR : Chédin et al. 1985, Chevallier et al. 1998) climatological dataset, previously extended to include variable atmospheric CO₂ concentrations. The regression estimates a weighted mean CO₂ concentration between the tropopause and about 400 hPa, with a maximum weight at about 200 hPa (Figure V.1). Individual retrievals are used here, in contrast to Chédin et al. (2003b) who averaged the retrievals in both time and space to study them.

Previous validations

The LMD TOVS retrievals (Chédin et al. 2003b) have been the first attempt to describe the CO₂ concentrations in the upper troposphere and in the tropical band directly from the observations. This pioneering effort has been followed by the evaluation of the product, based on comparisons with the few aircraft campaigns available, with models, and

on sensitivity studies. The conclusions of this evaluation can be summarized as follows : (i) the retrievals adequately identify CO₂ variations (the growth rate inter-annual variations, for example) only when averaged over at least a month and over very large regions (Chédin et al. 2003b); (ii) the limited information contained in the TOVS radiances does not allow the separation between CO₂ variations and those of other atmospheric signals, like ozone variations, over smaller spatial and temporal scales (iii) such regional biases, however, have less of an impact on the 12-hour difference between day time and night time retrievals and a consistent link between this difference and biomass burning emissions at regional scale has been established (Chédin et al., 2005).

From these previous studies, one can foresee that surface fluxes inferred from TOVS would be affected by some regional biases induced by those of the retrievals. The TOVS data are used here as a testbed for a methodology that will be applied to the forthcoming retrievals, from AIRS and OCO for instance.

The Observation Error Covariance Matrix

The observation error covariance matrix R is a key component of the retrieval system (equations V.5-V.6) and a proper assessment of its elements, i.e., variances and correlations, is needed. As mentioned above in section V.2.2, R takes the errors of H into account in addition to the measurement errors. Local time and space variations of LMDZ CO₂ concentrations are used here as a surrogate for representativeness errors, following the approach described by Rödenbeck et al. (2003). Practically, for each model grid point and for each model time step, a standard deviation is computed for 16 values of the LMDZ simulation that uses the prior fluxes. The 16 values correspond to the eight latitude/longitude grid points surrounding the observation at the start of the time step and to the eight ones at the end. Representative-

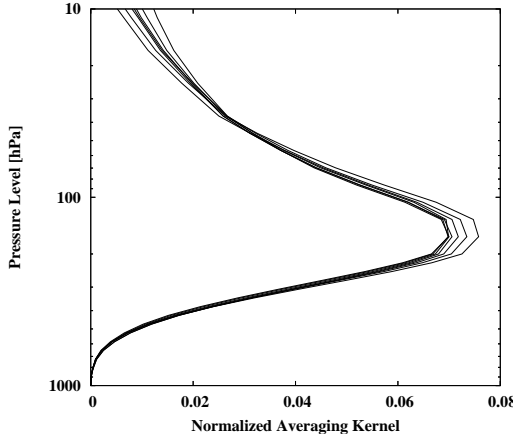


FIG. V.1 – Normalized averaging kernel of the TOVS CO₂ retrieval for seven different viewing angles of the TOVS instrument. The averaging kernel is defined here as $\partial\tilde{c}/\partial c(P)$, where \tilde{c} is the retrieval, $c(P)$ is the CO₂ atmospheric concentration at pressure level P . \tilde{c} and $c(P)$ are expressed in ppm Pa⁻¹. The averaging kernel has been estimated by finite differences based on model simulations.

ness error is defined as the monthly average of these standard deviations and the corresponding variances (typically a few tenths of ppm for upper-tropospheric observations) are added to the ones of the retrieval error. Correlations of the representativeness error are neglected.

Previous studies of the TOVS retrievals have focussed on monthly means at a horizontal resolution of 15° × 15° and the corresponding estimations of the product errors (e.g., Chédin et al. 2003b) are not relevant for the present one that uses individual retrievals. Accurate independent observations of CO₂ concentrations in the upper troposphere would be useful to build global statistics. For instance, an estimate of the error variance may be based on aircraft measurements, but these one are too sparse for an estimation of the error correlations. To circumvent this problem, model simulations are used here. Atmospheric profiles (temperature, humidity and ozone) and surface characteristics (temperature) have been extracted from the ECMWF archive. The fields correspond to the operational analyses valid at 12 UTC every 5 days for 365 days starting on 1 November 2003. The profiles are described on 60 ver-

tical levels. Only grid points whose latitude lies within 25° from the equator and with upper tropospheric relative humidity below 70% (i.e., about cloud-free at these altitudes) are kept. Together with a constant atmospheric CO₂ concentration of 370 ppm, those fields are used as input to two radiation models, depending on the wavelength of the TOVS channels. The first one is the narrow-band model Synsatrad (Tjemkes and Schmetz 1996) that simulates here the TOVS infrared channels. 3R-N (Chédin et al. 2003a) is another radiation model, applied here to the TOVS microwave channels. Synsatrad and 3R-N produce a set of simulated radiances, to which an estimate of the TOVS instrument noise is added (in the form of a Gaussian random perturbation). CO₂ concentrations are then retrieved from those pseudo data by the same artificial neural network that processed the TOVS archive. Finally, the retrievals are compared to the initial ‘true’ CO₂ value (370 ppm). The differences are interpreted as retrieval errors. Note that the artificial neural network training made use of only the 3R-N model for both infrared and microwave channels (Chédin et al. 2003b). The introduction of an independent model, i.e., Synsatrad, for the present study

can be seen as a surrogate for infrared spectroscopic errors.

The standard deviation of differences between the input to the radiation models and the output of the neural network reach 5.7 ppm for individual data. By consequence, variances of the TOVS retrieval errors are set to 36 ppm² here. Note that this is error corresponds to individual retrievals, in contrast to the previous studies (e.g., Rayner and O'Brien 2001) that used observations temporally averaged.

Figure V.2 displays the correlations of the differences as a function of the ground distance between two retrievals. By comparison, the transport resolution in this study is about 400 km along a parallel and 280 km along a meridian in the tropical belt. One may note that the error correlations are attenuated by as much as a twofold factor within about 500 km, i.e., from one grid point to about the next. Consequently, the following methodology is defined in the present study. TOVS data are subsampled so that each model grid point contains no more than one TOVS observation per grid point within any 6-hour time window and correlations between the selected observations are neglected. This approximation makes the covariance matrix R diagonal which simplifies the inference scheme.

To limit the impact of ozone-related regional biases (see section V.2.3), a quality control has been introduced that aims at removing the data in the presence of ozone extrema. Large ozone values in the upper troposphere are usually associated with stratospheric intrusion and are flagged here by a threshold on the absolute value of the potential vorticity on the 350 K isentropic surface. This threshold is 1 PVU = 10⁻⁶m² s⁻¹ K kg⁻¹. Ozone-poor air is more difficult to diagnose indirectly. The lowest quarter of the retrieved CO₂ values (i.e., less than 351 ppm for year 1990) were simply rejected since they may correspond to an ozone minimum aliased into a CO₂ minimum.

The number of TOVS retrievals that pas-

sed both the spatial screening and the quality control is illustrated in Figure V.3 for August 1990. Lower densities are observed in the cloud regions : mainly the inter-tropical convergence zone (ITCZ) and the stratocumulus areas off the West coast of the continents. In total 347,400 TOVS retrievals are used in the results presented here.

Background Flux Information

For background information, we use direct estimates of the surface carbon fluxes, including anthropogenic and natural components. Fossil fuel CO₂ emissions are from the EDGAR-3.0 emission database (Olivier et al. 1996). The data set is based on a combination of statistics on energy consumption, emission factors and population density maps, and the total emission was re-scaled to 6.1 Gt C per year for the year 1990. Air-sea CO₂ exchange is prescribed from the study by Takahashi and colleagues (2002), where a climatological extrapolated distribution of sea-air pCO₂ differences and a wind dependent gas exchange coefficient (Wanninkhof 1992) have been combined to produce monthly air-sea fluxes. The biosphere-atmosphere exchange of CO₂ is estimated by the Terrestrial Uptake and Release of Carbon (TURC) model (Lafont et al. 2002). TURC is a simple model of the biosphere driven by radiation, temperature, and humidity fields from ECMWF and by the Fraction of Absorbed Photosynthetically Active Radiation (FAPAR) from the SPOT4-VEGETATION sensor. SPOT4-VEGETATION data for the period between March 1998 and March 1999 are used here. The calculated daily fluxes have been redistributed throughout the day to account for the diurnal cycle of the fluxes. We used a simple scaling scheme where Gross Primary Production follows the incoming short-wave radiation and local air temperature. Finally the TURC model is forced to be carbon neutral on a yearly basis.

Current flux measurements do not allow us to estimate the errors of these prior fluxes.

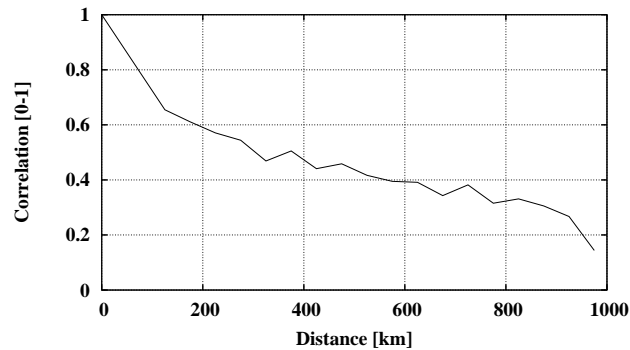


FIG. V.2 – Correlation of the TOVS retrieval errors as a function of the ground distance.

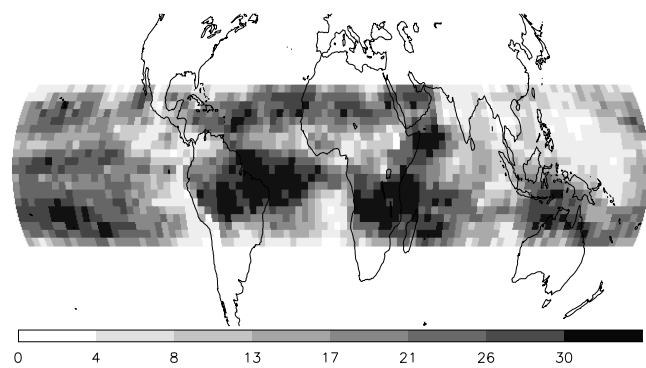


FIG. V.3 – Number of TOVS observations in each grid box of the LMDZ transport model after spatial filtering for August 1990.

The inference of CO₂ fluxes usually relies on *ad hoc* B matrices. Correlations are either neglected or specified per genotype as a function of the distance. Variances are either isotropic or specified from some biogeochemical considerations (e.g., Bousquet et al 2000, Rödenbeck 2003, Houweling et al. 2004). For instance they may be defined over land from a pattern of net primary productivity. The correlation lengths impose a smoothness constraint on the flux increments generated by the inversion system and the variance pattern favors some of the regions (i.e., the ones with the highest variance) for the increments to occur.

We tested two background error matrices. First results have been obtained with a simple background matrix, where error correlations are set to zero. When using the error statistics of all pixels, corresponding specified standard deviations of the flux errors globally sum up to 1.2 Gt C per year only. They are spread in time and space proportionally to grid size. Error standard deviations equal 1%, for the total columns at initial time in each grid box. An alternate inversion has been based on a matrix more consistent with what we guess from the carbon cycle (e.g., Rödenbeck et al. 2003). In this configuration of the B matrix, correlation lengths are set to 1000 and 500 km over ocean and land respectively for both fluxes and total columns. Correlations in time for fluxes are set to zero. Corresponding specified standard deviations of the flux errors globally sum up to 2 and 5 Gt C per year for ocean and land respectively and are spread in time and space proportionally to grid size over ocean and to the heterotrophic respiration flux modelled by TURC over land. Standard deviations of CO₂ total columns errors are set to 1% in each grid box, as above.

It turns out that the large misfit between the prior information and the TOVS data favors the simple B matrix, as will be described in the following. Therefore, the presentation of the results will focus on this config-

uration. The tests with the matrix based on bio-geochemical considerations are reported in section V.2.5.

Global Concentration Offset

Equations 1-7 implement the Bayes' theorem for the particular case of unbiased Gaussian statistics. The analysis is only supposed to account for random errors of the background and of the observations, as specified by the covariance matrices B and R. Biases therefore need to be removed from the inference system. Consistent with previous inversions, we calculate an offset of the atmospheric CO₂ by subtracting the mean of the departure statistics $Hx_b - y$ from the prior concentrations at the initial time step of the assimilation window.

V.2.4 Transport Model

Atmospheric inversion studies usually consider CO₂ as a passive tracer. Indeed, CO₂ is a rather stable gas in the troposphere and its chemical production from reduced carbon compounds may reasonably be neglected. Further, basic CO₂ climatologies are sufficient to properly account for the impact of CO₂ variations on meteorology via radiation. Consequently, the observation operator H in equations V.1-V.4 can be reduced to transport (large-scale and sub-grid) processes and to a convolution operator.

The present inference scheme relies on the off-line version of the LMDZ general circulation model (Sadourny and Laval 1984, Hourdin and Armengaud 1999). This version computes the evolution of atmospheric compounds based on an archive of transport fields : winds, convection mass fluxes and planetary boundary layer exchange coefficients. The archive is built from a prior integration of the complete general circulation model. In this study as in the one by Hourdin and Isartel (2000), the horizontal winds have been nudged towards ECMWF meteorological ana-

lyses during the preliminary simulation in order to realistically reproduce the actual meteorology.

The complete LMDZ model solves the primitive equations on a 3D eulerian grid. 19 sigma-pressure layers are used here to discretize the vertical axis. They correspond to a resolution of about 300-500 m in the planetary boundary layer (first level at 70 m height) and to a resolution of about 2 km at the tropopause. Large-scale advection of trace species follows the Eulerian framework described by Hourdin and Armengaud (1999). Deep convection is parameterized according to Tiedtke (1989) and the turbulent mixing in the boundary layer is based on Laval et al. (1981).

For comparison with the TOVS observations, the concentrations computed at their location are convolved with the function displayed in Figure V.1.

We investigated the retro-transport approach of Hourdin et al. (2005) to perform the adjoint operations in the inversion scheme (equation V.6). This approach exploits the time symmetry of Eulerian transport to minimize the development of the adjoint code. Unfortunately, the symmetry property does not strictly hold when space is discretized, as already discussed by Hourdin et al. (2005). We found that the accuracy of such retro-transport computations is not high enough for minimization algorithms like the conjugate gradient, that strictly require the quadraticity of the function to optimize. The retro-transport may be suitable for more flexible minimization algorithms, but they are likely to need more iterations to converge.

As a consequence, we manually coded the tangent-linear (H) and the adjoint (H^T) operators that correspond to the off-line version of LMDZ, line by line in order to reach the accuracy of the computer. Correctness of those models has been checked with the Taylor formula and by the identity between inner products that mathematically defines an adjoint.

V.2.5 Results

The inference scheme was run for the entire year 1990 at once. 30 iterations were used, which reduced the norm of the gradient by 10,000 times. The 30-iteration minimization required about 15 CPU days on an Intel P4 3 GHz processor. Note that the 10,000-fold reduction is theoretical because the minimization uses the tangent-linear of the non-linear transport model. The actual reduction of the norm is a factor 42 only. It is possible to iterate on the linearization point as is done in the ‘outer-loop’ of the ECMWF 4D-Var (e.g., Trémolet 2004) in order to come closer from the global minimum of the cost function. Tests of such an approach with the TOVS data did not significantly affect the results from the first minimization and are not reported in the following.

Estimation of the Error Reduction on the Surface Fluxes

As mentioned in section V.2.2, the Lanczos minimization scheme provides the leading eigenvectors of the second derivative of the cost function. The number of estimated eigenvectors is less than the number of iterations performed. From equation V.7, the error reduction from the background to the analysis can then be estimated as a truncated eigenvector expansion (Fisher and Courtier 1995). This property is exploited in the ECMWF analysis system to precondition the minimization and to estimate analysis error variance (Fisher and Andersson 2001). The accuracy of the error estimate increases with the number of eigenvectors used, but this must be offset against the computational cost of increasing the number of minimization iterations. Using more eigenvectors decreases the analysis error estimate, so that a truncated approximation is an over-estimate of the analysis error variance implied by the assumed statistics of observation and background errors.

Figure V.4 displays such an estimate of the

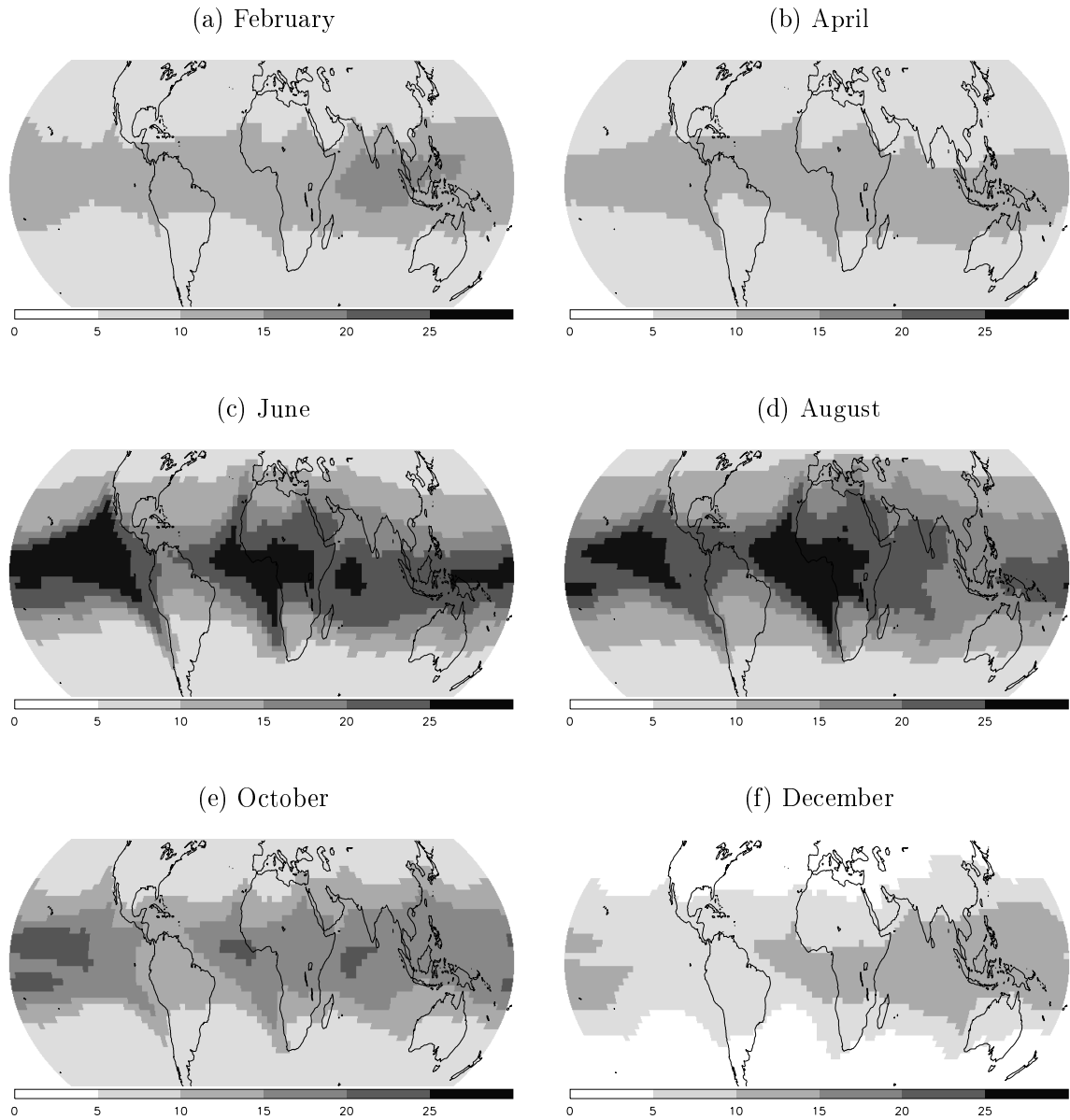


FIG. V.4 – Truncated estimate of the reduction of CO₂ day-time flux errors (in g C per m² per year) for six months of year 1990, as delivered by TOVS CO₂ retrievals. The error reduction is defined as the square root of the difference between the background error variances and the analysis error variances. As explained in the text, only the patterns are relevant, values are underestimated further to the truncation (10 eigenvectors are used out of about 200,000).

analysis error reduction for the day-time surface fluxes and for six months. The leading eigenvalue of the Hessian $\nabla^2 J(\chi)$ equals 1342 and the smallest eigenvalue retrieved is 30, knowing that by definition of χ (equation V.8) the eigenvalue spectrum further converges down to unity. The truncated eigenvector expansion provides those features of the error variance that have the largest spatial and temporal scales. Note that the error reduction is not related much to the observation location (Figure V.3) and even expands in the mid-latitudes. The error reduction is tightly linked with the main patterns of the general circulation in the tropics. The truncated error reduction is the largest in the ITCZ and in the trade wind regions that converge to this zone. The ascending branch of the Hadley circulation, which rapidly lifts air parcels from the boundary layer to the upper troposphere, obviously drives the analysis. Note that observations are restricted to clear sky here and sample the air outflowed from the tropical convection rather than the air in the convective towers themselves. The transport between other source regions, such as the subtropical high-pressure systems, and the upper troposphere is much slower and the flux analysis is consequently weakly constrained there. Comparing the error reduction for each month of the year, one can see a seasonal variation, with the largest signal in boreal summer, and the weakest in boreal winter, which follows the variations of the ITCZ intensity. Similarly, the fluxes are characterized by a smaller error reduction during the night (when convection is the weakest) than during the day (not shown) even though the number of day-time TOVS observations is about the same as the number of night time ones.

Additional iterations would increase the estimated error reduction and introduce smaller-scale patterns, but, by construction, they would not change the large-scale ones shown here. The Lanczos minimization scheme therefore gives an interesting, though

incomplete, indicator of the theoretical error reduction.

Estimation of the Satellite Information Content

As described by Fisher (2003), the Lanczos minimization algorithm also allows accurate estimation of two important measures of the observation information content. The first one is the degree of freedom for signal, expressed as (e.g., Rodgers 2000) :

$$d = \text{trace}(\mathbf{I} - \mathbf{AB}^{-1}) \quad (\text{V.9})$$

$$= N - \sum_i \lambda_i \quad (\text{V.10})$$

Where \mathbf{I} is the identity matrix, N is the dimension of the control vector \mathbf{x} and λ_i are the eigenvalues of \mathbf{AB}^{-1} . The degree of freedom for signal describes the number of independent pieces of information that the observations provide, given the prior information.

The second measure of the observation information content is given by the entropy reduction (e.g., Rodgers 2000) :

$$S = -\frac{1}{2} \log_2 |\mathbf{AB}^{-1}| \quad (\text{V.11})$$

$$= N - \sum_i \log_2(\lambda_i) \quad (\text{V.12})$$

S is the number of states, in bits, that can be distinguished using the observations in the space defined by the uncertainty of the prior information (whose metric is given by \mathbf{B}).

Note that Bayesian estimation shows how observations improve the knowledge about chosen variables : it is relative to some prior information. Consistently, d and S depend on the errors of the prior.

Engelen and Stephens (2004) studied the information content of the TOVS and AIRS radiance observations to infer CO₂ concentrations, based on those two quantities. The present study considers the step beyond, where surface fluxes are inferred. The dimension of this problem makes the estimation of $\sum_i \lambda_i$ and $\sum_i \log_2(\lambda_i)$ difficult. However, the change of variables defined by equa-

tion V.8 implies that the λ_i s are the eigenvalues of $\nabla_x^2 J(x)$, the leading ones being provided by the minimization algorithm. Moreover, the approach of Bai et al. (1996) allows to circumvent the unavailability of the trailing ones (Fisher 2003).

This approach has been applied to the 1990 TOVS data. Within 15 iterations, the entropy reduction converged to 341 and the degree of freedom for signal to 339. The former figure indicates that about 2^{341} states of the control vector (that can take an infinite number of values for each one of its 200,000 components) can be distinguished from a year's worth of TOVS data, given the specified prior information. The degree of freedom for signal allows the examination of the information content in the space of the observations. It shows that about 339 independent quantities can be measured from that year of TOVS data, given the specified prior information. One may compare the 339 independent quantities to the total number of observations available : 347,400. If these 339 information pieces were regularly spread between 20°S and 20°N and throughout the year (which is a rough approximation, as can be seen in Figure V.4), each one of them would cover a $22.5^\circ \times 22.5^\circ$ latitude-longitude surface. This simple calculation highlights the rather low resolution of the information about the CO₂ surface fluxes that can be extracted from upper tropospheric measurements. This rather low resolution stems from the highly diffusive nature of the atmosphere dynamics. Note that Chédin et al. (2003b, 2005) independently used the TOVS retrievals at resolution $15^\circ \times 15^\circ$, which is rather comparable to the present rough estimation. To summarize, given the specified errors of the observations and of the prior, the 347,400 CO₂ retrievals for year 1990 actually consist of 339 independent observations that allow to distinguish between 2^{341} states of the flux vector.

The Optimized Concentrations And Fluxes

The day-time flux increments for the 1990 analysis described above are illustrated in Figures V.5 and V.6 : April and August values are presented. In the same figures, the background fluxes, the mean CO₂ fields in the background, the analysis and the observations are displayed as well. As expected (section V.2.3), large differences can be seen between the background and the observation. The range for TOVS is about 7-9 ppm, with pronounced minima over the equatorial Pacific and in the subtropics in August. In contrast, the background mainly varies as a function of latitude within 4 ppm in April and 2 ppm in August. For each month shown, the analysis is a trade-off between the prior field and the observations, the weight of each being determined by the corresponding error covariance matrices and by the Jacobian of the transport model. The inference scheme adjusts the large-scale CO₂ patterns to fit the observations better for August than for April, consistent with the theoretical error reduction discussed in the previous section.

The corrections to the surface fluxes occur throughout the tropics (Figures V.5e and V.6e), spreading beyond the areas where the error diminishes the most as estimated in Figure V.4. The offset-correction on the concentrations mentioned in section V.2.3 makes the annual global averages of the flux increments close to zero, but locally the annual mean reaches several hundreds g C per m² per year, which is one order of magnitude larger than the increments obtained from the analysis of surface in situ measurements (see Figure 8d in Rödenbeck et al. 2003 for instance). The mismatch of about 4 ppm in the upper troposphere above the central Pacific implies an increment of the order of 3 GTC.yr⁻¹ over the eastern equatorial Pacific with LMDZ. Some of the increment patterns are clearly not realistic, since carbon uptake is inferred from the TOVS analysis in some of the tropical oceans, in contradiction with the ocean pCO₂ observa-

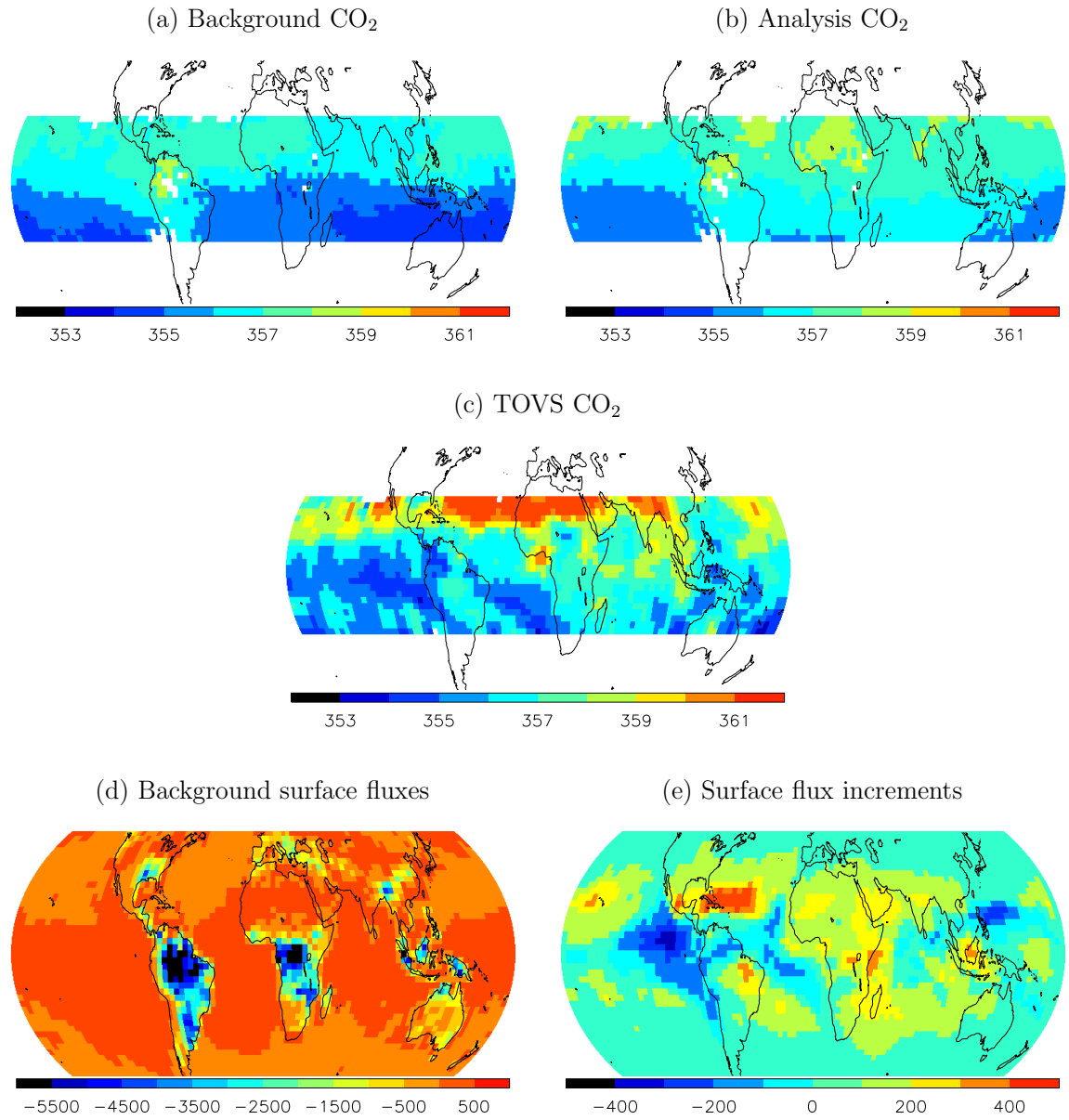


FIG. V.5 – Mean background (a), analysis (b) and TOVS (c) CO₂ concentrations, in ppm, for April 1990 and day-time flux background values (d) and increments (analysis minus background) (e), in g C per m² per year, for 1 April 1990.

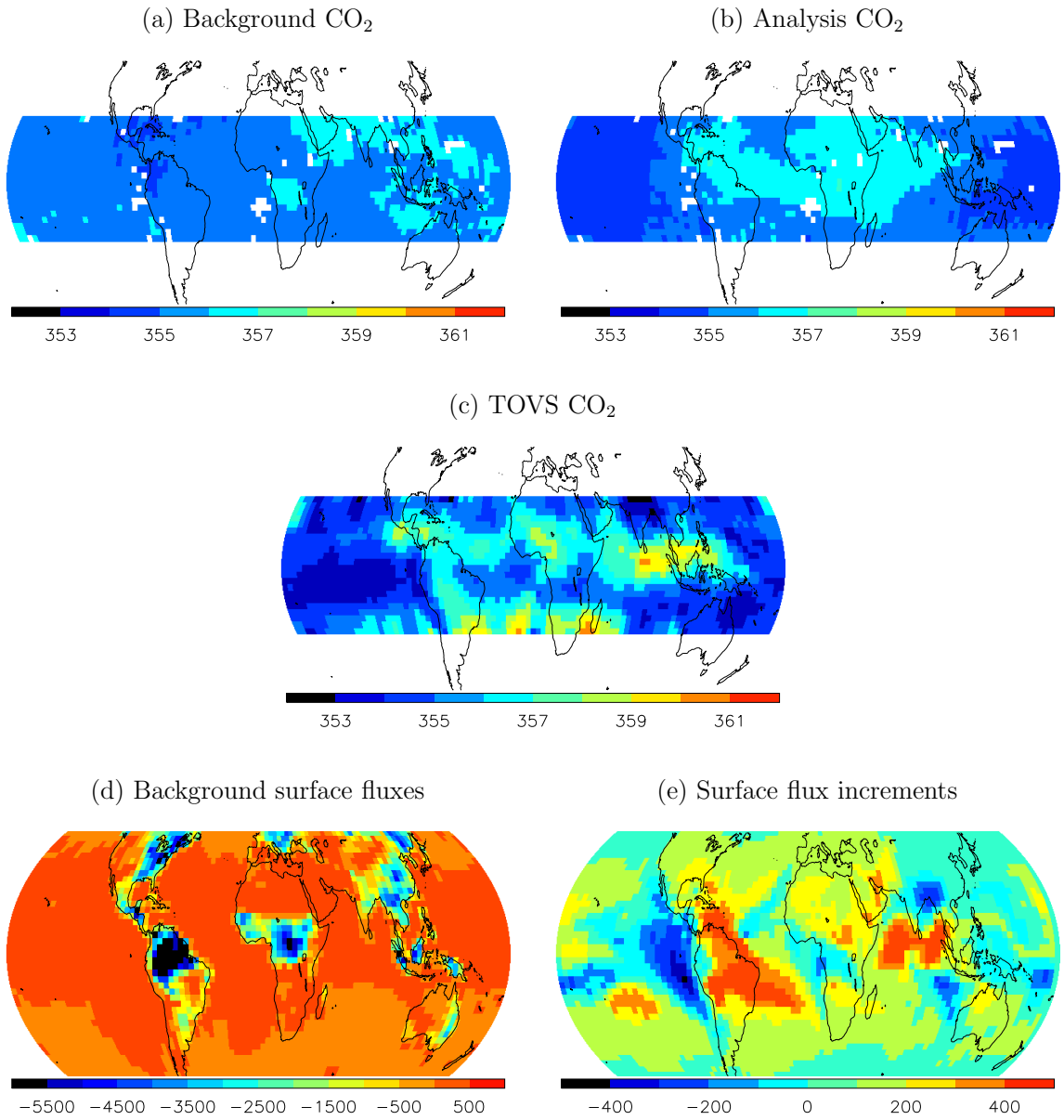


FIG. V.6 – Same as Figure V.5 for August 1990.

Site	(lat./long.)	Obs. Std.	(BG-Obs) RMS	(AN-Obs) RMS
ALT	(82.5 , -62.5)	5.2	3.5	3.7
MBC	(76.2 , -119.3)	5.3	3.7	3.9
BRW	(71.3 , -156.6)	6.1	3.7	3.8
STM	(66.0 , 2.0)	5.0	1.4	1.4
CBA	(55.2 , -162.7)	5.8	1.6	2.3
SHM	(52.7 , 174.1)	6.0	1.2	1.8
CMO	(45.5 , -124.0)	3.0	3.7	3.7
NWR	(40.0 , -105.6)	2.6	6.2	6.5
AZR	(38.8 , -27.4)	3.2	1.1	1.9
BME	(32.4 , -64.7)	3.1	1.1	1.4
BMW	(32.3 , -64.9)	2.8	1.0	1.5
MID	(28.2 , -177.4)	2.7	1.0	1.5
KEY	(25.7 , -80.2)	2.3	2.5	3.5
MLO	(19.5 , -155.6)	1.9	0.8	1.4
KUM	(19.5 , -154.8)	2.2	0.6	0.9
GMI	(13.4 , 144.8)	2.4	1.3	2.5
RPB	(13.2 , -59.4)	2.0	1.1	0.9
CHR	(1.7 , -157.2)	0.5	1.2	3.2
SEY	(-4.7 , 55.2)	0.9	1.5	1.3
ASC	(-7.9 , -14.4)	1.0	1.3	1.7
SMO	(-14.2 , -170.6)	0.4	1.1	1.1
CGO	(-40.7 , 144.7)	0.7	1.6	1.0
PSA	(-64.9 , -64.0)	1.1	1.7	1.0
SYO	(-69.0 , 39.6)	0.7	1.9	1.5
HBA	(-75.6 , -26.5)	0.7	1.6	1.2
SPO	(-90.0 , -24.8)	0.7	1.3	1.0

TAB. V.1 – Year 1990. RMS differences between the background (BG) or the analysis (AN) and the Globalview (Obs.) monthly means of carbon dioxyde concentrations (ppm) at various ground stations. The observations are independent from the analysis. The offset averaged over all the stations has been removed before the RMS computation. Each station is defined by a 3-letter acronym and a geographical position (latitude and longitude, in degrees). The standard deviation of the 12 Globalview monthly means is also indicated. Stations are ordered by decreasing latitude.

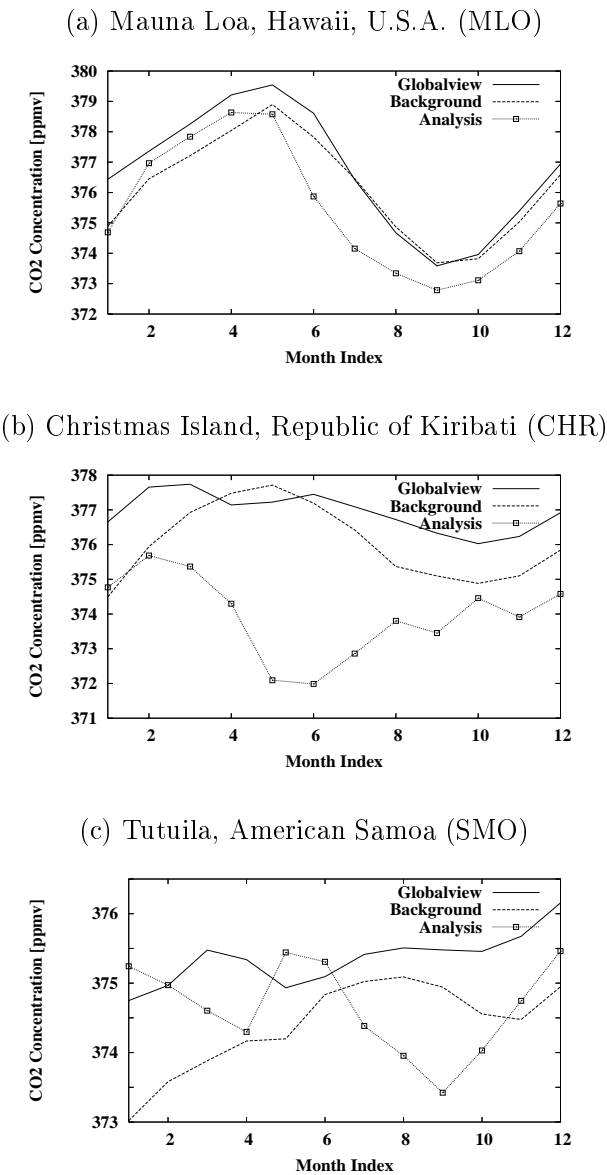


FIG. V.7 – 1990 time series of monthly mean CO₂ concentrations, in ppm, at three ground stations in Globalview, for the background and for the analysis. The Globalview identifier used in Table V.1 is given in parenthesis.

tions in these relatively well-observed basins (Takahashi 2002).

The flux increments are further evaluated against surface observations that are independent from the analysis (i.e., only the TOVS data are assimilated). To do so, we successively prescribed the prior and the analyzed fluxes as the boundary condition for the LMDZ transport model. The resulting monthly means of simulated CO₂ concentrations are compared to the values reported in the Globalview dataset for a series of ground stations (Globalview-CO₂ 2004). The Globalview monthly means are averages of smoothed measurements made at these observatories. The 1990 time series at three stations are shown in Figure V.7 as an illustration. Table V.1 summarizes the results by presenting the RMS statistics of the fit of the background and of the analysis to the Globalview monthly means for 1990 and 2003. The mean offset averaged over all the stations has been removed before the RMS computation. The prior RMS differences are usually about a couple of ppm. The analysis usually degrades them by a few tenth of ppm, except in the southern hemisphere, where the seasonal cycle is very small (so that the RMS difference is driven by its bias component). The conclusion of this evaluation is that, as expected (see section V.2.3), the flux patterns inferred from the TOVS satellite observations using the LMDZ model are less accurate than the prior fluxes.

Alternate Specification of the Background Errors

Results presented so far have relied on a crude specification of background flux errors, where correlations are neglected and where the same error (10^{-4} kg C per m² per hour) is attributed to each grid point flux. Complementary inversions have been performed with background errors from bio-geochemical considerations, as described in section V.2.3.

The main features of this alternate inversion with respect to the results presented can

be summarized as follows. First, the analysis fit to the CO₂ observations is about the same (2.7 ppm RMS difference in both cases). Second, the maps of theoretical error reduction reproduce the prescribed patterns of the prior error variance (here the heterotrophic respiration fluxes) in the tropics as at mid-latitudes (Figure V.8). Third, large flux increments occur at most latitudes with significant regional positive-negative dipoles (not shown). Fourth, the fit to the Globalview dataset is further degraded.

The realism of the analyzed fluxes appears to be less than with the diagonal background error matrix. This can be explained by the strong dipole increments needed to fit the biased TOVS data while a distinction is made now between areas of high prior errors and areas of low ones.

Note that Houweling et al. (2004) estimated the flux error reduction induced by upper tropospheric observations of CO₂ concentrations (their Figure 2c). Their results are based on simulated observations that are not restricted to the tropics. Their patterns over land are quite similar to our second configuration (Figure V.8), despite a very different inversion set up. They differ significantly from our two estimates (Figures V.4 and V.8) over the oceans, since they show a minimum in the tropical Atlantic for the error reduction, where our two configurations consistently show a maximum. The very large correlation lengths used by Houweling and his co-authors (1250 and 2000 km respectively over land and ocean) may explain the contradiction (Houweling, personal communication, 2005).

V.2.6 Discussion

The above results are an early step in inferring CO₂ surface fluxes from actual satellite observations. A variational scheme has been built that successfully processes satellite retrievals over long periods of time (here one year) and without averaging the data over weeks or months as is usually done. The in-

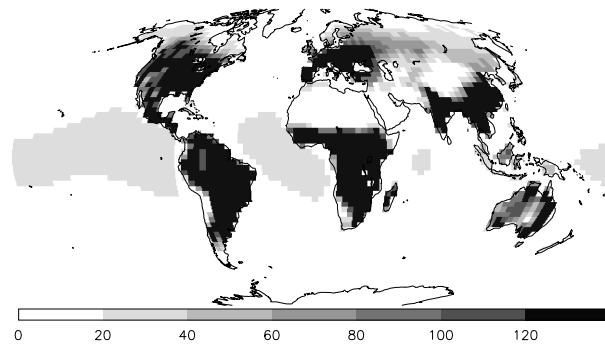


FIG. V.8 – Truncated estimate of the reduction of CO_2 day-time flux errors (in g C per m^2 per year) for August 1990, and for the inversion using a physically-based inversion matrix. The error reduction is defined as the square root of the difference between the background error variances and the analysis error variances. Note that a better convergence is obtained, which allows a better estimation of the eigenvectors. Therefore we use 14 eigenvectors here instead of 10 in Figure V.4. This explains the larger figures.

version system behaves consistently with the specifications of the inversion problem. However, the evaluation of the inferred fluxes indicates that these are less accurate than the prior fluxes given by a climatology. Our conclusion is that some of the inputs of the inversion scheme (observations, prior information and/or corresponding errors) are not consistent with each other.

The key inconsistent assumption that is violated is that there are no regional biases in the TOVS observations. Indeed systematic errors have been previously found in the TOVS dataset that cannot be resolved from the information contained in the TOVS radiances alone. It should be emphasized that the density of satellite measurements limits the impact of random errors and that consequently even poor-quality satellite retrievals should be superior to the existing flask network (Rayner and O'Brien 2001). However biases are damaging and should be removed or at least minimized. In practice it is difficult to envisage a bias-correction scheme given the lack of high-quality column-integrated CO_2 observations. Further, one might not trust the prior information enough to bias-correct the observations against it as is done in the field of numerical weather prediction (Harris and

Kelly 2001). A close collaboration between the people involved at some stage in the process of going from the raw satellite counts to elaborate products, like surface flux estimates, is required to diagnose and understand the sources of biases for a given satellite instrument.

Our study also points at the sensitivity of the inferred fluxes to the prior information, despite the large amount of satellite retrievals (we processed individual measurements). Indeed we find a large impact from changing the background errors. Their specification is important and should be refined in terms of variances, in terms of temporal correlations and in terms of spatial correlations.

Last but not the least, errors of the atmospheric transport model may also degrade the inversion. In particular, the quality of the sub-grid parameterizations (boundary layer turbulence and moist convection) may be essential, even though they suffer from large inaccuracies in current global models (e.g., Chevallier and Kelly, 2003).

V.2.7 Conclusion

A Bayesian inference scheme has been set up to link satellite CO_2 retrievals to the CO_2 surface fluxes. A variational formulation has

been chosen to cope with the large amount of satellite data. The scheme iteratively computes the optimum solution to the inference problem as well as an estimation of its error characteristics and some quantitative measures of the observation information content. The LMDZ model nudged with ECMWF winds provides information about the atmospheric transport to the inversion scheme. A surface flux climatology regularizes the inference problem.

The first dataset of satellite CO₂ retrievals from space, the one from TOVS established at LMD, has been used as a testbed for the whole method. The inferred fluxes are not judged realistic. We point at the sensitivity of the results to the formulation of the prior uncertainty and to the modelling of atmospheric transport. Most of all, regional biases in the observations hamper the inversion. On the one hand our study demonstrates the possibility to process the satellite CO₂ retrievals at high spatial and temporal resolutions. On the other hand it does not seem to be relevant for the TOVS data that would be more adequately used at very low resolution. The 26-yr archive of TOVS data may be used in the future in surface flux inversion as a constraint on the monthly zonal means of CO₂ concentrations. In such an inversion configuration, surface measurements would also be assimilated to constrain the smaller horizontal scales. So far only the night-minus-day-difference (NDD, Chédin et al. 2005) of the TOVS retrievals has proved to carry a significant CO₂-related emission signal at the regional level, which could worth further exploitation to constrain the inversion of sources and sinks, provided that the transport model is adapted to simulate biomass burning-induced convection.

The inversion scheme described here will allow us to investigate the use of the forthcoming CO₂ retrievals, like those of AIRS and OCO, that should be less prone to biases, at high resolution. Moreover four-dimensional inversion schemes of this type could form the

basis of ambitious multisensor data assimilation systems to estimate surface fluxes of key atmospheric compounds like CO₂, carbon monoxide, methane or aerosols.

Acknowledgments. Authors wish to thank R. Engelen (ECMWF), P. Rayner (LSCE) and F. Hourdin (LMD) for fruitful discussions, A. Idelkadi (LSCE) for help with the LMDZ model and F. Marabelle (LSCE) for computer support. This study was co-funded by the European Union under project GEMS. Suggestions from two anonymous reviewers have helped to improve the clarity of the article.

References

- Bai, Z., M. Fahey, and G. H. Golub (1996), Some large scale matrix computation problems, *J. Comput. Appl. Math.*, 74, 21–89.
- Bousquet, P., P. Peylin, P. Ciais, C. Quere, P. Friedlingstein, and P. Tans (2000), Regional changes in carbon dioxide fluxes of land and oceans since 1980, *Science*, 290, 1342–1346.
- Chédin, A., R. Saunders, A. Hollingsworth, N. A. Scott, M. Matricardi, J. Etcheto, C. Clerbaux, R. Armante and C. Crévoisier (2003), The feasibility of monitoring CO₂ from high resolution infrared sounders, *J. Geophys. Res.*, 108, doi :10.1029/2001JD001443.
- Chédin, A., N. A. Scott, C. Wahiche, and P. Moulinier (1985), The Improved Initialization Inversion method : a high resolution physical method for temperature retrievals from TIROS-N series. *J. Clim. Appl. Meteor.*, 24, 128–143.
- Chédin, A., S. Serrar, A. Hollingsworth, R. Armante, and N. A. Scott (2003a), Detecting annual and seasonal variations of CO₂, CO and N₂O from a multi-year collocated satellite-radiosonde data-set using the new Rapid Radiance Reconstruction Network (3R-N) model, *J. Quant. Spectrosc. Radiat. Transfer*, 77, 285–299.
- Chédin, A., S. Serrar, N. A. Scott, C. Crévoisier, and R. Armante (2003b), First global measurement of midtropospheric CO₂ from NOAA polar satellites : Tropical zone, *J. Geophys. Res.*, 108, doi :10.1029/2003JD003439.
- Chédin, A., S. Serrar, N. A. Scott, C. Pierangelo, and P. Ciais (2005), Impact of tropical biomass burning emissions on the diurnal cycle of upper tropospheric CO₂ retrieved from NOAA-10 satellite observations, *J. Geophys. Res.*, 110, D11309, doi :10.1029/2004JD005540.
- Chevallier, F., F. Chéruy, N. A. Scott, and A. Chédin (1998), A neural network approach for a fast and accurate computation of longwave radiative budget, *J. Appl. Meteor.*, 37, 1385–1397.
- Chevallier, F., and G. Kelly (2002), Model clouds as seen from space : comparison with geostationary imagery in the 11μm window channel, *Mon. Wea. Rev.*, 130, 712–722.
- Crévoisier C., S. Heilliette, A. Chédin, S. Serrar, R. Armante, and N. A. Scott (2004), Midtropospheric CO₂ concentration retrieval from AIRS observations in the tropics, *Geophys. Res. Lett.*, 31, doi :10.1029/2004GL020141.
- Dufour, E., and F.-M. Bréon (2003), Spaceborne estimate of atmospheric CO₂ column using the differential absorption method. *Appl. Optics*, 42, 3595–3609.
- Engelen, R. J., and G. L. Stephens (2004), Information content of infrared satellite sounding measurements with respect to CO₂. *J. Appl. Meteor.*, 43, 373–378.
- Engelen, R. J., E. Andersson, F. Chevallier, A. Hollingsworth, M. Matricardi, A. P. McNally, J.-N. Thépaut, and P. D. Watts (2004), Estimating atmospheric CO₂ from advanced infrared satellite radiances within an operational 4D-Var data assimilation system : methodology and first results. *J. Geophys. Res.*, 109, D19309, doi :10.1029/2004JD004777.
- Errico, R. M. (1997), What is an adjoint model ? *Bull. Amer. Meteo. Soc.*, 78, 2577–2591.
- Fisher, M. and P. Courtier (1995), Estimating the covariance matrices of analysis and forecast error in variational data assimilation, *ECMWF Technical Memorandum*, 220, 26 pp.
- Fisher, M., and E. Andersson (2001), Developments in 4D-Var and Kalman filtering. *ECMWF Technical Memorandum*, 347, 38 pp.
- Fisher, M. (2003), Estimation of entropy reduction and degrees of freedom for signal for large variational analysis systems, *ECMWF Technical Memorandum*, 397, 18 pp.
- Globalview-CO₂ (2004), Cooperative atmospheric data integration project - carbon dioxide. *CD-ROM, NOAA CMDL, Boulder, Colorado*, [also available on internet via anonymous FTP to ftp.cmdl.noaa.gov, path : ccg/co2/GLOBALVIEW].
- Gurney, K. R., R. M. Law, A. S. Denning, P. J. Rayner, D. Baker, P. Bousquet, L. Bruhwiler, Y. H. Chen, P. Ciais, S. Fan, I. Fung, M. Gloo, M. Heimann, K. Higuchi, J. John, T. Maki, S. Maksyutov, K. Masarie, P. Peylin, M. Prather, B. C. Pak, J. Randerson, J. Sarmiento, J., S. Taguchi, T. Takahashi, and C. W. Yuen (2002), Towards robust regional estimates of CO₂ sources and sinks using atmospheric transport models, *Nature*, 415 :6872, 626–630.

- Harris, B. A., and G. Kelly (2001), A satellite radiance bias correction scheme for radiance assimilation, *Q. J. Roy. Meteor. Soc.*, 127, 1453–1468.
- Hourdin, F., and A. Armengaud (1999), Test of a hierarchy of finite-volume schemes for transport of trace species in an atmospheric general circulation model, *Mon. Wea. Rev.*, 127, 822–837.
- Hourdin, F., and J.-P. Issartel (2000), Sub-surface nuclear tests monitoring through the CTBT xenon network, *Geophys. Res. Lett.*, 27, 2245–2248.
- Hourdin, F., O. Talagrand, and A. Idelkadi (2005), Eulerian backtracking of atmospheric tracers : II Numerical aspects, *Q. J. Roy. Meteor. Soc.*, *in press*.
- Houweling, S., F.-M. Bréon, I. Aben, C. Rödenbeck, M. Gloor, M. Heimann, and P. Ciais (2004), Inverse modeling of CO₂ sources and sinks using satellite data : a synthetic inter-comparison of measurement techniques and their performance as a function of space and time. *Atmos. Chem. Phys.*, 4, 523–538.
- Kaminski, T., P. J. Rayner, M. Heimann, and I. G. Enting (2001), On aggregation errors in atmospheric transport inversions, *J. Geophys. Res.*, 106(D5), 4703–4716.
- Ide, K., P. Courtier, M. Ghil, and A. Lorenc (1997), Unified notation for data assimilation : Operational, sequential and variational, *J. Met. Soc. Japan*, 75, 181–189.
- Lafont, S., L. Kergoat, G. Dedieu, A. Chevillard, E. Kjellström, U. Karstens, and O. Kolle (2002), Spatial and temporal variability of land CO₂ fluxes estimated with remote sensing and analysis data over western Eurasia, *Tellus*, 54B, 820–833.
- Lanczos, C. (1950), An iteration method for the solution of the eigenvalue problem, *J. Res. Nat. Bur. Standards*, 45, 255–282.
- Laval, K., R. Sadourny, and Y. Serafini (1981), Land surface processes in a simplified general circulation model, *Geophys. Astrophys. Fluid Dyn.*, 17, 129–150.
- Law, R. M., P. J. Rayner and Y. P. Wang (2004), Inversion of diurnally-varying synthetic CO₂ : network optimization for an Australian test case, *Global Biogeochem. Cycles*, 18, GB1044, doi :10.1029/2003GB002136
- Olivier, J. G. J., A. F. Bouwman, C. W. M. Van der Maas, J. J. M. Berdowski, C. Veldt, J. P. J. Bloos, A. J. H. Visschedijk, P. Y. J. Zandyelt, and J. L. Haverlag (1996), Description of EDGAR Version 2.0. A set of global emission inventories of greenhouse gases and ozone-depleting substances for all anthropogenic and most natural sources on a per country basis and on 1x1 grid, *RIVM/TNO report, December 1996. RIVM, Bilthoven, RIVM report nr. 771060 002. [TNO MEP report nr. R96/119]*.
- Rayner, P. J., and D. M. O'Brien (2001), The utility of remotely sensed CO₂ concentration data in surface source inversions, *Geophys. Res. Lett.*, 28, 175–178.
- Rayner, P. J., R. M. Law, and D. M. O'Brien (2002), Global observations of the carbon budget, 3. initial assessment of the impact of satellite orbit, scan geometry, and cloud on measuring CO₂ from space. *J. Geophys. Res.*, 107, D21, doi :10.1029/2001JD000618.
- Rodgers, C. D. (2000), Inverse methods for atmospheric sounding : theory and practice, *World Scientific*, 238 pp.
- Rödenbeck, C., S. Houweling, M. Gloor, and M. Heimann (2003), CO₂ flux history 1982–2001 inferred from atmospheric data using a global inversion of atmospheric transport. *Atmos. Chem. Phys.*, 3, 1919–1964.
- Rumelhart, D. E., G. E. Hinton, and R. J., Williams (1986), Learning internal representations by error propagation, in *Parallel distributed processing : Explorations in the macrostructure of cognition*, vol. 1, edited by D. E. Rumelhart and McClelland, MIT Press, pp. 318–362, MIT Press, Cambridge, Mass.
- Sadourny, R., and K. Laval (1984), January and July performance of the LMD general circulation model, *In New Perspectives in Climate Modeling, A.L. Bergerand C. Nicolis (eds.), Elsevier Press, Amsterdam*, 173–197.
- Takahashi, T., S. C. Sutherland, C. Sweeney, A. Poisson, N. Metzl, B. Tilbrook, N. Bates, R. Wanninkhof, R. A. Feely, C. Sabine, J. Olafsson and Y. Nojiri (2002), Global Sea-Air CO₂ Flux Based on Climatological Surface Ocean pCO₂, and Seasonal Biological and Temperature Effect, *Deep Sea Res. II*, 49, 1601–1622.
- Tiedtke, M. (1989), A comprehensive mass flux scheme for cumulus parameterization in large-scale models, *Mon. Wea. Rev.*, 117, 1179–1800.

- Tjemkes, S. A., and J. Schmetz (1997), Synthetic satellite radiances using the radiance sampling method, *J. Geophys. Res.*, **102D**, 1807–1818.
- Trémolet, Y. (2004), Diagnostics of linear and incremental approximations in 4D-Var. *Q. J. Roy. Meteor. Soc.*, **130**, 2233–2251.
- Turner, D. S. (1993), The Effect of Increasing CO₂ Amounts on TOVS Longwave Sounding Channels, *J. Appl. Meteor.*, **32**, 1760–1766.
- Turner, D. S. (1994), HIRS Sensitivity to CO₂ Mixing Ratio and a Pragmatic Correction Term, *J. Appl. Meteor.*, **33**, 1155–1162.
- Wanninkhof, R. (1992), Relationship between wind speed and gas exchange, *J. Geophys. Res.*, **97**, 7373–7382.
- Weaver, A.T., J. Vialard, and D.L.T. Anderson (2003), Three- and four-dimensional variational assimilation with a general circulation model of the tropical Pacific Ocean, Part 1 : formulation, internal diagnostics and consistency checks. *Mon. Wea. Rev.*, **131**, 1360–1378.

V.3 Diagnostics

Cette section reprend l'article de Chevallier et coll. (2007) paru dans *Journal of Geophysical Research*.

The Contribution of the Orbiting Carbon Observatory to the Estimation of CO₂ Sources and Sinks : Theoretical Study in a Variational Data Assimilation Framework

Frédéric Chevallier, François-Marie Bréon and Peter J. Rayner

Laboratoire des Sciences du Climat et de l'Environnement
Institut Pierre-Simon Laplace
Gif-sur-Yvette, France

Abstract. NASA's Orbiting Carbon Observatory (OCO) will monitor the atmospheric concentrations of carbon dioxide (CO₂) along the satellite subtrack over the sunlit hemisphere of the Earth for more than two years, starting in late 2008. This paper demonstrates the application of a variational Bayesian formalism to retrieve fluxes at high spatial and temporal resolution from the satellite retrievals. We use a randomization approach to estimate the posterior error statistics of the calculated fluxes. Given our error statistics for the prior fluxes (about 0.4 gC.m⁻² per day over ocean and 4 gC.m⁻² per day over vegetated areas) and the observations (2 ppm), we show error reductions of up to about 40% at weekly and gridpoint scales. We simulate the impact of biases by perturbing the observations and show that regional biases of a few tenths of a ppm in column-averaged CO₂ can bias the inverted sub-continental fluxes by a few tenths of a giga-ton of carbon.

V.3.1 Introduction

The carbon cycle in the Earth system results from the exchange of huge amounts of carbon compounds between the atmosphere,

the ocean, the biosphere, and the fossil reservoirs (several tens of Gt C per year). Since the cycle is nearly stationary on a yearly timescale, the annual global net flux at the interface between the atmosphere and the surface

is close to zero, with a relatively small gain for the atmosphere (about 3 Gt C per year, mainly of CO₂). This slight imbalance feeds back on another near-balanced budget, that of the energy exchange between the Earth system and outer space, via radiation processes. The importance of the topic has triggered numerous efforts to better quantify the carbon surface fluxes at all spatial scales.

The Orbiting Carbon Observatory (OCO, Crisp et al., 2004) has been chosen by NASA to remotely sense atmospheric CO₂ from space and is planned for launch in late 2008. From its high-resolution spectroscopic measurements of reflected sunlight, this instrument will provide the data needed to retrieve the column-averaged dry air mole fraction of CO₂, denoted X_{CO₂}, over the sun-lit part of the globe. The number of cloud-free soundings and precision per sounding will vary with latitude, cloud cover, aerosol optical depth, and other factors, but the minimum requirement of the mission is to achieve X_{CO₂} precision of 1 ppm for monthly averages over regional (1000 x 1000 km²) spatial scales. Building on the experience using in situ gas concentration measurements (e.g., Gurney et al., 2002), inverse methods will be applied to quantify the CO₂ surface sources and sinks from the OCO retrievals. The usefulness of satellite data for such a task has been demonstrated from simulations at relatively low spatial and temporal resolutions (Rayner and O'Brien, 2001; Pak and Prather, 2001; Houweling et al., 2004). Higher resolutions are being introduced thanks to a variational formulation of the Bayesian inversion problem (Chevallier et al., 2005b; Rödenbeck 2005). However, the inversion of existing satellite CO₂ products has not been successful so far most likely because of the existence of biases both in the observations and in the transport models (Chevallier et al., 2005a, 2005b; Houweling et al., 2005). Furthermore, some of these observations are restricted to the upper troposphere, which is only remotely connected to the sur-

face. In the light of these recent developments, this paper evaluates the usefulness of the forthcoming OCO measurements for characterizing surface fluxes, based on a series of observing system simulation experiments. The design of the experiments allows us to estimate some diagnostic quantities, like the degrees of freedom for signal or the error reduction, that are usually difficult to obtain for high dimensional problems. To summarize, our study approaches two distinct scientific problems : a methodological issue regarding variational systems in general, and the relevance of OCO to improve our knowledge about the carbon cycle. Our method and our data are described in the following section. Section V.3.3 presents the results, which are discussed in section V.3.3.

V.3.2 Method and Data

The steps in our observing system simulation experiments (OSSE) can be described as follows :

1. Use a climatology of surface fluxes as boundary conditions to a transport model and generate a set of pseudo observations
2. Perturb the pseudo-observations consistently with assumed observation error statistics
3. Perturb the surface flux climatology consistently with assumed error statistics
4. Perform a Bayesian inversion using the perturbed pseudo-observations as data and the perturbed climatology as the prior field.

The ingredients of this procedure are detailed in the next subsections.

The Inversion Scheme

Bayesian inference describes how observations y transform our knowledge about any related variables x . It actually shifts the

problem of estimating posterior probabilities $P(x|y)$ to that of estimating prior probabilities $P(x)$. In spite of the difficult definition of $P(x)$, Bayesian optimization has proven to be particularly useful in numerous fields. It is at the root of CO_2 surface flux estimations at the global scale (e.g., Gurney et al., 2002; Enting 2002). The main developments of the method for CO_2 since its introduction by Enting et al. (1995) are twofold. First the realism of its ingredients has been improved : the transport model H which simulates the atmospheric concentrations y from the surface fluxes x , and the error covariance matrices B and R that describe the error statistics, assumed to be Gaussian, for x and y respectively. Second, the spatial and temporal resolutions of x and y have been dramatically increased, thanks to the evolution of computer power and, only recently, to the implementation of a variational formulation to the optimization problem (Chevalier et al., 2005b; Rödenbeck 2005), as is done in numerical weather prediction (NWP).

In this study, the control variables x are the CO_2 surface fluxes either at daytime or at night-time, at each point of a $3.75^\circ \times 2.5^\circ$ (longitude-latitude) grid every eight days. Daytime and night-time fluxes are defined separately to account for the diurnal cycle of the biospheric fluxes. The motivation for the eight-day resolution is given further below from considerations about the prior errors. In the simulations presented, fluxes within any of the eight-day periods are interpolated in time from the control variables. The 3D carbon field at the start of the assimilation window is also included in the vector x but the length of the temporal window considered (one year) makes it play a minor role. The general circulation model of the Laboratoire de Météorologie Dynamique (LMDZ, Sadourny and Laval 1984, Hourdin and Armentaud, 1999), nudged to NWP winds, is our H operator. LMDZ is used here with 19 levels in the vertical and the same horizontal resolution as the surface fluxes.

The concentrations y are here individual OCO retrievals of X_{CO_2} , binned per orbit at the $3.75^\circ \times 2.5^\circ$ model resolution. As mentioned in the introduction, they are distributed in cloud-free sunlit areas only and therefore constrain the control variables in a complicated way. For instance, a midday X_{CO_2} observation is not influenced by the surface fluxes later in the day but may integrate significant information about the fluxes from the night before.

The variational inversion system of Chevalier et al. (2005b) allows us to find the optimal fluxes x_a that fit both the observations y with their specified error statistics R and the prior fluxes x_b with their specified error statistics B , by iteratively minimizing the cost function J defined by :

$$\begin{aligned} J(x) = & (x - x_b)^T B^{-1} (x - x_b) \\ & + (H(x) - y)^T R^{-1} (H(x) - y) \end{aligned} \quad (\text{V.13})$$

The number of iterations needed for the minimization of $J(x)$ to reach convergence depends not only on the degree of non-linearity and on the conditioning of the minimization problem, but also on the minimization strategy. The efficiency of the minimization algorithm is particularly crucial when the computational cost of each iteration is high. In our case, a single iteration using one-year worth of data takes about 7 CPU hours when using a 64-bit processor at 2.6 GHz. This high computation burden is explained by the necessity of running the transport model successively in forward mode (to compute $J(x)$) and in adjoint mode (to compute the gradient of $J(x)$) over the whole period at each iteration. Our minimization strategy follows the "inner loop/outer loop" approach developed at the European Centre for Medium-Range Weather Forecasts (ECMWF) where operational constraints impose a stringent limitation to the number of iterations for the NWP analyses. As initially described by Courtier et al. (1994), the minimization is decomposed into a succession of

minimizations for which the observation operator is linearized around the corresponding first-guess (using a first order Taylor expansion). The updates of the linearization constitute the outer loop of this system. The overall convergence of such an inner loop/outer loop approach depends on the validity of the tangent-linear hypothesis for the size of analysis increments considered (Trémolet, 2005). Note that even for the transport of a passive tracer, like CO₂, the spatiotemporal discretization of the advection equation imposes non-linear models to preserve the stability of the transport and to avoid numerical diffusion (e.g. Hourdin and Armengaud, 1999). However, the use of a linear model in the inner loop makes the cost function quadratic and allows one to use efficient algorithms like the conjugate gradient methods, as is done here. Conjugate-gradient methods require fewer iterations to converge if the Hessian (matrix of second derivatives J'') of J has a lower condition number (e.g., Andersson et al., 2000). Preconditioning techniques reduce the condition number of J'' by an appropriate change of variable. The perfect preconditioner is the change to $\mathbf{z} = (J''_x)^{-1/2}\mathbf{x}$, because it makes all the eigenvalues of the preconditioned Hessian J''_z equal to one and reduces the minimization to a single iteration when using steepest descent or conjugate gradient methods. To draw near to this ideal case, Courtier et al. (1994) estimate J''_x based on a randomized estimate of the covariance matrix of J'_x (the derivative of J with respect to \mathbf{x}), while Fisher and Courtier (1995) use the Lanczos algorithm to obtain the leading eigenvectors of J''_x . In our case the preconditioning with respect to the prior only, as suggested by Lorenc (1988), was found more practical despite its lesser efficiency : $\mathbf{z} = \mathbf{B}^{-1/2}\mathbf{x}$ is our minimization control variable rather than \mathbf{x} . Note that this change of variable is also used at ECMWF in the first minimization.

The configuration that we have selected is a two-iteration outer loop. 10 iterations are

performed in the first inner-loop minimization and 40 in the second. This set-up was chosen empirically after several tests. It provides numerically-stable results at a reasonable computational cost.

Observations

The atmospheric CO₂ fields used to simulate OCO X_{CO₂} data in the present study have been calculated from a climatology of carbon fluxes \mathbf{x}_{clim} used as the boundary condition for LMDZ. \mathbf{x}_{clim} is considered to be the truth for the present theoretical study.

The climatology includes three components. First, fossil fuel CO₂ emissions are defined from the EDGAR 3.0 emission database (Olivier et al., 1996). Second, air-sea CO₂ exchange is prescribed from Takahashi et al. (2002) with a sink of 1.8 Gt C per year. Last, the biosphere-atmosphere exchange of CO₂ is estimated by the Terrestrial Uptake and Release of Carbon (TURC) model (Lafont et al., 2002), which is annually balanced. The daily fluxes calculated by TURC have been redistributed throughout the day to account for the diurnal cycle of the fluxes resulting from the photosynthetic activity (M. Heimann, personal communication, 2003). The CO₂ concentrations at the initial time step of the LMDZ simulation are defined from a former simulation using fluxes optimized through the inversion of monthly surface in situ observations (Bousquet et al., 2000).

OCO will fly in the A-Train with a 705 km sun-synchronous polar orbit that provides global sampling on a 16-day (233 orbits) repeat cycle with a 13 : 18 local standard time equator crossing (Crisp et al., 2004). In these simulations, we assume that OCO is in the glint observing mode, where the instrument boresight is pointed off nadir at the specular reflection point. This mode increases the measurement signal-to-noise over water bodies and provides useful data over both land and ocean. OCO will continuously collect 12 to 24 soundings per second as the satellite

moves from pole to pole at 6.8 km per second along its near-polar, sun-synchronous orbit track. It therefore collects 490 to 980 samples each time it traverses a $3.75^\circ \times 2.5^\circ$ (longitude-latitude) LMDZ grid cell, and each grid cell is traversed two or three times during each 16-day repeat cycle. The sounding foot print size varies from less than 3 square km when observing the local nadir, to greater than 25 square km at the most extreme viewing angles. Note that the OCO instrument also has a nadir sampling mode, which is believed to be more favourable over land, but less favourable over ocean. The sampling of both modes is rather similar. Simulated X_{CO_2} have been individually sampled along the OCO orbit track at the glint location. Since only X_{CO_2} retrievals in clear sky conditions provide direct constraints on the surface fluxes, these samples were filtered for clouds. The sampling accounts for a climatological cloud cover (Rossow et al., 1996) as well as for cloud cover spatial correlation statistics (Bréon et al., 2005).

The sampled X_{CO_2} have been perturbed with the specified observation error statistics R following :

$$\mathbf{y} = \mathbf{y}_{clim} + \mathbf{V}^T \mathbf{v}^{1/2} \mathbf{p} \quad (V.14)$$

with $\mathbf{y}_{clim} = H(\mathbf{x}_{clim})$ the simulated X_{CO_2} . V and v are the eigenvalue and eigenvector matrices of the principal component analysis of R , so that $R = V^T v V$. p is a vector of size the number of observations, which is a realization of random variables with standard normal distributions.

In Eq. V.13, the observation error is defined with respect to the transport model. Therefore it includes the measurement error, the representativeness error (caused by differences in temporal and spatial resolutions between the observations and the model) and the transport model error. The simulations presented by Crisp et al. (2004) indicated random measurement errors between 0.8 and 1.7 ppm for retrievals from individual OCO X_{CO_2}

soundings. Representativeness and model errors are difficult to quantify but are usually considered to be of the order of 1 ppm for most surface stations (Rödenbeck et al., 2003). For simplicity we have assumed the total observation error standard deviation to be 2 ppm for all of our data. Following the usual approximation, correlations between the errors of different retrievals is neglected so that Equation V.14 reduces to :

$$\mathbf{y} = \mathbf{y}_{clim} + \mathbf{p} \quad (V.15)$$

Prior Information

The prior information \mathbf{x}_b is also specified to be consistent with the above-described "true" fluxes \mathbf{x}_{clim} and with their specified error matrix B :

$$\mathbf{x} = \mathbf{x}_{clim} + \mathbf{W}^T \mathbf{w}^{1/2} \mathbf{q} \quad (V.16)$$

q is a vector of size the dimension of x_b , which is a realization of random variables with standard normal distributions. W and w are the eigenvalue and eigenvector matrices of the principal component analysis of B , so that $B = W^T w W$. The covariance matrix B is defined below.

The correlations of B are assigned from basic considerations about the origin of errors in the prior fluxes. Since the processes involved are different for land and for sea, the errors are supposed to be uncorrelated between these two geotypes. Chevallier et al. (manuscript submitted to Geophys. Res. Lett., 2006) suggested that current prior errors for vegetation fluxes have significant temporal autocorrelations (i.e. larger than 0.5) within about a fortnight. For the sake of simplicity, land and sea fluxes are defined here with an eight-day temporal resolution and with zero temporal correlations from one eight-day period to the next. Spatial correlations are specified as a function of distance as, e.g., in the study by Rödenbeck et al. (2003). Correlation e-folding lengths are set to 500 km over land, which implies error patterns of about

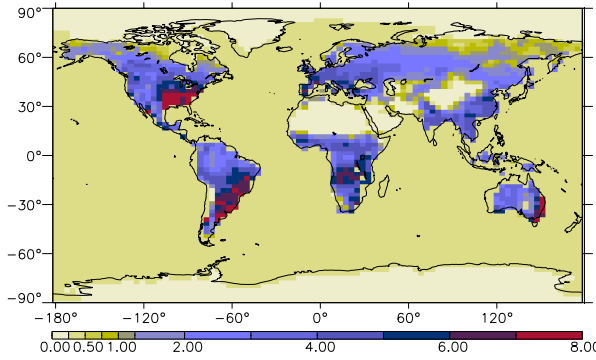


FIG. V.9 – Standard deviation of the prior errors, in gC.m^{-2} per day.

the size of France. This relatively small value is motivated by the large spatial variability of biospheric carbon fluxes that should tend to de-correlate errors. Spatial scales are larger over oceans and an e-folding length of 1000 km over the ocean was chosen. It specifies the size of coherent error patterns to be about that of the Bay of Bengal. Corresponding specified standard deviations of the flux errors globally correspond to 0.8 and 2.0 Gt C per year for ocean and land respectively and are spread in space proportionally to grid size over ocean and to the annual-mean heterotrophic respiration flux modelled by TURC over land. There is no seasonality in these errors. The resulting error standard deviations are shown in Fig. V.3.2. Standard deviations of the errors of the CO_2 concentrations at the initial time step of the LMDZ simulation are set to 1% in each grid box, with unity vertical correlations.

It is of interest to mention that the inversion of \mathbf{B} in Equation V.13 and its eigenvalue decomposition in V.16 are facilitated despite its large dimension because \mathbf{B} is block-diagonal (zero temporal correlations). Still, temporal correlations can be easily introduced as long as the matrix remains sparse, for instance using its principal components.

The Inversions

Five inversions have been performed. Each of them covers 12 months, using meteorological conditions valid for year 2003. They only differ from each other by the vectors of perturbations \mathbf{p} and \mathbf{q} (that have standard normal distribution, as explained in section V.3.2). The simulated OCO orbit and cloud cover give 243,689 independent observations at the horizontal resolution of the LMDZ transport model (the cloud screening removed 30% of the original data). By comparison, the dimension of the control vector is about 340,000 (i.e. twice-a-day grid-point fluxes every eight days during one year). OCO will actually provide hundreds of observations within a model grid box in most cases. However the existence of large correlations among the measurement errors and of the representativeness errors between these makes it difficult to assimilate them all individually. Therefore each one of the 243,689 observations may be considered either as an average value of the measurements along the corresponding portion of the satellite orbit, or as a sample of these. Depending on the actual value of the measurement error correlations within a model grid-box, this sub-sampling may underestimate the strength of the constraint available from the full OCO measurement dataset.

V.3.3 Results

A number of useful diagnostics about the inversion system are directly available as by-products of the inversions. This is particularly the case when the system satisfies consistency, such as ours, as ensured by V.14 and V.16. The diagnostics are detailed in the following.

Linearity of the Transport Model

The validity of the tangent-linear hypothesis used in the minimization can be evaluated in different ways (e.g. Janiskov et al., 2002). Here, the impact of non-linearities in the transport model can be simply noticed when studying the distribution of the variable $a = H(\mathbf{x}_b) - H(\mathbf{x}_{clim})$. From Equation V.16, a should be unbiased in the case of a linear operator since $\mathbf{W}^T \mathbf{w}^{1/2} \mathbf{q}$ is unbiased by definition (at least for large numbers of observations). This is actually only the case south of 50°N. Limiters of the tracer slopes in the advection scheme (Hourdin and Armengaud 1999), bias a by up to 0.8 ppm around the North Pole (not shown). Indeed they slightly slow down the poleward transport in the presence of the large surface gradients introduced by $\mathbf{W}^T \mathbf{w}^{1/2} \mathbf{q}$ between the vegetated areas of the Northern hemisphere and the polar cap, to preserve the monotonicity of the scheme.

The comparison between the reduction of the gradient of the quadratic cost function and the reduction of the real (non-linear) J' provides another evaluation of the tangent-linear hypothesis. In our case, the first ten iterations reduce the gradient of the quadratic J' by a factor between ten and twenty in the five inversions performed. The gradient reduction for the real J' is about the same. However, at the end of the second inner loop (see section V.3.2), significant differences are noticed between the two versions of the gradient. The quadratic J' is reduced by about a 20-fold factor when the real J' is reduced by a factor about 4 only. This feature justifies not adding

more iterations in the second inner loop, but a third inner loop may further reduce the discrepancy.

Condition Number of the Minimization

As discussed in section V.3.2, the rate of convergence of the minimization is largely determined by the condition number of J''_z . Further to our change of variable $\mathbf{z} = \mathbf{B}^{-1/2} \mathbf{x}$, the smallest eigenvalue of J''_z equals 1 and its condition number is its leading eigenvalue. As can be seen from Eq. V.13, J''_z does not depend on the values of the observations nor on the prior, but only on the spatiotemporal structure of their error statistics and the observation operator. Its leading eigenvalues are provided by the Lanczos algorithm as a by-product of the conjugate-gradient minimization (Fisher 1998). In our case, the condition number is about 41,600. By comparison, the condition number for the ECMWF weather analyses is about 3,000 when using the same conditioning as here (Andersson et al., 2000). Our very large condition numbers indicate that the observations are much more accurate than the prior or that the density of the observations is large compared to the surface flux error patterns (*ibid*). Both explanations may be valid for OCO.

Number of Iterations

The value of the cost function at the end of the minimization provides an interesting diagnostic of the convergence. Indeed, for a consistent system and given a realization of the observations \mathbf{y} , the cost function at the minimum $J(\mathbf{x}_a)$ is chi square distributed with expectation and variance equal to the number of observations N (e.g., Talagrand 1998, Mnard et al., 2000). Our idealized system is consistent by construction and $J(\mathbf{x})$ converges towards N indeed, starting from about 330,000 and reaching about 244,000, given about 243,689 observations. This result justifies non-pursuing the minimization after

our second inner loop.

Degrees of Freedom for Signal

The quantity $J_b(\mathbf{x}_a) = (\mathbf{x}_a - \mathbf{x}_b)^T B^{-1} (\mathbf{x}_a - \mathbf{x}_b)$ which is used for the computation of $J(\mathbf{x}_a)$ reflects the number of degrees of freedom for signal (DFS, e.g., Rodgers 2000). The DFS describes the number of independent pieces of information that the observations provide, given the prior information. $J_b(\mathbf{x}_a)$ is actually a small fraction of $J(\mathbf{x}_a)$ in our case. Even though the latter is rather stable after the second inner loop minimization, the former still increases from one iteration to the next and its value should be considered as a lower bound. We get numbers about 6000, which indicates that more than 6000 independent quantities about the fluxes can be measured from a year of OCO data. Unsurprisingly, the 244,000 OCO X_{CO_2} measurements yield significantly more surface flux information than the 347,000 TOVS measurements studied by Chevallier et al. (2005b) that were less accurate and restricted to the tropical upper troposphere (they had 340 DFS).

Error Reduction

The statistical characteristics of the analysis error are another very useful quantity. They will be one of the key metrics to evaluate the usefulness of the X_{CO_2} data product. Given unbiased Gaussian error statistics for the observations and the prior, and a linear transport model, the analysis errors are also unbiased and Gaussian, and can be fully described by a covariance matrix A . A can be written in various analytical forms (e.g., Rodgers, 2000). They are exact as long as the error statistics of the observations and of the prior are correctly described. All of these expressions require the inversion of matrices that are too large to be feasible for the current study. Instead of using these given exact expressions, we take advantage here of the fact that the statistics of the analysis errors are the sta-

tistics of the differences between \mathbf{x}_a and our truth \mathbf{x}_{clim} . Such an a posteriori estimation is all the more reliable since the statistical sample is large. The high computational cost of an inversion prevents the accumulation of many inversion results, but each one-year inversion inherently contains 45 global maps of 8-day fluxes. The five inversions thus generate an ensemble of 225 maps that allow us to estimate the annual-mean variance of the analysis errors of the eight-day fluxes. Note that temporal correlations are absent in our prior errors and in our observation errors, but are induced in the analysis by the atmospheric transport. Therefore the number of truly independent realizations of the eight-day fluxes is smaller. To estimate the errors on the monthly fluxes, 60 realizations are available.

The existence of spatial and temporal correlations in the analyzed flux increments makes the error reduction scale-dependent. Positive correlations between the errors of the individual fluxes (i.e. large increments in space or time) tend to increase the errors of the aggregated fluxes. Negative correlations (i.e. dipoles) have the opposite effect. Figure V.3.3 displays the global map of the estimated uncertainty reduction achieved by the analysis for eight-day fluxes and monthly fluxes. In both cases, daytime and night-time fluxes have been aggregated together. By definition, these error reductions are relative to our prior errors (section V.3.2) and would vary with other error characteristics. The map for eight-day (respectively monthly) fluxes displays error reduction of 0-15% (respectively 0-25%) for fluxes over oceans and over boreal forests, and of about 15-45% (respectively 20-50%) over other vegetated areas. The patterns are robust with respect to the individual realizations. For instance, using any two years only, out of the five available, gives the same patterns. Over land, they rather reproduce the patterns of the background errors (Fig. V.3.2), with larger reductions where the prior errors are larger, i.e. over the vegetated areas, and

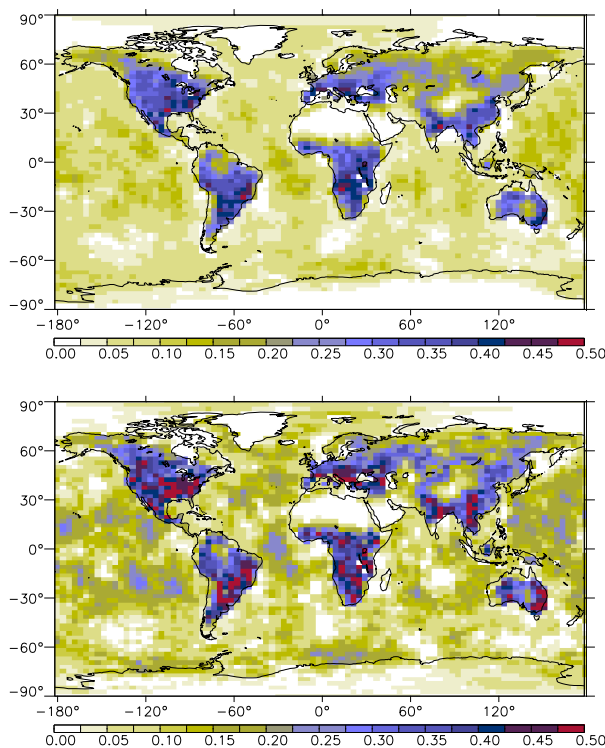


FIG. V.10 – Fractional error reduction of the eight-day mean (top) and of the monthly mean (bottom) grid point CO₂ surface fluxes. The error reduction is defined as $(1 - \sigma_a/\sigma_b)$, with σ_a the posterior error standard deviation and σ_b the prior error standard deviation.

smaller reductions where the prior errors are negligible, i.e. over the polar caps and over the deserts. Over the oceans, where our background errors are the same everywhere, the reduction patterns are driven by the meteorology and by the observation location, which are the same in the five simulations. The error reduction is smaller when separating day-time and night-time fluxes (not shown). This feature shows the existence of large negative correlations between the two types of fluxes, or, in other words, confirms the ambiguity of X_{CO_2} information with respect to surface fluxes at sub-daily timescales.

The impact of spatial aggregation is illustrated by aggregating the fluxes within the 11 land and 11 ocean regions defined in phase 3 of the Atmospheric Tracer Transport Model Intercomparison Project (TransCom3, Gurney et al., 2002). Together with the ice caps (23rd region with negligible fluxes and uncertainties), they cover the globe entirely. Figure V.3.3 presents the fractional change in flux uncertainty for the 22 regions. It emphasises the better constraint of the monthly fluxes vs. the eight-day ones, in particular over oceans. One may also notice that the TransCom3-scale error reduction is larger than at the grid point scale, in particular over land where the reduction rises to 50-80%. Indeed the ambiguity of the X_{CO_2} information with respect to the spatial location of the fluxes translates into negative spatial error correlations in the analysed fluxes, attenuated by our specified error correlation lengths (smaller over land than over oceans, section V.3.3).

Tolerance to Observational Biases

The error reduction estimated in the previous section is strictly theoretical. In practice, inadequate specifications of the error statistics introduce inconsistencies and prevent the inversions from converging on optimal fluxes. The detrimental impact of undetected regional biases in the observations has been underlined in several studies (e.g.,

Rayner et al., 2002, Patra et al., 2003). Chevallier et al. (2005a) quantified the tolerance of the inversion systems based on the statistics of the observation-minus-prior departures $d = y - Hx_b$. They indicate that biases larger than about one tenth of the variation of the departures are likely to degrade the quality of the analysis increments. The upper part of Figure V.3.3 shows the departure statistics in our simulations. Based on the former criterion, a few tenths of a ppm bias would be enough to affect the inversions to some extent, in particular over sea. We checked this property by introducing known biases in our simulated observations. There are several potential sources of biases in the satellite estimate of X_{CO_2} , each with a particular spatial and temporal pattern. As an example, we focus here on the potential impact of sub-micron aerosol particles, the optical thickness of which has a strong and variable spectral signature, which could be a source of error (O'Brien and Rayner 2002). These aerosols are mostly generated by anthropogenic activities and biomass burning. For the present experiment, we used 3D aerosol concentrations derived from the assimilation of satellite retrievals of aerosol optical depths into an atmospheric transport model (Generoso et al, 2007). For this exercise, we assume a bias (in ppm) in the OCO retrievals as five times the sub-micronic aerosol 850 nm optical thickness (unitless). The bias is defined so that it increases the observation value. The global average bias is 0.29 ppm while the 90th percentile is 0.49 ppm. With this choice, the bias is, on average, one order of magnitude smaller than the departure standard deviation (see Fig. V.3.3, bottom). Some regions show a more significant bias however, in particular downwind of China, North America and Europe. Regions of biomass burning (Sahel, South Africa, South and Central America) also show significant biases, but only during the corresponding season so that the impact on the annual mean is small. The large

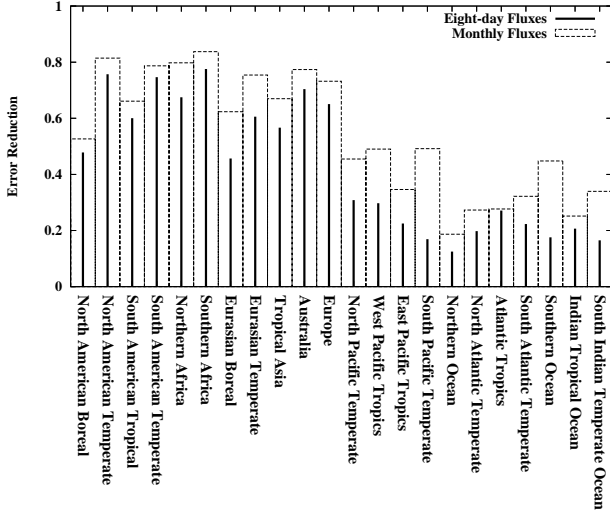


FIG. V.11 – Fractional error reduction of the CO₂ surface fluxes over the 22 TransCom-3 regions. Results for monthly as for eight-day fluxes are shown. As in Fig. V.3.3, the error reduction is defined as $(1 - \sigma_a/\sigma_b)$, with σ_a the posterior error standard deviation and σ_b the prior error standard deviation.

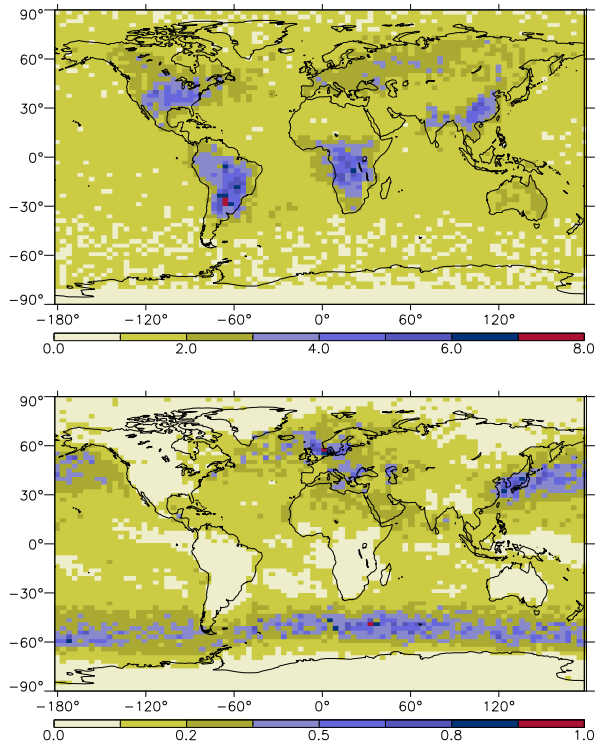


FIG. V.12 – The top figure shows the standard deviation (in ppm) of the observation-minus-prior departure. The bottom figure displays the ratio of the annual-mean bias introduced in the inversions to this standard deviation.

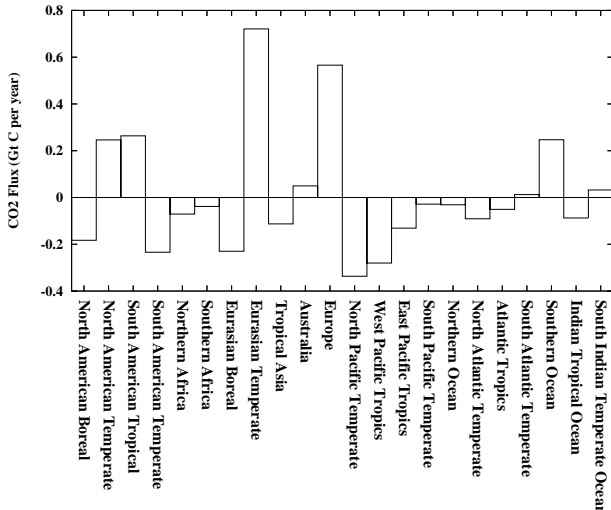


FIG. V.13 – Flux bias (in Gt C per yr) induced by the OCO bias of Fig. V.3.3 in each one of the 22 TransCom-3 regions.

values around 50S are the result of both marine aerosol load and small departure standard deviations.

The impact of the biases on the inversion is illustrated by the resulting bias in the annual carbon budget in each one of the 22 TransCom3 regions. As expected, significant biases occur in Europe (0.6 Gt C per yr), in temperate Eurasia (0.7 Gt C per yr), in Northern and Southern temperate America (0.25 Gt C per yr in both cases). Over the oceans, a 0.2 Gt C per yr bias is seen in the Southern ocean. Interestingly, the inversion system generates negative flux biases to conserve CO₂ mass between the areas where the observations are biased and the ones located downstream. For instance, the boreal Eurasian region, downstream of Europe, is biased by about -0.2 Gt C per yr. By comparison, the analysis error standard deviation for monthly fluxes is between 0.1 and 0.2 GtC per year in each region and the prior one between 0.1 and 0.7 Gt C per yr (not shown). The biased analysis has still smaller root mean square errors (RMSE) than the prior in all land regions, but Europe and temperate Eurasia. Owing to the small prior errors over ocean, the observation bias

cancels any RMSE improvement in these two regions.

V.3.4 Discussion and Conclusions

The variational formulation of Bayesian estimation plays an increasingly important role for the analysis of large numbers of observations, as is the case for satellite data. It circumvents the difficulty of inverting a large and possibly dense matrix in the search for the minimum variance solution. Unfortunately, unlike the formulation by a suite of matrix operations, the characterization of the uncertainty of this solution remains a challenge, which affects the conditioning of the minimization and hampers the computation of useful diagnostics, like the number of degrees of freedom for signal or the observation influence matrix. A few strategies have been proposed to estimate some quantities related to the analysis error covariance matrix, based on randomization (Rabier and Courtier, 1992; Fisher, 2003; Desroziers et al., 2005) or on reduced rank decomposition (Fisher and Courtier, 1995). More directly, the influence of observations on an assimilation system is also studied by comparison to independent

observations or with observing system simulation experiments (OSSE). For OSSEs, the truth is usually defined from another model, which is likely to be inconsistent with the specified prior errors. Our study combines an OSSE framework with a randomization approach to build OCO observations and prior fluxes that are perfectly consistent with their specified error statistics. This method relies on the availability of sufficiently-accurate reduced-rank eigenvector decompositions of the prior and of the observation errors. This is straight-forward for the observation error covariance matrix which is usually diagonal. The prior error covariance matrix is usually built in such a way that it has both realistic features and convenient mathematical properties (e.g., Derber and Bouttier, 1999), so that its eigenvalue decomposition may also be available despite its large dimension, as is the case here. Our approach allows one to directly estimate mean analysis error variances and the number of degrees of freedom for signal as by-products of the inversion. It also helps to choose the number of iterations of the minimization procedure. These possibilities may motivate the design of such OSSEs for both existing and future instruments. Additional benefit may be found for the minimization preconditioning, but this remains a topic for future work.

Our method has been applied to the estimation of the impact of the forthcoming OCO observations on the analysis of CO₂ surface fluxes. Other CO₂ observations could be usefully studied in a similar way (e.g., those from NASA's Atmospheric Infra-Red Sounder or those from the forthcoming Greenhouse Gases Observing Satellite planned by the Japan Aerospace Agency). Given our assigned error statistics for the prior fluxes and the observations, we show significant error reduction even at the weekly time scale and at the grid point resolution over land (15-45% over vegetated areas). The reduction over oceans becomes significant (20-40%)

only when aggregating at the oceanic-basin monthly scales. These results are consistent with the results from previous low-resolution studies. They are based on a series of reasonable assumptions about the error statistics, the importance of which needs to be stressed. The error statistics are assumed to be unbiased, Gaussian, uncorrelated for the observations, uncorrelated in time and correlated with an e-folding distance by geotype in space. Therefore our study should be considered as a best-case estimate and careful examination of each one of these hypotheses will be essential for optimal use of the OCO data. The existence of regional biases, or equivalently of strong spatial correlations, linked to scattering by clouds and aerosols, is of particular concern. We show that the failure to limit the regional biases to within a few tenths of a ppm would have a detrimental impact on the flux estimation. Therefore the usefulness of OCO observations for the study of the carbon cycle will depend on the quality control of the data. The assimilation of OCO observations in concert with another instrument would reduce the impact of the biases provided the biases of the two observing systems do not share the same space-time characteristics. A similar issue could be raised about the biases of the transport models that are used to link the atmospheric measurements to the boundary fluxes. It is important to stress that the exploitation of the surface network for flux inversion faces the same challenges. Other issues that still need to be addressed are the contributions of fossil fuel emissions and biomass-burning, whose distinct features are not studied here, i.e. a large spatiotemporal variability and an injection height possibly well above the surface.

In our reference case estimate, the uncertainty in the monthly carbon budget over Europe is reduced by 70%, leaving a residual uncertainty of about 0.16 Gt C per year (annual total). By comparison, the 2003 European summer drought induced an ano-

maly of about 0.5 Gt C (Ciais et al., 2005), so that such large climate induced anomaly should be detected by an observation system like OCO plus a suitable assimilation system. However it is very unlikely that a single CO₂-sensitive satellite instrument, like OCO, will be sufficient to address scientific questions about smaller signals (like the compliance to international treaties) or smaller scales (like the quantification of the role of peatlands raised by Sotocornola and Kiely, 2005). For instance, European fossil emissions are less than 1 Gt C per yr, while the reduction objective of the Kyoto protocol (see <http://unfccc.int/>) are of a few percent averaged on a five year period. The verification of European compliance with the Kyoto protocol therefore requires an accuracy of the order of 1 percent of current emissions, or 0.01 Gt C per yr. Our results indicate that such accuracy is not feasible with an OCO-like instrument alone. Following the example of numerical weather prediction, a multi-instrument strategy is desirable to build robust carbon cycle data assimilation systems.

Acknowledgments. Authors wish to thank M. Fisher (ECMWF), P. Peylin, P. Ciais (LSCE) and A.S. Denning (LSCE/CSU) for fruitful interactions, F. Delage (LSCE) for kind help with the plots, and F. Marabelle (LSCE) for computer support. D. Crisp, C. Miller (JPL), R. Engelen and A. Hollingsworth (ECMWF) provided useful comments on an earlier version of this article. Some of the computations were performed at the Centre de Calcul Recherche et Technologie (CCRT). The study was co-funded by the European Union under the project GEMS.

References

- Andersson, E., M. Fisher, R. Munro, A. McNally (2000), Diagnosis of background errors for radiances and other observable quantities in a variational data assimilation scheme, and the explanation of a case of poor convergence. Quart. J. Roy. Meteor. Soc., 126, 1455-1472.
- Baker, D. F., S. C. Doney, and D. S. Schimel (2006), Variational data assimilation for atmospheric CO₂. Tellus B, 58, 359-365.
- Bousquet, P., P. Peylin, P. Ciais, C. Quere, P. Friedlingstein, and P. Tans (2000), Regional changes in carbon dioxide fluxes of land and oceans since 1980, Science, 290, 1342-1346.
- Bréon, F. M., D. M. O'Brien and J. D. Spinhirne (2005), Scattering layer statistics from space borne GLAS observations. Geophys. Res. Lett., 32, doi :10.1029/2005GL023825.
- Chevallier, F., R. J. Engelen, and P. Peylin, 2005a : The contribution of AIRS data to the estimation of CO₂ sources and sinks. Geophys. Res. Lett., 32, L23801, doi :10.1029/2005GL024229.
- Chevallier, F., M. Fisher, P. Peylin, S. Serrar, P. Bousquet, F.-M. Bréon, A. Chédin, et P. Ciais, 2005b : Inferring CO₂ sources and sinks from satellite observations : method and application to TOVS data. J. Geophys. Res., 110, D24309, doi :10.1029/2005JD006390.
- Chevallier, F., N. Viovy, M. Reichstein, and P. Ciais (2006), On the assignment of prior errors in Bayesian inversions of CO₂ surface fluxes, Geophys. Res. Lett., 33, L13802, doi :10.1029/2006GL026496.
- Ciais, P., M. Reichstein, N. Viovy, A. Granier, J. Oge, V. Allard, M. Aubinet, N. Buchmann, C. Bernhofer, A. Carrara, F. Chevallier, N. De Noblet, A. D. Friend, P. Friedlingstein, T. Grnwald, B. Heinesch, P. Keronen, A. Knohl, G. Krinner, D. Loustau, G. Manca, G. Matteucci, F. Miglietta, J. M. Ourcival, D. Papale, K. Pi legaard, S. Rambal, G. Seufert, J. F. Sous-sana, M. J. Sanz, E. D. Schulze, T. Vesala, and R. Valentini (2005), Europe-wide reduction in primary productivity caused by the heat and drought in 2003, Nature, 437, 529-533.

- Courtier, P., J.-N. Thepaut, and A. Hollingworth (1994), A strategy for operational implementation of 4D-Var using an incremental approach. *Quart. J. Roy. Meteor. Soc.*, 120, 1367-1387.
- Crisp, D., R.M. Atlas, F.-M. Bréon, L.R. Brown, J.P. Burrows, P. Ciais, B.J. Connor, S.C. Donley, I.Y. Fung, D.J. Jacob, C.E. Miller, D. O'Brien, S. Pawson, J.T. Randerson, P. Rayner, R.J. Salawitch, S.P. Sander, B. Sen, G.L. Stephens, P.P. Tans, G.C. Toon, P.O. Wennberg, S.C. Wofsy, Y.L. Yung, Z. Kuang, B. Chudasama, G. Sprague, B. Weiss, R. Pollock, D. Kenyon, and S. Schroll (2004) .The Orbiting Carbon Observatory (OCO) Mission, *Advances in Space Research*, 34(4), 700-709.
- Derber, J. C. and F. Bouttier (1999), A reformulation of the background error covariance in the ECMWF global data assimilation system. *Tellus*, 51A, 195-221.
- Desroziers, G., P. Brousseau, B. Chapnik (2005), Use of randomization to diagnose the impact of observations on analyses and forecasts, *Quart. J. Roy. Meteor. Soc.*, 131, 2821-2837.
- Enting, I.G., C.M. Trudinger and R.J. Francey (1995), A synthesis inversion of the concentration and $\delta^{13}\text{C}$ atmospheric CO₂. *Tellus*, 47B, 35-52.
- Enting, I.G. (2002), *Inverse Problems in Atmospheric Constituent Transport*, Cambridge University Press.
- Fisher, M. (1998), Minimization algorithms for variational data assimilation, Seminar on Recent Developments in Numerical Methods for Atmospheric Modelling, 7-11 September 1998 [available from the librarian, ECMWF, Shinfield Park, Reading RG2 9AX, UK], 364-385.
- Fisher, M. (2003), Estimation of entropy reduction and degrees of freedom for signal for large variational analysis systems, *ECMWF Tech. Memo.* 397.
- Fisher, M., and P. Courtier (1995), Estimating the covariance matrices of analysis and forecast error in variational data assimilation, *ECMWF Tech. Memo.* 220.
- Generoso, S., F.-M. Bréon, F. Chevallier, Y. Balkanski, M. Schulz, and I. Bey (2007), Assimilation of POLDER aerosol optical thickness into the LMDz-INCA model : Implications for the Arctic aerosol burden, *J. Geophys. Res.*, 112, D02311, doi :10.1029/2005JD006954.
- Gurney, K. R., R. M. Law, A. S. Denning, P. J. Rayner, D. Baker, P. Bousquet, L. Bruhwiler, Y. H. Chen, P. Ciais, S. Fan, I. Fung, M. Gloor, M. Heimann, K. Higuchi, J. John, T. Maki, S. Maksyutov, K. Masarie, P. Peylin, M. Prather, B. C. Pak, J. Randerson, J. Sarmiento, J., S. Taguchi, T. Takahashi, and C. W. Yuen (2002), Towards robust regional estimates of CO₂ sources and sinks using atmospheric transport models, *Nature*, 415 :6872, 626-630.
- Hourdin, F., and A. Armengaud (1999), Test of a hierarchy of finite-volume schemes for transport of trace species in an atmospheric general circulation model. *Mon. Wea. Rev.*, 127, 822-837.
- Houweling, S., F.-M. Bréon, I. Aben, C. Rödenbeck, M. Gloor, M. Heimann, and P. Ciais (2004), Inverse modeling of CO₂ sources and sinks using satellite data : a synthetic inter-comparison of measurement techniques and their performance as a function of space and time. *Atmos. Chem. Phys.*, 4, 523-538.
- Houweling, S., W. Hartmann, I. Aben, H. Schrijver, J. Skidmore, G.-J. Roelofs, and F.-M. Bréon (2005), Evidence of systematic errors in SCIAMACHY-observed CO₂ due to aerosols. *Atmos. Chem. Phys.*, 5, 3003-3013.
- Ide, K., P. Courtier, M. Ghil and A. C. Lorenc (1997), Unified notation for data assimilation : operational, sequential and variational. *J. Meteor. Soc. Japan*, 75, 181-189.
- Intergovernmental Panel on Climate Change (2001), *Climate Change 2001 : The Scientific Basis*, 881 pp., Cambridge Univ. Press, New York.
- Janisková, M., J.-F. Mahfouf, J.-J. Morcrette, and F. Chevallier (2002), Linearized radiation and cloud schemes in the ECMWF model : development and evaluation. *Quart. J. Roy. Meteor. Soc.*, 128, 1505-1528.
- Lafont, S., L. Kergoat, G. Dedieu, A. Chevillard, E. Kjellström, U. Karstens, and O. Kolle (2002), Spatial and temporal variability of land CO₂ fluxes estimated with remote sensing and analysis data over western Eurasia, *Tellus*, 54B, 820-833.
- Lorenc, A.C. (1988), Optimal nonlinear objective analysis. *Quart. J. Roy. Meteor. Soc.*, 114, 2052-240.

- Mnard, R., S.E. Cohn, L.-P., Chang, L. Lang-Ping, P.M. Lyster (2000), Assimilation of Stratospheric Chemical Tracer Observations Using a Kalman Filter. Part I : Formulation, *Mon. Wea. Rev.*, 128, 2654-2671.
- O'Brien, D.M., and P.J. Rayner (2002), Global observations of the carbon budget, 2, CO₂ column from differential absorption of reflected sunlight in the 1.61 m band of CO₂. *J. Geophys. Res.*, 107(D18), 4354, doi :10.1029/2001JD000617.
- Olivier, J. G. J., A. F. Bouwman, C. W. M. Van der Maas, J. J. M. Berdowski, C. Veldt, J. P. J. Bloos, A. J. H. Visschedijk, P. Y. J. Zandyelt, and J. L. Haverlag (1996), Description of EDGAR Version 2.0. A set of global emission inventories of greenhouse gases and ozone-depleting substances for all anthropogenic and most natural sources on a per country basis and on 1x1 grid, RIVM/TNO report, December 1996. RIVM, Bilthoven, RIVM report nr. 771060 002. [TNO MEP report nr. R96/119].
- Pak, B.C., and M.J. Prather (2001), CO₂ source inversions using satellite observations of the upper troposphere, *Geophys. Res. Lett.*, 28, 4571-4574.
- Patra, P. K., S. Maksyutov, Y. Sasano, H. Nakajima, G. Inoue, and T. Nakazawa (2003), An evaluation of CO₂ observations with Solar Occultation FTS for Inclined-Orbit Satellite sensor for surface source inversion, *J. Geophys. Res.*, 108(D24), 4759, doi :10.1029/2003JD003661.
- Rabier, F., and P. Courtier (1992), Four-dimensional assimilation in the presence of baroclinic instability. *Q. J. R. Meteorol. Soc.*, 118, 649-672.
- Rayner, P. J., and D. M. O'Brien (2001), The utility of remotely sensed CO₂ concentration data in surface source inversions, *Geophys. Res. Lett.*, 28, 175-178.
- Rayner, P. J., R. M. Law, D. M. O'Brien, T. M. Butler, and A. C. Dilley (2002), Global observations of the carbon budget 3. Initial assessment of the impact of satellite orbit, scan geometry, and cloud on measuring CO₂ from space, *J. Geophys. Res.*, 107(D21), 4557, doi :10.1029/2001JD000618.
- Rödenbeck, C., S. Houweling, M. Gloor, and M. Heimann (2003), CO₂ flux history 1982-2001 inferred from atmospheric data using a global inversion of atmospheric transport. *Atmos. Chem. Phys.*, 3, 1919-1964.
- Rödenbeck, C. (2005), Estimating CO₂ sources and sinks from atmospheric mixing ratio measurements using a global inverse of atmospheric transport. Technical Reports, Max-Planck-Institut für Biogeochemie 6.
- Rodgers, C. D. (2000) : Inverse methods for atmospheric sounding : theory and practice, World Scientific, 238 pp.
- Rossow, W.B., A.W. Walker, D.E. Beuschel, and M.D. Roiter (1996), International Satellite Cloud Climatology Project (ISCCP) Documentation of New Cloud Datasets. WMO/TD-No. 737, World Meteorological Organization, 115 pp.
- Sadourny, R., and K. Laval (1984), January and July performance of the LMD general circulation model, In *New Perspectives in Climate Modeling*, A.L. Bergerand C. Nicolis (eds.), Elsevier Press, Amsterdam, 173-197.
- Sottocornola, M., and G. Kiely (2005), An Atlantic blanket bog is a modest CO₂ sink, *Geophys. Res. Lett.*, 32, L23804, doi :10.1029/2005GL024731.
- Takahashi, T., S. C. Sutherland, C. Sweeney, A. Poisson, N. Metzl, B. Tilbrook, N. Bates, R. Wanninkhof, R. A. Feely, C. Sabine, J. Olafsson and Y. Nojiri (2002), Global Sea-Air CO₂ Flux Based on Climatological Surface Ocean pCO₂, and Seasonal Biological and Temperature Effect, *Deep Sea Res. II*, 49, 1601-1622.
- Talagrand, O. (1998), A posteriori evaluation and verification of analysis and assimilation algorithms, Proceedings of the Workshop on Diagnosis of Data Assimilation Systems, 2-4 Nov 1998, European Centre for Medium-Range Weather Forecasts, Reading, UK, 17-28.
- Trémolet, Y. (2005), Diagnostics of linear and incremental approximations in 4D-Var, *Quart. J. Roy. Meteor. Soc.*, 130, 2233-2251.

Annexe A

Bibliographie

Les références citées dans les articles reproduits plus haut sont détaillées séparément à la fin de chaque article. La bibliographie complète de l'auteur est donnée en annexe C.

- Baker, D. F., S. C. Doney et D. S. Schimel (2006), Variational data assimilation for atmospheric CO₂, *Tellus*, 58B, 359-365.
- Bauer, P., P. Lopez, D. Salmond, A. Benedetti, S. Saarinen et M. Bonazzola (2006a), Implementation of 1D+4D-Var assimilation of precipitation affected microwave radiances at ECMWF, Part II : 4D-Var, *Q. J. Roy. Met. Soc.*, 132, 2307-2332.
- Bauer, P., E. Moreau, F. Chevallier et U. O'Keeffe (2006b), Multiple-scattering microwave radiative transfer for data assimilation applications, *Q. J. Roy. Met. Soc.*, 132, 1259-1281.
- Bayes, T. (1763), An essay towards solving the doctrine of chances, *Philosophical Transactions of the Royal Society of London*, 53, 370-418.
- Bellhouse, D. (2002), On some recently discovered manuscripts of Thomas Bayes, *Historia Mathematica*, 29, 383-394.
- Bjerknes, V. (1904), Das Problem der Wettervorhersage, betrachtet vom Standpunkte der Mechanik und der Physik, *Meteor. Z.*, 21, 1-7.
- Bocquet, M. (2005), Reconstruction of an atmospheric tracer source using the principle of maximum entropy. II : Applications, *Q. J. Roy. Met. Soc.*, 131, 2209-2224.
- Burlaud, C., G. Deblonde et J.-F. Mahfouf (2007), Simulation of satellite passive microwave observations in rainy atmospheres at the Meteorological Service of Canada, *IEEE Trans. on Geoscience and Remote Sensing*, 45, 2276-2286.
- Chevallier, F. (2007), Impact of correlated observation errors on inverted CO₂ surface fluxes from OCO measurements, *Geophys. Res. Lett.*, 34, L24804, doi :10.1029/2007GL030463.
- Chevallier, F., F. Chéry, N. A. Scott, et A. Chédin (1998), A neural network approach for a fast and accurate computation of a longwave radiative budget. *J. Appl. Meteor.*, 37, 1385-1397.
- Chevallier, F., J.-J Morcrette, F. Chéry et N. A. Scott (2000), Use of a neural network-based longwave radiative transfer scheme in the ECMWF atmospheric model, *Q. J. R. Meteor. Soc.*, 126, 761-776.
- Chevallier, F., P. Bauer, G. Kelly, C. Jakob, et A. P. McNally (2001), Model clouds over oceans as seen from space : comparison with HIRS/2 and MSU radiances. *J. Climate*, 14, 4216-4229.
- Chevallier, F., et J.-F. Mahfouf (2001), Evaluation of the Jacobians of infrared radiation models for variational data assimilation, *J. Appl. Meteor.*, 40, 1445-1461.

- Chevallier, F., P. Bauer, J.-F. Mahfouf et J.-J. Morcrette (2002), Variational retrieval of cloud profile from ATOVS observations, *Q. J. R. Meteor. Soc.*, 128, 2511-2526.
- Chevallier, F., et G. Kelly (2002), Model clouds as seen from space : comparison with geostationary imagery in the $11\mu\text{m}$ window channel. *Mon. Wea. Rev.*, 130, 712-722.
- Chevallier, F. et P. Bauer (2003), Model rain and clouds over oceans : comparison with SSM/I observations, *Mon. Wea. Rev.*, 131, 1240-1255.
- Chevallier, F., P. Lopez, A. M. Tompkins, M. Janisková et E. Moreau (2004), The capability of 4D-Var systems to assimilate cloud-affected satellite infrared radiances, *Q. J. R. Meteor. Soc.*, 130, 917-932.
- Chevallier, F., R. J. Engelen et P. Peylin (2005a), The contribution of AIRS data to the estimation of CO₂ sources and sinks, *Geophys. Res. Lett.*, 32, L23801, doi :10.1029/2005GL024229.
- Chevallier, F., M. Fisher, P. Peylin, S. Serrar, P. Bousquet, F.-M. Bréon, A. Chédin et P. Ciais (2005b), Inferring CO₂ sources and sinks from satellite observations : method and application to TOVS data, *J. Geophys. Res.*, 110, D24309, doi :10.1029/2005JD006390.
- Chevallier, F., G. Kelly, A. J. Simmons, S. Uppala, et A. Hernandez (2005c), High clouds over oceans in the ECMWF 15-year and 45-year re-analyses. *J. Climate*, 18, 2647-2661.
- Chevallier, F., N. Viovy, M. Reichstein et P. Ciais (2006), On the assignment of prior errors in Bayesian inversions of CO₂ surface fluxes, *Geophys. Res. Lett.*, 33, L13802, doi :10.1029/2006GL026496.
- Chevallier, F., F.-M. Bréon et P. J. Rayner (2007), The contribution of the Orbiting Carbon Observatory to the estimation of CO₂ sources and sinks : theoretical study in a variational data assimilation framework, *J. Geophys. Res.*, 112, D09307, doi :10.1029/2006JD007375.
- Coumet, E. (1970), La Théorie du Hasard est-elle ne par hasard ?, *Annales Économies Sociétés Civilisations*, 3, 574-598.
- Cournot, A.-A. (1843), *Exposition de la théorie des chances et de la probabilités*, Hachette, Paris.
- Daston, L. J. (1988), *Classical probability in the Enlightenment*, Princeton University Press.
- Dercourt, J. (2004), *Les flux d'étudiants susceptibles d'accéder aux carrières de recherche, l'exemple de l'Ile-de-France dans le cadre national*, Rapport à l'Académie des sciences, http://www.academie-sciences.fr/publications/rapports/rapports.html/rapport_JD0604.htm
- Diu, B. et B. Leclerc (2005), *La physique mot à mot*, Odile Jacob.
- Dubovik, O., T. Lapyonok, Y. J. Kaufman, M. Chin, P. Ginoux, R. A. Kahn et A. Sinyuk (2008), Retrieving global aerosol sources from satellites using inverse modeling, *Atmos. Chem. Phys.*, 8, 209-250.
- Einstein, A., B. Podolsky et N. Rosen (1935), Can quantum-mechanical description of physical reality be considered complete? *Phys. Rev.*, 47, 777-780.
- Emmons, L. K., et coll. (2004), Validation of Measurements of Pollution in the Troposphere (MOPITT) CO retrievals with aircraft in situ profiles, *J. Geophys. Res.*, 109, D03309, doi :10.1029/2003JD004101
- English, S. J., J. R. Eyre et J. A. Smith (1999), A cloud-detection scheme for use with satellite sounding radiances in the context of data assimilation for numerical weather prediction, *Q. J. R. Meteor. Soc.*, 125, 2359-2378.
- Enting, I. G., C. M. Trudinger et R. J. Francey (1995), A synthesis inversion of the concentration and δC^{13} of atmospheric CO₂, *Tellus*, 47B, 35-52.
- de Finetti, B. (1937), La prévision : ses lois logiques, ses sources subjectives. *Annales de l'I.H.P.*, 7, 1-68.

- Fienberg, S. E. (2006), When did Bayesian inference become "Bayesian"? *Bayesian Analysis*, 1, 1-40.
- Fisher, M., M. Leutbecher et G. A. Kelly (2006), On the equivalence between Kalman smoothing and weak-constraint four-dimensional variational data assimilation, *Q. J. R. Meteor. Soc.*, 131, 3235-3246.
- Fisher, M. et E. Andersson (2001) : Developments in 4D-Var and Kalman filtering. *ECMWF Technical Memorandum*, 347, 38 p.
- Fisher, M. et D. J. Lary (1995), Lagrangian four-dimensional variational data assimilation of chemical species *Q. J. R. Meteor. Soc.*, 121, 1681-1704.
- Gauss, C. F. (1809), *Theoria motus corporum coelestium in sectionibus conicis solum ambientium*, Perthes and Besser, Hamburg.
- Hacking, I. (1975), *The emergence of probability*, Cambridge University Press.
- Hegerl, G.C., F. W. Zwiers, P. Braconnot, N.P. Gillett, Y. Luo, J.A. Marengo Orsini, N. Nicholls, J.E. Penner et P.A. Stott (2007), Understanding and Attributing Climate Change. In : Climate Change 2007 : The Physical Science Basis. Contribution of Working Group I to the Fourth Assessment Report of the Intergovernmental Panel on Climate Change [Solomon, S., D. Qin, M. Manning, Z. Chen, M. Marquis, K.B. Averyt, M. Tignor and H.L. Miller (eds.)]. Cambridge University Press, Cambridge, United Kingdom and New York, NY, USA.
- IPCC (2005), *Guidance Notes for Lead Authors of the IPCC Fourth Assessment Report on Addressing Uncertainties*. IPCC, Genève. <http://www.ipcc.ch/pdf/supporting-material/uncertainty-guidance-note.pdf>
- Hadot, P. (2004), *Le voile d'Isis*, Gallimard.
- Hahn, R. (2004), *Le système du monde - Pierre Simon Laplace, un itinéraire dans la science*, Gallimard.
- Haimberger, L. (2005), Homogenization of radiosonde temperature time series using ERA-40 analysis feedback information. *ERA-40 Project Report Series*, 23, 68 p.
- Hakami, A., D. K. Henze, J. H. Seinfeld, T. Chai, Y. Tang, G. R. Carmichael et A. Sandu (2005), Adjoint inverse modeling of black carbon during the Asian Pacific Regional Characterization Experiment, *J. Geophys. Res.*, 110, doi :10.1029/2004JD005671.
- Hald, A. (1990), *A history of probability and statistics and their applications before 1750*, Wiley, New York.
- Ho, Y. C. et Lee, R. C. K. (1964), A Bayesian approach to problems in stochastic estimation and control, *IEEE Transactions on Automatic Control*, 9, 333-339.
- Janisková, M., J.-F. Mahfouf, J.-J. Morcrette et F. Chevallier (2002), Linearized radiation and cloud schemes in the ECMWF model : development and evaluation, *Q. J. R. Meteor. Soc.*, 128, 1505-1528.
- Jaynes, E. T. (2003), *Probability theory : the logic of science*, G. L. Bretthorst (ed.), Cambridge University Press.
- Kalman, R. E. (1960), A new approach to linear filtering and prediction problems, *Transactions of the American Society of Mechanical Engineers, J. Basic Eng.*, 82, 34-45.
- Kaplan, L. D. (1959), Inferences of atmospheric structures from satellite radiance measurements, *J. Opt. Soc. Amer.*, 49, 1004-1007.
- Keil, C., A. Tafferner et T. Reinhardt (2006), Synthetic Satellite Imagery in the Lokal-Modell, *Atmos. Res.*, 82, 19-25.
- Kolmogorov, A. N. (1941), Interpolation and extrapolation of stationary random sequences (en Russe), *Izv. Akad. Nauk. SSSR Ser. Mat.*, 5, 3-14. Traduction anglaise dans *Selected Works of*

- A. N. Kolmogorov II*, A. N. Shiryagev (ed.), 272-280 (Kluwer Academic Publishers, Dordrecht, The Netherlands).
- Krasnopolksky, V. M., M. S. Fox-Rabinovitz et D. V. Chalikov (2005), New approach to calculation of atmospheric model physics : accurate and fast neural network emulation of long wave radiation in a climate model, *Mon. Wea. Rev.*, 133, 1370-1383.
- Krüger, L., L. J. Daston et M. Heidelberger (1987), *The probabilistic revolution. Volume 1 : ideas in history*, MIT Press, Cambridge, MA.
- Krüger, L., G. Gigerenzer et M. S. Morgan (1987), *The probabilistic revolution. Volume 2 : ideas in the sciences*, MIT Press, Cambridge, MA.
- Laplace, P. S. (1774), Mémoire sur la probabilité des causes par les événements, *Sav. Etr.*, 6, 621-656.
- Laplace, P. S. (1781), Mémoire sur les probabilités, *Mém. Acad. R. des Sci. Paris pour 1778*, 227-332.
- Laplace, P. S. (1812), *Théorie analytique des probabilités*, Courcier, Paris.
- Law, R. M., R. J. Matear, et R. J. Francey (2008), Comment on "Saturation of the Southern Ocean CO₂ Sink Due to Recent Climate Change" *Science*, 319, doi :10.1126/science.1149077
- Le Dimet, F.-X. et O. Talagrand (1986), Variational assimilation of meteorological observations : theoretical aspect, *Tellus*, 38A, 97-110.
- Le Quéré, C., C. Rödenbeck, E.T. Buitenhuis, T. J. Conway, R. Langenfelds, A. Gomez, C. Labuschagne, M. Ramonet, T. Nakazawa, N. Metzl, N. Gillett et M. Heimann (2007), Response to Comments on "Saturation of the Southern ocean CO₂ sink due to recent climate change", *Science*, 319, doi :10.1126/science.1147315
- Lewis, J. M. et J. C. Derber (1985), The use of adjoint equations to solve a variational adjustment problem with advective constraints, *Tellus*, 37A, 309-322.
- Lorenc, A. (1986), Analysis methods for numerical weather prediction, *Quart. J. Roy. Met. Soc.*, 112, 1177-1194.
- Matricardi, M., F. Chevallier, G. Kelly, et J.-N. Thépaut (2004), Improved general fast radiative transfer model for the assimilation of radiance observations, *Q. J. R. Meteor. Soc.*, 130, 153-173.
- Meirink, J. F., H. J. Eskes et A. P. H. Goede (2006), Sensitivity analysis of methane emissions derived from SCIAMACHY observations through inverse modelling, *Atmos. Chem. Phys.*, 6, 1275-1292.
- Michalak, A. M., A. Hirsch, L. Bruhwiler, K. R. Gurney, W. Peters et P. P. Tans (2005), Maximum likelihood estimation of covariance parameters for Bayesian atmospheric trace gas surface flux inversions, *J. Geophys. Res.*, 110, D24107, doi :10.1029/2005JD005970.
- Moivre, A. de (1718), *The doctrine of chances : or, a method of calculating the probability of events in play*, London.
- Moreau, E., P. Bauer et F. Chevallier (2003), Variational retrieval of rain profiles from spaceborne passive microwave radiance observations, *J. Geophys. Res.*, 108(D16), 4521, doi :10.1029/2002JD003315.
- Parrish, D. F. et J. C. Derber (1992), The National Meteorological Center's spectral statistical-interpolation analysis system, *Mon. Wea. Rev.*, 120, 1747-1763.
- Peuch, A., J.-N. Thépaut et J. Pailleux (2000), Dynamical impact of total-ozone observations in a four-dimensional variational assimilation, *Q. J. Roy. Met. Soc.*, 126, 1641-1659.
- Peters, W., A. R. Jacobson, C. Sweeney, A. E. Andrews, T. J. Conway, K. Masarie, J. B. Miller, L. M. P. Bruhwiler, G. Pétron, A. I. Hirsch, D. E. J. Worthy, G. R. van der Werf, J. T. Randerson, P.

- O. Wennberg, M. C. Krol, et P. P. Tans (2007), An atmospheric perspective on North American carbon dioxide exchange : CarbonTracker *Proc. of the Nat. Acad. of Sc.*, 104, 18925-18930.
- Popper, K. R. (1959), *The Logic of Scientific Discovery*, Routledge.
- Prigogine, I. (1996), *La fin des certitudes*, Odile Jacob.
- Raupach M. R., Marland G., Ciais P., Le Quéré C., Canadell J. G. et Field, C. B. (2007), Global and regional drivers of accelerating CO₂ emissions, *Proc. of the Nat. Acad. of Sc.*, 104, 10288-10293, doi :10.1073/pnas.0700609104
- Rödenbeck, C. (2005), Estimating CO₂ sources and sinks from atmospheric mixing ratio measurements using a global inverse of atmospheric transport. Technical Reports, Max-Planck-Institut für Biogeochemie 6.
- Saunders, R., P. Brunel, S. English, P. Bauer, U. O'Keefe, P. Francis, P. Rayer (2006), RTTOV-8 - Science and validation report, *NWP-SAF report*, NWPSAF-MO-TV-007.
- Shafer, G. et V. Vovk (2006), The sources of Kolmogorov's *Grundbegriffe*, *Statistical Science*, 21, 70-98.
- Stavrakou, T. et J.-F. Müller (2006), Grid-based versus big region approach for inverting CO emissions using Measurement of Pollution in the Troposphere (MOPITT) data, *J. Geophys. Res.*, 111, D15304, doi :10.1029/2005JD006896.
- Stigler, S. M. (1986), *The history of statistics - The measurement of uncertainty before 1900*, Harvard University Press.
- Szyndel, M., G. Kelly et J-N. Thépaut (2005), Evaluation of calibration and potential for assimilation of SEVIRI radiance data from Meteosat-8, *EUTMETSAT/ECMWF Fellowship Programme Research Report no. 15*.
- Tebaldi, C., R. L. Smith, D. Nychka et L. O. Mearns (2005), Quantifying uncertainty in projections of regional climate change : a Bayesian approach to the analysis of multimodel ensembles, *J. of Clim.*, 18, 1524-1540.
- The International Ad Hoc Detection and Attribution Group (IADG) (2005), Detecting and attributing external influences on the climate system : a review of recent advances. *J. of Clim.*, 18, 1291-1314.
- Tocqueville (de), A. (1840), *De la démocratie en Amérique*, 2, Paris.
- Wiener, N. (1949), *Extrapolation, interpolation, and smoothing of stationary time series*, Wiley, New York.
- Zickfeld, K., J. C. Fyfe, M. Eby et A. J. Weaver (2008), Comment on "Saturation of the Southern Ocean CO₂ Sink Due to Recent Climate Change", *Science*, 319, doi :10.1126/science.1146886
- Zupanski, D., A. S. Denning, M. Uliasz, M. Zupanski, A. E. Schuh, P. J. Rayner, W. Peters, and K. D. Corbin (2007), Carbon flux bias estimation employing Maximum Likelihood Ensemble Filter (MLEF), *J. Geophys. Res.*, 112, D17107, doi :10.1029/2006JD008371

Annexe B

Curriculum vitae

Frédéric CHEVALLIER

Laboratoire des Sciences du Climat et de l'Environnement (LSCE)
Unité mixte de recherche du CEA, du CNRS et de l'UVSQ (UMR 1572)

L'Orme des Merisiers, Bat 701, Point courrier 129
91191 Gif sur Yvette CEDEX, France
④ +33 (0) 1 69 08 77 29 ; ✉ frederic.chevallier@lsce.ipsl.fr
<http://www-lsce.cea.fr/Pisp/6/frederic.chevallier.html>

THÈMES DE RECHERCHE

Assimilation de données
Modélisation du cycle du carbone
Modélisation du rayonnement atmosphérique
Télédétection

EXPÉRIENCES PROFESSIONNELLES

2003 - présent Ingénieur chercheur CEA au Laboratoire des Sciences du Climat et de l'Environnement (LSCE, Gif-sur-Yvette)
1998 - 2003 Chercheur au Centre Européen pour les Prévisions Météorologiques à Moyen Terme (CEPMMT, Reading, GB)
1994 - 1997 Doctorant au Laboratoire de Météorologie Dynamique (LMD, Palaiseau)

ÉTUDES

1998 Doctorat « Méthodes Physiques en Télédétection », université Paris 7
La modélisation du transfert radiatif à des fins climatiques : une nouvelle approche fondée sur les réseaux de neurones artificiels, 230 p.
1994 DEA « Méthodes Physiques en Télédétection », université Paris 7
1993 Maîtrise de Physique, université Rennes 1
1991 DEUG de mathématiques et de physique, université Rennes 1
1989 Baccalauréat scientifique

PUBLICATIONS

Auteur ou coauteur de plus de 40 publications dans des revues de rang A (indice $h = 16$, liste donnée en annexe C), de plus de 35 publications dans des actes de colloques et de 20 rapports techniques.

CONTRATS DE RECHERCHE

2009 - présent	Investigateur et coordinateur LSCE du projet européen <i>Monitoring Atmospheric Composition and Climate</i> (MACC)
2008 - présent	Investigateur et coordinateur LSCE du projet européen <i>Geoland-2 - Towards an operational GMES land monitoring core service</i>
2008 - présent	Investigateur et coordinateur LSCE du projet européen <i>Coordination Action Carbon Observation System (COCOS)</i>
2007 - présent	Investigateur du projet ESA <i>Observation techniques and mission concept for the analysis of the global carbon cycle</i>
2006 - présent	Investigateur du projet ESA <i>CArbon flux Modelling using Earth observation Land products for Initiation and by Assimilation</i> (CAMELIA)
2006 - présent	Investigateur et coordinateur LSCE du projet européen <i>Quantification, understanding and prediction of carbon cycle and other GHG gases, in Sub-Saharan Africa</i> (CARBOAFRICA)
2006 - présent	Investigateur du projet européen <i>HYdrogen, Methane and Nitrous oxide : trend variability, budgets and interactions with the biosphere</i> (HYMN)
2006 - présent	Investigateur du projet ANR <i>Aménager l'Utilisation des Terres et des Ressources de l'Environnement en Modélisant les Écosystèmes aNTropiques</i> (AUTREMENT)
2006 - présent	Investigateur du projet ANR <i>Theoretical Developments of Data Assimilation Models for Climate Extremes</i> (AssimilEx)
2005 - présent	Investigateur et coordinateur LSCE du projet européen <i>Global Earth-system Monitoring using Satellite and in-situ data</i> (GEMS)
2005 - présent	Investigateur du projet ESA <i>TRopospheric composition and Air Quality</i> (TRAQ)
2004 - 2007	Investigateur du projet européen <i>GMES products & services, integrating EO monitoring capacities, to support the implementation of European directives and policies related to "land cover and vegetation"</i> (GEOLAND)
2000 - 2003	Investigateur du projet conjoint entre Eumetsat, the Met Office, le CEPMMT et MétéoFrance <i>Centres d'Applications Satellitaires - Prévision Numérique du Temps</i> (SAF NWP)
1999	Investigateur du projet ESA/ESTEC 13151/98/NL/GD en préparation de <i>Earth Radiation Mission</i>

PRODUCTION SCIENTIFIQUE PUBLIQUE NON LITTÉRAIRE

- Créeur et administrateur d'un site Internet de suivi de la biosphère terrestre en temps semi-réel
<http://www.lsceorchidee.cea.fr>
- Production d'une banque de données de profils atmosphériques échantillonnés (1999, mise à jour en 2002 et 2006), téléchargeable sur
http://www.metoffice.gov.uk/science/creating/working_together/nwpsaf_public.html
- Production d'un code informatique générique d'inversion de type « 1D-Var » (1999, mise à jour en 2000, 2002, 2003 et 2004), téléchargeable sur
http://www.metoffice.gov.uk/science/creating/working_together/nwpsaf_public.html

ENCADREMENT

avr. 2008 - présent	Katja Hungershoefer, post-doctorante au LSCE (50%)
juin 2007 - sept. 2008	Claire Carouge, post-doctorante au LSCE (50%) - article Carouge et coll., 2008 (cf. annexe C)
avr. 2007 - présent	Isabelle Pison, post-doctorante au LSCE (75%) - article Pison et coll., 2008 (cf. annexe C)
avr. 2007 - présent	Audrey Fortems, stagiaire M2 puis CDD ingénieur au LSCE (80%)
mai - sept. 2006	Marion Devaux, stagiaire ingénieur et M2 au LSCE (70%)
oct. 2005 - présent	François Delage, CDD ingénieur au LSCE (30%)
oct. 2005 - déc. 2008	Thomas Lauvaux, doctorant au LSCE (30%) - articles Lauvaux et coll., 2007, 2008a, 2008b (cf. annexe C)
2004 - 2006	Jérôme Demarty, post-doctorant au LSCE (50%) - article Demarty et coll., 2007 (cf. annexe C)
2004	Sylvia Generoso, doctorante au LSCE (30%) - article Generoso et coll., 2007 (cf. annexe C)
2002	Emmanuel Moreau, post-doctorant au CEPMMT (30%) - article Moreau et coll., 2003 (cf. annexe C)

ADMINISTRATION DE LA RECHERCHE

2008	Examinateur dans le jury de thèse de Thomas Lauvaux, UVSQ
2007 - présent	Responsable de l'équipe Inversion-Assimilation-Télédétection du LSCE (20-30 personnes)
2007 - présent	Membre du comité d'utilisateurs du pôle de compétences en chimie atmosphérique ETHER (CNES, CNRS)
2007	Co-organisateur de <i>4th International Workshop on Greenhouse Gas Measurements from Space</i> , CNES, Paris, 25-27 juin 2007
2007	Examinateur dans le jury de thèse de Nicolas Huneeus, université de Lille
2005 - présent	Membre du conseil scientifique du programme <i>assimilation</i> de l'INSU
2005	Participation à la prospective de la commission spécialisée océan-atmosphère de l'INSU
2004 - présent	Rapporteur de projets de recherche soumis à NSF (USA), NOAA/CDEP (USA), NERC (GB), et l'ANR (F)
2003	Membre du comité de programmation de <i>Third conference on artificial intelligence applications to the environmental science</i> , Long Beach, CA, 9-13 février 2003
2003	Membre du comité de programmation de <i>EUMETSAT meteorological satellite conference</i> , Weimar, Allemagne, 29 septembre - 3 octobre 2003
1998 - présent	Rapporteur d'une soixantaine d'articles pour <i>J. Appl. Meteor.</i> , <i>Q. J. R. Meteor. Soc.</i> , <i>J. Geophys. Res.</i> , <i>Mon. Wea. Rev.</i> , <i>Geophys. Res. Lett.</i> , <i>IEEE Trans. on Geoscience and Remote Sensing</i> , <i>Biogeosciences</i> et <i>Atmos. Chem. Phys.</i>

REPRÉSENTATION DU PERSONNEL

2008	Élu au conseil du laboratoire du LSCE
2006 - 2008	Suppléant élu au conseil du laboratoire du LSCE
2001 - 2003	Représentant élu des consultants au CEPMMT

Annexe C

Publications scientifiques

Articles publiés dans des revues à comité de lecture

Le nombre de citations obtenu par chaque article dans la littérature scientifique est indiqué en date du 10 décembre 2008 (source : *Web of Science*).

1. F. Chéruy, **F. Chevallier**, J.-J. Morcrette, N. A. Scott, et A. Chédin, 1996 : Une méthode utilisant les techniques neuronales pour le calcul rapide de la distribution verticale du bilan radiatif terrestre, *C. R. Acad. Sci. Paris, 322, IIb*, 665-672. Cité 13 fois.
2. **F. Chevallier**, F. Chéruy, N. A. Scott, et A. Chédin, 1998 : A neural network approach for a fast and accurate computation of a longwave radiative budget. *J. Appl. Meteor., 37*, 1385-1397. Cité 74 fois.
3. N. A. Scott, A. Chédin, R. Armante, J. Francis, C. Stubenrauch, J.-P. Chaboureau, **F. Chevallier**, C. Claud, et F. Chéruy, 1999 : Characteristics of the TOVS Pathfinder Path-B database. *Bull. Amer. Meteo. Soc., 80*, 2679-2702. Cité 48 fois.
4. F. Chéruy et **F. Chevallier**, 2000 : Regional and seasonal variations of the clear sky atmospheric longwave cooling over tropical oceans. *J. Climate, 13*, 2863-2875. Cité 4 fois.
5. **F. Chevallier**, A. Chédin, F. Chéruy, et J.-J. Morcrette, 2000 : TIGR-like atmospheric profile databases for accurate radiative flux computation. *Q. J. R. Meteor. Soc., 126*, 777-785. Cité 26 fois.
6. **F. Chevallier**, F. Chéruy, R. Armante, C. J. Stubenrauch, et N. A. Scott, 2000 : Retrieving the clear-sky vertical longwave radiative budget from TOVS : comparison of a neural network-based retrieval and a method using geophysical parameters. *J. Appl. Meteor, 39*, 1527-1543. Cité 3 fois.
7. **F. Chevallier**, J.-J Morcrette, F. Chéruy, et N. A. Scott, 2000 : Use of a neural network-based longwave radiative transfer scheme in the ECMWF atmospheric model. *Q. J. R. Meteor. Soc., 126*, 761-776. Cité 27 fois.
8. **F. Chevallier** et J.-J. Morcrette, 2000 : Comparison of model fluxes with surface and top-of-the-atmosphere observations. *Mon. Wea. Rev., 128*, 3839-3852. Cité 17 fois.
9. **F. Chevallier**, P. Bauer, G. Kelly, C. Jakob, et A. P. McNally, 2001 : Model clouds over oceans as seen from space : comparison with HIRS/2 and MSU radiances. *J. Climate, 14*, 4216-4229. Cité 29 fois.

10. **F. Chevallier** et J.-F. Mahfouf, 2001 : Evaluation of the Jacobians of infrared radiation models for variational data assimilation. *J. Appl. Meteor.*, 40, 1445-1461. Cité 16 fois.
11. L. Garand, D. S. Turner, M. Larocque, J. Bates, S. Boukabara, P. Brunel, **F. Chevallier**, G. Deblonde, R. Engelen, M. Hollingshead, D. Jackson, G. Jedlovec, J. Joiner, T. Kleespies, D. S. McKague, L. McMillin, J.-L. Moncet, J. R. Pardo, P. J. Rayer, E. Salathe, R. Saunders, N. A. Scott, P. Van Delst, et H. Woolf, 2001 : Radiance and Jacobian intercomparison of radiative transfer models applied to HIRS and AMSU channels. *J. Geophys. Res.*, 106 :D20, 24017-24031. Cité 36 fois.
12. **F. Chevallier** et G. Kelly, 2002 : Model clouds as seen from space : comparison with geostationary imagery in the $11\mu\text{m}$ window channel. *Mon. Wea. Rev.*, 130, 712-722. Cité 22 fois.
13. M. Janisková, J.-F. Mahfouf, J.-J. Morcrette, et **F. Chevallier**, 2002 : Linearized radiation and cloud schemes in the ECMWF model : development and evaluation. *Q. J. R. Meteor. Soc.*, 128, 1505-1528. Cité 18 fois.
14. **F. Chevallier**, P. Bauer, J.-F. Mahfouf et J.-J. Morcrette, 2002 : Variational retrieval of cloud profile from ATOVS observations. *Q. J. R. Meteor. Soc.*, 128, 2511-2526. Cité 16 fois.
15. **F. Chevallier** et P. Bauer, 2003 : Model rain and clouds over oceans : comparison with SSM/I observations. *Mon. Wea. Rev.*, 131, 1240-1255. Cité 18 fois.
16. V. Krasnopolsky et **F. Chevallier**, 2003 : Some neural network applications in environmental sciences. Part II : advancing computational efficiency of environmental numerical models. *Neural Networks*, 16, 335-348. Cité 17 fois.
17. E. Moreau, P. Bauer, et **F. Chevallier**, 2003 : Variational retrieval of rain profiles from spaceborne passive microwave radiance observations. *J. Geophys. Res.*, 108(D16), 4521, doi :10.1029/2002JD003315. Cité 11 fois.
18. **F. Chevallier**, P. Lopez, A. M. Tompkins, M. Janisková et E. Moreau, 2004 : The capability of 4D-Var systems to assimilate cloud-affected satellite infrared radiances. *Q. J. R. Meteor. Soc.*, 130, 917-932. Cité 12 fois.
19. R. J. Engelen, E. Andersson, **F. Chevallier**, A. Hollingsworth, M. Matricardi, A. P. McNally, J.-N. Thépaut, et P. D. Watts, 2004 : Estimating atmospheric CO_2 from advanced infrared satellite radiances within an operational 4D-Var data assimilation system : methodology and first results. *J. Geophys. Res.*, 109, D19309, doi :10.1029/2004JD004777. Cité 16 fois.
20. M. Matricardi, **F. Chevallier**, G. Kelly, et J.-N. Thépaut, 2004 : An improved general fast radiative transfer model for the assimilation of radiance observations. *Q. J. R. Meteor. Soc.*, 130, 153-173. Cité 20 fois.
21. E. Moreau, P. Lopez, P. Bauer, A. M. Tompkins, M. Janisková et **F. Chevallier**, 2004 : Variational retrieval of temperature and humidity profiles using rain rates versus microwave brightness temperatures. *Q. J. R. Meteor. Soc.*, 130, 827-852. Cité 25 fois.
22. E. Andersson, P. Bauer, A. Beljaars, **F. Chevallier**, E. Hölm, M. Janisková, P. Källberg, G. Kelly, P. Lopez, A. McNally, E. Moreau, A. J. Simmons, J.-N. Thépaut et A. Tompkins, 2005 : Assimilation and modeling of the atmospheric hydrological cycle in the ECMWF forecasting system. *Bull. Amer. Meteo. Soc.*, 86, 387-402, doi :10.1175/BAMS-86-3-387. Cité 34 fois.

23. **F. Chevallier**, 2005 : Comments on "New approach to calculation of atmospheric model physics : accurate and fast neural network emulation of long wave radiation in a climate model". *Mon. Wea. Rev.*, 133, 3721-3723. Cité 2 fois.
24. **F. Chevallier**, G. Kelly, A. J. Simmons, S. Uppala, et A. Hernandez, 2005 : High clouds over oceans in the ECMWF 15-year and 45-year re-analyses. *J. Climate*, 18, 2647-2661. Cité 3 fois.
25. **F. Chevallier**, R. J. Engelen, and P. Peylin, 2005 : The contribution of AIRS data to the estimation of CO₂ sources and sinks. *Geophys. Res. Lett.*, 32, L23801, doi :10.1029/2005GL024229. Cité 9 fois.
26. **F. Chevallier**, M. Fisher, P. Peylin, S. Serrar, P. Bousquet, F.-M. Bréon, A. Chédin, et P. Ciais, 2005 : Inferring CO₂ sources and sinks from satellite observations : method and application to TOVS data. *J. Geophys. Res.*, 110, D24309, doi :10.1029/2005JD006390. Cité 9 fois.
27. P. Ciais, M. Reichstein, N. Viovy, A. Granier, J. Ogée, V. Allard, M. Aubinet, N. Buchmann, C. Bernhofer, A. Carrara, **F. Chevallier**, N. De Noblet, A. D. Friend, P. Friedlingstein, T. Grnwald, B. Heinesch, P. Keronen, A. Knohl, G. Krinner, D. Loustau, G. Manca, G. Matteucci, F. Miglietta, J. M. Ourcival, D. Papale, K. Pilegaard, S. Rambal, G. Seufert, J. F. Soussana, M. J. Sanz, E. D. Schulze, T. Vesala, et R. Valentini, 2005 : Europe-wide reduction in primary productivity caused by the heat and drought in 2003, *Nature*, 437, 529-533. Cité 182 fois.
28. C. Prigent, **F. Chevallier**, F. Karbou, P. Bauer, et G. Kelly, 2005 : AMSU-A land surface emissivity estimation for numerical weather prediction assimilation schemes. *J. Appl. Meteor*, 44, 416-426. Cité 14 fois.
29. S. M. Uppala, P. W. Källberg, A. J. Simmons, U. Andrae, V. da Costa Bechtold, M. Fiorino, J. K. Gibson, J. Haseler, A. Hernandez, G. Kelly, X. Li, K. Onogi, S. Saarinen, N. Sokka, R. P. Allan, E. Andersson, K. Arpe, M. A. Balmaseda, A. C. M. Beljaars, L. van de Berg, J. Bidlot, N. Bormann, S. Caires, **F. Chevallier**, A. Dethof, M. Dragosavac, M. Fisher, M. Fuentes, S. Hagemann, E. Hólm, B. J. Hoskins, L. Isaksen, P. A. E. M. Janssen, R. Jenne, A. P. A. McNally, J.-F. Mahfouf, J.-J. Morcrette, N. A. Rayner, R. W. Saunders, P. Simon, A. Sterl, K. E. Trenberth, A. Untch, D. Vasiljevic, P. Viterbo, et J. Woollen, 2005 : The ERA-40 Reanalysis. *Q. J. Roy. Met. Soc.*, 131, 2961-3012. Cité 572 fois.
30. P. Bauer, E. Moreau, **F. Chevallier**, et U. O'Keeffe, 2006 : Multiple-scattering microwave radiative transfer for data assimilation applications. *Q. J. Roy. Met. Soc.*, 132, 1259-1281. Cité 10 fois.
31. **F. Chevallier**, N. Viovy, M. Reichstein, et P. Ciais, 2006 : On the assignment of prior errors in Bayesian inversions of CO₂ surface fluxes. *Geophys. Res. Lett.*, 33, L13802, doi :10.1029/2006GL026496. Cité 5 fois.
32. S. Generoso, F.-M. Bréon, **F. Chevallier**, Y. Balkanski, M. Schulz et I. Bey, 2006 : Assimilation of POLDER optical thickness into the LMDZ-INCA model : implications for the Arctic aerosol burden. *J. Geophys. Res.*, 112, D02311, doi :10.1029/2005JD006954. Cité 4 fois.
33. Y. K. Tiwari, M. Gloor, R. J. Engelen, **F. Chevallier**, C. Rödenbeck, S. Körner, P. Peylin, B. H. Braswell, M. Heimann, 2006 : Comparing CO₂ retrieved from AIRS with model predictions : implications for constraining surface fluxes and lower-to-upper troposphere transport. *J. Geophys. Res.*, 111, D17106, doi :10.1029/2005JD006681. Cité 10 fois.

34. **F. Chevallier**, 2007 : Impact of correlated observation errors on inverted CO₂ surface fluxes from OCO measurements. *Geophys. Res. Lett.*, 34, L24804, doi :10.1029/2007GL030463. Cité 1 fois.
35. **F. Chevallier**, F.-M. Bréon, et P. J. Rayner, 2007 : The contribution of the Orbiting Carbon Observatory to the estimation of CO₂ sources and sinks : Theoretical study in a variational data assimilation framework. *J. Geophys. Res.*, 112, D09307, doi :10.1029/2006JD007375. Cité 10 fois.
36. J. Demarty, **F. Chevallier**, A. D. Friend, N. Viovy, S. Piao et P. Ciais, 2007 : Assimilation of global MODIS leaf area index retrievals within a terrestrial biosphere model. *Geophys. Res. Lett.*, 34, L15402, doi :10.1029/2007GL030014.
37. M. Labonne, F.-M. Bréon, et **F. Chevallier**, 2007 : Injection height of biomass burning aerosols as seen from a spaceborne lidar. *Geophys. Res. Lett.*, 34, L11806, doi :10.1029/2007GL029311. Cité 5 fois.
38. C. Carouge, P. Peylin, P. J. Rayner, P. Bousquet, **F. Chevallier** et P. Ciais (2008) : What can we learn from European continuous atmospheric CO₂ measurements to quantify regional fluxes, Part 2 : Sensitivity of flux accuracy to inverse setup. *Atmos. Chem. Phys. Discuss.*, 8, 18621-18649.
39. R. J. Engelen, S. Serrar et **F. Chevallier**, 2008 : Four-dimensional data assimilation of atmospheric CO₂ using AIRS observations, *J. Geophys. Res.*, doi :10.1029/2008JD010739, sous presse.
40. A. Hollingsworth, R. J. Engelen, C. Textor, A. Benedetti, O. Boucher, **F. Chevallier**, A. Dethof, H. Elbern, H. Eskes, J. Flemming, C. Granier, J. J. Morcrette, P. Rayner, V.-H Peuch, L. Rouil, M. Schultz, A. Simmons, et the GEMS consortium, 2008 : The Global Earth-system Monitoring using Satellite and in-situ data (GEMS) Project : Towards a monitoring and forecasting system for atmospheric composition. *Bull. Amer. Meteo. Soc.*, 89, 1147-1164, doi :10.1175/2008BAMS2355.1
41. T. Lauvaux, O. Pannekoucke, C. Sarrat, **F. Chevallier**, P. Ciais, J. Noilhan, et P.J. Rayner, 2008 : Structure of the transport uncertainty in mesoscale inversions of CO₂ sources and sinks using ensemble model simulations, *Biogeosciences Discuss.*, 5, 4813-4846.
42. T. Lauvaux, M. Uliasz, C. Sarrat, **F. Chevallier**, P. Bousquet, C. Lac, K. J. Davis, P. Ciais, A. S. Denning, et P. J. Rayner, 2008 : Mesoscale inversion : first results from the CERES campaign with synthetic data. *Atmos. Chem. Phys.*, 8, 3459-3471.
43. I. Pison, P. Bousquet, **F. Chevallier**, S. Szopa, et D. A. Hauglustaine : Multi-species inversion of CH₄, CO and H₂ emissions from surface measurements. *Atmos. Chem. Phys. Discuss.*, 8, 20687-20722.
44. C. Prigent, E. Jamouillé, **F. Chevallier** et F. Aires, 2008 : A parameterization of the microwave land surface emissivity between 19 and 100 GHz, anchored to satellite-derived estimates. *IEEE Trans. Geosci. Remote Sens.*, 46, 344-352. Cité 1 fois.
45. **F. Chevallier**, A. Fortems, P. Bousquet, I. Pison, S. Szopa, M. Devaux, et D. A. Hauglustaine (2009), African CO emissions between years 2000 and 2006 as estimated from MOPITT observations, *Biogeosciences*, 6, 103-111.
46. G. Toulemonde, A. Guillou, P. Naveau, M. Vrac et **F. Chevallier**, 2009 : Autoregressive models for maxima and their applications to CH₄ and N₂O. *Environmetrics*, sous presse.

De l'application de la théorie analytique des probabilités pour l'étude de l'atmosphère

Résumé : Le théorème dit « de Bayes » est un modèle mathématique de l'apprentissage. Il décrit comment l'apport d'une nouvelle information améliore la connaissance d'un phénomène. Découvert en 1774 par Pierre Simon Laplace, il fournit une solution générique aux problèmes inverses et est devenu une référence essentielle pour les méthodes d'estimation statistique. Son succès témoigne de sa flexibilité et de sa rigueur pour le traitement des observations. Son application pour l'étude d'un problème particulier fait appel à des savoirs variés, car chacune des composantes d'un système d'inversion requiert un travail spécialisé, sur le problème scientifique étudié, sur les observations, sur la modélisation, ou sur l'ingénierie informatique. Mais elle doit être guidée par une compétence spécifique liée à la théorie des probabilités.

Nous présentons plusieurs questions fondamentales autour du théorème de Bayes. Comment spécifier les statistiques d'erreur des différentes informations disponibles ? Toute observation est-elle utile ? Comment relier les variables observées et les variables d'étude ? Comment appliquer le théorème dans le cas de problèmes de grandes dimensions ? Les réponses à ces questions sont étayées dans le cadre de deux problèmes scientifiques. Le premier est l'assimilation des informations fournies par les satellites sur les nuages et la pluie dans les modèles numériques mis en œuvre pour la prévision météorologique. Le deuxième problème scientifique concerne l'estimation des flux de dioxyde de carbone à la surface du globe.

On the application of the analytical theory of probabilities for the study of the atmosphere

Abstract : Bayes' theorem is a mathematical model of learning. It describes how new information improves our knowledge about any phenomenon. Discovered in 1774 by Pierre Simon Laplace, it provides a generic solution to inverse problems and has become a reference for statistical estimation. Its success reflects its flexibility and rigor for the treatment of observations. Its application to a specific problem involves diverse skills, because each component of an inversion system requires a dedicated study, on the problem itself, on the observations, on modeling, or on engineering science. But it must be guided by the theory of probability.

We present some fundamental issues about Bayes theorem. How to assign error statistics to the available information pieces ? Are all observations useful ? How to link the observed variables and the variables of study ? How to apply the theorem in the case of large-dimension problems ? The answers to these questions are documented based on two scientific problems. The first is the assimilation of satellite information about clouds and rain in numerical weather forecast models. The second scientific problem concerns the estimation of the carbon dioxide fluxes at the Earth surface.